Cranfield University

Gudrun Winkler

Effects of configuration on the operation of membranes in membrane biological reactors

School of Applied Sciences
Centre for Water Science

PhD Thesis

CRANFIELD UNIVERSITY

SCHOOL OF APPLIED SCIENCES
CENTRE FOR WATER SCIENCE

PHD THESIS

GUDRUN WINKLER

Effects of configuration on the operation of membranes in membrane biological reactors

Supervisor: Professor Tom Stephenson

January 2011

This thesis is submitted in partial fulfillment of the requirements for the degree of Doctor of Philosophie.

Abstract

The aim of this work included the investigation of the impact of membrane material properties on fouling propensity and permeate flux decline in MBR biomass systems. Furthermore, the impact of membrane configuration on the respective fouling behaviour was of interest. A direct comparative study of different membrane module configurations including a multi-tubular membrane (MT), a single flat sheet module (FS) and a hollow fibre (HF) pilot scale module was undertaken. Membrane module filtration performances, especially with respect to their fouling propensity under varying hydraulic conditions, were investigated to ultimately evaluate the impact of varying parameters such as aeration and biomass make up on fouling and to determine optimised operational parameters. Subsequently, a range of different membrane materials, such as flat sheet membrane samples made of polyethylene (PE), polyethersulfone (PES), polysulfone (PS) and polyvynilidene fluoride (PVDF) and a single-tube made of PVDF and PES were characterised and their fouling propensity to MBR biomass was studied at bench-scale.

Critical flux trials were conducted using a novel flux step method including relaxation periods and (where configuration permitted) backwash cycles to be able to study the different filtration behaviours deriving from different membrane configurations. Trials at different aeration rates of SAD_m 0.5 $Nm^3m^2h^{-1}$ to 2.0 $Nm^3m^2h^{-1}$ at three different MLSS contents showed that filtration performance varied significantly for the different membrane configurations tested. This was first be explained by the application of the aeration in the different configurations (in-side-out to outside-in filtration) and furthermore in changed sludge filterability due to the effects on the biomass during the side-stream vessel passage. For instance, the MT module showed an increased critical flux with increased aeration intensity and lower MLSS content, whereas for the HF and FS module the critical flux, J_c, decreased with increasing aeration intensity and J_c increased furthermore with increasing MLSS content.

The FS and HF modules displayed a better filtration performance at high MLSS contents with clear correlations between the critical flux and permeability and the MLSS concentration. Conversely, the MT module exhibited a better performance at a concentration of 7 $g.L^{-1}$. However, in all cases no clear correlation could generally be found between the fouling observed and other biomass characteristics. Overall, at the more typical MLSS concentration of 12 $g.L^{-1}$ for the operation of membrane bioreactors, the HF module was found to show the best performance based on the data of this study and where filtration tests were all undertaken at

short-term. Long-term fouling study might reveal different results.

Investigation of membrane materials at bench-scale revealed very different behaviours for the range of materials tested. Deviations of samples from the same material were found to be quite high, especially for the PVDF 0.15 μm material. This emphasized the high inhomogeneity which may occur during membrane manufacturing. The best filtration performances were observed with the PE 0.4 μm and PVDF 0.08 μm. The trials furthermore revealed that a clear selection of a most favourable material is impossible; for example the membrane PVDF 0.15 μm displayed much lower filtration performance than the PVDF 0.08 μm suggesting that fouling is not only linked to the type of material but also to other parameters such as pore size and surface/material preparation. Single-tube trials furthermore revealed results opposed to the flat sheet material. Bench-scale trials undertaken simultaneously to pilot scale trials revealed opposing trends. A more detailed analysis of the materials and processes would then be needed to fully understand the mechanisms occurring.

Acknowledgements

I would like to express my gratitude to all those who made it possible to complete this thesis.

First of all, I would like to thank Prof. Tom Stephenson to whom I am deeply indebted to for overseeing this project in its most critical stage and I would like to express my gratitude for all his support and his unfailing patience. I would like to thank Prof. Simon Judd for offering me the chance to participate in this very interesting project and for not only introducing me to the the European MBR network, but also to the legendary *world of membranes*. I would also like to thank Dr. Bruce Jefferson and Dr. Marc Pidou for their guidance throughout this project.

This work was carried out as part of the 6^{th} Framework Program "EUROMBRA" and the European Commission is gratefully thanked for the financial support. All project partners are thanked for the very interesting meetings and fruitful discussion, with special thank you to TorOve Leiknes as our project coordinator and Steffen Bütehorn, Corinne Cabassud and Adriano Joss as workpackage leaders.

I would furthermore like to thank all the membrane suppliers who contributed sample materials, with special thanks to Dirk Volmering from KMS Puron for his special side-stream vessel contribution, and the companies Berghof and Toray for their pilot scale module contribution. John from Model Products, Wootton, and his team are greatly acknowledged for their excellent work, John for his diligent advise while designing and setting up the pilot plant. A special thank you goes furthermore to Roland Härtel for his excellent tailor-made contribution: the pump program!

I would like to thank the Water Science staff, Rukhsana, Jane, Ian, Nigel, Paul and Keith for being so helpful all the time, with special thanks to Rukhsana and Ian for their help during the pilot plant set up. Ian is furthermore acknowledged for his help and encouragement during various moments of pilot hELl despair.

I am furthermore grateful to Martino, Aurelien and Sarah for their precious help during their placements.

A special thank you to the *Hempel-Tussis*, Katja and her crazy sister Manja. I still can not believe you chose to spend your holidays in the middle of nowhere to help a pregnant friend filtering some *shit* samples. I owe you my deepest gratitude.

I would like to say a big thank-you to all the friends and colleagues I met along the way. There are too many to name, but heartfelt thanks to everyone and I am happy and grateful that our paths met and I hope they'll meet again.

Especially, I would like to thank Mel, Cynthia and Ai, the *ladies* of North Crawley, for our wonderful times in "Cottey"; Max & Sil for sharing the "Mellor-fun"; Adrien, Axelle, Davide, Ewan, Jerry, John, Nacho, Nic, Pantelis, Ruben for sharing the pilot hELl experience; lady Nathalia for baptising SHIMA and for all the cheerful moments especially when everything seemed to get lost; and furthermore thank you to Meiky and Yura for all your support and cheering up.

Last but not least I would like to express my love and gratitude to my family, my parents and my in-laws, my brothers and sister for all their warm support in every matter. A special thank you to mum and dad for your believe in me, to my mum for never rejecting a *"Kultur-Tante"*-call and to my dad for keeping up so bravely the loneliness during the various *"Kultur-Tante"*-trips. Nothing would have been possible without your love and support.

I would like to emphasize my inexpressible thankfulness to my -*meanwhile*- husband Marko "Ruschmuba" for enduring another *"island"* episode, and for his endless devoted support and encouragement. Dedicating your holidays to sludge filtration experiments during *our* special circumstances has never been taken for granted. Thank you for always being there for me and for simply making my life so cheerful.

And finally a big hearted **thank you** to the biggest surprise within this PhD, to Emil, our little Knuffel. Nothing would be the same without you: Thank you for having chosen to join our lives.

Contents

Title Page i

Abstract vi

Acknowledgements viii

Table of Contents xiii

List of Figures xv

List of Tables xxii

Abbreviations and Notation xxv

1. Introduction 1

2. Literature Review 5

2.1. Membrane Separation Process 5

2.2. Membranes and Membrane Module Classification 12

2.2.1. Membrane materials 13

2.2.1.1. Overview of membrane materials applied within MBR systems 13

2.2.1.2. Impact of membrane material properties on filtration performance in MBRs 18

2.2.2. Membrane Modules and Configuration 21

2.2.3. Membrane Technology in Wastewater Treatment 24

2.3. Foulants and fouling control concepts in MBRs 27

2.4. Configurational Aspects on Overall Costs 35

3. Aims and Research Objectives 39

4. Materials and Methods 41

4.1. General 41

4.2. Materials 42

4.2.1. Membrane Materials 42

4.2.2. Pilot Plant . . . 44
4.2.2.1. Design and Set Up . . . 44
4.2.2.2. Operation . . . 47
4.2.2.3. Cleaning and Clean Water Trials . . . 49
4.2.2.3.1. Side-stream Modules . . . 49
4.2.2.3.2. Submerged Module . . . 50
4.2.2.4. Pilot Plant Start Up Phase . . . 51
4.2.2.4.1. Membrane modules filtration performance . . . 51
4.2.2.4.2. Biomass parameters . . . 55
4.2.2.4.3. Summary . . . 56
4.2.3. Bench-scale . . . 57
4.2.3.1. Flat Sheet Test Cell Device . . . 57
4.2.3.2. Single-tube Test Device . . . 59
4.3. Methods . . . 60
4.3.1. Membrane Characterisation . . . 60
4.3.1.1. Surface characterisation . . . 60
4.3.1.1.1. Atomic Force Microscope - AFM . . . 60
4.3.1.1.2. Scanning Electron Microscopy (SEM) . . . 61
4.3.1.1.3. Contact Angle Measurements and Determination of Surface Free Energy . . . 61
4.3.1.2. Filtration Protocol - Critical Flux, Continuous Flux . . . 63
4.3.1.2.1. Critical Flux . . . 63
4.3.1.2.2. Continuous Flux . . . 63
4.3.1.3. Calculation of filtration parameters . . . 65
4.3.1.3.1. Temperature Correction . . . 65
4.3.1.3.2. Permeability . . . 66
4.3.1.3.3. Determination of Filtration Resistances . . . 66
4.3.1.3.4. Determination of Fouling Rates and Novel Critical Flux Parameters . . . 68
4.3.1.4. Fractionation of Potential Foulants . . . 72
4.3.1.4.1. Bench-scale material . . . 72
4.3.1.4.2. Pilot-scale and full-scale material . . . 72
4.3.2. Wastewater and Biomass Characterisation . . . 73
4.3.2.1. Sampling . . . 73
4.3.2.2. SMP and EPS extraction . . . 73
4.3.2.2.1. Preparation of Solid Free Fraction (SMP) . . . 73
4.3.2.2.2. Extraction of Extracellular polymeric substances (EPS) 74
4.3.2.2.2.1. EPS extraction via heating method . . . 74
4.3.2.2.2.2. EPS extraction via CER . . . 74

4.3.2.3. Standard analytical procedures . . . 75
4.3.2.4. Protein and Carbohydrate determination . . . 76
4.3.2.4.1. Protein determination . . . 76
4.3.2.4.2. Carbohydrates . . . 77
4.3.2.5. UV-VIS Adsorbance - SUVA . . . 78
4.3.2.6. High performance size exclusion - HPSEC . . . 79
4.3.2.7. Mixed liquor suspended solids, total solids and volatile solids . 80
4.3.2.7.1. Suspended Solids - MLSS content . . . 80
4.3.2.7.2. Total Solids . . . 80
4.3.2.7.3. Volatile Solids . . . 81
4.3.2.8. Particle Size and particle surface . . . 81
4.4. Statistical Analyses . . . 83

5. Results & Discussion:
Critical flux trials under different flux step protocols **85**
5.1. Scope . . . 85
5.2. Comparison of critical flux trials with and without relaxation/backwash at MLSS 12 g.L^{-1} . . . 88
5.2.1. Permeability . . . 88
5.2.2. Fouling rates - dP/dt . . . 95
5.2.3. Residual fouling rates - $dP_{p,s}/dt$ . . . 100
5.3. Summary . . . 102

6. Results & Discussion:
Comparison of critical fluxes at varying MLSS concentration **105**
6.1. Scope . . . 105
6.2. Comparison of critical trials with and without relaxation/backwash at varying MLSS concentration . . . 106
6.2.1. Permeability . . . 106
6.2.2. Fouling rates dP/dt and $dP_{p,s}/dt$ . . . 107
6.2.3. Cake layer resistance R_{cl} . . . 112
6.2.4. Summary . . . 114
6.3. Critical Flux at pilot scale - Comparison to consecutive filtration runs and sub-critical long-term fouling . . . 116
6.3.1. Critical Flux Trials under Consecutive Filtration . . . 116
6.3.2. Sub-critical continuous filtration . . . 118
6.4. Critical flux of different membrane materials at varying MLSS - Bench-scale trials 120
6.5. Summary . . . 122

7. Results & Discussion:
Fouling control by air scouring **127**
7.1. Scope . . . 127
7.2. Permeability Development of Critical Flux Trials at different SAD_m and MLSS content . . . 129
7.2.1. MT module . . . 129
7.2.2. FS module . . . 133
7.2.3. HF module . . . 135
7.3. Fouling rates - dP/dt, $dP_{p,s}/dt$ . . . 138
7.3.1. MT module . . . 138
7.3.2. FS module . . . 138
7.3.3. HF module . . . 139
7.4. The positive effects of low membrane aeration . . . 143
7.5. Summary . . . 145

8. Results & Discussion:
Biomass Properties and their potential impact on filtration performance **151**
8.1. Scope . . . 151
8.2. Overall biomass characteristics and effluent quality of the pilot plant . . . 152
8.3. Soluble microbial products and their potential impact on the filtration performance . . . 158
8.4. Particle size . . . 161
8.5. Floc rupture - SMP release, SMP retention and HPSEC profiles . . . 163
8.6. Summary . . . 168

9. Results & Discussion:
Impact of membrane material properties **173**
9.1. Scope . . . 173
9.2. Membrane Surface Characterisation . . . 174
9.3. Membrane Filtration Resistances - R_t, R_m, R_{cl}, R_{rev}, R_{irrev} . . . 182
9.4. Fractionation of potential membrane foulants . . . 184
9.5. Comparison of Attached Foulants on Membrane Materials after biomass filtration from MBR full scale plant . . . 189
9.6. Summary . . . 191

10. Overall Summary **195**

11. Conclusions **197**

12. Future Aspects **199**

References **214**

A. Sludge Filterability - DFC$_m$ **217**

A.1. Scope . . . 217
A.2. Measurements of resistance to filterability - ΔR_{20} . . . 217
A.2.1. Aeration Tank *(ΔR_{20AT})* . . . 217
A.2.2. Retentate Lines of Air-lift Sidestream Modules *(ΔR_{20Ret})* . . . 219
A.2.2.1. Constant Aeration - Low to High Permeate Fluxes . . . 219
A.2.2.2. Varying Aeration - SAD$_m$ trials . . . 220
A.3. Impact of biomass parameters on ΔR_{20} variations . . . 222
A.3.1. Biomass parameters during critical flux trials at varying aeration rates (SAD$_m$ trials) . . . 222
A.3.2. Biomass parameters during constant aeration trials . . . 228
A.4. Impact of operational parameters on ΔR_{20} ratios . . . 230
A.4.1. Critical flux trials at varying aeration rates (SADm trials) . . . 230
A.4.2. Continuous filtration at constant aeration rates . . . 231
A.5. Membrane filtration performance and ΔR_{20} variations . . . 233
A.6. ANNEX: DFCm filtration trials - Correlation Graphs . . . 237
A.6.1. Corresponding graph to Figure A.3 . . . 237
A.6.2. Corresponding graph to Figure A.4 . . . 238

B. Biomass Parameter - Summary of overall process operation **241**

B.1. Monitoring of biomass changes during constant HRT . . . 241
B.1.1. Monitoring of overall biomass and SMP changes at constant operation without side-stream operation . . . 241
B.1.1.1. Influent values . . . 242
B.1.1.2. Elimination rates and observed retention . . . 246
B.1.2. Monitoring daily fluctuation of biomass properties on a 2-hourly basis . 249
B.1.2.1. Variation of particle size distribution in the aeration tank . . . 249
B.1.2.2. Variation of particle size distribution in sidestream retentate lines . . . 251
B.1.2.3. Impact of SMP variation on particle size distribution . . . 254
B.1.2.4. Changes of SMP in supernatant due to changes in particle size distribution . . . 254

List of Figures

1.1. MBR fouling roadmap - fouling factors and operational design parameters - modified according to Zhang *et al.* (2006) 3

2.1. Filtration spectrum of pressure driven membrane technologies (adapted from Melin and Rautenbach, 2004; Pinnekamp and Friedrich, 2006; Peeters and Theodoulou, n.d.) 5
2.2. Schematic presentation of cake blocking and pore blocking 7
2.3. Schematic presentation of pressure distribution in membrane and cake layer and acting forces on single particles 9
2.4. Example of acting drag forces due to permeate flow on particle in suspension . 10
2.5. Schematic presentation of the critical flux concept with J_c in its strong and weak form 11
2.6. Membrane classification (adapted from Melin and Rautenbach, 2004; Baumgarten, 2007;) 12
2.7. Membrane material classification - Modified according to Rautenbach and Albrecht (1989) with MF/UF/NF applications considered in this study being highlighted 14
2.8. Schematic presentation of various membrane structures according to Günder (2001), illustrating SEM images taken from membrane samples available within this study *(note: orange arrow indicated direction of permeate flow)* 15
2.9. Comparison of permeability and packing density of different commercially available modules for MBR application (data taken from Judd, 2006) 22
2.10. Schematic overview of MBR process configuration: *(a)* side-stream, *(b)* air-lift side-stream, *(c)* submerged (iMBR) with membrane integrated into aeration tank, *(d)* submerged (iMBR) with separated membrane tank 25
2.11. Comparison costs for MBR vs SB-BB for industrial wastewater treatment (paper industry; data from Möbius and A.Helble, 2006). 36

3.1. Aims and Objectives - Effects of investigated operational parameters on performance of different configurations 40

4.1. Scheme of Pilot Plant 45

4.2. Pictures of Pilot Plant 46
4.3. Continuous filtration operation during start up phase from Aug 2007 - Dec 2007 52
4.4. HF1 Module - Module Clogging and Fibre twisting 54
4.5. Observed retention of SMP values during start-up period 56
4.6. Flat Sheet Test Cell Device: Measurements 58
4.7. Flat Sheet Test Cell Device: Scheme of system and Picture 58
4.8. Single-tube Test Device 59
4.9. Critical Flux Scheme 64
4.10. Critical flux determination of classical incremental flux step 69
4.11. Critical flux determination for novel filtration protocol - dP/dt, dPp,s/dt, dPi,s/dt 70
4.12. Protein Calibration with BSA solution 77
4.13. Carbohydrate Calibration with glucose as standard solution 78

5.1. Sample graph of critical flux determination: *(a)* classical filtration protocol without relaxation/backwash; *(b)* novel filtration protocol with 2 filtration cycles including relaxation/backwash 87
5.2. Comparison of permeability curves of membrane modules at critical flux trials with/without backwash or relaxation at biomass filtration trials (MLSS $12gL^{-1}$; SAD_m= 1.0 (FS, HF) and 1.5 (MT) $Nm^3m^{-2}h^{-1}$) and post-sludge clean water trials 89
5.3. Permeability curves for critical flux trials at $MLSS = 12\ gL^{-1}$ - comparison without and with backwash/relaxation 91
5.4. dPdt curves for critical flux trials at $MLSS = 12\ gL^{-1}$ - comparison with and without backwash/relaxation 95
5.5. Residual fouling rates: $dP_{p,s}/dt$ for critical flux trials at $MLSS = 12\ gL^{-1}$ . . 101

6.1. Permeability curves for different critical flux protocols at varying MLSS content 107
6.2. Comparison of determined fouling rates dP/dt and $dP_{p,s}/dt$ for the two different flux step protocols - MT module 109
6.3. Comparison of determined fouling rates dP/dt and $dP_{p,s}/dt$ for the two different flux step protocols - FS module 110
6.4. Comparison of determined fouling rates dP/dt and $dP_{p,s}/dt$ for the two different flux step protocols - HF module 111
6.5. Comparison of cake layer resistance R_{cl} of critical flux trials of the two different filtration protocols 113
6.6. Figure: comparison of critical flux values of different critical flux protocols . . . 114
6.7. Fouling rates dP/dt for consecutive critical flux trials - without cleaning between trials 117

6.8. Continuous filtration trials using relaxation/backwash protocol: *(a)* MLSS 6 g.L^{-1}; *(b)* MLSS 12 g.L^{-1}. 119
6.9. Comparison of J_c to MLSS content of *(a)* flat sheet material and *(b)* single-tube 121
6.10. Correlation of J_c with MLSS content of retentate lines ($MLSS_{RET}$) - fixed SAD_m 123

7.1. Resulting CFV from chosen SAD_m rates for different module configurations and varying MLSS content. 128
7.2. Permeability curves for critical flux trials at different aeration rates and varying MLSS content - MT module 130
7.3. Comparison of determined critical flux J_c and applied aeration intensity at varying MLSS contents - MT module 132
7.4. Permeability curves for critical flux trials at different aeration rates and varying MLSS content - FS module 134
7.5. Comparison of determined critical flux J_c and applied aeration intensity at varying MLSS content - FS module 135
7.6. Comparison of determined critical flux J_c and applied aeration intensity at varying MLSS content - HF module 136
7.7. Permeability curves for critical flux trials at different aeration rates and varying MLSS content - HF module 137
7.8. Fouling rates (classical dP/dt vs peak fouling $dP_{p,s}/dt$) for critical flux trials at different aeration rates and varying MLSS content - MT module 140
7.9. Fouling rates (classical dP/dt vs peak fouling $dP_{p,s}/dt$) for critical flux trials at different aeration rates and varying MLSS content - FS module 141
7.10. Fouling rates (classical dP/dt vs peak fouling $dP_{p,s}/dt$) for critical flux trials at different aeration rates and varying MLSS content - HF module 142
7.11. Permeability values at 30 LMH step vs dewatering of the individual sidestream module 144
7.12. Comparison of determined critical flux J_c for different aeration rates at varying MLSS content. 145
7.13. Comparison of determined critical flux J_c and aeration intensity at more typical MLSS ranges: this study and literature 146

8.1. Floc size distribution within the 2.2 m^3 membrane aeration - overall variation within this study *(a)* vs MLSS content *(b)* vs time of plant operation. 154
8.2. Variation of SMP throughout this study vs *(a)* MLSS content, *(b)* particle size and *(c)* time of pilot plant operation. 155
8.3. Concentration of soluble microbial products per varying MLSS content of biomass for critical flux trials at different aeration rates 158

8.4. Impact of soluble microbial product concentration on permeability development - critical flux trials at different aeration rates and varying MLSS content 159
8.5. Permeability per changing MLSS content of biomass for critical flux trials at varying aeration rate vs. *(a)* particle size; *(b)* particle fractionation; 162
8.6. Impact of pump shear rate on floc size development Example of floc size development between biomass taken from aeration tank (AT) and bench-scale cross-flow of flat sheet test cell device 164
8.7. Sample of changes in supernatant molecular composition during sidestream operation and retention due to membrane filtration - HPSEC profiles 167

9.1. Scanning electron microscope - Selection of pictures of PVDF membrane samples (virgin material) at varying magnitudes 174
9.2. Scanning electron microscope - Selection of pictures of different membrane samples (virgin material) at varying magnitudes 175
9.3. Determined surface roughness (RMS and R_A) for different flat sheet membrane material 177
9.4. Atomic force microscope - Sample of AFM pictures of different membrane samples (virgin material) 177
9.5. Determination of *(a)* contact angle ° for different flat sheet membrane materials and varying wetting liquids and *(b)* the resulting surface tension parameters in $mJ.m^{-2}$ 180
9.6. Determined filtration resistances according to resistance-in-series method for different flat sheet membrane materials 183
9.7. Comparison of attached potential foulants and biomass resistance 186
9.8. Extracted potential foulants from membrane materials *(a, b)* mechanical cleaning, *(c, d)* alkaline cleaning 188
9.9. Comparison of extracted foulants from membrane surface in this study to literature 193

A.1. Sludge filterability (results of DFCm measurements) - daily variations within the aeration tank 218
A.2. Sludge filterability (results of DFCm measurements): Daily average values ($\Delta R_{20\,AT}$) of samples taken from the aeration tank 219
A.3. Sludge filterability (results of DFCm measurements) - comparison of ΔR_{20} values for aeration tank and ratio of $\frac{\Delta R_{20\,Ret}}{\Delta R_{20\,AT}}$ - *(a)* first stage of experiment: constant aeration and low to high permeate fluxes; *(b)* second stage of experiment: critical flux trials with varying SAD_m 221
A.4. Sludge filterability (results of DFCm measurements) - Correlation of $\frac{\Delta R_{20\,Ret}}{\Delta R_{20\,AT}}$ with - *(a)* SAD_m rates; *(b)* date 222

A.5. Sludge filterability (results of DFCm measurements) - SMP values of varying SADm trials . . . 224
A.6. Sludge filterability (results of DFCm measurements) - Correlation of ΔR_{20} with *(a)* Volatile Suspended Solids; *(b)* Particle Size; *(c)* COD_{sludge}; *(d)* pH . . . 226
A.7. Sludge filterability (results of DFCm measurements) - Correlation of ΔR_{20} with *(a)* Carbohydrates per gVSS; *(b)* Proteins per gVSS; *(c)* DOC per gVSS; *(d)* Sum SMP per gVSS . . . 227
A.8. Sludge filterability (results of DFCm measurements) - Correlation of ΔR_{20} with biomass parameters during constant aeration trials . . . 229
A.9. Sludge filterability (results of DFCm measurements) - Correlation of $\frac{\Delta R_{20\ Ret}}{\Delta R_{20\ AT}}$ with *(a)* SAD_p; *(b)* $SRT_{side-stream}$; *(c)* CFV; *(d)* Sludge $Dewatering_{side-stream}$ 231
A.10. Sludge filterability (results of DFCm measurements) - $\frac{\Delta R_{20\ Ret}}{\Delta R_{20\ AT}}$ development during constant aeration trial vs *(a)* Sludge dewatering during the passage of the sidestream vessel; *(b)* Ratio of total solids (retentate line/aeration tank) . . 232
A.11. Sludge filterability (results of DFCm measurements) - Permeability of sidestream modules vs. *(a)* SAD_m; *(b)* $\frac{\Delta R_{20\ Ret}}{\Delta R_{20\ AT}}$ . . . 233
A.12. Sludge filterability (results of DFCm measurements) - Module performance: fouling resistance R_f vs. *(a)* SAD_m; *(b)* $\frac{\Delta R_{20\ Ret}}{\Delta R_{20\ AT}}$ . . . 234
A.13. Sludge filterability (results of DFCm measurements) - Module filtration performance: *(a)* classical $d\mathrm{TMP}/d\mathrm{t}$ vs SAD_m; *(b)* classical $d\mathrm{TMP}/d\mathrm{t}$ vs $\frac{\Delta R_{20\ Ret}}{\Delta R_{20\ AT}}$ *(c)* peak-step $d\mathrm{TMP}_{p,s}/d\mathrm{t}$ vs SAD_m; *(d)* peak-step $d\mathrm{TMP}_{p,s}/d\mathrm{t}$ vs $\frac{\Delta R_{20\ Ret}}{\Delta R_{20\ AT}}$ . . . 235
A.14. Correlation of DFCm resistance to filtration measurement and ratio of P/C for bulk phase of the biomass sample. . . . 236
A.15. Sludge filterability (results of DFCm measurements) - comparison of ΔR_{20} values aeration tank and retentate lines - *(a)* first stage of experiment: constant aeration and low to high permeate fluxes; *(b)* second stage of experiment: critical flux trials with varying SADm . . . 237
A.16. Sludge filterability (results of DFCm measurements) - Correlation of $\frac{\Delta R_{20\ Ret}}{\Delta R_{20\ AT}}$ with - *(a)* SADm rates; *(b)* date - individual module trendlines . . . 238
A.17. Sludge filterability (results of DFCm measurements) - Correlation of $\frac{\Delta R_{20\ Ret}}{\Delta R_{20\ AT}}$ with *(a)* SAD_p; *(b)* $SRT_{side-stream}$; *(c)* CFV; *(d)* Sludge $Dewatering_{side-stream}$: showing individual module trendlines. . . . 239

B.1. *(a)* Variation of SMP, MLSS and pH during monitoring period at HRT 10. *(b)* Correlation of MLSS vs. VSS. . . . 242
B.2. Variation of soluble microbial products measured within the influent (feed) and the supernatant of the aeration tank. . . . 243
B.3. Example of HPSEC profiles of the influent, the supernatant of the aeration tank and permeate of the submerged HF module; MLSS content 12 $g.L^{-1}$ . . . 245

B.4. Soluble microbial products: Elimination rate vs *(a)* time and *(b)* sludge loading rate; *(b)* permeate loading rate vs sludge loading rate during monitoring period at HRT 10. 247
B.5. Retention of soluble microbial products during monitoring period at HRT 10. 248
B.6. Daily variations of floc size distribution within the 2.2 m^3 membrane aeration tank. *(a)* Sample of Mastersizer profile for one monitoring day, *(b)* $d_{0.5}$ floc size development without side-stream modules operation, *(c)* $d_{0.5}$ floc size development with side-stream module operation 250
B.7. Sample of variation of floc size distribution between samples of the 2.2 m^3 membrane aeration tank and the retentate lines of the side-stream modules at 8h00 during sampling trial at MLSS 4 $g.L^{-1}$ 252
B.8. Observed particle fractionation during operation of the side-stream modules: *(a)* MT module, *(b)* FS module, *(c)* HF module 253
B.9. Correlation between *(a)* hourly changes of particle size $dd_{0.5}/dt$ vs. hourly changes of influent ratios P_{INF}/C_{INF} ($dP_{INF}/C_{INF}/dt$, and *(b)* correlation between P_{INF}/C_{INF} ratios and particle size of the aeration tank during the 3 months monitoring period) 254
B.10. Correlation of observed particle fractionation during operation of the sidestream modules vs. fractionation of SMP during 2-hr-monitoring trial:*(a)* MT module, *(b)* FS module, *(c)* HF module 255
B.11. Sample of changes in supernatant molecular composition during sidestream operation - HPSEC profiles 256

List of Tables

2.1. Properties, advantages and disadvantages of different membrane configurations used in wastewater treatment processes (adapted from Judd, 2006; Pinnekamp and Friedrich, 2006; Stephenson *et al.*, 2000) 23
2.2. Available Membrane Modules - from Santos and Judd (2010) 26
2.3. Examples of application of different membrane module configuration 34
2.4. Specific energy demand per membrane filtration process (Baumgarten, 2007) . . 35

4.1. Overview of tested membranes 43
4.2. Overview of membrane modules operated at pilot scale 46
4.3. Start up of pilot plant: Chosen filtration parameters 48
4.4. HRT and biomass parameters during pilot plant start up-phase: Aug 2007 - Dec 2007 55
4.5. Contact angle measurement - surface tension (γ_L), surface tension components (γ_L^{LW}, γ_L^{AB}) and parameters (γ_L^-, γ_L^+) $[mJ.m^2]$ of the used high-energy contact angle liquids at 20°C 62
4.6. Summary of undertaken critical flux protocols 65
4.7. Filtration protocol for continuous fluxes 66
4.8. Critical flux determination - Data analysis 71
4.9. Analytical standard methods 75
4.10. Elution times from protein with known molecular weights 79

5.1. Comparison of permeability values, permeability loss per module for critical flux trials (with and without backwash/relaxation) at fixed SAD_m and MLSS 12 $g.L^{-1}$ 94
5.2. Comparison of average classical fouling rates dP/dt for different critical flux trials (n=4,5,6) at fixed SAD_m and MLSS 12 $g.L^{-1}$ 96
5.3. Comparison of critical flux fouling rates 103
5.4. Typical fouling rates from full scale application; range of fouling rates from pilot plant results - MLSS 12 $g.L^{-1}$; fixed aeration rate 104

6.1. Overview of results for critical flux filtration tests with different critical flux protocol and at varying MLSS content (fixed SAD_m) 115

6.2. Comparison of impacts of MLSS on critical fluxes - literature data and this study 124
6.3. Comparison of impacts of MLSS on critical fluxes - literature data and this study 125

7.1. Typical aeration rates [SAD_m in $N.m^3m^{-2}h^{-1}$] 128
7.2. Comparison of effects of aeration on critical flux - MT 148
7.3. Comparison of effects of aeration on critical flux - FS 149
7.4. Comparison of effects of aeration on critical flux - HF 150

8.1. Biomass and supernatant parameters throughout this study - classified according to operated HRT 156
8.2. Effluent quality of MBR pilot plant throughout this study - classified according to operated HRT 157
8.3. Biomass and SMP parameter for critical flux trials of different flat sheet membrane material 165
8.4. Examples of data from literature - soluble microbial products (SMP), particle sizes - part 1 170
8.5. Examples of data from literature - soluble microbial products (SMP), particle sizes - part 2 171

9.1. Summary of determined membrane material characterisation parameters 181
9.2. Amount of extracted potential foulants from membrane material challenged with MBR biomass 185
9.3. Comparison of extracted foulants from PVDF 0.08μm flat sheet membrane material - short-term vs. long-term fouling 190

A.1. Summary of biomass parameters during DFCm - SADm trial 225
A.2. Summary of biomass parameters during DFCm - Constant aeration trial 228

B.1. Ratio of soluble microbial products determined in influent samples and supernatant of the aeration tank throughout the study 244

Abbreviations & Notation

Latin Abbreviations & Symbols

A_m	membrane area	m^2
A_x	Observed attachment of compound x	%
Carbs	carbohydrates	$mg.L^{-1}$; $mg.g^{-1}$.VSS
CFV	cross-flow velocity	$m.s^{-1}$
DFCm	Delft Fitration Characterisation method	
DO	dissolved oxygen	$mg.L^{-1}$
DOC	dissolved organic carbon	$mg.L^{-1}$; $mg.g^{-1}$.VSS
dP/dt	fouling slope	$mbar.min^{-1}$
dR/dt	fouling velocity	$m^{-1}.s^{-1}$
dR_{20}	slope of resistance increase	10^{12} m^{-1}
EPS	extracellular microbial product	
FS	flat sheet	
HF	hollow fibre	
HRT	hydraulic retention time	h
J	permeate flow, flux	$l.m^{-2}.h^{-1}$; LMH
J_{20}	flux normalised to 20°C	$l.m^{-2}.h^{-1}$; LMH
J_c	critical flux	$l.m^{-2}.h^{-1}$,
J_{cw}	critical flux in its weak form,	$l.m^{-2}.h^{-1}$; LMH
K	permeability	$(l.m^{-2}.h^{-1}).bar^{-1}$; $LMH.bar^{-1}$
K_{20}	flux normalised to 20°C	$(l.m^{-2}.h^{-1}).bar^{-1}$; $LMH.bar^{-1}$
K_{LMH30}	permeability at flux of LMH30	$(l.m^{-2}.h^{-1}).bar^{-1}$; $LMH.bar^{-1}$
LMH	flux of membrane	$l.m^2.h^{-1}$
m	mass (load)	$g.s^{-1}$
MF	microfiltration	
MLSS	mixed liquor suspended solids	$g.L^{-1}$ or %
MT	mutlti-tubular	

MWCO	molecular weight cut off	kDa
PAN	Polyacrylonitrile	
PE	Polyethylen	
PES	Polyethersulfone	
PP	Polypropylene	
Prots	proteins	$mg.L^{-1}$; $mg.g^{-1}$.VSS
PS	Polysulfone	
PVDF	Polyvinylidene difluoride	
R	resistance	10^{12} m^{-1}
R_A	surface roughness (average)	nm
R_m	intrinsic membrane resistance	10^{12} m^{-1}
R_{20}	resistance normalised to R20	10^{12} m^{-1}
R_b	biomass resistance	10^{12} m^{-1}
R_{cl}	cake layer resistance	10^{12} m^{-1}
R_f	foulant resistance	10^{12} m^{-1}
R_{irrev}	irreversible resistance	10^{12} m^{-1}
R_{rev}	reversible resistance	10^{12} m^{-1}
R_t	total resistance	10^{12} m^{-1}
RMS	surface roughness (root-mean-square)	nm
RO	reverse osmosis	
SAD_m	specific aeration demand per membrane area	$Nm^3m^{-2}h^{-1}$
SAD_p	specific aeration demand per permeate	$Nm^3m^{-3}h^{-1}$
SMP	soluble microbial product	$mg.L^{-1}$; $mg.g^{-1}$.VSS
SRT	solid retention time	d
S_x	observed retention of compound x	%
TMP	trans-membrane pressure	mbar
TSS	total solids	$g.L^{-1}$
UF	ultra-filtration	
V	volume	m^3
VSS	volatile suspended solids	$g.L^{-1}$ *or* %
VTS	volatile totals solids	$g.L^{-1}$ *or* %
W_{sl}	work of adhesion	$mJ.m^2$

Greek Symbols

$\Delta G_{iwi}{}^{*}$	Gibbs free energy	$mJ.m^2$
dP/dt	fouling slope	$mbar.min^{-1}$
dR/dt	fouling velocity	$m^{-1}.s^{-1}$
dR_{20}	slope of resistance increase	10^{12} m^{-1}
γ_S^{LW}	Liftshitz-van der Waals surface free energy	$mJ.m^2$
γ_S^{+}	electron-accepting surface free energy	$mJ.m^2$
γ_S^{-}	electron-donating surface free energy	$mJ.m^2$
γ_S^{AB}	acid-base surface free energy	$mJ.m^2$
γ_S	surface tension (solid)	$mJ.m^2$
γ_{SL}	interfacial surface tension	$mJ.m^2$

1. Introduction

Membrane applications have been in intensive use throughout the last decade in applications mainly relating to biotechnology and food processing industries. The first commercial introduction of membranes to wastewater applications was initiated by Dorr-Olivier in the late 1960's with their so-called Membrane Sewage Treatment (MTS) system, consisting of a biological treatment step and an external ultrafiltration module (Bemberis *et al.*, 1971).

The development of membrane biological reactors experienced its first big boost in the 1980's in Japan, initiated by the "Aqua Renaissance Program '90" in order to develop an innovative wastewater treatment concept with a small footprint and high effluent quality suitable for water re-use (Kimura, 1991). Since then, MBRs gained more and more acceptance in international markets for being the choice of technology for conventional wastewater treatment plants (Judd, 2006), with an average annual growth rate for the global MBR market of 10.9% and an expected approach of US$363 million in 2010 (Atkinson, 2006).

The main advantages of MBRs to conventional activated sludge plants are:

- *Enormous amelioration of effluent water quality:* MBR effluents were found to meet the requirements of the EU Bathing Water Directive (EC/160/75) (Günder (2001), Melin *et al.* (2006)).
- *Possible water Re-use:* Due to the high effluent quality, effluents are re-usable for e.g. domestic use, process water or irrigation, which leads to reduction in water costs and can be of essential impact in arid and semi-arid regions suffering from water shortages.
- *Lower investment costs:* MBR treatment plants may have less investment costs due to omission of final sedimentation and downsizing of the activated sludge stage (higher bacterial concentration within the activated biomass allows higher productivity of the activated sludge stage)
- *Small footprint:* MBR treatment plants can reduce the required space to 50% of conventional treatment plants. This is especially of advantage where space is a limiting factor, e.g. within an extension or new construction of treatment plants where available building ground is limited or where it might be an advantageous choice of enhancing the capacity of present treatment plants. Furthermore, MBRs play a promising role in decentralised wastewater solutions, e.g. household plants.

- *Avoidance of bulking sludge problems:* Occurrence of bulking and floating sludge problems leading to unacceptable effluent quality of final clarifiers is theoretically not an issue affecting effluent quality of MBR systems.

Furthermore, there are configurational advantages, such as independent control of solid retention time (SRT) and hydraulic retention time (HRT) , which results in the potential to grow slow-growing bacteria such as nitrifying and methanogen bacteria, and is hence providing a higher flexibility of operation. The possibility of running MBRs at very high sludge age and with almost unlimited MLSS concentrations also enables to adapt the biomass to wastewater usually difficult to treat; such as, for example, leachate wastewater (Lyko *et al.*, 2005).

However, *fouling* is an inherent phenomenon of any membrane process, which leads to lower efficiencies of the overall process. In order to overcome permeability losses due to fouling, overall maintenance regimes, such as frequent air flushing/scouring, backwashing and chemical cleaning, have to be applied to remove the foulants. These strategies in turn increase the overall energy demands and maintenance costs of the membrane system. As such, finding suitable strategies to reduce fouling and hence increase the module performance has been a challenge for all membrane processes, including MBRs.

Fouling factors within MBR filtration processes are part of a highly complex interaction of membrane configuration (material properties, permeate flow and flux concept, module configuration), hydrodynamic conditions (submerged, side-stream, aeration with air scouring, cross-flow velocity) and process control & biomass make-up (MLSS concentration, SRT, HRT, organic shock loading).

The major aspects for the selection of membranes in terms of fouling prevention are material properties, such as pore size distribution, hydrophilicity and surface charge; while configurational choices such as hydrodynamical conditions (flow concept, aeration, relaxation) and applied flux concepts (applied trans-membrane pressure (TMP)) may be adjusted to reduce short- and long-term fouling behaviour (Le-Clech *et al.* (2006); Zhang *et al.* (2006), Figure 1.1).

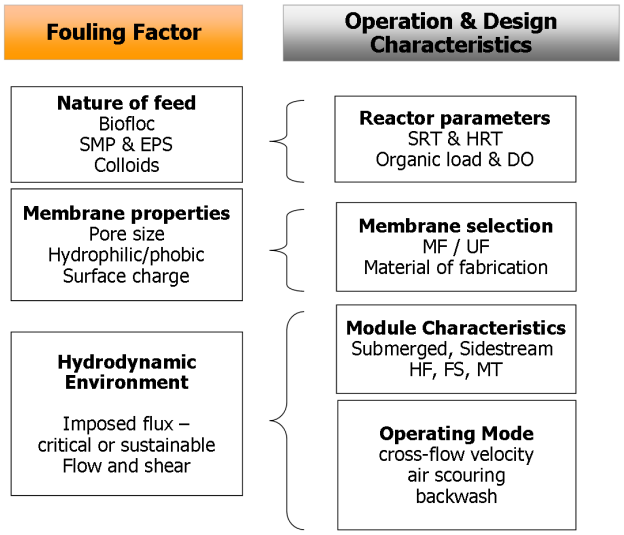

Figure 1.1.: MBR fouling roadmap - fouling factors and operational design parameters - modified according to Zhang *et al.* (2006)

The preferred pore size for MBRs is usually within the range of Microfiltration and Ultrafiltration, and recently also within Nanofiltration (Judd, 2006; Rosenberger, 2003). As with any filtration process, pore size or more likely pore size distribution and bulk solution characteristics strongly relate to membrane fouling. However, due to the complex nature of feed characteristics within MBR systems, opposing trends have been reported within literature depending on the pore size and the type of biomass (Judd, 2006; Le-Clech *et al.*, 2006; Rosenberger, 2003; Zhang *et al.*, 2006). Further studied membrane material properties are surface characteristics, such as hydrophobicity, streaming potential and surface roughness.

Despite the influence of membrane material and membrane module configuration, various predominant suspected fouling factors originating from feed and biomass characteristics are, obviously influenced by the complexity of the system, very often antithetically discussed in literature (Judd, 2006; Le-Clech *et al.*, 2006; Rosenberger, 2003; Zhang *et al.*, 2006).

Amongst the discussed parameters for *feed & biomass characteristics and process controll* are:

- Mixed liquor concentration (MLSS) (Defrance *et al.*, 2000; Le-Clech *et al.*, 2003b; Lee *et al.*, 2001; Rosenberger, 2003; Rosenberger *et al.*, 2005)
- Particle or floc size (Wisniewski and Grasmick, 1998)
- Soluble microbial products (SMP) and Extracellular polymer products (EPS), as mainly Proteins, Polysaccharides and Humic Substances (Huang *et al.*, 2000; Ognier *et al.*, 2002; Rosenberger *et al.*, 2005; Rosenberger and Kraume, 2002)

- Colloids (Bouhabila *et al.*, 2001; Defrance *et al.*, 2000)
- Organic loading (He *et al.*, 2005b,a)
- Solid retention time (SRT) (Han *et al.*, 2005; Huang *et al.*, 2001)

The vast amount of opposing results reported in literature appear to be based on the fact that the number of boundary conditions seems to be indefinite, as not only the feed characteristics are important, but also the configurational choice including the type of membrane material and operational parameters. Most data reported in literature is gained through various changes and examination in the operational parameters, but are quite often based on one single configurational set up or on comparison of different configurations with different bioreactors, hence resulting in varying biomass properties.

2. Literature Review

2.1. Membrane Separation Process

Membranes are applied in water and wastewater treatment as a physical separation process (liquid permeation). The separation range varies from macro particle, e.g. mixed liquor suspended solids to low molecular species, e.g. salts and micro pollutants, according to the type of filter pore size selected (Figure 2.1).

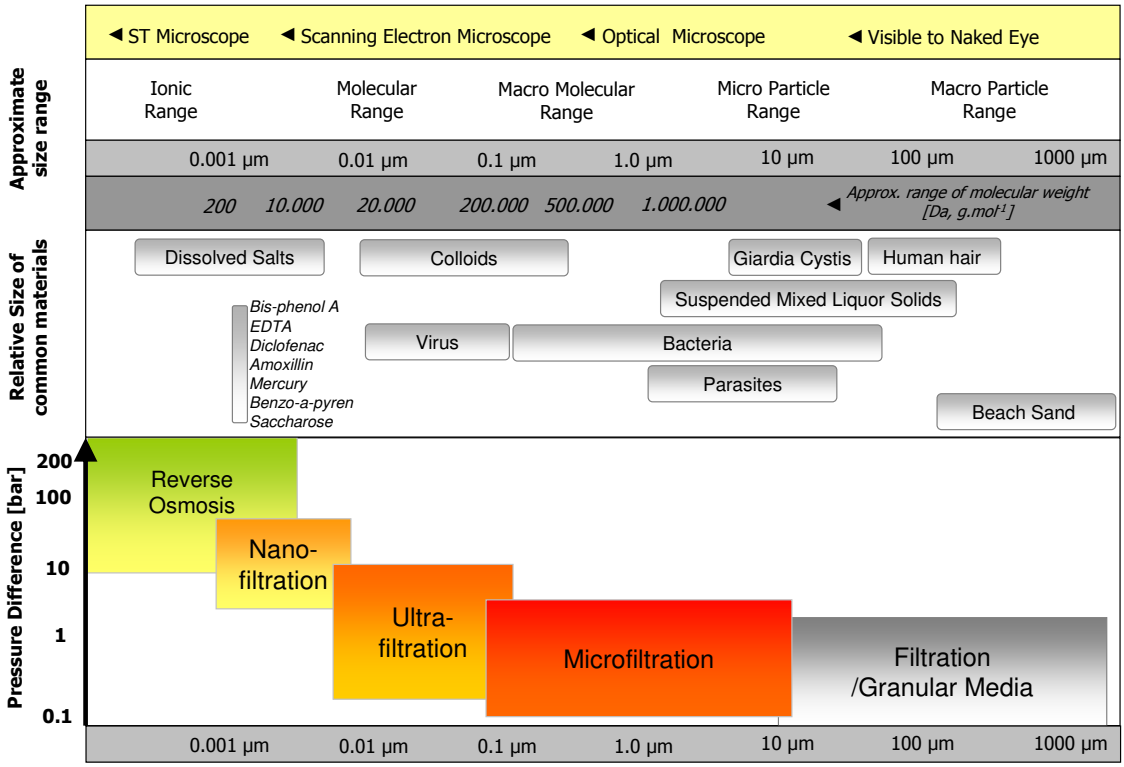

Figure 2.1.: Filtration spectrum of pressure driven membrane technologies (adapted from Melin and Rautenbach, 2004; Pinnekamp and Friedrich, 2006; Peeters and Theodoulou, n.d.)

The separation process for membrane filtration is based either on size exclusion or solution-diffusion transport processes depending on the type of membrane application. Though the membranes are strictly categorized into

- porous membranes and
- diffusion (dense) membranes

to distinguish between the two types of transport processes, it has to be born in mind that both types of processes may coexist during real membrane filtration (Pinnekamp and Friedrich, 2006).

For any liquid permeation process, the membrane functions as a filter separating the permeate from the feed with the trans-membrane pressure difference being the driving force of the process. The effective force is derived from either positive pressure on the feed side or negative pressure at the permeate side. Depending on the type of filtration process, the trans-membrane pressure (TMP) may vary from 0.1 bar to 70 bar, and for some applications like reverse osmosis TMP may even reach 200 bar (Figure 2.1; Pinnekamp and Friedrich, 2006; Melin and Rautenbach, 2004).

The pressure difference describing the trans-membrane pressure is thus generally defined by the pressure on the feed side of the membrane minus the pressure on the permeate side: $TMP = p_{feed} - p_{permeate}$ (Günder, 2001). To overcome higher trans-membrane pressure differences, the pressure gradient needs to be increased and hence processes with higher TMP usually also require higher pump energy on either permeate or feed side.

The occurring trans-membrane pressure is hence not only impacted by the pressure head from the feed side and the pressure created on the permeate side, but also by the cake layer resistance (R_{cl}) and resistance of the membrane (R_m) itself (Figure 2.3*(a)*). The accumulation of particles and solutes on the membrane surface is, amongst others, one of the main factors opposing the driving force and thus increasing the overall resistance to the filtration process (Stephenson *et al.*, 2000). Furthermore, foulants attaching onto the surface or entering the membrane pores mainly contribute to an increasing inefficiency of the overall filtration process.

Membrane fouling during biomass filtration is a highly complex process of various interacting parameters, such as (Judd, 2006; Stephenson *et al.*, 2000):

- intrinsic membrane resistance
- trans-membrane pressure
- cross-flow velocity
- permeate flux
- particle size distribution of the bulk phase
- viscosity of the bulk phase
- agglomeration behaviour of the bulk phase
- interacting forces between particles within the bulk phase
- surface interaction between the membrane and particles and solutes of the bulk phase

The majority of membrane fouling processes *per se* can be described as the increase in trans-membrane pressure with either a gel or cake layer formation on the membrane surface (cake formation phenomenon) increasing the resistance of the cake layer or small solute and fine particles enter the membrane pores leading to pore blocking, which in turn would increase the membrane resistance itself (Figure 2.2). While gel layer or cake layer formation is generally considered to be reversible, the pore blocking is mainly irremovable leading to irrecoverable increase of membrane resistance.

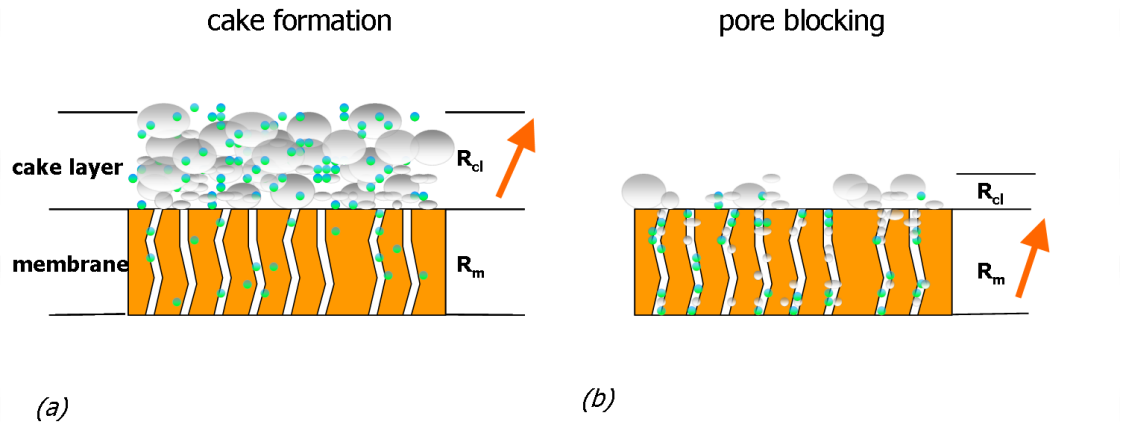

Figure 2.2.: Schematic presentation of (a) cake blocking and (b) pore blocking.

Generally, because of the enormous varying causes and interactions, the definition of the term *fouling* is not consistently used within in literature (Rosenberger, 2003). Commonly, any pressure loss resulting in flux decline is declared as fouling. Processes causing flux decline can involve (Judd, 2006; Melin and Rautenbach, 2004; Ripperger, 1992):

- adsorption of macromolecular and/or colloidal matter on the membrane surface
- adsorption of small particles in membrane pores
- adhesion and growth of microorganism on the membrane surface (biofouling)
- precipitation of solutes on the membrane surface (scaling)
- membrane aging

The term *fouling* can thus furthermore be diverted into (Hilal *et al.*, 2005):

- particulate and colloidal fouling
- inorganic fouling
- organic
- biofouling

One major aspect which also leads to a dramatic decline in permeability and is occurring in membrane filtration especially at high solid content suspension, such as MBRs, is the phenomenon of clogging or sludging of the membrane module's void area/separation area. With MBR set ups being mostly submerged systems, it is consequently difficult to distinguish if a sharp increase in membrane resistance is either derived from biomass fouling or from clogging of the void area of the module.

To predict fluxes derived from steady state membrane filtration processes, several models have been developed to simulate diffusion processes; concentration polarisation effects include Brownian diffusion in laminar and fully turbulent flow processes, and also to describe dynamic pore and cake formation processes (Belfort *et al.*, 1994; Fane, 1986; Hermia, 1982; Romero and Davis, 1990). Models based on Brownian diffusion were found to under predict fluxes of suspensions with particles > 1 μm. To overcome the so-called flux paradox (Green and Belfort, 1980), terms for shear induced diffusion and inertial lift were included (Davis and Sherwood, 1990; Zydney and Coloton, 1986). While models based on the Brownian diffusion theory are applicable for molecular solutions and solutions within sub-micron-particle ranges, the models based on shear induced diffusion were found to be more suitable for suspensions with particles $> 1\mu$m (Nguyen, 2004).

Another type of model found to be suitable within multi-disperse solutions is based on the theory that particle deposition onto the membrane surface is governed by the balance of a combination of drag and lift forces acting on the particle (Figure 2.3). Additional to the hydrodynamic forces of drag and lift, adhesive and friction force are acting on a deposited particle (Altmann and Ripperger, 1997). While cross flow velocity and permeate flow are determining the amplitude of drag and lift forces, and interactions of particles or particle membrane-surface determine the frictions forces, the adhesive forces are being caused by van der Waals forces and also by electrostatic interactions (Altmann and Ripperger, 1997).

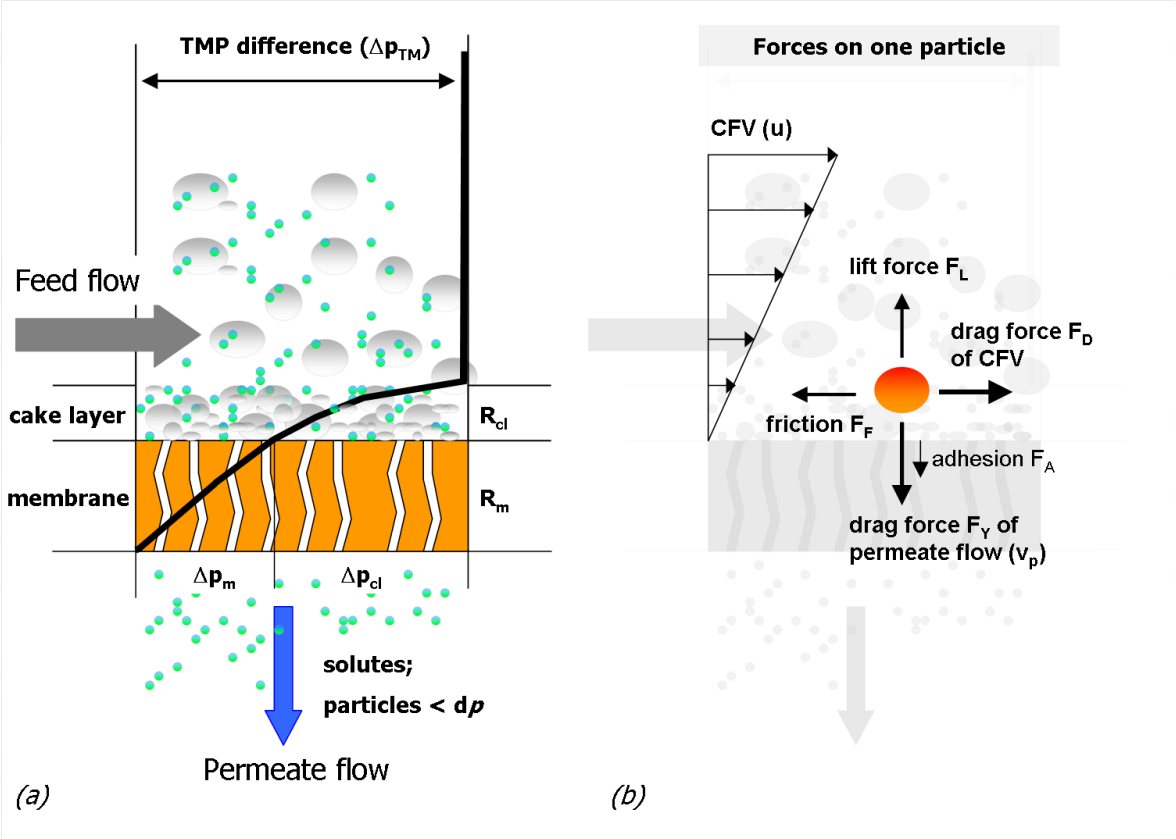

Figure 2.3.: Schematic presentation of *(a)* pressure distribution in membrane and cake layer and *(b)* acting forces on one single particle.

Altmann and Ripperger (1997) showed within their proposed model, that particle deposition onto the membrane surface is mainly governed by the balance of the lift and drag forces of the permeate flow, with smaller particles being more likely to accumulate on the membrane surface at higher permeate fluxes. In cases that adhesion and friction forces are higher than the hydrodynamic forces, the particle deposition is likely to become irreversible, which is most likely for small particles, as only in smaller particle range are adhesive and friction forces higher than the corresponding hydrodynamic forces (Altmann and Ripperger, 1997).

The dependency of the hydrodynamic forces on particle size is described as follows (Altmann and Ripperger, 1997):

- lift force $F_L \approx d_p^3$
- drag force of cross-flow velocity $F_D \approx d_p^2$
- drag force of permeate flow $F_\gamma \approx d_p$

To illustrate, the example of acting forces on one particle in low concentrated suspension (Figure 2.4) reveals that lift forces exceed drag forces of permeate flow for particles with a diameter > 10 μm (Nguyen, 2004). As a consequence, those particles are not expected to be deposited on the membrane surface, whereas smaller particles will be transported to the membrane surface and are more likely to build up deposition. For lower permeate flows, the force balance will be shifted towards smaller particles, hence leading to the insight that for smaller permeate drag forces only smaller particles will be likely to deposit onto the membrane surface (Altmann and Ripperger, 1997; Nguyen, 2004). Furthermore, it is ascertained that this force balance is responsible for the possibility to increase membrane fluxes by flocculating processes, thus binding the smaller particle fraction of the suspension (Nguyen, 2004) .

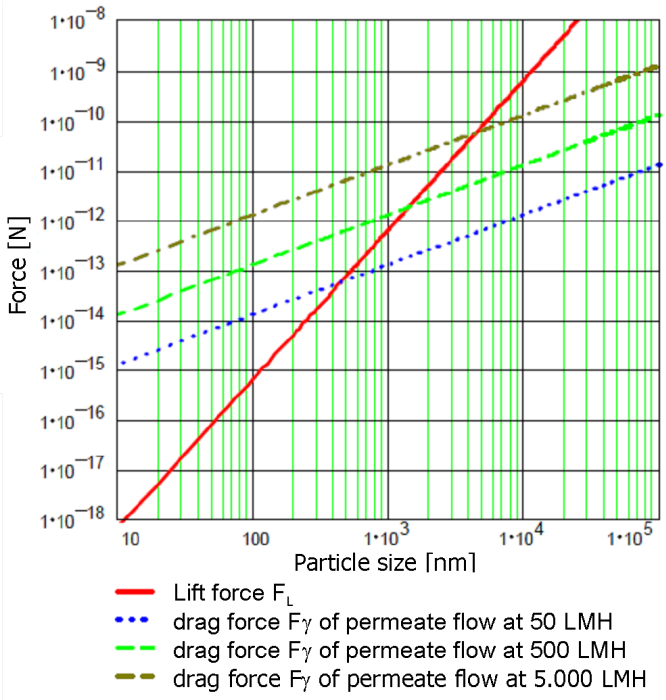

Figure 2.4.: Example of acting drag forces due to permeate flow on particle in suspension (figure taken from Altmann and Ripperger, 1997; Nguyen, 2004; boundary condition given in Nguyen (2004): cross-flow velocity of 1.5 m.s^{-1} and low concentrated suspension).

In the complex matrix of MBR filtration, however, where the fluid dynamics are hard to predict and the high concentrated biomass is most likely to adsorb onto the membrane surface and use the membrane as growth support regardless of any convection flow to the membrane surface (Zhang *et al.*, 2006), defining a comprehensive mechanistic model to successfully describe membrane fouling seems more or less impossible (Drews, 2010). For instance, Howell *et al.* (2004) stated that a model describing a current test series revealed only a limited fit while applying to previous studies leading to the assumption that membrane fouling history will always represent an unpredictable parameter. Such membrane history will also depend on cleaning cycles, cleaning regime and the membrane's material response to these factors.

Fouling determination has been undertaken using varying approaches, one amongst them which is highly reported in literature and frequently used as a short-term test, is the so-called critical flux concept. While having been reported to show limitations to full scale applications with general fouling trends being one order of magnitude smaller, and also providing difficulties when comparing results deriving from different researches due to an arbitrary definition of the concept *per se* (Bacchin *et al.*, 2006), the critical flux concept can be an essential tool for short-term comparisons of biomass filtration, membrane characterisation respectively. The critical flux concept goes back to Field *et al.* (1995) and is generally defined as the flux in which the permeability differs compared to the intrinsic clean water permeability (Figure 2.5).

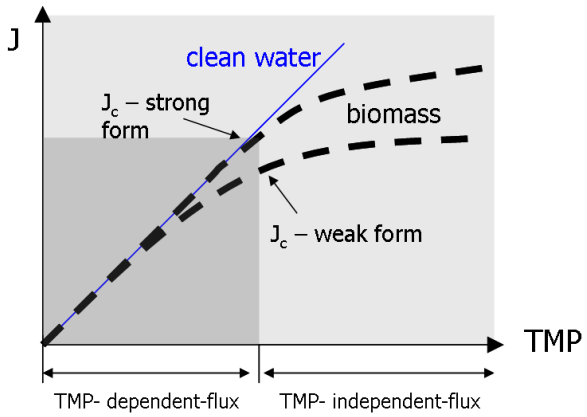

Figure 2.5.: Schematic presentation of the critical flux concept with J_c in its strong and weak form relating to the clean water flux (adapted from Field *et al.*, 1995;).

2.2. Membranes and Membrane Module Classification

Membranes used for MBRs can be divided into their material classification, their module configuration and the MBR configuration itself, whereas MBR configuration is dependent on the flow concept and the feed concept respectively; the restraint of membranes in the MBR reactor, and the type of permeate extraction (Figure 2.6).

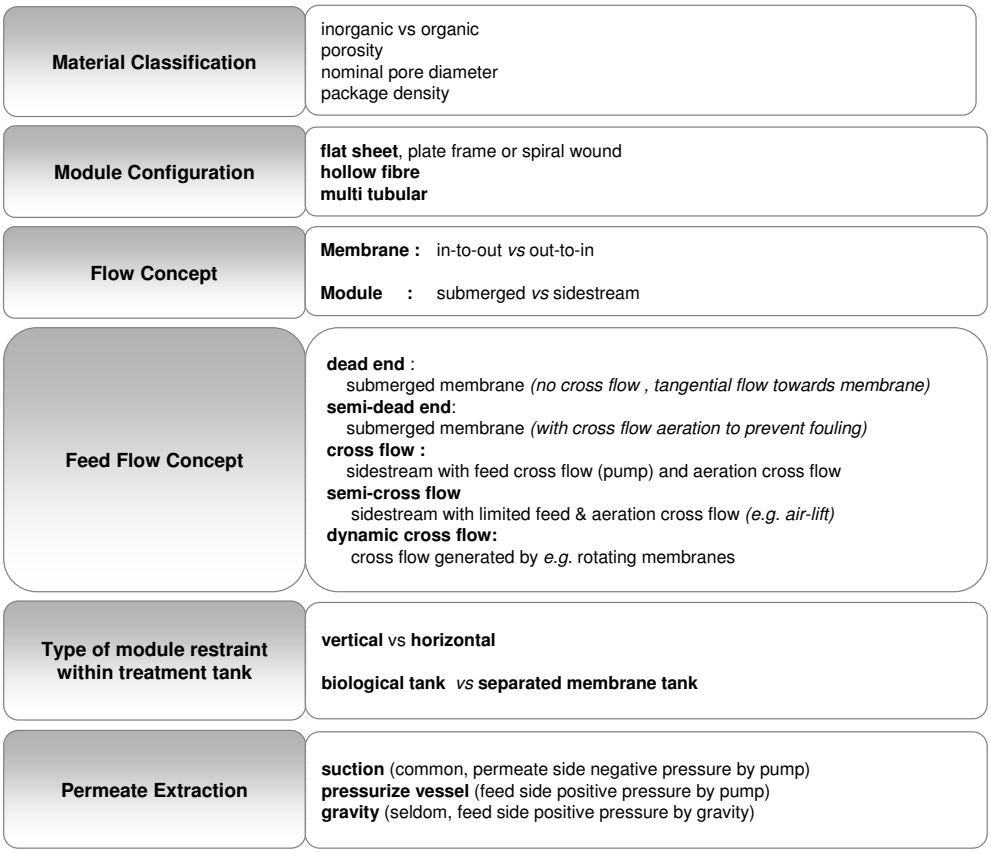

Figure 2.6.: Membrane classification (adapted from Melin and Rautenbach, 2004; Baumgarten, 2007;)

Major specifications for the choice of different configurations are usually the type of wastewater to be treated, the costs (investigations and maintenance), the permeate yield per membrane and the control of fouling or clogging propensity during long term runs (Judd, 2006; Melin and Rautenbach, 2004).

2.2.1. Membrane materials

2.2.1.1. Overview of membrane materials applied within MBR systems

The most important membrane (material) qualities are (Rautenbach and Albrecht, 1989):

- high selectivity
- high permeability
- mechanical stability
- temperature stability
- chemical resistance

Rautenbach and Albrecht (1989) placed high selectivity as first choice, as low permeability can be compensated for to a certain extent by an increase in membrane surface area. Rautenbach and Albrecht (1989) furthermore stated that for general membrane application, low selectivity can lead to multi-stage processes where significant wastewater effluent consent is required, which in most cases is not economical compared with established conventional processes. Within MBR systems, however, permeability plays a major role, as the use of MF and UF membranes usually reaches the consent of the wastewater treatment plant (Günder, 2001; Judd, 2006; Melin *et al.*, 2006) but the major problem to tackle remains to be permeability losses due to fouling. Furthermore, a low-print footage of a wastewater treatment plant is a high cost advantage, which can be the main factor for a particular choice of technology.

Even though clean water permeability is stated as not being the most important parameter of membranes for application in MBRs, it has to be stressed that obtaining a certain process flux is the crucial design parameter for MBR applications (Pearce, 2008). A lower flux will consequently lead to an increase in capital cost, due to effects on membrane area and footprint, and more importantly to a likely increase in maintenance costs due to higher costs for permeate suction, air scouring and cleaning (Judd, 2006; Pearce, 2008). Fluxes for clean water permeability, however, need to be compared to filtration performances during activated sludge filtration as a gel layer formation can reveal a sudden drop of fluxes. For instance, due to gel layer formation resulting from concentration polarisation on the membrane surface, fluxes were reported to decrease within seconds from initially over 600 LMH to typically 60 LMH for ultrafiltration membranes (Baker, 2004).

Besides permeability, a high mechanical stability and a high chemical resistance to cleaning reagents are also crucial parameters for membranes used in MBR systems (Judd, 2006; Melin and Rautenbach, 2004; Pearce, 2008; Pinnekamp and Friedrich, 2006).

The preferred pore size for MBRs is usually within the range of microfiltration and ultrafiltration (Judd, 2006; Rosenberger, 2003). Micro- and ultrafiltration membranes used for

wastewater solid-liquid separation can be produced in various ways and are, with regards to their material, either classified by their structure (symmetrical, asymmetric, dynamically formed porous membranes), by their construction material (inorganic vs. organic) or by their nominal pore size (micro-, ultrafiltration) (Rautenbach and Albrecht, 1989; Figure 2.7).

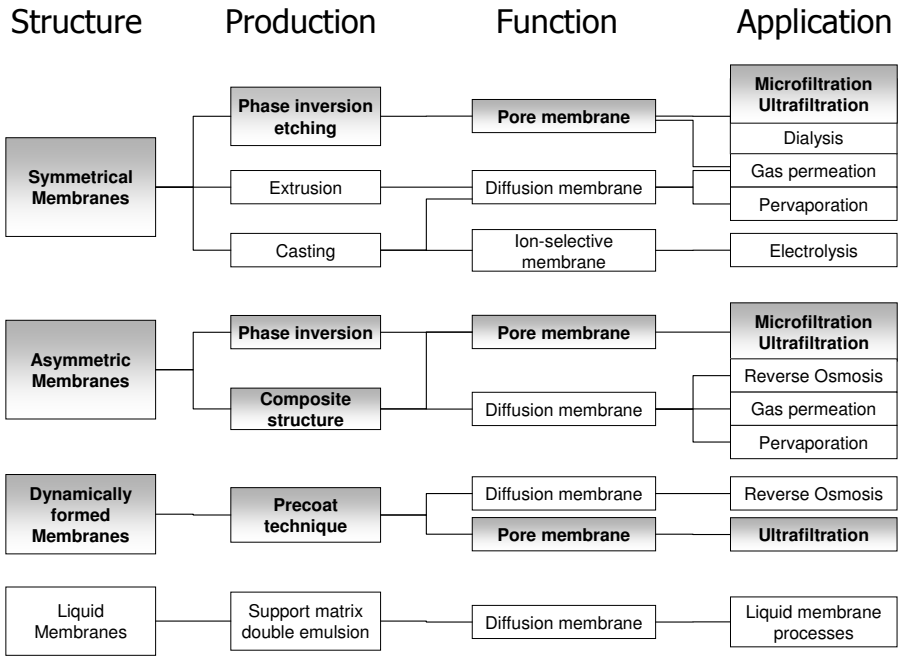

Figure 2.7.: Membrane material classification - Modified according to Rautenbach and Albrecht (1989) with MF/UF/NF applications considered in this study being highlighted

While a symmetrical membrane is of roughly a similar homogeneous construction over its depth, an asymmetrical membrane usually consists of two layers; one active filtration layer and one supportive layer (Baker, 2004; Pinnekamp and Friedrich, 2006; Figure 2.8). With the supportive layer being generally very porous and its only purpose providing mechanical strength to the membrane, the active filtration layer determines the membrane's separation properties and this layer should remain as thin as possible to keep the initial membrane filtration resistance as low as possible (Pinnekamp and Friedrich, 2006; Stephenson *et al.*, 2000). Whilst the top layer and the supportive layer of phase inversion membranes are made of similar material, composite membranes consist of two different types of materials so that both layers can be optimised regarding their required properties (Baker, 2004; Pinnekamp and

Friedrich, 2006).

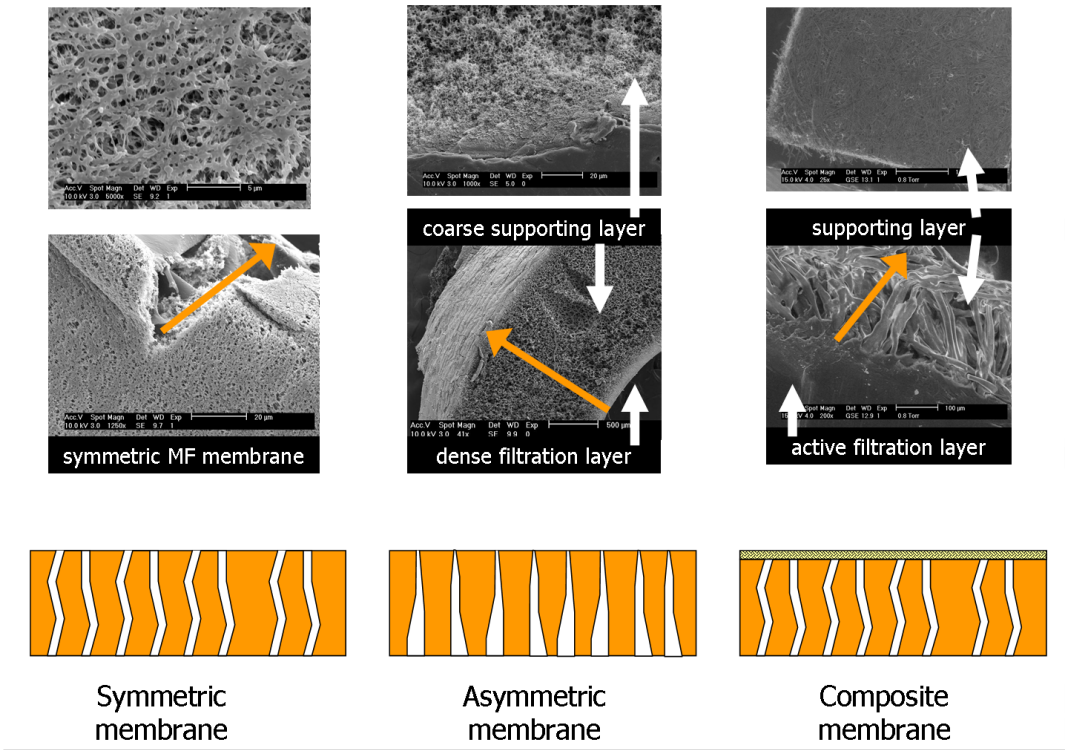

Figure 2.8.: Schematic presentation of various membrane structures according to Günder (2001), illustrating SEM images taken from membrane samples available within this study *(note: orange arrow indicated direction of permeate flow)*

Available types of membranes materials comprise of organic (polymeric) and inorganic (ceramic/metallic) materials with polymeric membranes being used most commonly within MBR technology (Judd, 2006; Mulder, 1997). Ceramic membranes, such as aluminium, zirconium, silicium and titanium oxide composites, show higher hydraulic, thermal and chemical resistance than polymeric materials, but are limited in their geometry and are furthermore significantly more expensive (Mallevialle *et al.*, 1996; Mulder, 1997).

To give a rough estimation, Stephenson *et al.* (2000) disclosed the production costs of simple polymeric membranes as less than 10 GBP per m^2 membrane, while the costs for ceramic ultrafiltration or microfiltration membranes were reported to well exceed 1,000 GBP per m^2 membrane. However, the use of ceramic membranes might be expanding as their higher hydraulic and chemical strength may compensate higher costs due to longer membrane lifetime (Cicek *et al.*, 1999).

Zhang *et al.* (2005) reported the successful application of a stainless steel membrane module with a nominal pore size of 0.2 μm on a bench-scale MBR, whereas usually metallic membrane

filters have very special applications which are not necessarily related to MBR technology (Judd, 2006; Mulder, 1997).

Recent research also concentrates on finding appropriate low rejection membranes based on non-woven fabric (Chang *et al.*, 2001, 2003; Fuchs *et al.*, 2005; Judd, 2006; Meng *et al.*, 2005; Moghaddam *et al.*, 2002; Seo *et al.*, 2002). However, a pilot scale demonstration of an non-woven fabric (NWF) at the Industrial Research Institute (ITRI) in Taiwan showed significant internal fouling with organic material within a few days of operation, leading to a drop in permeability to very low values (Judd, 2006). Nevertheless, it has to be admitted that the replacement costs of such material is very low and ongoing research into these materials for MBR technology may suggest the commercialisation of non-woven materials in the future (Judd, 2006). Furthermore, Zahid and El-Shafai (2011) recently reported the successful application of three different textile materials as filtration media in MBRs. Effluents of all three set ups (Acrylate, Polyester or Nylon on a stainless steel tube as the supporting material) tested over a period of 60 days in MBR were found to meet Saudi Arabian and Egyptian regulatory standards for use in agricultural irrigation. The average trans-membrane pressures were reported to vary between 0.2 to 0.4 bar at fluxes of 14.6 to 15.1 LMH with corresponding HRT of 8.0 to 8.9 hours . Despite the fact that the set up was mentioned to represent a cost-effective alternative to commercially available MBR materials, Zahid and El-Shafai (2011) stated furthermore that during the operating period of 60 days, flux recovery of the textile material could be achieved by mechanical cleaning solely, hence reducing maintenance costs further by the absence of chemicals as cleaning agents.

Polymeric membranes can be manufactured from any polymer in principal, whereas only a limited number of materials meet the requirements for the application of membrane separation. The most common materials used for membranes in MBRs are (Judd, 2006):

- Polysulfone (PS)
- Polyethersulfone (PES)
- Polypropylene (PP)
- Polyethylen (PE)
- Polyvinylidene difluoride (PVDF)
- Polyacrylonitrile (PAN)

Main differences of the commercially used polymeric membrane materials are; their ability to modify their properties in terms of pore size and mechanical strength, the hydrophilicity of the material's surfaces, their chemical resistance and last but not least the overall production costs (Baker, 2004; Judd, 2006; Pearce, 2008). For instance, PVDF membranes show limited ability for modifying pore size properties and are hence mainly made as coarse ultrafiltration

membrane or within the microfiltration range (Pearce, 2008). PVDF membranes have also been shown to reveal excellent strength, flexibility and adequate permeability (Pearce, 2008), but are, on the other hand, known to create high production costs.

PP and PE membranes are two polymeric membranes which can only be produced in microfiltration range, but are inexpensive in production and reveal reasonable strength, a general hydrophilic surface and the susceptibility to oxidation can be improved by surface modification (Baker, 2004; Pearce, 2008).

PS and PES membranes on the other hand, can be produced in a broad range of pore sizes with a narrow pore size distribution and the surface properties can be modified through polymer blend. As both types of material are produced in large quantities, production costs are cheaper compared to PP, PE or PVDF (Mulder, 1997). However, due to the very good performance of PVDF membranes and the resulting higher membrane lifetime, several companies offer membrane modules made of PVDF and consequently this polymer is currently dominating the MBR market (Pearce, 2008).

A very recent market survey revealed that $\approx 20\%$ of the listed iMBR materials are made of PES/PS material, whereas over 55 % of the membrane materials for the total iMBR market are made of PVDF (Santos and Judd, 2010). Amongst the 25% of remaining products, materials such as PAN (polyacrylnitril) and PVA (polyvinyl alcohol) were reported to be used.

2.2.1.2. Impact of membrane material properties on filtration performance in MBRs

Despite the important role of configuration and hydrodynamic changes on the maintenance of high fluxes (see section 2.2.2, page 21), an adequate membrane morphology is expected to contribute significantly to the overall process optimisation. Zhang *et al.* (2006) proposed that within their *road map of fouling*, membrane material properties such as pore size distribution, hydrophilicity, surface roughness and surface charge, were major aspects for the selection of membranes in terms of *fouling prevention* (Figure 1.1, page 3).

As with any filtration process, *pore size* or more likely *pore size distribution* and bulk solution characteristics strongly relate with regards to membrane fouling (Le-Clech *et al.*, 2006; Pinnekamp and Friedrich, 2006). However, likely due to the complex nature of feed characteristics within MBR systems, opposing trends have been reported within literature depending on the pore size and the type of biomass (Judd, 2006; Le-Clech *et al.*, 2006; Rosenberger, 2003). This can partly also be attributed to the wide variety of materials studied (pore size distribution, material, hydrophilicity), the complex and wide differences of bulk characteristics and last but not least the conditions of hydraulic performances and the type and duration of tests applied.

While generally a higher porosity is beneficial for higher fluxes, the interrelation of membrane fouling to pore size is stronlgy dependent on the characterisation of the feed solution. Le-Clech *et al.* (2003b) compared submerged MT modules with different pore sizes (200 kda, 0.1 μm, 1 μm) and different lumen diameter under varying MLSS concentrations (4, 8 and 12 g.L^{-1}) and varying aeration rates. During the conducted critical flux trials, no effect of pore size on J_c was observed other than at lowest pore size (200kDa) and low MLSS values.

Hughes and Field (2006) compared the resistance to filtration of microfiltration PS membranes (0.1 μm, 0.2 μm, cone-and-plate test cell, 44.12 cm^2) under washed, unwashed yeast and yeast extracted EPS solution at low concentration (0.97 g.L^{-1}, 0.73 g.L^{-1}, 0.14 g.L^{-1}) and observed a similar fouling rate for the unwashed yeast (0.2 mbar.min^{-1}), a small increased fouling rate for the 0.2 μm membrane for the unwashed yeast (0.51 mbar.min^{-1} to 0.48 mbar.min^{-1}), but a significantly higher fouling rate of the EPS solution on the 0.2 μm membrane (0.2 mbar.min^{-1} to 0.08 mbar.min^{-1}). Furthermore, Hughes and Field (2006) observed that a regime of cleaning and filtration repetition cycles would affect most the 100kDa tested nanofiltration membrane where an average increase of 19% in intrinsic membrane resistance (R_m) was measured after each experiment and cleaninig cycle, whereas the same experiments exhibited on microfiltration membranes (0.1 μm, 0.2 μm, same manufacturer, same material) did reveal an increase of R_m after each cycle from 0.4% to 2.5%.

Mueller and Davis (1996) studied effects of varying membrane morphologies with the same nominal pore size of 0.2 μm on protein fouling and concluded that the tested PC and CE membranes with higher surface porosity yielded in higher permeability, but also revealed extensive internal fouling prior to external fouling took place. The tested PVDF and PS membranes

on the other hand, showed lower porosity with few pores which led to lower permeability and quick external pore blocking by proteins. Furthermore, modified microfiltration membranes with hydrophilic-coated membrane surfaces were found to exhibit lower fluxes, but similar fouling patterns to unmodified membranes (Mueller and Davis, 1996).

Jin *et al.* (2009) compared different pore-sized ceramic flat sheet membranes (80, 100, 200 and 300nm) in submerged mode with MLSS ranging around 5 $g.L^{-1}$, where no influence of EPS could be found and the rejection rate was observed to be higher, the smaller the pore size. In overall, Jin *et al.* (2009) concluded that the membrane with the biggest pore size exhibited the highest fouling potential, while fouling potential was observed to be the least for the membrane with the smallest pore size.

Another crucial aspect during membrane filtration comparison is the length of the investigation period. For instance, He *et al.* (2005a) compared five different PES ultrafiltration membranes with pore size ranging from 20 kDa to 700 kDa for their suitable application in anaerobic wastewater filtration. While during the initial start-up, the flux decline of the smaller pore size membrane was reported to be most significantly due to concentration polarization. This changed over long-term filtration with the 700 kDa membrane having been reported to exhibit pore clogging. The authors attributed this to the higher membrane surface roughness and stated furthermore that the flux decline of the high MWCO membrane was difficult to recover.

In addition, not only does the pore size determine the membrane fouling tendency, but also material related characterizations, such as membrane material and its hydrophilicity. For instance, Kimura *et al.* (2006) investigated fouling of different NOM fractions on different membrane materials (PAN 80kDa, PAN 100kDa, PVDF 0.1 μm, PE 0.1 μm). Between the two MF membranes tested, the PVDF 0.1 μm exhibited a higher fouling rate for irreversible fouling than the PE 0.1 μm. No significant irreversible fouling was observed for the two ultrafiltration membrane materials. Alkaline extraction revealed that hydrophilic fraction was responsible for the irreversible fouling which the authors mentioned was in occurrence in one of their previous studies (Kimura *et al.*, 2004). Opposite trends to the observations made by Kimura *et al.* (2006), were reported by Yamato *et al.* (2006) while analysing different fouling behaviour between two different types of membrane material modules (PE and PVDF) with the same pore size (0.4 μm). In this study, the PE membrane was found to foul more rapidly than the PVDF membrane module and fouling was dominated by irreversible foulants. The PVDF membrane on the other hand, was reported to be fouled mainly due to increased carbohydrate concentration within the mixed liquor, which was consequently reversible. Attached foulants desorbed from the membrane surface could not be related to the extent of fouling observed during filtration performance.

Several research studies were conducted on *surface modification* of membrane to enhance the surface hydrophilicity and hence to reduce the fouling propensity. Polymeric membranes, such as polyethylene (PE), polypropylene (PP), poly-vinildylene fluoride (PVDF), and polysul-

phone (PS), naturally being more hydrophobic can be blended with hydrophilic polymers or surface treated to make them hydrophilic (Gander *et al.*, 2000). For instance, several studies have shown that hydrophobicity in UF and MG play an important role in fouling in terms that hydrophilic membrane tend to suffer less from flux decline than hydrophobic ones (Fane *et al.*, 1991; Futamura *et al.*, 1994; Gekas and Hallström, 1990; Persson *et al.*, 1993).

Surface coating with polyelectrolytes was shown to slightly increase hydrophilicty of naturally hydrophobic PES membranes (Kochan *et al.*, 2009). However, the applied surface coating was also shown to increase membrane rejection significantly and consequently decrease the permeability of the coated membranes. Surface plasma-treatment was also shown to be a suitable surface modification method, however long-term experiments did reveal a higher permeability decline of the modified membrane than the unmodified one (Tyszler *et al.*, 2006).

Nevertheless, Buetehorn *et al.* (2009) reported in a summary of different research tasks the successful application of analytical tools for membrane surface characterization to identify surface modification of membranes and consequently elucidating optimised residence time for chemical post-treatment during membrane manufacture. The membrane optimisation was furthermore reported to have been successfully verified during 15 months of pilot testing for wastewater treatment.

A significant increase in permeability was also reported to occur after wetting PES hollow fibre and PS flat sheet membrane materials with isopropyl alcohol and ethanol respectively (Kochan *et al.*, 2009). However, while the higher permeability lasted partially for clean water trials, filtration performance with supernatant of activated sludge did not show any enhancement.

Roudman and DiGiano (2000) reported also an increase in permeability after membrane surface treatment, where the membrane was reported to have become more hydrophilic after treatment and subsequent ultra pure water permeation, but after permeation of NOM containing water surface energy was found to have approached the same surface energy as the untreated membrane, indicating NOM adsorption.

A protein (BSA) fouling study conducted by Marchese *et al.* (2003) on surface modified PES membranes with PVP (polyvinyl-pyrrolidone) to increase permeability while remaining selective revealed that due to its hydrophobicity PVP acts as a prevention to BSA pore blockage to some extent.

2.2.2. Membrane Modules and Configuration

The term *configuration* can be used for either the module configuration or how the module is integrated within the bioreactor, hence representing the process configuration of the overall treatment process. Membrane module configurations applied in wastewater treatment are

- Plate-and Frame/ Flat Sheet (FS)
- Hollow Fibre (HF)
- Multi-Tubular (MT)

The technical requirements for optimised module configuration are derived from the purpose of the membrane module itself. In general, and also for filtration in MBRs, typical requirements include (Judd, 2006; Melin and Rautenbach, 2004; Stephenson *et al.*, 2000):

- even cross-flow along the membrane surface
- low pressure loss, hence low permeability loss (low fouling/scaling propensity)
- high packing density
- low production costs
- low cleaning demands and possibility for efficient low cost cleaning
- low replacement costs
- low clogging propensity

The **flat sheet** membrane is generally mounted onto a support plate with drainage and arranged in parallel within cascade modules. Flat sheet panels are generally low in packing density, but can compensate with higher permeability values (table 2.1). The main disadvantage of this type of module is the lack of backwash as fouling control. However, as the usual flat sheet membrane modules are restricted to relaxation periods during filtration only (as applying backwash would detach the materials from their supporting panel), the new generation of (mainly ceramic) flat sheet materials comprise this disadvantage and show resistance to backwash pressures of up to 1000 mbar (Agfa-Gevaert NV, 2010; Grelot *et al.*, 2007; ItN Nanovation AG, 2010).

Hollow fibre modules are usually are self-supporting membrane tubes with an internal diameter (ID) of 0.5 to 5.5 mm. Some modules, so called capillary tubes, use fine fibres with an ID of less than 0.5 mm. The thin membrane tubes are usually pressure proof with moderately applicable backwash flows. One major advantage of this is the high packing density, however it also allows susceptibility to module clogging/sludging.

Multi-tubular modules modules are usually side-stream operated modules, but are very rarely used submerged. Generally tubular modules are not pressure proof and hence require an

additional supporting tube. The permeate flow is opposed to that of HF and FS in wastewater application, from in-to-out, which consequently also leads to susceptibility of lumen clogging. However, due to the very good controllable hydrodynamics within the tubes, sludging problems can generally be avoided.

Some of the desirable module characteristics conflict one another, and as such a compromise has to be made according to the priority of needs. For example, self-supporting materials have to be used for HF or MT, which consequently results in higher initial membrane resistances and hence lower permeability rate per square-meter of membrane in comparison to flat sheet membrane material where the thin membrane material is mounted on an additional frame support. On the other hand, these lower permeability rates can be easily compensated with higher package density per module, hence increasing the membrane area per module and furthermore leading to usually smaller footprints for HF submerged membrane concepts than for flat sheet. To illustrate, data from full scale modules commercially available for MBR application was taken from Judd (2006) and permeability rates for clean water was plotted against the packing density of the membrane module (Figure 2.9). Notably, the PAN flat sheet material indicated with a nominal pore size of only 40kDa revealed clean water permeability as high as the microporous PE 0.4 μm membrane. Furthermore, Kimura *et al.* (2004) observed a very good filtration performance of PAN material compared to others, regardless of the very low nominal pore size of the membrane surface.

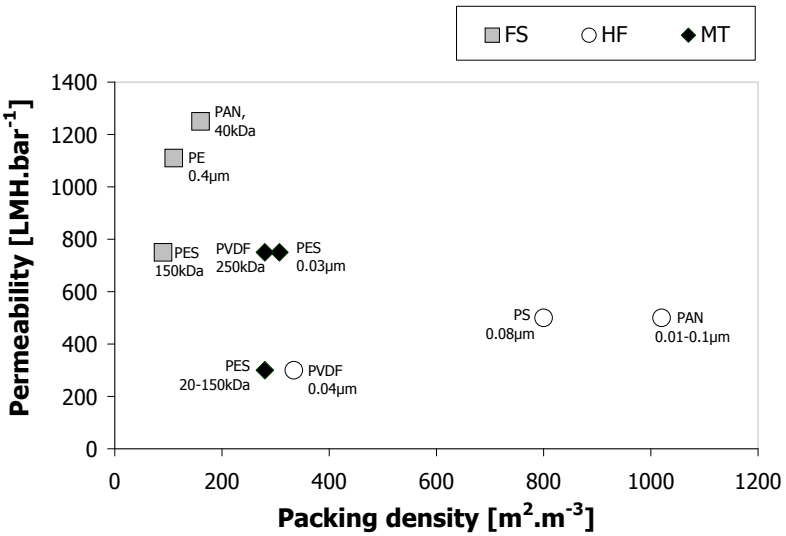

Figure 2.9.: Comparison of permeability and packing density of different commercially available modules for MBR application (data taken from Judd, 2006)

Table 2.1.: Properties, advantages and disadvantages of different membrane configurations used in wastewater treatment processes (adapted from Judd, 2006; Pinnekamp and Friedrich, 2006; Stephenson *et al.*, 2000)

Membrane Module	**Multi-Tubular**	**Hollow Fibre**	**Flat Sheet**
Permeate flow concept	in-to-out	out-to-in in-to-out	out-to-in
Flow concept	cross-flow semi-cross-flow	(semi-)dead-end semi-cross-flow	(semi-)dead-end semi-cross-flow
Feed flow concept	sidestream (very rarely submerged)	submerged (very rarely sidestream)	submerged
inner diameter; separation* [mm]	5.5 - 25mm	0.25 - 5.5 mm 0.04-0.25 mm	4* to 8*
Packing density [$m^2.m^{-3}$]	<80-300	<1.000 <10.001	<100-200
typical intrinsic permeability [$LMH.bar^{-1}$]	200 - 1000	200 - 800	500 - 2000
typical net flux [LMH]	20 - 100	20 - 30	15 - 25
Recommended MLSS [$g.L^{-1}$]	15 - 30	10 - 15	10 - 15
Energy consumption (membrane only) [$kWh.m^3$]	2 - 10	0.3 - 0.6	0.3 - 0.6
Advantages	• low pressure loss • high cross-flow velocities possible • low risk to plugging/clogging at high cross-flow velocities • backflush at high fluxes	• high packing density • low specific production costs • backflush at moderate fluxes	• low risk to clogging • possibility of single membrane replacement
Disadvantages	• low packing density	• low to moderate resistance to pressure • susceptible to module/fibre clogging • in-to-flow: suceptible to plugging	• low packing density • for most configuration no backflush possible

High packing density generally comes with higher sludging propensity. This problem can be overcome by applying optimum operational conditions. Some suppliers also innovate their products to overcome disadvantages derived from the type of configuration, and new membrane market penetration is likely to shift the former necessary compromises. For instance, hollow fibre membrane modules derived from Kochmembrane systems (Puron) are less prone to fibre sludging as the hollow fibres are mounted on one side only (the permeate withdrawal), while the other end is floating free.

Furthermore, ceramic membranes, known for their strength and lifetime but also for their formerly high production costs, are currently entering the MBR market at reasonable prices and with package plant designs ready to serve small communities (ItN Nanovation AG, 2010). Flat sheet membranes made of PUR/PVC are reported to withstand backwash pressures of up to 1000 mbar (Agfa-Gevaert NV).

2.2.3. Membrane Technology in Wastewater Treatment

Two main MBR process configurations exist; immersed (submerged MBR, iMBR) or side-stream (sMBR) (Judd, 2006). While side-stream MBR systems are frequently used within industrial applications and actually go back to the first stages of MBRs (Smith *et al.*, 1969; Sutton, 1997), nowadays submerged or immersed MBR systems are preferably used for communal wastewater treatment plants.

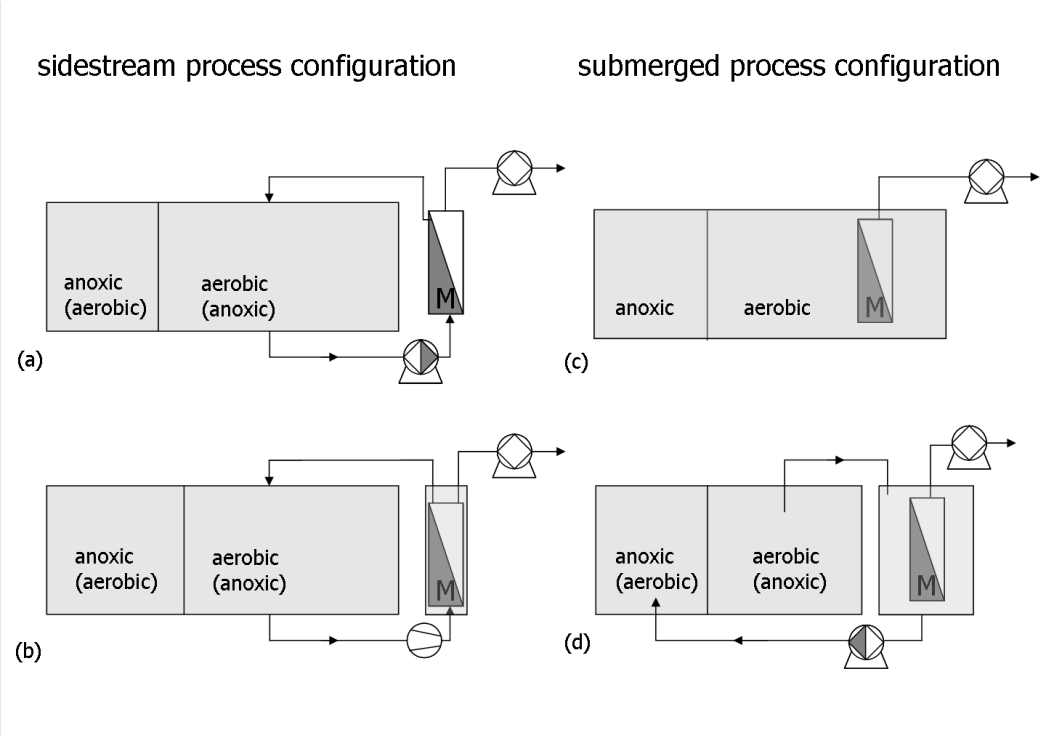

Figure 2.10.: Schematic overview of MBR process configuration: *(a)* side-stream, *(b)* air-lift side-stream, *(c)* submerged (iMBR) with membrane integrated into aeration tank, *(d)* submerged (iMBR) with separated membrane tank

The submerged process itself can be diverted into MBR plants having the membrane submerged into the aeration tank or into a separated biomass tank. While the side-stream MBR usually only refers to the classical side-stream concept, nowadays it is getting more and more common to apply so called air-lift systems, meaning the membrane is placed as a quasi sidestream configuration outside the bioreactor, while the biomass is mainly passed by using aeration only. This air-lift concept is mainly applied on multi-tubular membranes and also hollow fibre membranes, where the membrane module is placed within an extra membrane holding vessel. However, apart from a few drinking water plants, the HF side-stream concept has not been frequently used.

Furthermore, there are submerged systems (e.g. some *Kubota* full scale plants) which are using gravity for permeate extraction. This is without doubt playing a major role in the overall costs as it is saving installation costs and moreover maintenance costs of pumps (such as electricity), but might also place limitations in reactions to higher hydraulic loads, especially when the membranes permeability have declined significantly. Huber and Martin Systems provide flat sheet membrane panels with additional shear to control fouling created by rotating the membrane panels/disc respectively. While this technique provides a significant advantage

in fouling control, additional energy consumption has to be considered. A summary of most of the currently available membrane module configurations is provided in table 2.2 (Santos and Judd, 2010).

The general advantage of placing membranes into separated membrane compartments are: *(a)* better control of MLSS content with the biomass, *(b)* avoiding changes in feed hitting the membranes directly, and *(c)* disconnecting the membrane compartment from the biomass for maintenance, e.g. intensive cleaning or membrane replacement. The disadvantages are usually: *(a)* higher foot-print of the plant and *(b)* higher maintenance due to additional pumps.

Table 2.2.: Available Membrane Modules - from Santos and Judd (2010)

Immersed (iMBR)		Sidestream (sMBR)
Flat sheet	*Hollow fibre*	*Multitube/multichannel*
A3–*MaxFlow*[DE]	Asahi Kasei–*Microza*®[JP]	Berghof–*HyPerm-AE; HyPerflux*[DE]
Alfa Laval[SE]	Beijing Origin Water Technology Co.[CN]	Norit X-Flow–*Norit Airlift*[TMNL]
Brightwater–*Membright*®[IRL]	*Ecologix–EcoFlon*[TM], *EcoFil*[CN]	Orelis Environment–*Kerasep*®[FR]
Colloide–*Sub snake*[NIR]	ENE Co., Ltd.–*SuperMAK*[KR]	MEMOS Membranes Modules Systems GmbH[DE]
Ecologix–*Ecoplate*[TM], *EcoSepro*[CN]	GE Zenon–*ZeeWeed*®[US]	
Huber–*VRM*®; *VUM*®/*GreyUse*[DE]	Hangzhou H-Filtration Membrane Technology Engineering Co., Ltd.–*MR*[CN]	
Jiangsu Lantian Peier Memb. Co. Ltd.[CN]	Koch Membrane Systems–*Puron*®[US]	*Hollow fibre*
KOReD–*Neofil*[KR]	Korean Membrane Systems–*KSMBR*®[KR]	Ultraflo–*Ultraflo*®[SG]
Kubota–ES/EK[JP]	Litree–*LH3*[CN]	Polymem–*Immem*[TMFR]
Microdyn-Nadir–*BioCel*®[DE]	Memstar–SMM[SG]	
Pure Envitech Co., Ltd.–*ENV1S*[KR]	Mitsubishi Rayon–*Sterapore SUR*®; *Sterapore SADF*®[JP]	*Flat disc ceramic*
Shanghai Megavision Memb. Tech.[CN]	Philos[KR]	KERAFOL Keramische Folien GmbH[DE]
Shanghai SINAP Membrane Science & Technology Co., Ltd.[CN]	Porous Fibers S.L.–*Micronet*®[SP]	Grundfos–*Biobooster*[DK]
Toray–*TRM*[JP]	SENUO Filtration Technology Co., Ltd.–*SENUOFIL*[CN]	
Vina Filter–*Vinap*[CN]	Shanghai Dehong Biology Medicine Science & Tech. Development Co., Ltd.[CN]	
Weise–*MicroClear*®[DE]	Siemens Water Tech.–*Memjet*[TM DE]	
	Sumitomo–*PoreFlon*®[JP]	
	Superstring MBR Tech. Corp.–*SuperUF*[CN]	
	Tianjin Motimo–*FP AIV*[CN]	
	Vina Filter–*F08*[CN]	
	Zena Membranes–*P5*[CZ]	

CN: China/Taiwan; CZ: Czech Republic; DE: Germany; DK: Denmark; FR: France; IRL: Southern Ireland; JP: Japan; KR: Korea; NIR: Northern Ireland; NL: Netherlands; SE: Sweden; SG: Singapore; SP: Spain; US: United States.

2.3. Foulants and fouling control concepts in MBRs

Fouling control in MBR comprises of several concepts, from the general set up (design parameters such as load, F:M ratio, type of membrane material and membrane configuration) *to* pre-treatment of the influent *to* optimised operation conditions in order to control hydrodynamics of the membrane module compartment (Figure 1.1, page 3).

Pre-treatment of the feed is generally undertaken by applying appropriate fine screens in order to filter out materials which could impair the overall operational performance of the MBR by clogging and tressing membrane modules. Such materials include hair, debris, lint and other fine material (Le-Clech, 2010). While conventional fine screens with average gaps of 2.0 mm were found to result in insufficient removal of the fine material, very fine screens with gaps as small as 0.5 mm are generally applied within MBR systems (Judd, 2006; Le-Clech, 2010). Furthermore, chemical processes are used to establish chemical boundary conditions which the membrane material is able to withstand. Such processes include precipitation, coagulation, flocculation, anti-scalants and pH-adjustment (Hilal *et al.*, 2005), however, these are mainly used for industrial applications.

Operational parameters to control clogging and fouling formation on the membrane surface include the following (Drews, 2010; Judd, 2006; Stephenson *et al.*, 2000):

1. Biological Parameters
    - SRT
    - HRT
    - loading rate/type of feed
    - MLSS (also eventually soluble microbial products, extracellular products)
    - dissolved oxygen level; nitrate concentration
2. Hydraulic Parameters
    - cross-flow velocity due to configuration
    - type of filtration (constant flux, constant TMP)
    - filtration cycles and filtration duration
    - aeration (rate, intermittent; coarse, fine aeration)
    - cleaning procedure (intervals, chemicals)

As indicated in Chapter 1, effects of different **biological parameters** are reported in opposing trends with regards to overall membrane filtration performance by numerous researches in literature and intensive summaries have been published (Chang *et al.*, 2002; Drews, 2010; Judd, 2006; Le-Clech *et al.*, 2006; Meng *et al.*, 2009).

The main aspects for biological operational parameters which can be influenced by membrane operators and which are usually also indicated with an optimum range by membrane module suppliers are commonly activated sludge parameters, such as SRT, HRT, MLSS,viscosity, DO content, temperature, pH and sludge loading rates. Within MBR research these parameters have been extended to particle size, fractional dimension, soluble microbial products and extracellular microbial products.

MLSS content is generally know to contribute to cake layer formation and is therefore one of the first suspects to contribute to fouling in MBRs. However, opposing trends have been reported with cake layer resistance either decreasing or increasing with MLSS content or threshold values for MLSS. For instance, no impact of either MLSS, EPS or viscosity on the sludge filterability could observed by Rosenberger and Kraume (2002) while comparing various sludge samples from 8 different MBRs using a flat sheet test cell device (MLSS was reported to range from 2 to 24 $g.L^{-1}$).

Schwarz *et al.* (2007) observed a threshold value for MLSS concentration of $\approx$ 5 $g.L^{-1}$, below which the hypothesis that J_{crit} decreases with increasing MLSS is true. Above a MLSS concentration of $\approx$ 5 $g.L^{-1}$, flux-management techniques to prevent serious cake formation were stated to be more important than MLSS. Trussell *et al.* (2007) revealed within a very concise overview of several studies conducted on a HF submerged (ZENON) membrane, that the exposure time towards high MLSS content resulted in a greater permeability decline in permeability with MLSS. Itonaga *et al.* (2004) investigated the operation of pilot scale submerged HF and stated an upper limit for MLSS concentration for efficient operation of MBRs, which was suggested to be around 10 $g.L^{-1}$. An exponential relationship of increasing filtration resistance with increasing MLSS has been reported by Meng *et al.* (2006), investigating fouling aspects on a PE 0.1 μm hollow fibre membrane with MLSS content ranging from 5 to 25 $g.L^{-1}$. Wu and Huang (2009) also observed a threshold value for MLSS concentration, which was determined with 10 $g.L^{-1}$. Below that threshold value no impact of MLSS on filtration resistance could be observed on a bench-scale MF hollow fibre (0.4 PE), while above the threshold value a linear increase in filtration resistance with increasing MLSS content was found to be statistically significant.

Feed water characteristics were reported to play a major role in filtration performance by Guglielmi *et al.* (2007a); Lyko *et al.* (2008b), with Lyko *et al.* (2008b) finding that the F:M ratio for full scale plants influences sludge filterability. An increased fouling rate with increased **ratio of P/C** within the feed was reported by Arabi and Nakhla (2008), with the highest fouling at a ratio of P/C $\approx$ 8:1 and lowest fouling at P/C ratio at $\approx$ 2:1. Lower

EPS concentration at higher P/C rates was found to result in smaller flocs and higher cake resistance (Arabi and Nakhla, 2008).

SRT is also being reported to play an important role when assessing the fouling propensity of activated sludge. Pollice *et al.* (2007) reported sludge filterability and capillary suction time to be at a minimum for SRT in the range of 40-80 days, with SRT tested from 20 days to complete retention. Furthermore, in a literature survey Pollice *et al.* (2005) stated that higher SRT might be beneficial due to lower EPS carbohydrate content for sub-critical filtration conditions, but come in turn with higher MLSS levels thus exposing higher fouling propensity at super-critical filtration scenarios. A trend in higher fouling propensity at lower SRT due to higher EPS was also observed by others (Ahmed *et al.*, 2007). Furthermore, (Masse *et al.*, 2006) reported lower EPS in biomass deriving from MBR with increasing SRT.

Lee *et al.* (2003) investigated microfiltration HF membrane made of PP and suggested fouling could be related to EPS composition of the biomass. The study furthermore indicated that the overall fouling resistance improved with increasing SRT, whereas it was not indicated if this improvement might also be influenced by the membrane exposure over time. However, hydrophobicity of the biomass, biomass surface charge and microbial activity were stated as potential key factors in estimating resistance caused by microbial floc.

Soluble microbial products (SMP) and **extracellular microbial products (EPS)** are thought to contribute to membrane fouling, but with opposing trends being reported. The opposing observations might be influenced by the different membrane configurations used within the various research studies. In terms of different membrane configurations, for instance, Drews *et al.* (2007) stated after having determined a non impact of carbohydrates on ultra filtration flat sheet membranes (PAN and PES, ≈ 0.037 μm) that higher susceptibility to carbohydrate fouling could be found for microfiltration membranes, and largely hollow fibre membranes.

For long term trials, this was also observed by Torres *et al.* (2008) while comparing Kubota flat sheet and Zenon HF MBR pilot plants for wastewater treatment of oil refinery. After 6 months of operation, both plants were found to meet the local legislative requirements regarding the effluent quality (CONAMA 357, Brazil) , whereas in regards to the overall performance, the HF module did show much higher permeability values during the start of the pilot plant. On the contrary to the FS module MBR, the permeability decline had not reached a stabilized plateau state after 5 months of operation. The authors suggested this might indicate the higher susceptibility of the HF module to irreversible fouling, hence the result of pore penetrating macromolecules and fine colloids.

However, Itonaga *et al.* (2004) reported no clear correlation between measured dissolved organic matter (DOC, carbohydrates, proteins) and membrane fouling on two parallel run HF submerged MBRs. Instead, colloidal fractions within the supernatant seemed to play an im-

portant role in membrane fouling (Itonaga *et al.*, 2004). In fact, Fan *et al.* (2006) also reported colloidal TOC being the main fouling parameter with J_c decreasing with increasing colloidal TOC, whereas no clear relationship could be drawn to MLSS content which varied from 7 to 21g.L^{-1}. Furthermore, J was reported to decrease with increasing soluble carbohydrates and increasing EPS, whereas EPS was directly related to colloidal TOC. Humic substances and proteins showed less impact.

Fan *et al.* (2006) drew a empirical relationship to estimated J_c from colloidal organic carbon content, but stated that the correlation is expected to be highly influenced by the membrane, module configuration and operating parameters. Similar conclusions have been drawn by Howell *et al.* (2004) where a model was fitted for one type of experiment, however could not be applied to previous fouling studies. Howell *et al.* (2004) stated this being most likely affected by the complexity of the nature of membrane filtration where the impact of membrane fouling history on future filtration performances is very unlikely to be predictable

On the other hand, Hai *et al.* (2005) compared the filtration performance of a FS and HF module with same nominal pore size (0.4μm) and indicated that the FS was observed to foul slightly more than the HF. Also permeability was reported to be unrecoverable following a mechanical cleaning. Similar observations were reported by Howe *et al.* (2007), where microfiltration and ultra filtration membranes of both types, flat sheet and hollow fibre were compared for their fouling propensity. Flat sheet membranes made of 0.22 μm PVDF and 100kda PS were found to foul more rapidly than hollow fibre membranes made either of 0.1 μm PVDF and 100kda PS (Howe *et al.*, 2007). However, Howe *et al.* (2007) stated furthermore that no straightforward conclusion could be drawn for filtration assessment between the different configurations as fabrication process of the membrane material might have had an enormous impact.

At this point it should be reiterated that difference will also derive from the operational set up, hence the conditions of membrane testing. Le-Clech *et al.* (2005) also revealed higher critical fluxes for a submerged multi-tubular membrane than for a side-stream operated MT membrane. Aeration efficiency on fouling control was also reported to be higher for the submerged module. Furthermore, as previously indicated the membrane material will also impact on the observed fouling behaviour. Alvarez-Vazquez *et al.* (2008) compared the fouling of a ceramic and polymer membrane trialled in the same high fouling conditions and reported critical fluxes of 36 and >60 LMH for the polymeric and ceramic membrane respectively.

A comparative study of side-by-side filtration at five different MBR pilot plants in Hawaii (Babock Jr. *et al.*, 2007), reported an optimum filtration performance at a MLSS content of 10-12 g.L−1 for a MLSS range from 6-16 g.L−1 being tested. During the comparative study all six MBRs revealed similar good treatment and effluent quality reaching standards suitable for water recycling. The authors concluded that the major differences between the individual techniques would be nitrification/denitrification capacities, and maintenance and

operational costs, which are mainly influenced by power requirements, membrane cleaning frequency, robustness of the system (Babock Jr. *et al.*, 2007). However, detailed figures estimating the overall difference in costs for the systems tested were not stated. Overall, there be difficulties in directly assessing the performance of the different configurations reported in literature as they are usually operated according to indicated optimised operation conditions provided by membrane suppliers, which may differ widely.

To reduce negative impacts of potential foulants, current research also investigates the addition of polymers or activated carbon to reduce macromolecular substances within the bulk phase to enhance filtration performance (Iversen *et al.*, 2009), whereas the techniques for full scale applications seem to still be facing limitations.

Hydraulic Parameters

Hydraulic operational parameters applied to create a reduction in particle deposition on the membrane surface are

- aeration
- air sparging
- back pulsing
- backwash

All the above mentioned measurements are undertaken to increase shear on the membrane surface in order to help reduce permeability decline resulting from cake layer formation or polarisation concentration.

High shear dynamic filtration is furthermore reported to be a promising technology especially for applications requiring high selectivity and high concentration factors, as the benefits of rotating or vibrating membranes on reducing the concentration polarization and thus increasing the flux have been well documented (Jaffrin, 2008). A significant reduction in membrane production costs, and furthermore a simpler construction and less frequent membrane replacement by using ceramic membranes have been considered to enhance the potential market application significantly (Jaffrin, 2008). However, apart from the two previously mentioned set up by Huber and Martin Systems, dynamic filtration is not frequently used within MBRs for wastewater treatment, which is mainly due to the necessity of a low cost solution rather than high selectivity.

The measurements for particle deposition control differ according to the set up, but are also influenced by new market materials. For instance, hollow fibre membranes are generally reported to withstand high backwash regimes, which in turn help to maintain high permeabilities.

Within MBR systems, however, the formation of a loose and porous cake layer might be beneficial to prevent pore penetration of fine material. This porous cake layer is suspected to be destroyed by frequent backwash regimes.

However, Grelot *et al.* (2007) investigated the fouling behaviour of a novel back flushable flat sheet material (A3 water solution, 0.2μm PVDF) which was arranged in a double deck system. The optimum net flux was determined with 26.4 LMH and gave a stable permeability of around 500-600 LMH.bar^{-1} at SADm of 0.34 Nm^{3}m^{2}2h^{-1} and a filtration/relaxation cycle of 8 min on/ 2 min off. The suspected higher fouling of modules within double deck configuration was not observed. While the biomass filtration performance reported was in range with other materials reported (table 2.3), it would be interesting to compare the long-term fouling behaviour of this new configuration with and without backwash to investigate the potential drawback of backwashing on irreversible and irrecoverable foulants.

Wu *et al.* (2008) reported a better filtration performance with higher initial flux (60 LMH) for a very short period prior to the individual filtration cycle. This improved filtration performance was attributed to lower pore penetration due to the creation of a porous cake layer.

Membrane aeration is used for general supply of oxygen to the biomass, but also to scour the membrane surface to control fouling and gel layer formation. While fine bubble aerators are used for oxygen supply, aerators used for fouling control are generally of coarse bubble aeration. Membrane scouring has been found to show positive effects on membrane filtration performance due to reduction of particle deposition or reduction of concentration polarization (Wintgens *et al.*, 2003), whereas the advantages of increased aeration were also reported to be effective only up to a threshold value above which a further increase in aeration did not result in further membrane filtration improvements (Bouhabila *et al.*, 1998; Le-Clech *et al.*, 2003b; Ueda *et al.*, 1997).

Nywening and Zhou (2009) reported a proportional relationship between stable fouling resistance and permeate flux, and an inverse relationship to scouring aeration intensity, derived from experiments on a HF pilot scale plant (Zenon, ZW-500G-SMC). The authors also reported that the effects of permeate and aeration on fouling ratios were found to be independent which led to an empirical relationship.

Ndinisa *et al.* (2006) reported a threshold value of aeration similar to the studies on single or multi-tubular tubes systems, on a bench-scale flat sheet module (Kubota, A4 size) above which no further increase in fouling control was observed. Meng *et al.* (2008) carried out a comprehensive study on membrane fouling in submerged membrane bioreactors operated under different aeration intensities and reported negative impacts of too low and too high aeration rates on membrane performance. While the lower aeration intensity was reported to lack reduction of particle deposition, the very high aeration rate created floc rupture and

hence resulted in higher fouling potential of the bulk phase.

Overall, the increased membrane filtration performance with increased aeration is related to the higher cross-flow velocity cause by the altered aeration, however there are also reports in literature where increased cross-flow velocity did not result in an increased membrane filtration performance (Busch *et al.*, 2007; Drews *et al.*, 2010; Prieske *et al.*, 2008). A threshold value has been reported for aeration rates above which the contradictory observed increase in cake layer resistance with increasing aeration rate would result in better fouling control (Busch *et al.*, 2007). The suggested aeration rate was 0.1 m^3 per seconds for the HF module application the model was developed for (Busch *et al.*, 2007).

Conversely, Drews *et al.* (2010) observed lower critical fluxes with higher cross-flow velocity at constant aeration rates, whereas increasing aeration at constant cross-flow velocity resulted in increased critical fluxes. The observations were attributed to the balance of lift and drag forces similar to the model of Altmann and Ripperger (1997). Within their CFD validated calculations, the lower critical flux could be related to a sub micron critical particle size of 0.85 μm at the higher cross flow velocity of 0.4 $m.s^{-1}$. Lowering the cross flow velocity resulted in a larger diameter for critical particle size (3 μm at CFV of 0.2 $m.s^{-1}$)and subsequently led to higher critical fluxes (8 LMH instead of 2 LMH, Drews *et al.* (2010)). The parameter determining the increased critical flux with increased aeration at constant cross flow velocity would consequently be the different shear force exhibited on the membrane surface.

Table 2.3.: Examples of application of different membrane module configuration

Config. Type	supplier	material	pore size [µm]	permeability raw water [LMH.bar^{-1}]	permeability sludge [LMH/bar]	packing density per module [m²/m³]	MLSS [g/l]	typical flux [l.m^{-2}h^{-1}]	SAD$_m$ [Nm³.m²h^{-1}]	Cleaning	Fouling control	References
FS	Kubota	Chlorinated PE	0.4	1110	200-800	115	9-15.4	8.3-42	0.75	NaOCl, Oxalic Acid	relaxation	Beverijk wastewater treatment plant
FS	Toray Industries	PVDF	0.08	1200	300-400	135	12-16	24.3	0.2-0.4	NaOCl. Citric acid	relaxation	Heenvliet
FS	Agfa-Gevaert NV	PES/PVP	<0.02	1000			8-15	10-60	0.35-0.7	bases, oxidant, tenside, acid	relaxation + active backwash (up to 1bar)	Industrial: Mortsel, Belgium Muncipal: Xanten-Vynen. Germany
HF	Mitsubishi Rayon Engineering	PES	0.04		140-200	485	8.9-11.6	5-30.6	0.28-0.38	NaOCl, acid	relaxation+backwash	Beverijk wastewater treatment plant
HF	Zenon Environmental	PVDF	0.04		200-350	300	10.4-11.2	20-35	0.54	NaOCl. Citric acid	relaxation+backwash; air sparging	Beverijk wastewater treatment plant
MT	Norit X-Flow	PES	0.03	750	75-250	307	8	15-50	0.33-0.6	NAOCL, Ultrasil	high backwash	Beverijk wastewater treatment plant

2.4. Configurational Aspects on Overall Costs

The main drawback for elevated installation of MBR plants is still their higher specific costs per cubic meter of wastewater treatment compared to conventional activated sludge plants. Commonly, these differences in costs are considered to derive from the main operational costs for MBRs, which are attributed to higher aeration costs necessary for membrane air scouring and usual higher oxygen demand due to higher MLSS content of the biomass. However, the required pre-treatment steps with fine screens are incurring additional costs compared to conventional activated sludge plants (Wintgens, 2005).

Costs for MBRs depend strongly on the configuration and the size of the MBR plants. Smaller MBR plants usually come with higher specific costs per cubic meter of permeate. For instance, the MBR Roedingen with 2.200 PE was indicated to have a specific energy demand of 1.7 to 2.7 kWh per m^3 of permeate, whereas the specific energy costs of the much bigger MBR plant Nordkanal, with its 80.000 PE were indicated on average 0.89 $kWh.m^{-3}$ (Wintgens, 2005). The latter value represented approximatively only 0.3 $kWh.m^{-3}$ in additional costs compared to a conventional activated sludge plant of similar size (Wintgens, 2005).

Specific energy requirements for membrane systems vary widely with the submerged systems considered being the most cost effective due to the lack of pumps (table 2.4).

Table 2.4.: Specific energy demand per membrane filtration process (Baumgarten, 2007)

membrane	filtration process	specific energy demand
MF, UF	dead-end	0.1 - 0.3 $kWh.m^3$
MF, UF	semi-cross-flow	0.5 - 2.0 $kWh.m^3$
MF, UF	cross-flow	2.0 - 10.0 $kWh.m^3$
NF, RO	cross-flow	0.5 - 5.0 $kWh.m^3$

Overall the costs determining the specific costs per treated cubic meter wastewater are (Melin and Rautenbach, 2004):

1. Investment cost
2. Maintenance cost
3. Capital cost

Fletcher *et al.* (2007) investigated the costs of different configurations based on single household MBRs and concluded that CAPEX costs would decline significantly with increasing PE, with MT design being lower HF, lower FS modules. However, CAPEX and OPEX costs were reported to be interchangeable with one declining and the other one increasing, and hence total costs differed significantly with HF configuration at the lower cost end and MT at the upper (Fletcher *et al.*, 2007).

However, the assumption for the costs consideration undertaken by Fletcher *et al.* (2007) included pump systems for the MT configuration. Therefore, OPEX might be significantly reduced by applying a LE (low energy) MT membrane only, such as an air-lift side-stream configuration, even when consequently lowering the assumed flux.

A further advantage which should not be neglected is the opportunity of water re-use of membrane effluents. For instance, Möbius and A.Helble (2006) compared the costs for a MBR and a SB-BB designed to treat industrial wastewater deriving from the paper industry. They concluded that the MBR plant would have resulted in 30% higher investment costs and 67% higher annual overall costs compared to the standard SB-BB with higher maintanance costs for the MBR consisting mainly of energy requirements, chemicals and membrane replacements (Figure 2.11).

However, major advantages of the MBR system were considered to be the significantly lower foot-print and the high quality of effluent fulfilling standards for internal water recycling, which would in turn result in a major reduction of the overall costs compared to the SB-BB system.

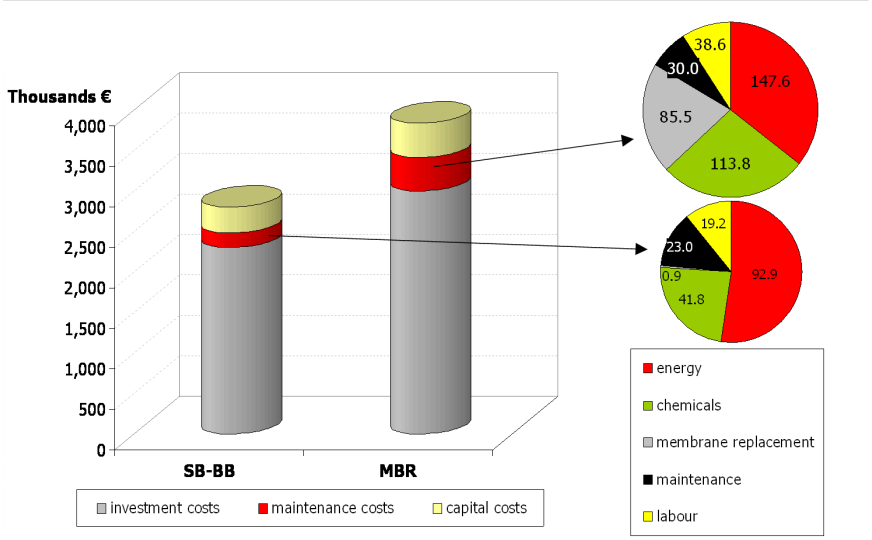

Figure 2.11.: Comparison costs for MBR vs SB-BB for industrial wastewater treatment (paper industry; data from Möbius and A.Helble, 2006).

Membrane replacement costs experienced a rapid decline during the last two decades since the first full scale plants went into operation. So did the average cost per square meter of membrane of a *Kubota* membrane sheet dropping from $400 in 1992 to less than $50 in 2005 (Judd, 2006). Higher installation capacities, optimised plant design and operation furthermore resulted over time in a decline of the costs per cubic meter of permeate (Judd, 2006).

Further improvements regarding the overall cost of MBRs are expected if the MBR market is to undergo a concept of standardisation as it had been undertaken, for instance, for RO market (De Wilde *et al.*, 2007). However, according to the survey undertaken by De Wilde *et al.* (2007), the current market situation including the ongoing research on process improvements did not reach a final state and hence the immediate introduction of a standardisation might be counterproductive.

A full scale investigation was undertaken by Brannock *et al.* (2010) to determine the energy requirements on complete mixing of sludge by comparing two full scale plants and concluded that even though both plants were close complete mixing, due to the lower packing density the flat sheet pilot plant required more energy per square meter of membrane area to achieve the same state of mixing as the hollow fibre pilot plant. The conclusion was that the hollow fibre module was more energy efficient than the flat sheet module.

Brepols *et al.* (2008) provided an overview of retrofitted full scale wastewater plants with MBR technology, and concluded that with an adequate diligence of the planning engineer, MBR technology provides several promising aspects of upgrading conventional wastewater treatment plants, especially in cases where higher effluent quality parameters need to meet regulations, e.g. for water reuse.

Yoon *et al.* (2004) untertook a cost estimation for aeration and sludge treatment of MBRs and for a wastewater of 400 $mg.L^{-1}$, the steady state model was expected to increase from 11 $g.L^{-1}$ to 15 $g.L^{-1}$ MLSS when HRT was decreased from 16h to 12h. The economical optimum was considered under the above conditions to be HRT 16h and MLSS 11 $g.L^{-1}$, which would then result in a minimum air requirement of 13.3 $m^3.min^{-1}$ when influent was 100 $m^3.d^{-1}$.

An optimum air requirement was also reported by Garces *et al.* (2007), whereas Verrecht *et al.* (2008) concluded that a reduction in flux to half of its value would result in energy savings of 45%.

3. Aims and Research Objectives

The proposed research is to investigate the effects of configurational aspects on the operation of membranes in MBRs. As previously described there is a very complex interacting process influencing the rate of fouling and hence permeability losses during the process of activated sludge filtration. While many researches studied intensively the impact of varying process parameters, such as organic loading, F/M ratio and varying aeration intensity on the specific fouling phenomenon, the set up is quite often based on a single configuration. This research focuses on a direct comparison of three different full-scale sized membrane configurations operated in parallel as air-lift side-stream mode from a $2.2m^3$ aeration tank.

The three air-lift side stream operated modules are a multi-tubular membrane (MT), a single flat sheet module (FS) and a hollow fibre (HF) module, where special membrane holding vessels are designed to facilitate the operation of FS and HF membranes in air-lift side-stream mode with simulative separation distances prevalent in submerged modus. For hydrodynamic comparison, the filtration path length of each membrane module was fixed to 1.45m. The aeration tank itself consists of an internal submerged HF module (membrane area, $A=17.5m^2$) which is functioning as a HRT control module and enables the operation of the side-stream modules decoupled from the overall hydraulic overall performance of the pilot plant.

Filtration performances are compared under steady and unsteady state operations of the biomass with different MLSS (mixed liquor suspended solid) content. The overall performance is assessed throughout the operation while running at constant specific aeration demands and varying fluxes for each air-lift module by applying the so called critical flux concept. Biomass properties and potential foulant parameters (such as suspended solids, total solids, particle size, COD, proteins and carbohydrate concentration in supernatant and permeate lines) are monitored for each defined condition.

In parallel to the aeration trials of the pilot plant, bench-scale material tests are conducted to allow an eliminative approach for fouling effects on different materials while being of the same configuration. Flat sheet and single tube materials are tested for the varying membrane resistances (intrinsic, cake layer, reversible and irreversible fouling) and also for desorbed potential foulants on their surfaces. Membrane materials are furthermore analysed for their surface characteristics to determine whether hydrophobicity, porosity or surface energy have an impact on their fouling propensities.

The evaluation of the outcomes of all different research tasks will be interlinked under the aspect of cost assessments of MBRs (Figure 3.1).

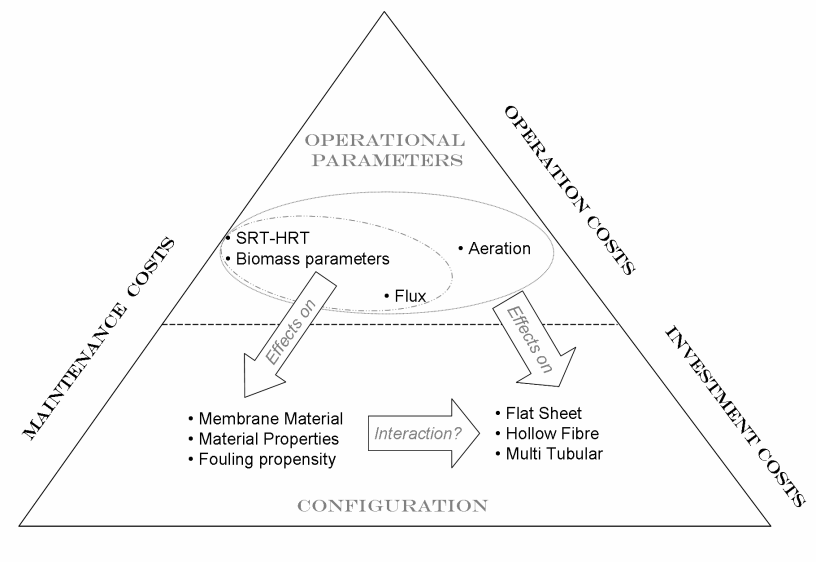

Figure 3.1.: Aims and Objectives - Effects of investigated operational parameters on performance of different configurations

4. Materials and Methods

4.1. General

The proposed research was to investigate the effects of configurational aspects on the operation of membranes in membrane biological reactors (MBRs). Core experiments were undertaken at a pilot plant, designed and set up to allow a direct comparison of the three most commonly used membrane configurations for MBRs within wastewater treatment. The three configurations were a multi-tubular membrane (MT), a single flat sheet module (FS) and a hollow fibre (HF) module. All three modules were operated in parallel as air-lift side-stream mode from one 2.2m^3 biological aeration tank to allow a direct comparison under same biological condition and fixed hydraulic operation mode (same SAD_m, same membrane path length, operation as air-lift sidestream in a confined vessel).

The pilot plant was set up at Cranfield University Pilot Hall and fed with real domestic sewage and allowed an individual flow control for each side-stream module decoupled from the pilot plant's overall hydraulic condition. Tests were undertaken to study the effects of varying aeration scenarios under different biomass parameters on each module performance using short-term critical flux tests and long-term subcritical tests. Biomass properties and potential foulant parameters (such as suspended solids, total solids, particle size, COD, proteins and carbohydrate concentration in supernatant and permeate lines) were monitored for each trial.

In parallel to the aeration trials of the pilot plant, bench-scale material tests were conducted to allow an eliminative approach for fouling effects on different materials while being of the same configuration. Different flat sheet and single-tube materials were tested for the varying membrane resistances (intrinsic, cake layer, reversible and irreversible fouling) and also for adsorbed potential foulants on their surfaces. Membrane materials were furthermore analysed for their surface characteristics to determine the impact of hydrophobicity, porosity and surface energy on membrane fouling propensity.

4.2. Materials

4.2.1. Membrane Materials

The membranes tested and analysed consisted of different commercially available polymeric materials which were at the time amongst the most commonly applied in MBRs:

- chlorinated polyethylene (PE)
- polyethylsulfone (PES)
- polyvinylidene difluoride(PVDF)
- polysulphone (PS).

Flat sheet material tests were run in parallel to the pilot scale trials to allow an eliminative approach for differences in filtration performance deriving from either hydrodynamical impacts either due to configurational aspects or due to material properties. Flat sheet materials were therefore chosen due to their availability for use in full-scale MBRs and their potential match to the pilot plant modules in terms of materials and pore size.

An exact match in terms of material comparison between pilot scale and bench-scale materials was given for the flat sheet material (T01-T10) and the flat sheet membrane module (FS), and also for single-tube membrane (sMT-04) and the multi tubular module (MT). A complete overview of the different tested materials and their respective pore size is summarised in Table 4.1.

Table 4.1.: Overview of tested membranes

ID	material	pore size [μm]	separation[(a)] or diameter[(b),(c)] [mm]
BENCH-SCALE - flat sheet material			
K01 - K10	PE	0.4	9 [(a)]
M01 - M10	PES	0.04 (150kDa)	9 [(a)]
P01 - P05	PS	0.05	9 [(a)]
T01 - T10	PVDF	0.08	9 [(a)]
B01 - B05	PVDF	0.15	9 [(a)]
BENCH-SCALE - single-tube material			
sMT01	PES	tbi	11.7 [(b)]
sMT02	PES	tbi	11.7 [(b)]
sMT03	PES	tbi	8 [(b)]
sMT04	PVDF	0.03	8 [(b)]
PILOT-SCALE - membrane material			
MT	PVDF	0.03	8 [(b)]
FS	PVDF	0.08	6
HF1	PS	0.08 (300kDa)	1.4 [(c)]
HF	PES	0.04	2.4 [(c)]
AK (HF)	PVDF	0.1	-

[(a)] separation distance of flat sheet test cell device; [(b)] inner diameter of lumen; [(c)] outer diameter of fibre

4.2.2. Pilot Plant

4.2.2.1. Design and Set Up

The MBR pilot plant was designed and set up to enable a direct comparison of three different membrane module configurations; a multi-tubular membrane (MT), a single flat sheet module (FS) and a hollow fibre (HF) module. The three different types of modules were all operated in parallel in air-lift side mode from a 2.2m^3 aeration tank to allow a direct comparison under fixed hydraulic conditions (air-lift side-stream solely, same SAD_m, same membrane path length; Figure 4.1 and 4.2).

A special vessel made of persplex-glass (Model Products, Wootton, UK) was designed to facilitate the operation of the flat sheet membrane (FS) in air-lift side-stream mode. After a first stage operation of the pilot plant, it became necessary to exchange the first HF side-stream module (HF 1, manufactured to be operated in air-lift mode) to a second different type of hollow fibre module (HF), where the holding vessel was also specially designed for this purpose. For both vessels of FS and HF, simulative separation distances prevalent in submerged modus were chosen for their design. The design of the HF vessel also considered a separation panel at the entrance of the feed line to prevent the biomass from hitting the membrane fibres at a right incidence angle. The multi-tubular module (MT) arrived purpose-built from the membrane manufacturer.

For hydrodynamic comparison, the filtration path length of each side-stream membrane module was fixed to $1.45m$ where possible. The aeration tank itself consisted of an internal submerged HF module (membrane area, A=$17.5m^2$) which functioned as a HRT-control module and enabled the operation of the side-stream modules decoupled from the hydraulic overall performance of the pilot plant. All used membranes in pilot scale and their main parameters are summarised in Table 4.2.

Permeate was withdrawn under suction from each module using peristaltic pumps (Watson Marlow, Falmouth, UK model *620DuN* (MT), *520Du* (HF, FS) and Varmeca/Watson Marlow (submerged HRT-control module); PP1-PP4 in Figure 4.1). Each membrane module was facilitated with an individual clean-in-place (CIP) tank where permeate was collected for individual monitoring of permeate quality and separated backwash operation per module, where module configuration permitted. To decouple the operation of the side-stream membranes from the overall performance of the pilot plant, the permeate collected in the individual side-stream-CIP tanks was looped back into the main aeration tank via gravity.

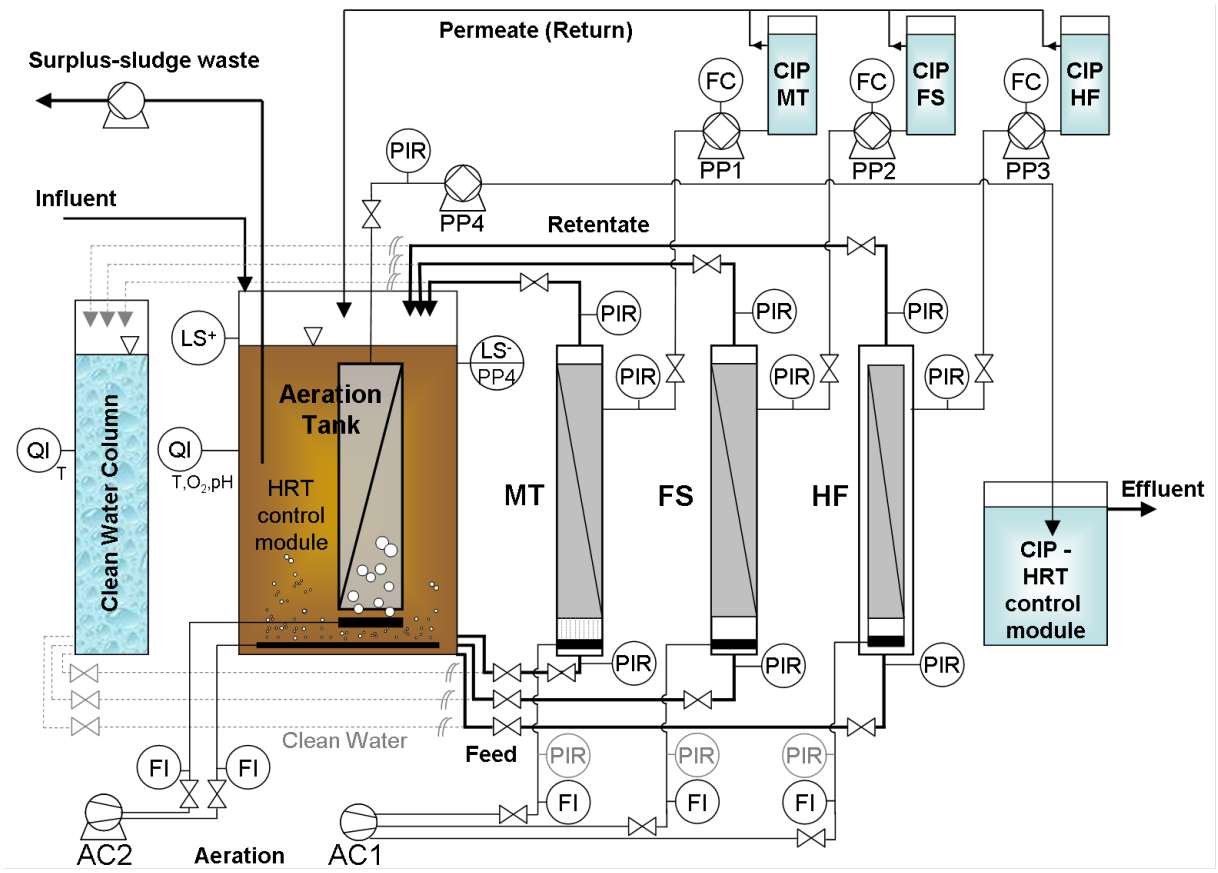

Figure 4.1.: Scheme of Pilot Plant

Pressure was measured in each permeate line (MT, FS, HF and HRT-control module) using voltage (0-5V) vacuum pressure transducers (Sensit, -1 to 1 bar, -0.5 to 0.5 bar respectively, RM&C, Padley, UK & ALTHEN GmbH, Kelkheim, Germany) with a high accuracy of of 0.15% FS. Pressure for each side-stream module at inlet (feed line) and outlet (retentate line) was monitored using a voltage (0-5V) pressure transducer ranging from 0 bar to 1 bar (RS, Corby, UK) with an accuracy of 0.25% FS. The trans-membrane pressure (TMP) of each membrane was recorded and monitored online on a computer using two data loggers (Pico data logging system, ADC-16 and PicoLog data acquisition software, Pico technology Ltd., Cambridge, UK). Due to experienced signal interference caused by the quantity of voltage pressure transducers connected to each data logger, the terminal boards of the data logger were equipped with 330nF capacitors (Kemet, RS, Corby, UK) in addition to the required 10k metal film resistors (Tyco Electronics; RS, Corby, UK) for signal conversion (all calculations according to data-logger manufacturer: Pico technology Ltd, Cambridge, UK).

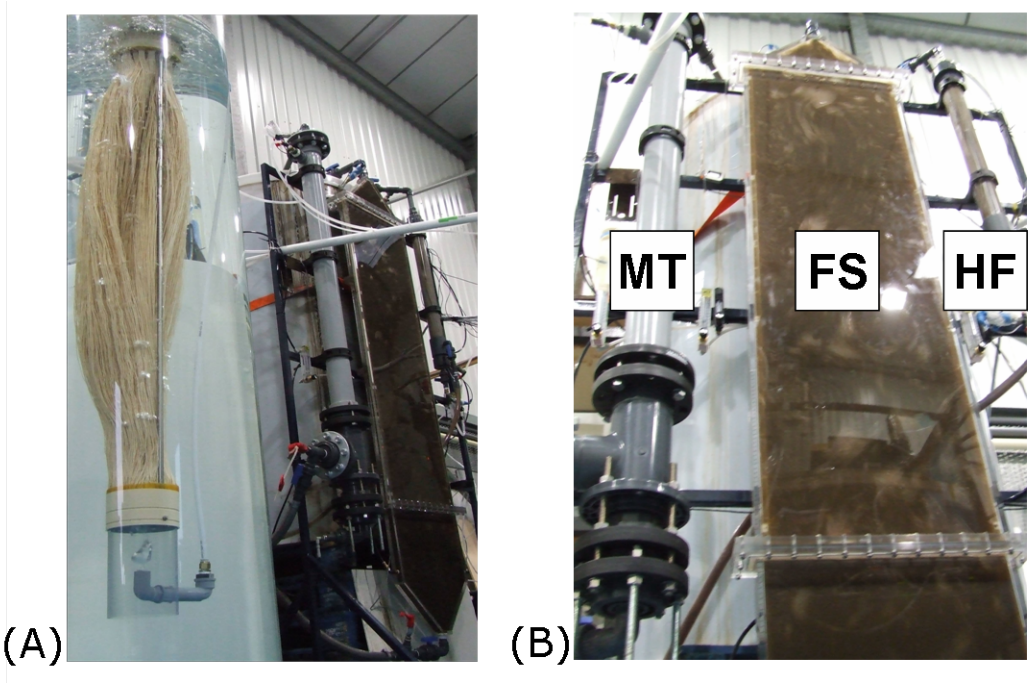

Figure 4.2.: Pictures of Pilot Plant: (A) HRT-control module prior installation, (B) MT, FS and HF1 running under biomass filtration

Table 4.2.: Overview of membrane modules operated at pilot scale

ID	Type of Membrane	Operation Mode	Filtration Length [m]	Membrane Surface Area [m^3]	Packing Density [m^2m^{-3}]	Material	Nominal pore size [μm]
MT	Multi Tubular	Air-lift sidestream	1.45	3.10	364	PVDF	0.03
FS	Flat Sheet	Air-lift sidestream	1.45	1.40	76	PVDF	0.08
HF1	Hollow Fibre	Air-lift sidestream	0.75	3.04	632	PS	0.05
HF	Hollow Fibre	Air-lift sidestream	1.45	2.75	242	PES	0.04
AK	Hollow Fibre	Submerged - HRT control	1.5	17.5	n.a. (5.3)	PVDF	0.1

Air was supplied to the bottom of each individual membrane module to allow membrane scouring (coarse bubble aeration) and to provide an air-lift to each side-stream module. The FS membrane was fitted with an aeration tube simulating an air supply similar to a full scale application, while the MT, HF and submerged HRT-control module were equipped with an individual aeration system deriving from the membrane manufacturers. Air supply was controlled using two different types of air rotameters (Key Instruments, RS, Corby, UK) enabling the range of a specific membrane aeration demand (SAD_m) per module from 0.1 to 2.0 $Nm^3m^{-2}h^{-1}$. Aeration for biomass growth was distributed to the aeration tank via plate air diffusers (fine bubble aeration) and was also controlled using airflow meters (Key Instruments, RS, Corby, UK). For certain experiments the air flow between the individual airflow meters and membrane modules were also monitored for air pressure changes (pressure transducers, 0-1 bar, 0.25% FS accuracy, RS, Corby, UK).

Air was provided via two air compressors (AC1 and AC2, Figure 4.1). AC 1 was the main line air compressor for the Cranfield University Pilot Hall, where the air was cooled and filtered and mist and oil separated before being distributed via main rings to the individual working bays. AC 2 was a stand-alone air compressor (Model Products, Wootton, UK) used as a back-up aeration system for emergencies and was solely connected to the core parts of the pilot plant the aeration tank, and the submerged HRT-control module.

The aeration tank was equipped with a level control float switch (RM&C, Padley, UK) for the influent (fed by gravity from main ring system of the pilot hall) and a relay-level-switch (RS, Corby, UK) which was connected to the permeate pump of the HRT-control module (PP4, Figure 4.1) to enable an automatic stop of permeate withdrawal at a critical low level set for the top end of the HRT-control module.

Temperature was monitored at different levels via two submerged digital thermometers (RS, Corby, UK), and pH and dissolved oxygen (Hanna Instruments Ltd, Leighton Buzzard, UK) were measured on-site, in-situ (biomass of aeration tank) and ex-situ (retentate lines).

4.2.2.2. Operation

The MBR pilot plant was set up at Cranfield University Pilot Hall where it was fed with raw sewage deriving from the on-site primary settler of Cranfield University wastewater treatment works. The wastewater was considered to be of municipal character and the consented dry weather flow (DWF) for this wastewater treatment works was given as approximately 675 m^3h^{-1} (Le-Clech, 2002).

The pilot plant was initially seeded with return-activated sludge (RAS) taken from a nearby conventional activated sludge plant (Cotton Valley STW, Anglian Water, Milton Keynes). The biomass was mixed with sewage (2:1), aerated and after 12 hours of acclimatisation the

membrane filtration was initiated at low to moderate fluxes with an initial chosen SAD_m value of $0.5 Nm^3m^{-2}h^{-1}$ per module. Intermittent filtration cycles with short backwash cycles, where configuration allowed, were chosen (Table 4.3) and incrementally increased to reach an HRT value of 32 hrs. The installation of the HRT-control module (AK) was able to be carried out three months after the starting up-phase and HRT values were subsequently decreased from 36 hours (without AK) to 24 hours (with AK).

After the start up phase it became necessary to exchange the originally installed hollow fibre side-stream module (HF1) with an alternativew manufactured hollow fibre module (HF) due to re-occurring clogging problems with HF1. All tests thereafter were run with this second HF module (HF) (Table 4.2).

Table 4.3.: Start up of pilot plant: Chosen filtration parameters

Parameter	MT	FS	HF 1
Flux range [LMH]	8.0 - 22.3	10.0 - 18.0	3.7 - 9.0
Filtration	540 s	540 s	540 s
Relaxation	50 s	60 s	50 s
Backwash	10 s	-	10 s
Backwash intensity	equal to operated flux	-	equal to operated flux
SAD_m $[Nm^3m^{-2}h^{-1}]$	0.5	0.5	0.5 - 1.25

The pilot plant was operated under varying conditions, accomplishing tests under alternating biomass parameters. Parts of the main experiments were run under certain MLSS contents, where HRT was adapted to reach the targeted MLSS content.

The research at pilot scale was divided into two sections:

- Short term filtration tests - Critical flux trials under varying operational parameters (steady and unsteady state, varying MLSS and SAD_m values)
- Long term fouling tests - Continuous filtration to verify short term fouling tests and to identify daily fluctuation of sludge filterability and potential foulants (fixed SAD_m, varying fluxes)

4.2.2.3. Cleaning and Clean Water Trials

4.2.2.3.1. Side-stream Modules

Intensive clean water tests were conducted prior the start-up of the pilot plant. A special clean water column (CWC; Model Products, Wootton, UK) was set up in parallel to the aeration tank to allow an intensive mechanical cleaning of the side-stream modules and clean water tests prior to and after each test trial. The CWC consisted of approximately 200L working volume and was filled with fresh tap water for each individual test. The column was set up to enable an individual working system completely decoupled from the biomass filtration unit (Figure 4.1). The feed lines were set up to be interchangeable between feed connectors of the aeration tank and the CWC, and the retentate lines of each side-stream module were equipped with an extension to be attached for clean water trials. Permeate lines were chosen to be of flexible hose material and could therefore easily be switched from the CIP tanks of the side-stream modules to the clean water column. Temperature of the water was monitored with a submerged digital thermometer (RS, Corby, UK).

Prior to each critical flux trial, the membrane modules were methodically cleaned. Mechanical cleaning of the side-stream modules was conducted by attaching the modules to the CWC and flushing them with clean tap water under intermittent aeration. In case of heavy clogging (MT module), a series of rapid increase-decrease of aeration intensity combined with a quick 75% opening-closing of the valve situated at the MT retentate line and a moderate to high backwash intensity with clear water (tap water, $J_{20} > 35$ LMH) while the feed-line was detached proved to be most effective to push out the high density sludge causing the lumen clogging. Flushing of the membrane modules was repeated after renewing the water of the CWC until the water remained adequately clear. Clean water tests were undertaken for all side-stream modules and chemical cleaning was added when required to maintain permeability rates. Prior to each new set of experiments, chemical cleaning was conducted notwithstanding from overall permeability performance.

Chemical cleaning was undertaken with either sodium hydroxide solution (NaOH, pH 11) or sodium hypochlorite solution (NaOCl, 500 $mg.L^{-1}$ and 1000 $mg.L^{-1}$) according to the degree of fouling. Membranes were first mechanical cleaned, the clean water column was refilled with fresh water and chemicals were applied to the membranes under low flow rates via the permeate lines. It has to be noted that, according to the membrane manufacturer, an in-situ cleaning with gentle backwash was also possible for the flat sheet module (FS). Chemicals were left soaking for 2 hours and the membranes were subsequently flushed for a further 30 minutes with clean water (CWC) at an aeration rate of 0.5 $Nm^3m^{-2}h^{-1}$. Clean water tests were conducted and in cases where the permeability recovery rates showed to be lower than 90%, the cleaning procedure was repeated and the type of cleaning solution was changed when considered necessary.

4.2.2.3.2. Submerged Module

Intensive clean water test were carried out prior to installation of the HRT-control module (Figure 4.2). The submerged module served as an HRT-control module solely and was operated in continuous mode without any relaxation or backwash cycle. Chemical cleaning was conducted whenever permeability deteriorated considerably, the latest when TMP value increased above 350 mbar, which became necessary on average every 4-5 months of operation. The HRT-control module was chemically cleaned in-situ by gently backwashing in either sodium hydroxide solution (NaOH, pH 11) or sodium hypochlorite solution (NaOCl, 500 $mg.L^{-1}$ and 1000 $mg.L^{-1}$) according to the degree of fouling. The membrane was soaked for 2 hours, operation was initiated at low to moderate flux and permeability was compared to the initial clean water permeability of the virgin membrane material. In cases of insufficient results, the cleaning procedure was repeated until moderate permeability could be achieved. Intensive ex-situ cleaning became necessary once during the operation over a period of 20 months. For this ex-situ cleaning the membrane module was taken out of the bioreactor and firstly mechanically cleaned (hosed-down with tap water), and then soaked for 24 hours in 0.1% sodium hypochlorite solution. During this ex-situ cleaning procedure of the HRT-control module, the side-stream modules were operated under moderate fluxes to maintain the biomass.

4.2.2.4. Pilot Plant Performance - Start-Up Phase

After a clean water testing of the modules, the pilot plant was sludge seeded with RAS from a nearby full-scale conventionally activated sludge plant, the modules were initiated at low to moderate fluxes and permeate suction was incrementally increased or stabilised over the following weeks. The air lift aeration rate was fixed at a SAD_m value of 0.5 $N m^3 m^{-2} h^{-1}$ for each module and intermittent filtration cycles with short backwash cycles, where configuration allowed, were chosen as previously described (Table 4.3, page 48).

4.2.2.4.1. Membrane modules filtration performance

All modules showed a significant drop in permeability under biomass filtration compared to the determined clean water permeability. While the clean water permeability for the **MT** module was 720 LMH/bar, the permeability during the start-up phase dropped from 250 LMH/bar to an average of 50 LMH/bar during the operational period (Figure 4.3). Similar results were found for the **FS** module ($K_{intrinsic} \approx 950$ LMH/bar; $K_{startup} \approx 100$ LMH/bar; $K_{average} \approx 50$ LMH/bar) and **HF1** module ($K_{intrinsic} \approx 120$ LMH/bar; $K_{startup} \approx 80$ LMH/bar; $K_{average} \approx 22$ LMH/bar).

While the HF1 module already revealed a TMP increase at low flux during the first hours of operation, both the MT and the FS module only showed an increase of TMP taking place after flux increase (Figure 4.3). The flux increase during the unstabilised period was necessary as the HRT of the pilot plant needed to be decreased from 95 hours down to 32 hours. After the installation of a submerged HRT-control module (Nov 2007), the pilot plant could be operated at relevant HRTs (starting with 24 hours down to 8 hours) and all side-stream modules were able to run independently from the overall hydraulic conditions of the pilot plant.

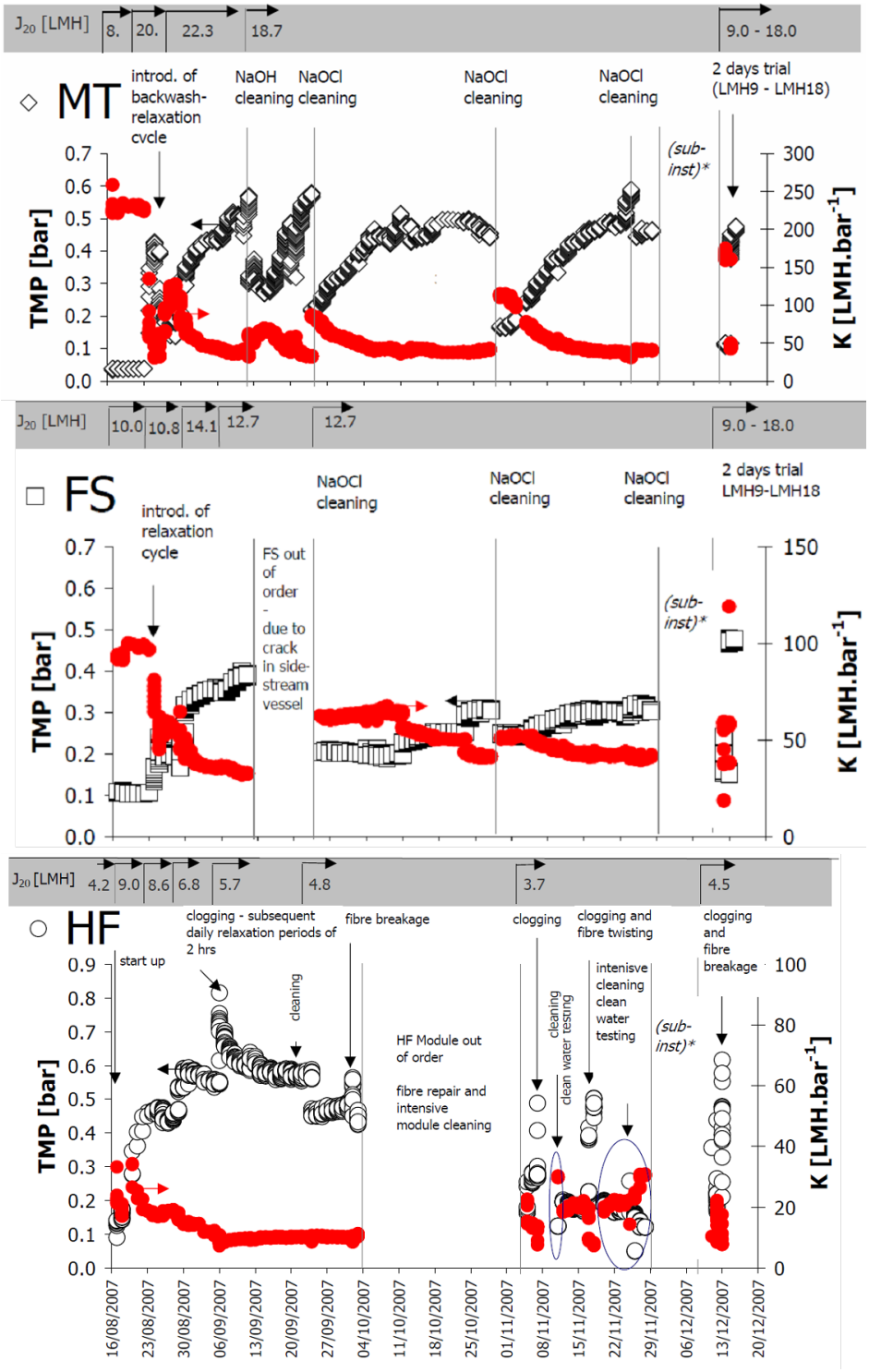

Figure 4.3.: Continuous filtration operation during start up phase from Aug 2007 - Dec 2007. Transmembrane pressure and permeability development per air-lift sidestream module. (*sub-inst. shut down of pilot plant due to installation of HRT-control module)

Multi-tubular module

Even though the module was operated at a relatively low aeration rate for this type of configuration ($SAD_m = 0.5\ N m^3 m^{-2} h^{-1}$ only) and without cross-flow pumping, the filtration performance could be kept at moderate fouling rates ($TMP < 0.5 bar$) at constant fluxes of $J_{20} \approx 18\ LMH$, where an in-situ cleaning ($1000 ppm$ of NaOCl for 2 hours) after 1.5 to 2 months seemed to be sufficient.

Flat sheet module

After a shut-down of the line due to a crack in the side-stream Plexiglas vessel, the FS module showed, similarly to the MT module, a relatively stable operational condition ($TMP < 0.25 bar$) at $J_{20} \approx 12.7\ LMH$, with an identical in-situ cleaning regime.

Hollow fibre module

The HF module revealed a steady TMP rise and hence permeability decline after having started biomass filtration even without flux increase. After one week of operation, the average trans-membrane pressure was recorded with 0.45 bar resulting in a permeability of less than 20 LMH/bar (Figure 4.3). After another week of operation (filtration cycle of 540 s / 50s off / 10 s backwash with flux of backwash equivalent to flux of filtration mode, $SAD_m = 0.5\ N m^3 m^{-2} h^{-1}$), the module exhibited a rapid increase in trans-membrane pressure resulting in a significant flux decline and a further decrease of permeability. At this stage, it was decided to increase the aeration rate from $SAD_m = 0.5\ N m^3 m^{-2} h^{-1}$ to $SAD_m = 0.75\ N m^3 m^{-2} h^{-1}$. After three weeks of operation, the module was found to be heavily clogged with biomass which resulted in a disruption of biomass cross-flow and a major TMP increase occurred from 0.55 *bar* up to 0.82 *bar*. Thereafter, the permeate flux was lowered to an average of $J_{20} \approx 5.5\ LMH$ and a daily relaxation period of 2 hours was introduced. The TMP could be stabilised at around 0.6 *bar* and after a first cleaning with a sodium hydroxide solution at pH 11 (duration: 2 hours), the TMP dropped to below 0.5 *bar*.

However, after one more week of operation ($J_{20} \approx 4.8\ LMH$, $SAD_m = 0.75\ N m^3 m^{-2} h^{-1}$), the module suddenly revealed several broken fibres (resulting in a high amount of biomass inside the CIP tank) and the fibre bundle itself was found to be twisted inside the module housing. The module was shut down and removed for a thorough cleaning and fibre repair. In total, 6 fibres were identified to have been broken and were pinned down according to the instructions given by the manufacturer. Even after a thorough cleaning was applied, it was found that, finally, the module could not be operated under stable conditions during biomass filtration for a period longer than 24 hours. The highest possible flux after an intensive cleaning procedure (recovery rate of initial permeability was 2/3 after 1000 ppm of NaOCl cleaning for 2 hours)

and one full week of clean water flushing was found to be 9 LMH, but only for clean water filtration. A filtration trial of the cleaned module with a flux of 9 LMH resulted in a complete clogging and fibre twisting after only 5 hours of operation. This setback re-occurred during trials under increased aeration rates of up to $\mathrm{SAD}_m = 1.25\ N\mathrm{m}^3\mathrm{m}^{-2}\mathrm{h}^{-1}$.

Even a biomass filtration trial of the cleaned module at a very low permeate flux of 3.7 LMH with an aeration increase from $\mathrm{SAD}_m = 0.5$ to 0.75 $N\mathrm{m}^3\mathrm{m}^{-2}\mathrm{h}^{-1}$ resulted in slight clogging at the bottom of the bundle after the first 10 hours of operation and a complete membrane vessel clogging and twisted fibre bundle after 55 hours of operation (Figure 4.4). After this, the module was sent back to the manufacturer for analysis.

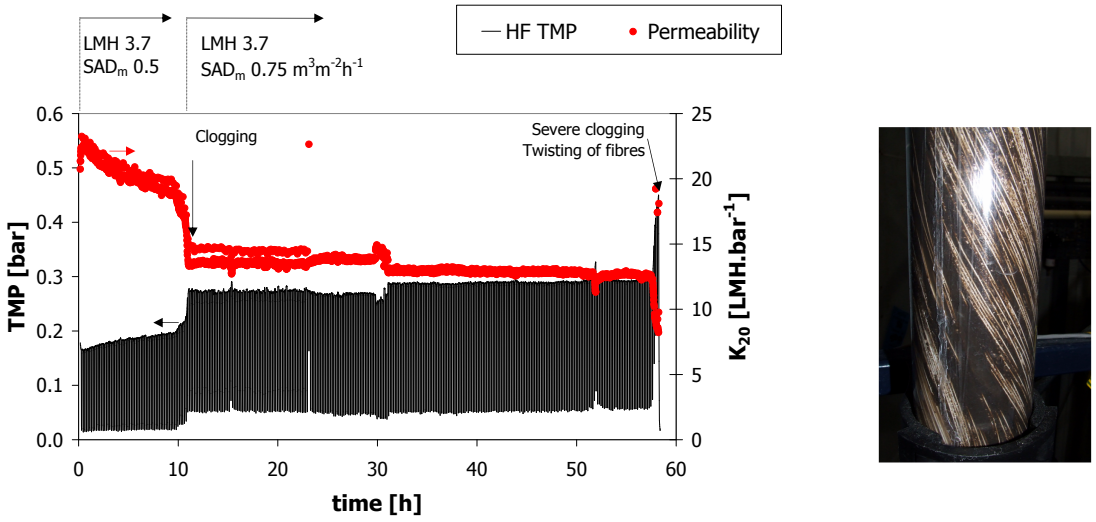

(a) *(b)*

Figure 4.4.: HF1 Module - Re-start at low flux and increased aeration rates after intensive module cleaning: reoccurring event of clogging, fibre twisting and fibre breakage. (a) TMP and permeability development, (b) picture of the clogged module with twisted fibres.

4.2.2.4.2. Biomass parameters

During the start-up phase (Aug 2007 - Dec 2007), the pilot plant biomass was adapted and partially stabilised. The HRT during the start-up period was 95 hours and was decreased to an average of 32 hours over the testing period, where a further decrease to 24 hours took place after the installation of a submerged HRT-control module (Nov 2007). The MLSS content changed from an initial value of 6.1 gL^{-1} to an average of 4.5 gL^{-1} MLSS (Table 4.4). After installation of the HRT-control module and operation at moderate HRTs, more relevant values of MLSS content could be achieved. The COD removal rates during the reported period were all within satisfactory ranges from 82.0% to 97% with an average removal rate of 95%.

Table 4.4.: HRT and biomass parameters during pilot plant start up-phase: Aug 2007 - Dec 2007

Parameter	HRT [h]	MLSS [gL^{-1}]	SMP_{Prote}	SMP_{Carb}	SMP_{DOC}	COD_{Effl} [mgL^{-1}]	COD removal [%]
Minimum	24	2.0	9.4	7.8	32.2	10.0	82.0
Maximum	95	6.1	31.8	13.6	45.2	45.6	97.2
Average	32	4.5	17.9	21.5	39.5	22.5	94.5

Initial measurements were undertaken to determine possible differences in fouling control of the three air-lift side-stream modules. Values for SMP content of proteins and carbohydrates (polysaccharides) varied between 9.4 and 31.8 mgL^{-1} for proteins and between 7.8 and 21.5 mgL^{-1} for carbohydrates (Table 4.4). No significant impact between the values of SMP content and TMP increases could be observed during this start-up period, which may, however, be due to the short period of observation and the unstabilised biomass conditions. Results for observed retention rates of potential foulants ($S_{Proteins}$, $S_{Carbohydrates}$, S_{DOC}) showed that, though operated at constant low hydraulic flux and the same aeration rates, the retention performances of each module varied significantly (Figure 4.5 - representing one week of measurements during the unstabilised period). Surprisingly, the observed carbohydrate retention of the HF module resulted in significantly high negative retention values, which may have been caused by concentration or accumulation of carbohydrates at the membrane surface, enhanced by the low air-lift efficiency observed for this particular module.

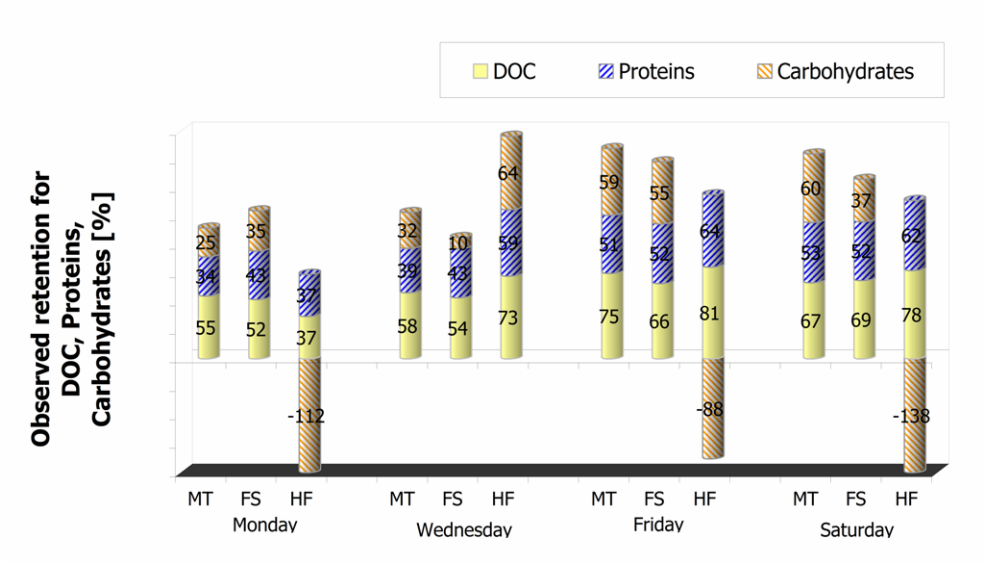

Figure 4.5.: Observed retention of SMP values during start-up period

4.2.2.4.3. Summary

During the start-up period between September 2007 and December 2007, the HF side-stream module (HF1) revealed operational problems due to re-occurring clogging of the membrane vessel. These periods of clogging made an increase of aeration necessary, which in turn seemed to cause fibre breakage. Those clogging problems seemed to occur due to an inefficient air-lift based on the narrow space between the fibre bundle and membrane holding vessel, which mainly became effective at higher operated permeate fluxes. A second HF side-stream module (HF) was commissioned, which was fitted into a specially designed holding vessel to allow a better air-lift of the biomass while simulating separation distances used at full scale. This module (HF) was operated from February 2008 onwards and all filtration performance results reported hereafter are based on that second HF module (HF). From November 2007 onwards, the HRT-control module could be installed into the bioreactor and the pilot plant was subsequently run at relevant HRTs ranging from 8 hours to 24 hours, where all pilot module trials could run decoupled from the overall hydraulic performance. Monitored SMP values did not reveal any significant impact on the TMP evaluation observed during this start-up period.

4.2.3. Bench-scale

Bench-scale tests were determined to identify the potential impact of different biomass parameters on the filtration performance of different commercially available membrane materials. The bench-scale section was divided into flat sheet materials and single-tube materials. An overview of all tested membrane materials are given in Section 4.2.1, where bench-scale materials are also specified as materials used for pilot scale experiments.

4.2.3.1. Flat Sheet Test Cell Device

Bench-scale filtration experiments were conducted on aperplex-glass membrane test cell with an active filtration area of 0.0153 m^2, a filtration path length of 170 mm and a separation distance of 9 mm (Figure 4.6).

Generally, the system was composed of a 9 L batch vessel from which the biomass, and water respectively, was pumped at constant cross-flow velocity ($0.2ms^{-1}$) by a centrifugal pump over the membrane surface (Figure 4.7).

Trans-membrane pressure (TMP) changes were monitored online (Permeate line: 0-5V pressure transducer of 0.15% FS accuracy; -0.5 to 0.5 bar and -1 to 1 bar; RM&C, Padley, UK & ALTHEN GmbH, Kelkheim, Germany. Feed and Retentate line: 0-5V pressure transducer of 0.25% FS accuracy; 0 to 1 bar; RS, Corby, UK) and fluxes were recorded. The temperature was measured (submerged thermometer; RS, Corby, UK) and regulated when necessary using a waterbath with thermostatic control (immersion thermostat GD120; Grant Instruments Ltd, Cambridge, UK).

Critical flux tests were undertaken with

- biomass derived from a full scale MBR plant (Wessex Water, Swanage: design flow for this MBR plant is given with 12.700 m^3d^{-1} and a total membrane area of 15.840 m^2. Further details see Judd, 2006)
- biomass derived from the pilot plant

Membrane materials were furthermore analysed for their clean water permeability, cake layer permeability and post-cleaning permeability using ultra pure water and a filtration protocol according to the critical flux protocol (section 4.3.1.3 and 4.3.1.2, page 63-65). Between each critical flux experiment biomass and the clean water tests, the equipment was flushed several times and the test cell including all piping systems were cleaned thoroughly with tap water and subsequently flushed with ultrapure water.

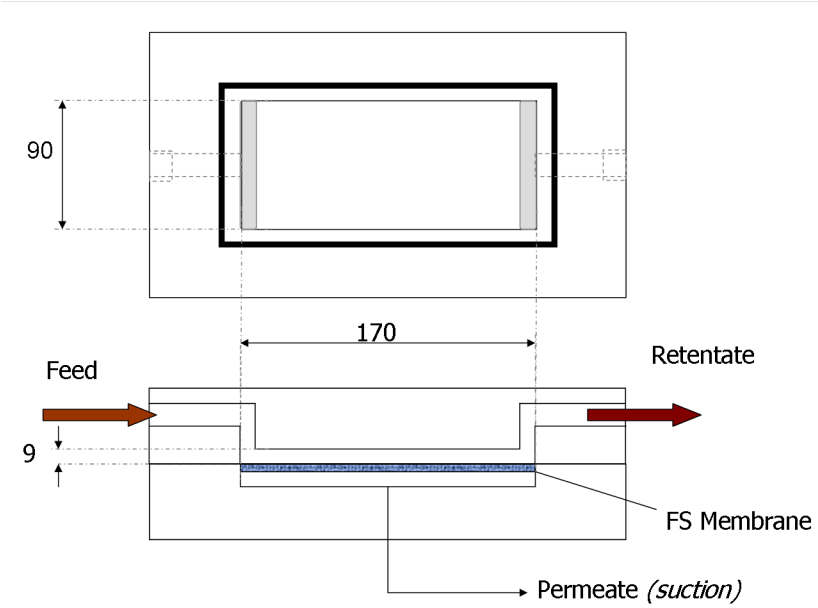

Figure 4.6.: Flat Sheet Test Cell Device: Measurements

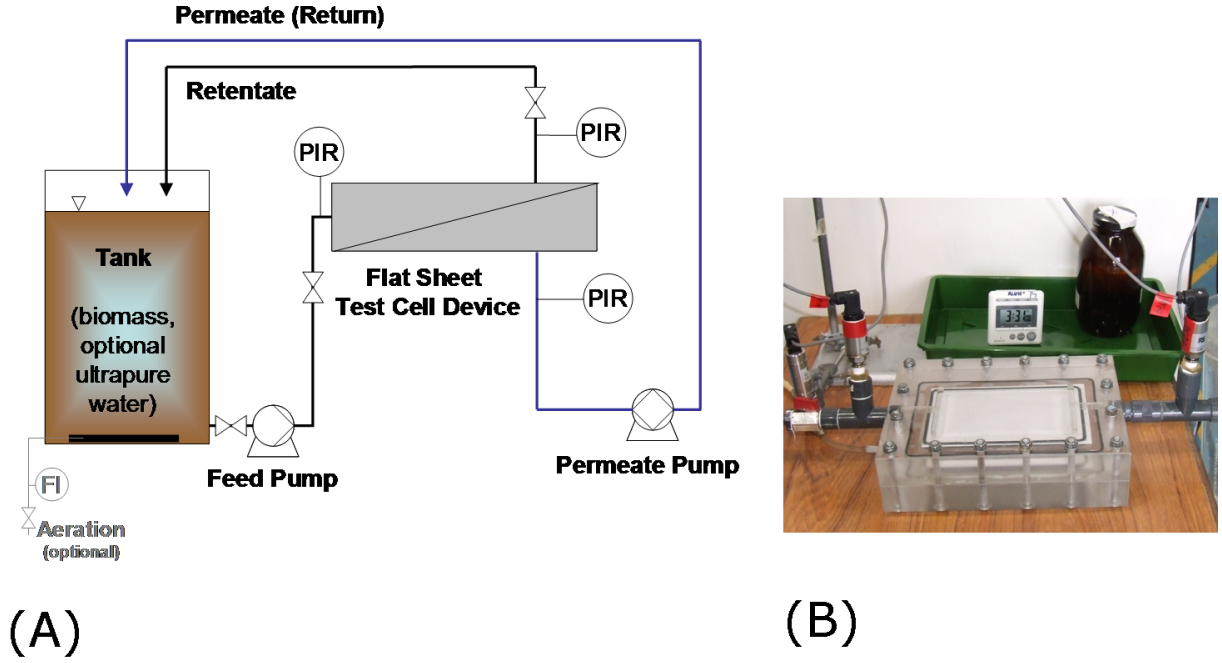

Figure 4.7.: Flat Sheet Test Cell Device: (A) Scheme of single flat sheet device and (B) Picture of flat sheet test device

4.2.3.2. Single-tube Test Device

A single-tube test cell device was set up in parallel to the existing single flat sheet device (Figure 4.8) to enable the comparison of different tube materials under tests run similarly to the flat sheet trials. Single-tubes were potted in clear persplex-glass tube (Model Products, Wootton, UK) with a length of 1.0m, providing an active filtration length of 0.97m.

Critical flux tests were undertaken with biomass deriving from the pilot plant using an incremental flux increase similar to the pilot scale experiments (section 4.3.1.2, page 63). The membrane materials were furthermore analysed for their clean water permeability, cake layer permeability and post-cleaning permeability using ultra pure water and a filtration protocol according to the critical flux protocol (section 4.3.1.3 and 4.3.1.2, page 63-65). Analogue to the flat sheet experiments, all equipment was cleaned thoroughly in between critical flux trials and clean water tests. For each test, trans-membrane pressure (TMP) changes were monitored online (Permeate line: PT of -0.5 to 0.5 bar and -1 to 1 bar, RM&C, Padley, UK & ALTHEN GmbH, Kelkheim, Germany; Feed and Retentate line: PT of 0 to 1 bar, RS, Corby, UK) and fluxes were recorded.

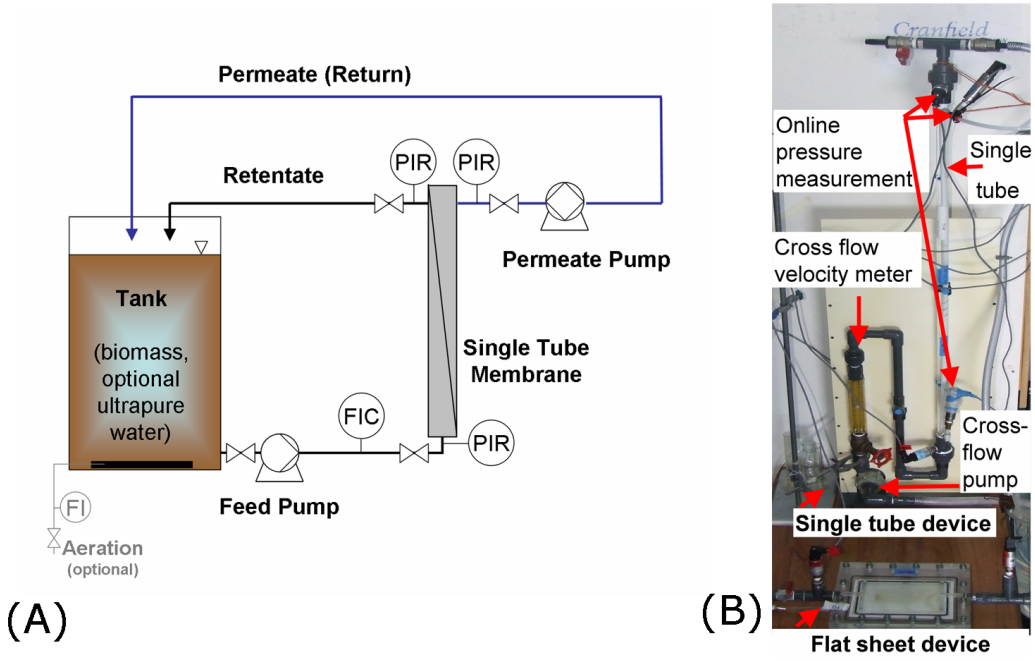

Figure 4.8.: Single-tube Test Device: (A) Scheme of single-tube test device and (B) Picture of single-tube and flat sheet test devices.

4.3. Methods

4.3.1. Membrane Characterisation

Different commercially available membranes (flat sheet material and single-tube material) were tested for their surface characteristics and filtration performances. Membrane materials tested included polymeric membranes made of PVDF, PES, PS and PE with varying pore sizes (Table 4.1). Membranes were analysed for their surface properties (RMS surface roughness, contact angle, surface energy, SEM imaging), for their filtration performance (ultra pure water permeability, critical flux trials, cake layer resistances) and also for adsorption of potential foulants onto the membrane surfaces (foulant fractionation; cake layer, reversible and irreversible fouling resistance).

4.3.1.1. Surface characterisation

4.3.1.1.1. Atomic Force Microscope - AFM

Atomic force microscopy is a powerful technique to allow imaging of non-conducting surfaces down to the sub-nanometre level without the need for any additional sample preparation.

The atomic force microscope is run in two basic modes: *contact* and *tapping*. In *contact mode* the AFM tip is in contact with the surface continuously, whereas in *tapping mode* (also called intermittent contact mode) the AFM cantilever is vibrated above the sample surface, so the tip is only in contact with the surface intermittently. This helps to reduce shear forces associated with the tip movement. For most imaging in AFM tapping mode is the recommended mode. Contact mode AFM is only used for specific applications, such as force modulation where the tip is pushed into the surface in order to measure local variations in hardness.

AFM images were taken using either a Veeco Explorer system or a Veeco Dimension 3000 (Veeco Instruments, Santa Barbara, California, USA) in tapping mode using silicon probes (SFM silicon probes, Veeco Explorer: 0.1-0.025 Ohm-cm Antimony (n) doped Si, non-coated tapping mode cantilevers for VEECO AFM; FESP-CLBR; Veeco Dimension: pointprobe plus PPP-cont with a nominal radius at 20 nm, HRF Silicon and Veeco Instruments).

4.3.1.1.2. Scanning Electron Microscopy (SEM)

A scanning electron microscope (SEM) can be a powerful analytical tool to study the structure of microfiltration membranes (pore size 0.08 to 10 μm). A beam of high-energy primary electrons hits the membrane surrounded by a vacuum, so that low-energy secondary electrons are stricken out of the very first molecule layers of the conductive material surface. The intensity of the signal, which is increasing with a decreasing distance between emitter and membrane surface, is recorded by a detector. Therefore, zones of a higher level (like areas with adsorbed foulants, for example) appear as bright spots on the screen. During the experiment, the emitter is moved along the fixed membrane, so that the whole surface structure can be scanned. Concurrently, x-rays are emitted while the membrane surface is bombarded with high energy electrons. By analysing the x-rays, the chemical composition of a sample down to 1 m depth is observable, which can be used for the identification of inorganic fouling on membranes. This is known as the electron dispersion analysis system (EDAS).

Samples were analysed using Philips XL-30 scanning electron microscopes (Philips Analytical, Munich, Germany) to provide a high resolution field emission microscopy and EDAS. A sample preparation was carried out by coating samples with palladium as the conducting layer. Images were obtained using a 10kV accelerating voltage and varying magnifications. Higher accelerating voltages were avoided as beam damage was observed on the specicims.

4.3.1.1.3. Contact Angle Measurements and Determination of Surface Free Energy

Contact angle measurements are used to characterise the wettability or hydrophobic/hydrophilic characteristics of membranes (Melin and Rautenbach, 2004). Contact angle measurements are taken using the sessile drop method, whereby a droplet of the wetting liquid was placed onto the membrane surface and the contact angle is determined by the angle between the membrane surface and the tangent at the drop boundary.

Samples were pre-washed for 24 hours in DI water (membrane surface up-side down) to remove any coating layer or dried in desiccators and kept in Petri-dishes prior to taking measurements. Membrane samples of material B and P (Table 4.1, page 43) were washed in sodium hydroxide solution (NaOH, pH 11, 40°C) to remove surface coating as indicated by membrane manufacturer.

A 10 μL drop of each wetting liquid (Table 4.5) was dispensed on the prepared membrane surface and allowed to come into equilibrium. Images of the drop were taken using a Jai-CV-M90 Interlaced CCD camera and contact angles were measured from both sides of the drop using Image Pro Plus software. Each membrane material was analysed on 10 random surface samples. All wetting chemicals were purchased from Sigma-Aldrich (Gillingham, UK) and chosen to determine the hydrophobicity and the surface free energy (van Oss, 2003) of the membrane samples (Table 4.5).

Table 4.5.: Contact angle measurement - surface tension (γ_L), surface tension components (γ_L^{LW}, γ_L^{AB}) and parameters (γ_L^-, γ_L^+) $[mJ.m^2]$ of the used high-energy contact angle liquids at 20°C

Liquid	**CAS**	γ_L	γ_L^{LW}	γ_L^{AB}	γ_L^-	γ_L^+	**Reference**
			Polar				
Water (ultrapure, 8MΩ)	7732-18-5	72.8	21.8	51.0	25.5	25.5	van Oss (2003)
Glycerol	56-81-5	64.0	34.0	30.0	57.4	3.9	van Oss (2003)
Ethylene glycol	107-21-1	48.0	29.0	19.0	47.0	1.9	Yildirim (2001)
Formamide	75-12-7	58.0	39.0	19.0	39.6	2.3	van Oss (2003)
Dimethylsulfoxide	67-68-5	44.0	36.0	8.0	30.0	0.5	Ozcan and Hasirci (2008)
			Apolar				
Diiodmethane	75-11-6	50.8	50.8		≈ 0.01	0.0	van Oss (2003)
1-Bromonaphthalene	90-3-11	44.4	44.4		0.0	0.0	Yildirim (2001)

The determination of surface free energy parameters of the membrane material was carried out according to the matrix method proposed by van Oss (2002)

$$\begin{bmatrix} (\gamma_{L1}^{LW})^{1/2} & (\gamma_{L1}^-)^{1/2} & (\gamma_{L1}^+)^{1/2} \\ (\gamma_{L2}^{LW})^{1/2} & (\gamma_{L2}^-)^{1/2} & (\gamma_{L2}^+)^{1/2} \\ (\gamma_{L3}^{LW})^{1/2} & (\gamma_{L3}^-)^{1/2} & (\gamma_{L3}^+)^{1/2} \end{bmatrix} \begin{bmatrix} (\gamma_S^{LW})^{1/2} \\ (\gamma_S^+)^{1/2} \\ (\gamma_S^-)^{1/2} \end{bmatrix} = \frac{1}{2} \begin{bmatrix} \gamma_{L1}(1+\cos\theta_1) \\ \gamma_{L2}(1+\cos\theta_2) \\ \gamma_{L3}(1+\cos\theta_3) \end{bmatrix} \tag{4.1}$$

The work of adhesion W_{SL} between water and membrane surfaces was determined according to the acidbase approach of the Young-Dupre equation (Ozcan and Hasirci, 2008; van Oss, 2002)

$$W_{SL} = 2(\sqrt{\gamma_S^{LW}\gamma_L^{LW}} + \sqrt{\gamma_S^+\gamma_L^-} + \sqrt{\gamma_S^-\gamma_L^+}) \tag{4.2}$$

and γ_{SL} as the interfacial surface tension of two interacting surfaces (e.g. membrane surface and water) according to the equation (Ozcan and Hasirci, 2008):

$$\gamma_{SL} = \gamma_S + \gamma_L - 2(\sqrt{\gamma_S^{LW}\gamma_L^{LW}} + \sqrt{\gamma_S^+\gamma_L^-} + \sqrt{\gamma_S^-\gamma_L^+}) \tag{4.3}$$

4.3.1.2. Filtration Protocol - Critical Flux, Continuous Flux

4.3.1.2.1. Critical Flux

The concept of Critical Flux has been intensively used for fouling determination of membranes in membrane filtration systems. Research studies over the last decade have created several aspects under which critical fluxes are defined (Bacchin *et al.*, 2006; Espinasse *et al.*, 2002; Field *et al.*, 1995; Howell, 1995; Le-Clech *et al.*, 2003c).

This study is using the empirical approach first described by Field *et al.* (1995) where the critical flux is defined as the flux below which *'a decline of flux with time does not occur; above it fouling is observed'* (Le-Clech, 2002), combined with a novel filtration protocol which is aimed to enable a better comparison of the respective pilot trials to membrane operation in full scale MBRs (Figure 4.9).

Critical Flux tests were undertaken with a novel filtration protocol, where the flux step consisted of two filtration cycles including relaxation and backwash where module configuration permitted (Figure 4.9 *(b)* and *(c)*). This protocol was chosen as common critical flux determination is based on sole filtration which might provide an overestimation of critical fluxes due to the absence of cake layer controlling operational parameters, such as relaxation and backwash.

To complete the research, a number of critical fluxes were undertaken, according to the classical incremental step increase (Figure 4.9*(a)*). Throughout the research, changes in flux step height became necessary to follow certain operational protocols and a summary of all critical flux filtration protocols used is provided in Table 4.6 (page 65).

4.3.1.2.2. Continuous Flux

Continuous filtration trials were undertaken for the start-up phase of the pilot plant (see Table 4.3, page 48), bench-marking trials of biomass parameters and sub-critical flux trials. All continuous flux studies were undertaken with the same filtration protocol where varying fluxes were applied (Table 4.7, page 66).

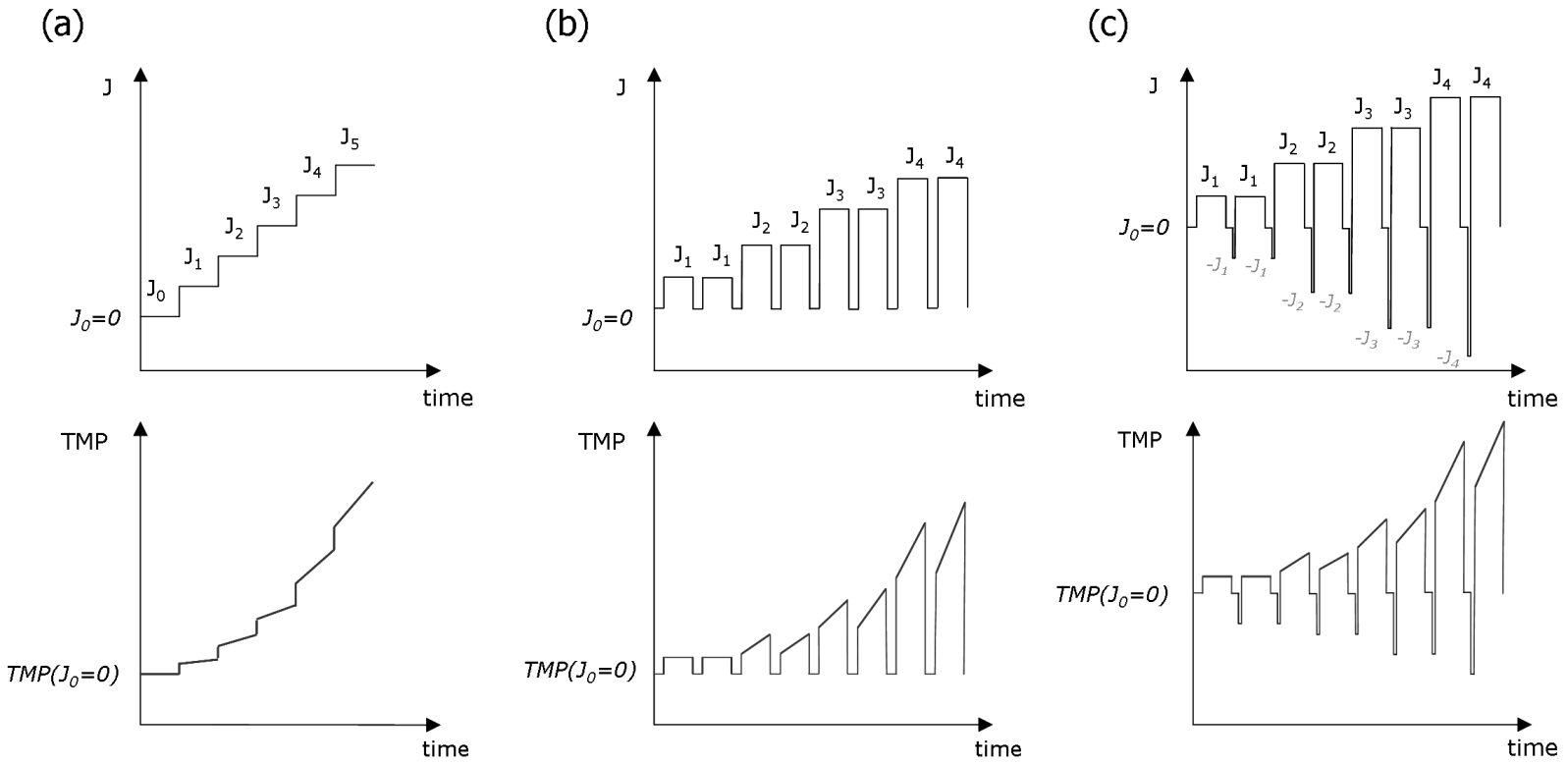

Figure 4.9.: Critical Flux Scheme: (a) classical incremental increase with no relaxation and no backwash, (b) novel filtration protocol with 2 filtration cycles per step including relaxation periods, (c) filtration protocol like *(b)* but including short backwash intervals

Table 4.6.: Summary of undertaken critical flux protocols

ID	step height	step length	filtration cycle			backwash intensity	aeration	cross-flow
	[LMH]	[filtration cycle]	filtration [s]	relaxation [s]	backwash [s]		(air)	(cf)
bench-scale - flat sheet material								
BS-1	2	one	600	-	-	-	no	constant
BS-2	3	two	540	60	-	-	no	constant
BS-3	3	two	540	60	-	-	yes	constant - air lift
bench-scale - single-tube material								
ST-1	5	one	600	-	-	equal to flux	no	constant
ST-2	5	two	540	50	10	equal to flux	no	constant
pilot-scale								
FS-1	3	two	540	60	-	-	yes	air-lift
FS-2	5	two	540	60	-	-	yes	air-lift
MT-HF-1	3	two	540	50	10	equal to flux	yes	air-lift
MT-HF-2	5	two	540	50	10	equal to flux	yes	air-lift
FS-MT-HF	5	one	900	-	-	-	yes	air-lift

BS - bench-scale flat sheet; ST - single-tube (bench-scale);

MT - multi-tubular (pilot-scale); FS - flat sheet (pilot-scale); HF - hollow fibre (pilot-scale)

4.3.1.3. Calculation of filtration parameters

4.3.1.3.1. Temperature Correction

To compensate for the increasing permeate flux with decreasing viscosity of the permeate, temperature correction was calculated according to Rautenbach and Albrecht (1989) (equation 4.4), where $T = 20°C$ was used as reference temperature and the normalised flux is indicated as J_{20}:

$$\frac{J_t}{J_{20}} = 1.025^{T-20} \tag{4.4}$$

with T = Temperature in $°C$.

Table 4.7.: Filtration protocol for continuous fluxes

Parameter	MT	FS	HF
Flux range [LMH]	3.0 - 30.0	3.0 - 30.0	3.0 - 30.0
Filtration	540 s	540 s	540 s
Relaxation	50 s	60 s	50 s
Backwash	10 s	-	10 s
Backwash intensity	equal to operated flux	-	equal to operated flux

4.3.1.3.2. Permeability

Permeability of membrane materials was conducted according the different filtration protocols applied for biomass filtration (Figure 4.9). Permeability of membranes (either bench or pilot scale) was determined using ultra pure water and following the protocol according to that applied for the individual critical flux trial, but in any case without applying the backwash option to avoid an increase in permeability; e.g for the post-sludge trial by backwashing steps. Permeability tests were conducted for the virgin membrane state (prior to first sludge exposure), cake layer permeability and reversible/irreversible fouling. Permeability was temperature corrected and expressed as K_{20} in $LMH.bar^{-1}$ according to the following equation:

$$K_{20} = \frac{J_{20}}{P} \tag{4.5}$$

4.3.1.3.3. Determination of Filtration Resistances

Membranes were analysed in bench-scale experiments for their varying permeabilities prior to, during and after sludge exposure and also after a chemical cleaning step using the respective bench-scale test devices (Section 4.2.3).

The membrane resistances were calculated using Darcy's law and applying a modified membrane resistance in-series determination (Bae and Tak, 2005; Field *et al.*, 1995). As analyses within these experiments were conducted under incrementally increasing and subsequently decreasing fluxes, the membrane resistance determination was defined for data points gained at a flux of J = 20 LMH = $J_{20(LMH20)}$ and J = 21 LMH = $J_{20(LMH21)}$.

The resistances of each step at $J_{20(LMH20)}$, $J_{20(LMH21)}$ respectively, were determined according to the following equations:

$$J = \frac{\Delta p}{\eta \cdot R_t} \tag{4.6}$$

$$\text{with } R_t = R_m + R_c + R_f \tag{4.7}$$

$$\text{and } R_f = R_{rev} + R_{irrev} \tag{4.8}$$

where

J = the permeation flux ($m^3m^2s^{-1}$)

Δp = the transmembrane pressure (TMP in Pa)

η = the viscosity of the permeate (Pa s)

R_t = the total resistance (m^{-1})

R_m = the intrinsic resistance (m^{-1})

R_c = the cake layer resistance (m^{-1})

R_f = the fouling resistance (m^{-1})

R_{rev} = the reversible fouling resistance (m^{-1})

R_{irrev} = the irreversible fouling resistance (m^{-1})

Clean water permeability of the virgin membrane material conducted with ultrapure water determined the *intrinsic membrane resistance* R_m.

The *total membrane resistance* R_t was taken as the median at the peak period ($J_{20(LMH20)}$, $J_{20(LMH21)}$) of the critical flux filtration steps under biomass filtration.

Cake layer and *reversible/irreversible fouling resistances* were determined measuring the membrane's permeabilities with ultrapure water after the biomass filtration step (post-sludge permeability, $R_{post-sludge}$=R_{m2}) and after the alkaline cleaning step ($R_{post-clean}$ = R_{m3}). The fouling resistance was subsequently calculated as R_f = R_{m2} - R_m. The reversible and irreversible fouling resistances could furthermore be differentiated from $R_{post-sludge}$ = R_{m2} and $R_{post-clean}$ = R_{m3} according to R_{rev} = R_{m2} - R_{m2} and R_{irrev} = R_{m3} - R_m.

4.3.1.3.4. Determination of Fouling Rates and Novel Critical Flux Parameters

Analyses of critical flux steps varied according to the filtration protocol applied (Table 4.6). While fouling parameters of the classical incremental flux step method were analysed according to Le-Clech *et al.* (2003c) (classical dP/dt, Figure 4.10), new parameters were introduced for the novel filtration protocol helping to illustrate further degrees of fouling rates ($dP_{p,s}/dt$ and $dP_{i,s}/dt$, Figure 4.11).

For each flux step (n) of the *classical incremental flux step method*, the initial trans-membrane pressure (TMP_i), defined as the trans-membrane pressure measured after the initial sudden increase, and the peak TMP (TMP_p), defined as the TMP value at the end of the filtration cycle, were determined as the average of 10 measurements (1 measurement/second) to compensate for deviations deriving from oscillations of the pressure gauge. From these two parameters, the average transmembrane pressure (P_{ave}), the fouling rate dP/dt (representing the slope m^n of increase in filtration resistance, Figure 4.10) and the fouling velocity dR/dt were calculated (Table 4.8).

For each flux step (n) of the *novel flux step method*, the initial (TMP_i) and peak trans-membrane pressure (TMP_p) were determined for each filtration cycle *(n_A and n_B)* resulting in four relevant TMP values per flux step: $TMP_{i,A}$, $TMP_{p,A}$ for cycle n_A and $TMP_{i,B}$, $TMP_{p,B}$ for cycle n_B (Figure 4.11).

From these TMP values, fouling parameters similar to the classical flux step method were analysed for each filtration cycle: the average trans-membrane pressure per filtration cycle ($P_{ave,A}$, $P_{ave,B}$), the fouling rate dP/dt per filtration cycle ($dP_A/dt = m_A^n$ and $dP_B/dt = m_B^n$, Figure 4.11) and the fouling velocity dR/dt per filtration cycle (dR_A/dt, dR_B/dt, Table 4.8).

To provide a possible estimation of potential fouling rates applicable for full scale filtration, it was decided to use two filtration cycles per flux step and to determine the so-called initial or root-step fouling rate $dP_{i,s}/dt$ (slope $m_{i,s}^n$) and the peak step fouling rate $dP_{p,s}/dt$ (slope $m_{p,s}^n$) between the respective filtration cycles (n_A, n_B; Figure 4.11). This method was elaborated on to ameliorate the comparability of short-term critical flux tests to long-term filtration experiments and also between different filtration protocols (fouling rate increase between backwash and non backwash critical flux trials). Furthermore, these values also enabled the calculation of novel fouling velocities between root (initial) and peak TMP values per flux step (Table 4.8).

Fouling parameters for continuous filtration trials were analysed as analogues with the initial trans-membrane pressure representing the starting point and the peak trans-membrane pressure representing the respectively indicated peak trans-membrane pressure at the indicated time interval (TMP(t_n)).

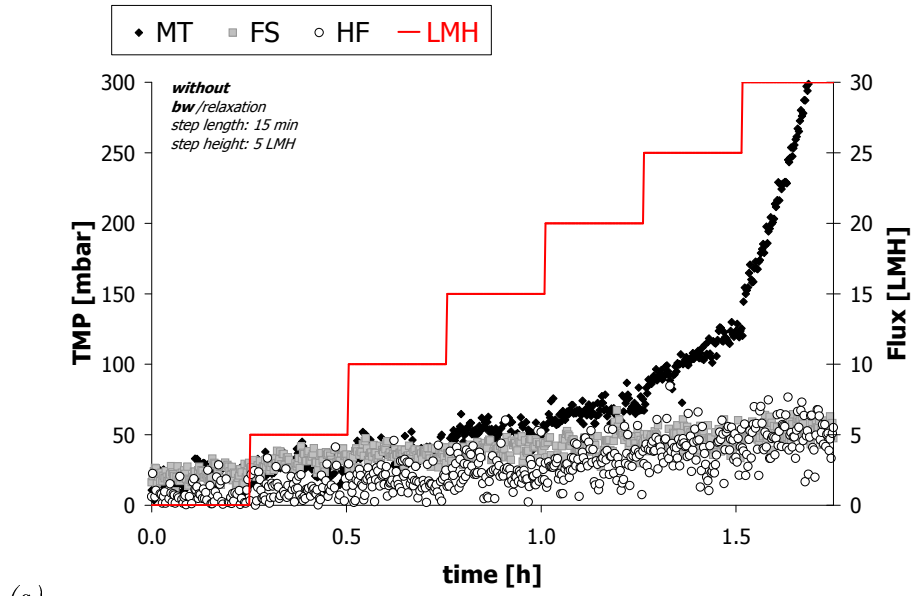

(a)

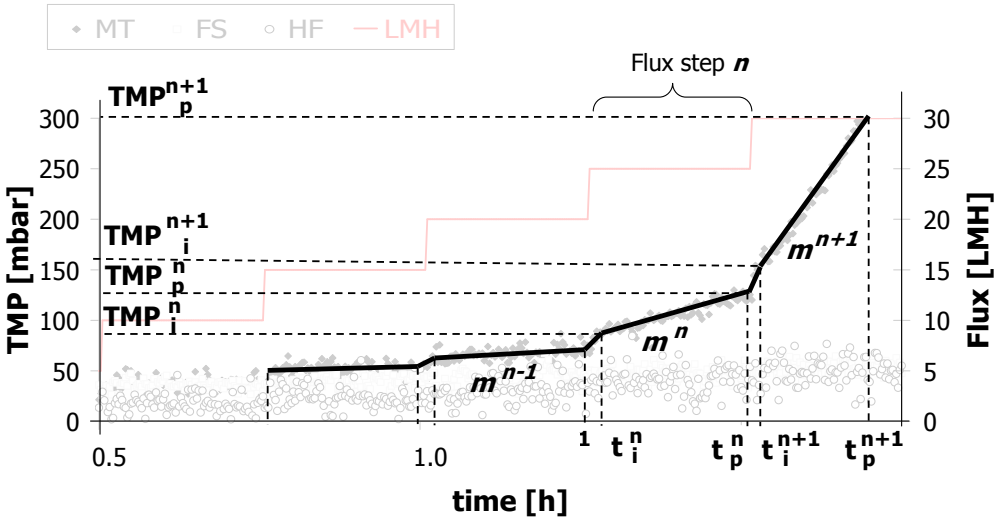

(b)

Figure 4.10.: Critical flux determination of classical incremental flux step: *(a)* Sample curve - illustration of first 6 flux steps; *(b)* Determination of dP/dt according to Le-Clech *et al.* (2003c).

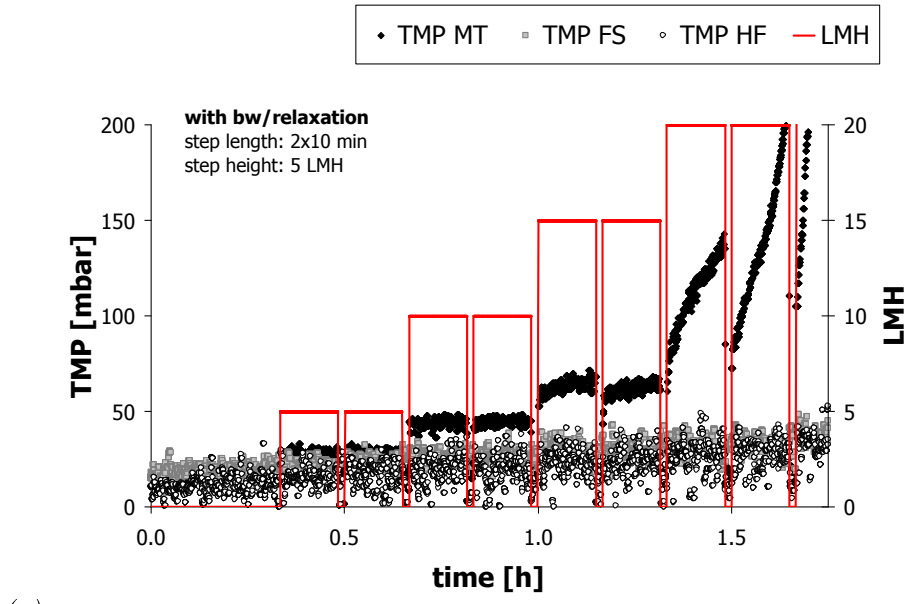

(a) *(b)*

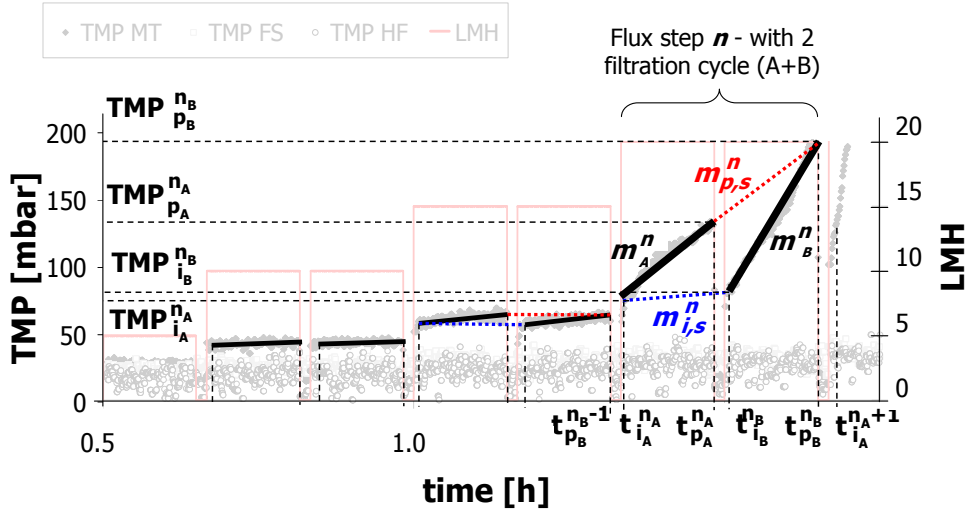

Figure 4.11.: Critical flux determination for novel filtration protocol: *(a)* Sample curve - illustration of first 4 flux steps; *(b)* Determination of dP/dt, $dP_{p,s}/dt$, $dP_{i,s}/dt$.

Table 4.8.: Critical flux determination - Data analysis

Parameter		Symbol	Unit	Calculation
general equations				
Flux		J_{20}	L.m^{-2}h^{-1} ($\equiv LMH$)	Equation 4.4; page 65
Mean permeability		$K_{20,ave}$	LMH.bar^{-1}	Equation 4.5; page 66, with $P = P_{ave}$
Resistances (total, fouling, cake layer)		R_t, R_f, R_{cl}	m^{-1}	Equation 4.6,4.7; page 67
classical incremental flux step method - without backwash [1]				
Mean trans-membrane pressure		P_{ave}	mbar	$P_{ave} = \frac{TMP_i^n + TMP_p^n}{2}$
Fouling rate	classical	dP/dt	mbar.min^{-1}	$dP/dt\ (\equiv m^n) = \frac{TMP_p^n - TMP_i^n}{t_p^n - t_i^n}$
Fouling velocity	classical	dR/dt	m^{-1}.s^{-1}	$dR/dt = \frac{R(TMP_p^n) - R(TMP_i^n)}{t_p^n - t_i^n}$
novel filtration protocol - including backwash/relaxation [2]				
Mean trans-membrane pressure		P_{ave}	mbar	$P_{ave(A,B)} = \frac{TMP^n_{i(A,B)} + TMP^n_{p(A,B)}}{2}$
Fouling rate	classical	dP/dt	mbar.min^{-1}	$dP/dt\ (\equiv m^n_{A,B}) = \frac{TMP^n_{p(A,B)} - TMP^n_{i(A,B)}}{t^n_{p(A,B)} - t^n_{i(A,B)}}$
	root,step	$dP_{i,s}/dt$	mbar.min^{-1}	$dP_{i,s}/dt\ (\equiv m^n_{i,s}) = \frac{TMP^n_{i,B} - TMP^n_{i,A}}{t^n_{i,B} - t^n_{i,A}}$
	peak,step	$dP_{p,s}/dt$	mbar.min^{-1}	$dP_{p,s}/dt\ (\equiv m^n_{p,s}) = \frac{TMP^n_{p,B} - TMP^n_{p,A}}{t^n_{p,B} - t^n_{p,A}}$
Fouling velocity	classical	dR/dt	m^{-1}.s^{-1}	$dR/dt = \frac{R(TMP^n_{p(A,B)}) - R(TMP^n_{i(A,B)})}{t^n_{p(A,B)} - t^n_{i(A,B)}}$
	root,step	$dR_{i,s}/dt$	m^{-1}.s^{-1}	$dR_{i,s}/dt = \frac{R(TMP^n_{i,B}) - R(TMP^n_{i,A})}{t^n_{i,B} - t^n_{i,A}}$
	peak,step	$dR_{p,s}/dt$	m^{-1}.s^{-1}	$dR_{p,s}/dt = \frac{R(TMP^n_{p,B}) - R(TMP^n_{p,A})}{t^n_{p,B} - t^n_{p,A}}$

With: ^{n}: step number; $_i$: initial; $_p$: peak; $_s$: step; $_{A,B}$: filtration interval of step (s↪B-A).

For detailed illustration of calculation parameters: see [1] Figure 4.10*(b)*; [2] Figure 4.11*(b)*

4.3.1.4. Fractionation of Potential Foulants

To identify the effect of potential foulants on the overall filtration performance of the membrane materials, bench-scale materials and long-term exposed pilot and full scale materials were examined for potential attached foulants, such as colloidal carbons, proteins and carbohydrates.

4.3.1.4.1. Bench-scale material

Following the biomass filtration trial (critical flux step), membranes were analysed for their potential attached foulants, divided into cake layer foulants and removable foulants (reversible fouling) which were extracted using an ultrapure water (cake layer) and alkaline cleaning (reversible fouling) step.

Flat sheet membrane material was placed in a zipper bag, and for cake layer removal $50mL$ of deionised water, and for alkaline cleaning step (reversible fouling) $50mL$ of NaOH solution (pH 11), were added to the sample. The materials were flattened and immersed in solution, and were shaken at a bench-top platform shaker (Fisher Scientific, Loughborough, UK); for ultrapure water solution for 1 hour at $200rpm$ and for NaOH for 2 hours at $200rpm$. The solutions were collected and analysed for their protein, carbohydrate and organic carbon content, while the membranes were subsequently analysed for their permeability.

Single-tube membranes were analysed according to the protocol of the flat sheet membranes, while the amount of cleaning solution (ultrapure water, NaOH-solution) was reduced to $40mL$ and the membranes were thoroughly closed on the top and bottom of the membrane to avoid any liquid loss prior to placing the tubes on the bench-top platform shaker.

4.3.1.4.2. Pilot-scale and full-scale material

Pilot-scale flat sheet modules and material deriving from long-term used full-scale flat sheet modules were also analysed for foulants attached to the surfaces. Membranes were separated in grid squares sizes according to the flat sheet test cell device and ultrapure water permeability was performed prior to and after cleaning steps (ultrapure water cleaning, NaOH-cleaning). Solutions for analyses of potential attached foulants were collected during the cleaning procedure according to the protocol described previously.

4.3.2. Wastewater and Biomass Characterisation

4.3.2.1. Sampling

Samples for analysis were collected in wide neck amber glass bottles (Fisher Scientific, Loughborough, UK) which had been pre-cleaned thoroughly and rinsed in acetone. Sample points at the pilot plant were the middle of the aeration tank, the retentate lines of the air-lift side-stream modules and the individual permeate lines. Samples were collected according to the individual test trial run, which were

- *continuous run:* three times a week
- *critical flux trials:* one sample of biomass tank at the start of the experiment and a full set of sampling at the advancing step of $J = 30\ LMH$

Samples for *bench-scale tests* were taken at the start of experiment (biomass sample) and at advancing step of $J = 20\ LMH$ (biomass and permeate). Samples were taken immediately to the laboratories of Cranfield University and stored in the wastewater cold room at $4°C$ until analysing was conducted, not longer than 3 hours after sampling.

4.3.2.2. SMP and EPS extraction

4.3.2.2.1. Preparation of Solid Free Fraction (SMP)

Preparation of wastewater and sludge fractions (supernatant) free of suspended solids was required for the determination of soluble COD, soluble protein, soluble carbohydrates, nitrite, nitrate and DOC, UV and turbidity analyses. The solid free fractions of sludge samples were prepared by centrifuging samples for 10 minutes at different speed rates/centrifugal forces:

- 3,000 g
- 4,5000 g
- 10,000 g

in a Rotana 96 R centrifuge (Hettich, Tuttlingen, Germany). The supernatant produced was decanted and filtered through a glass fibre filter (Schleicher and Schuell, Grade GF 52) to remove any residual suspended particles. Raw wastewater samples were filtrated without the centrifuging step. Sample analyses according to the common protocol of EUROMBRA were undertaken at a centrifugal force of 10,000 g and are the results which are reported most in this thesis unless otherwise stated.

4.3.2.2.2. Extraction of Extracellular polymeric substances (EPS)

Samples for analysis of extracellular polymeric substances (EPS) were prepared according to two different protocols which were

1. extraction via a heating method
2. extraction with cation-exchange resin (CER).

4.3.2.2.2.1. EPS extraction via heating method

Extracellular polymeric substances (EPS) extraction was based on a modified heating method according to Zhang *et al.* (1999). 200 ml of biomass of a thoroughly mixed activated sludge sample was centrifuged at 10,000g for 10 minutes and the supernatant was decanted. 200 ml of DI water was added to the sludge pellet and the content was thoroughly mixed (hand shaken) to resuspend the sludge pellet. The samples were placed into a water bath and heated at 80°C for 10 minutes. The bottles were centrifuged while still hot at 10,000 g (4,500 g respectively) for 20 minutes. The supernatant was filtrated through a 70 mm Schleicher & Schuell Grade GF 52 glass fibre filter paper (Patterson Scientific, Bedfordshire, UK). The supernatant gained was used for analysis of (cell-bound) EPS (= EPS_{HEAT}).

4.3.2.2.2.2. EPS extraction via CER

Extracellular polymeric substances (EPS) extraction using a cation-exchange resin (CER) was undertaken according to protocol reported by Frølund *et al.* (1995, 1996).

The buffer solution with pH 7.0 consisted of 2 mM Na_3PO_4, 4 mM NaH_2PO_4, 9 mM NaCl and 1 mM KCl (all chemicals Fisher Scientific, Loughborough, UK). The cation-exchange resin (CER) was supplied from Dowex® Marathon® (91973, Sigma-Aldrich, Gillingham, UK).

70-75g CER was weighed out per gram of volatile suspended solids (gVSS) of the sludge sample and equilibrated for 1 hour in the buffer solution (pH7). A 200mL sludge sample was centrifuged at 2,000g *(10,000g respectively)* for 10 minutes at 20^{o}C. The supernatant was removed ('centrifugate'= soluble microbial products (SMP)) and the sludge pellet was re-suspended in a buffer solution to reach a final volume of 200mL. The re-suspended sludge was transferred to an extraction vessel and the equilibrated cation-exchange resin (70-75g per gVSS) was added.

The suspension was stirred for 2 hours at 600ppm and subsequently the CER was allowed to settle. The supernatant was removed and centrifuged at 10,000 g for 10 minutes at 20^o and filtered through a 70 mm Schleicher & Schuell Grade GF 52 glass fibre filter paper (Patterson Scientific, Bedfordshire, UK). The supernatant gained was used for analysis of (cell-bound) EPS (= EPS_{CER}).

4.3.2.3. Standard analytical procedures

Temperature and dissolved oxygen (DO in mgL^{-1}) were measured on-site using a Jenway 9071 portable dissolve oxygen meter. Samples were analysed at the laboratories using the following standard analytical tools and procedures (Table 4.9).

Table 4.9.: Analytical standard methods

Parameter	Unit	Equipment/Tools
pH	-	HI 8424 pH meter (Hanna Instruments, Leighton Buzzard, UK)
Conductivity	μS	Jenway 3540 pH and conductivity meter (Camlab Ltd, Cambridge, UK)
Turbidity	NTU	Turbidimeter Hach 2100N (Camlab Ltd, Cambridge, UK)
Dissolved organic carbon (DOC)	mgL^{-1}	Organic carbon analyser Shimadzu TOC-5000A (Shimadzu, Milton Keynes, UK)
Chemical Oxygen Demand (COD)	mgL^{-1}	Merck Cell Tests (Merck (VWR International), Poole, UK)
Ammonium (NH^{4+})	mgL^{-1}	Merck Cell Tests; Merck (VWR International), Poole, UK
Nitrate (NO^{3-})	mgL^{-1}	Merck Cell Tests; Merck (VWR International), Poole, UK
Nitrite (NO^{2-})	mgL^{-1}	Merck Cell Tests; Merck (VWR International), Poole, UK
Phosphate ($PO_4{}^{3-}$)	mgL^{-1}	Merck Cell Tests; Merck (VWR International), Poole, UK

4.3.2.4. Protein and Carbohydrate determination

4.3.2.4.1. Protein determination

Protein concentration was measured using a modified method according to Lowry *et al.* (1951) and Frølund *et al.* (1995). *Reagents* were all purchased from Sigma-Aldrich (Gillingham, UK) and prepared as follows: A: 143 mM NaOH and 270 mM Na2CO3
B: 57 mM CuSO4
C: 124 mM Na2-Tartat
D: mixture of reagents A, B, C in ratio of 100:1:1 (always prepared on day of measurements)
E: Folin-Cioucalteu-reagent (1:2 in DI water)

The analysis was carried by adding $1.5mL$ of sample into a thoroughly pre-cleaned glass cell test tube and mixed rapidly with $2.1mL$ of reagent D using a Vortex-Mixer (Fisher Scientific, Loughborough, UK) and left for 10 minutes at room temperature. $0.3mL$ of reagent E was added rapidly (Vortex-Mixer), the test tube was sealed with a lid and subsequently left for another 45 minutes at room temperature. Samples were always analysed in triplicates.

Adsorption was measured at $750nm$ (AquaNova 6000 spectrophotometer, Camlab, UK) against an ultra pure water blank. For CER extracted EPS samples, the extraction buffer solution was used as blank. Measurements were taken three times from each tube by turning the tube slightly within the spectrophotometer cell to reduce influences of tube surface anomalies. Where necessary samples were diluted to keep adsorbance below 1.0.

Calibration was carried out with protein standard bovine serum albumin (BSA, Sigma-Aldrich, Gillingham, UK) as Protein Standard. As the standard curve for calibration adsorbance against protein concentration (Figure 4.12) is not linear (Lowry *et al.*, 1951), the Protein concentration (P in mgL^{-1}) was calculated according the following equation (Coakley and James, 1978):

P = *Protein [mg/L]:*

$$P = \frac{87.829 \cdot A}{1-0.403 \cdot A} \tag{4.9}$$

where A = *mean of measured absorbance:*

$$A = \frac{P}{0.403 \cdot P+87.829} \tag{4.10}$$

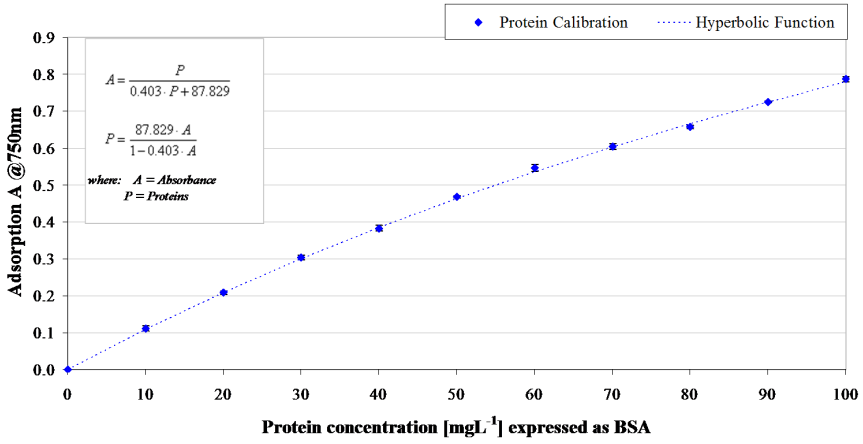

Figure 4.12.: Protein Calibration with BSA solution

4.3.2.4.2. Carbohydrates

Carbohydrates were analysed according to Dubois *et al.* (1956).

Reagents
5% (w/w) phenol solution (Sigma - Aldrich, Gillingham UK)
97% sulphuric acid (97%Fisher Chemicals, Loughborough, UK)

The *analysis* was undertaken by pipetting $1.0mL$ of sample into a thoroughly pre-cleaned glass cell test tube, then $1mL$ of 5% phenol-solution was added and mixed thoroughly using a Vortex-Mixer (Fisher Scientific, Loughborough, UK). Samples were left for 10 minutes at room temperature and $5mL$ of 97% sulphuric acid was added rapidly (in stream) to ensure a fast reaction of both reagents (heating reaction). Samples were left for cooling for 5 minutes at room temperature, and tubes were sealed and mixed again. After another 25 minutes left at room temperature, the samples were measured for their adsorbance. Samples were always analysed in triplicates.

Adsorption was measured at $490nm$ (AquaNova 6000 spectrophotometer, Camlab, UK) against an ultra pure water blank. For CER extracted EPS samples the extraction buffer solution was used as blank. Measurements were taken three times from each tube by turning the tube slightly within the spectrophotometer cell to reduce influences of tube surface anomalies. Where necessary, samples were diluted to keep adsorbance below 1.0. Calibration (Figure 4.13) was carried out using glucose as standard (D-glucose monohydrate).

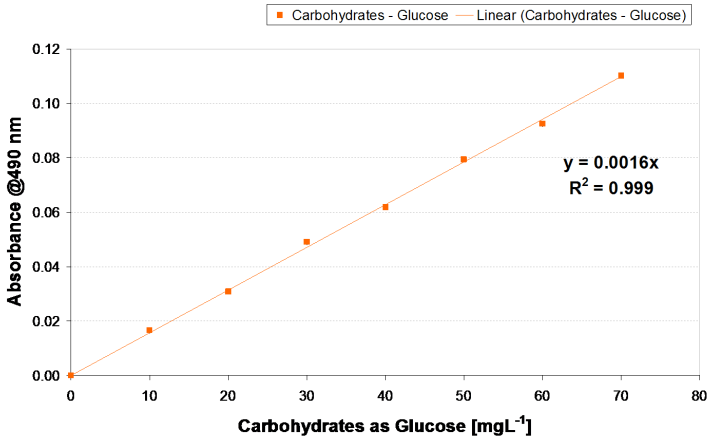

Figure 4.13.: Carbohydrate Calibration with glucose as standard solution

4.3.2.5. UV-VIS Adsorbance - SUVA

Ultraviolet absorbance at a wavelength of $254nm$ (UV_{254} in m^{-1}) was measured using UV quartz cuvette and a Jenway UV/Visible spectrophotometer (Jenway 6505, Patterson Scientific Ltd, Luton, UK), where ultra pure water was used as a blank for calibration.

Specific UV absorbance (SUVA) was calculated as the UV absorbance at $254nm$ (m^{-1}) divided by the DOC (mgL^{-1}) using the following equation:

$$\text{SUVA } [Lmg^{-1}m^{-1}] = \frac{UVA}{DOC} \cdot 100 \tag{4.11}$$

$$\text{with UVA } [cm^{-1}] = \frac{A}{d} \tag{4.12}$$

where

UVA = the calculated UV absorbance of the sample in cm^{-1}

A = the measured UV absorbance at 254nm

d = the quartz cell path length in cm^{-1}

4.3.2.6. High performance size exclusion - HPSEC

HPSEC analysis using a High Pressure Liquid Chromatography (HPLC) apparatus (Shimadzu VP series, Shimadzu, Milton Keynes, UK) was undertaken for liquid samples analogues a method used by Germain (2004). A BIOSEP-SEC-S3000 column was used with a 7.8 mm inner diameter x 30 cm and was fitted with a GFC-3000 disc 4.0 mm inner diameter x 30 mm and a security guard column (Phenomenex UK, Cheshire, UK). The UV detection was set to a wavelength of 254 nm.

Elution times from protein with known molecular weights (Sigma Aldrich, UK) were determined according to Germain (2004) (Table 4.10):

Table 4.10.: Elution times from protein with known molecular weights (Germain, 2004)

Molecular weight [kDa]	**Elution time [min]**
12.4	8.72
29	8.55
66	7.12
150	6.81
200	6.38
443	5.83
669	5.69

4.3.2.7. Mixed liquor suspended solids, total solids and volatile solids

4.3.2.7.1. Suspended Solids - MLSS content

Suspended Solids (SS) or Mixed Liquor Suspended Solid (MLSS) content is determined by Standard Method 2540D (APHA, 1998). Schleicher & Schuell Grade GF 52 glass fibre filter papers (Patterson Scientific, Bedfordshire, UK) are ignited in a furnace at 550°C for 1 hour and then cooled in a desiccator until required. The pre-ignited filter papers are weighed immediately prior to use. Well mixed samples are filtered under a vacuum through the pre-ignited and pre-weighed filter papers. The volume is chosen to yield a dried residue between 2.5 mg and 200 mg. The filter papers are subsequently dried in an oven at 105°C overnight, cooled in a desiccator and reweighed. The suspended solids content is calculated according to the following equation:

$$\text{SS } [\text{mgL}^{-1}] = \frac{(m_{105} - m_c) \cdot 1000}{V_s} \tag{4.13}$$

where

m_{105}= weight of dried residue + dish in mg

m_c = weight of crucible in mg

V_s= volume of sample in mL

4.3.2.7.2. Total Solids

Total solids (TS) is determined by Standard Method 2540B (APHA, 1998) for liquid samples. Porcelain crucibles are pre-ignited in a furnace at 550°C for 1 hour and cooled in a desiccator until required. The crucibles are pre-weighed and fluid sludge is pipetted together with a well-mixed homogeneous sample into the pre-weighed crucible. The volume of sample is chosen in a volume of 10 to 30 mL to yield a residue of between 2.5 mg and 200 mg. The crucible is left overnight in a 105°C drying oven and the evaporated samples are transferred to desiccator for cooling and then re-weighed. Total Solids (TS in mg total solids per L) content is determined according to the following equation:

$$\text{TS } [\text{mgL}^{-1}] = \frac{(m_{105} - m_c) \cdot 1000}{V_s} \tag{4.14}$$

where

m_{105} = weight of dried residue + dish in mg

m_c = weight of crucible in mg

V_s = volume of sample in mL

All analysed sludge samples are carried out in triplicates. The cycle of drying, cooling, desiccating and weighting is repeated until a constant weight is obtained, or until weight change is less than 4% of previous weight or 0.5 mg, whichever is less.

4.3.2.7.3. Volatile Solids

Volatile Suspended Solid (VSS) and Volatile Total Solid (for liquid samples, VTS) contents are determined by Standard Method 2540E (APHA, 1998). The residue obtained from Standard Method 2540D (SS) and 2540B (TS) respectively are ignited at 550° C for 2 hours in a furnace and then cooled in a desiccator upon removal. The dish (crucible or filter paper) is re-weighed and the volatile solids content is calculated according to equation below.

$$\text{VSS, VTS } [\text{mgL}^{-1}] = \frac{(m_{105} - m_{505}) \cdot 1000}{V_s} \tag{4.15}$$

where

m_{105} is the weight of the dish containing the dried mass, in mg

m_{505} is the weight of the dish containing the ignited dry mass, in mg

V_s is the volume of sample in mL

4.3.2.8. Particle Size and particle surface

Sludge particle sizes were measured using the Malvern Mastersizer 2000 particle analyser (Malvern Instruments Ltd, Worcestershire, UK). The Mastersizer uses an optical unit to detect the light scattering pattern of sludge particles dispersed in deionised water. Diluted sludge suspensions were circulated through a measurement cell where the particle fields were exposed to an analysing laser beam. The pattern of light scatter could be used to calculate the particle sizes that created the scatter by using Mie theory, which predicts the way light is absorbed and scattered by spherical particles.

All sludge samples were analysed using the same standard operating procedure. The stirrer was set at 350 rpm. Sludge samples were added to the water tank (filled with permeate from

the respective membrane modules), supplying the particle suspension to the measurement cell until the laser obscuration (fraction of light lost by scattering and absorption from the analyser beam) was between 10% and 20%. Ten measurement cycles are taken with a 3 second delay between cycles and an average measurement is calculated. The measurement time was set at 20 second (at 1000 snaps/second) in order to ensure that particle size distributions of the sludges were adequately represented by allowing coarser particles enough time to flow through the measurement beam.

The Mastersizer measurement is volume-based and according to Mie theory, assumes that the particles causing light absorption and scatter are perfect spheres. Consequently, the results are both volume based and expressed in terms of equivalent spheres. The percentage volume of particles is plotted against particle size (μm). The following parameters were reported:

- Mass Median Diameter (D [v, 0.5]): the particle size (μm) at which 50% of the sample is smaller and 50% is larger
- D [v, 0.1]: the particle size (μm) below which 10 % of the sample lies
- D [v, 0.9]: the particle size (μm) below which 90 % of the sample lies
- D [4, 3]: the volume mean diameter (μm)
- D [3, 2]: the surface area mean diameter (sauter mean) (μm)
- SpSA: specific surface area (m^2g^{-1})

To assess the potential floc rupture which was expected to have occurred due to exerted shear on the biomass while passing the side-stream modules, the **particle fractionation (FI)** was calculated using the following equation:

$$\text{FI } [\%] = \frac{d_{0.5RET}}{d_{0.5AT}} \cdot 100 \tag{4.16}$$

where

$d_{0.5\ \text{RET}}$ = particle size of the retentate line

$d_{0.5\ \text{AT}}$ = particle size of the aeration tank

4.4. Statistical Analyses

Describing membrane fouling by comprehensive mechanistic model seems to be currently impossible due to the very complex interaction of biomass make-up, configuration and membrane properties (Drews, 2010).

Due to the complex interaction, a statistical analysis was performed to assess the potential impact of determined foulants on membrane filtration performance or membrane fouling by applying simple linear Person correlation using the data software STATISTICA (StatSoft, Inc.).

As parameters may not be linear dependent, and some data in this work did not provide enough sets to allow a sufficient degree of freedom for tailored tests, data points were furthermore compared graphically for assessing empirical relationship. Generally, graphical data plots were compared applying linear or potential correlation, but where necessary the best-fit was provided for assessing potential empirical correlation.

5. Results and Discussion: Critical flux trials under different flux step protocols

5.1. Scope

The phenomenon of fouling of membranes within MBR filtration processes still remains a process difficult to predict. This is likely due to the very complex interaction of membrane material, hydrodynamic configuration and biomass make-up. Due to the complexity of the system, describing critical fluxes by a comprehensive mechanistic model is to-date considered as impossible (Drews, 2010). Short-term tests are therefore an inevitable tool to compare filtration performances of membranes (material or configuration) and to predict the membranes applicability within the media to be filtered. Filtration modes such as relaxation or backwash are routinely applied within full scale applications as fouling control parameters (Judd, 2006; Stephenson *et al.*, 2000) and are thus important parameters which might need to be considered when modelling fouling propensity within short-term tests, especially when comparing different membrane configurations.

The classical flux step protocol (Field *et al.*, 1995), probably most commonly used within many research studies (Bacchin *et al.*, 2006), is, however, limited to continuous filtration and is hence not allowing representation of the differences between the varying membrane configuration. Moreover, the fouling determined for each subsequent step is prestressed by the existing fouling of its precursor step which might lead to an overestimation of the critical flux and which furthermore does not allow prediction of reversibility (Bacchin *et al.*, 2006). For instance, Le-Clech *et al.* (2003c) reported higher TMP values during the decreasing loop than during the increasing loop for all critical flux trials conducted.

To identify the applicability of short-term critical flux tests for use in a full scale operation facilitating a comparison between different membrane module configurations, two different filtration protocols were applied under fixed aeration rates (SAD_m in $m^3 m^{-2} h^{-1}$ of 1.5 (MT) and 1.0 (FS, HF)):

a) classical incremental flux step protocol according Le-Clech *et al.* (2003c)

b) novel filtration protocol with 2 filtration cycles per flux step, including relaxation and backwash

The tests were conducted according to the filtration protocol described previously (see Material & Methods section 4.3.1.2, page 63) and data analyses for fouling parameters were conducted according to the determination methods described in the Material & Methods section 4.3.1.3 (page 65).

Repetition trials for each filtration mode at fixed aeration rates were undertaken at a MLSS content of 12 g.L^{-1} ($n = 4, 6$) and tests were completed with duplicated trials ($n = 2, 3$) at two further MLSS values (3-4 g.L^{-1}, 6-7 g.L^{-1}, see Chapter 6). It was aimed to undertake critical flux trials as sets at varying seasons whereas each individual test series within the set were undertaken within the shortest period of time, to avoid changes in biomass. Finally, the novel filtration protocol was also deployed for consecutive filtration runs and sub-critical long-term fouling trials (Chapter 6). To complete the study, filtration experiments on bench-scale materials were conducted in parallel to the pilot scale filtration trials.

A comparison of TMP vs. flux profiles between both flux step methods revealed the anticipated discrepancy between classical fouling rates dP/dt of the individual filtration steps (Figure 5.1). While the classical flux step method commonly showed higher fouling propensity (higher P_{ave}, lower $K_{20,ave}$) than the backwash/relaxation flux step protocol, classical dP/dt rates were found to be higher for the backwash/relaxation filtration mode due to the nature of the filtration cycle.

This effect could be well observed especially for higher fluxes and for declining steps (illustrated for the MT module in Figure 5.1). Similar results were observed by Germain (2004), where higher fouling rates (expressed as dP$/d$t) were reported for critical flux trials with backwash than for classical critical flux trials while overall filtration performance increased whilst applying backwash mode.

As higher classical dP/dt rates for the novel flux step protocol were anticipated, the novel flux step protocol consisted consequently of two filtration cycles per flux step, which subsequently allowed the calculation of fouling parameters expressed as dP/dt or dR/dt as either *classical* dP/dt, *root (initial) fouling rate* $dP_{i,s}/dt$ or *peak fouling rate* $dP_{p,s}/dt$ per flux step (Table 4.8, page 71), whereas preference should be given to the peak fouling rate $dP_{p,s}/dt$ due to the potential depiction of fouling incline expected over long term filtration.

All parameters indicated in Table 4.8 (page 71) were calculated for each individual test and assessed for their relevancy on the fouling propensity of the respective module and a selection of the most pertinent results will be represented and discussed during the following sections.

Furthermore, statistical analyses were performed to determine the potential impact of various biomass and bulk parameters on the overall filtration performance, with results being reported within Chapter 8.

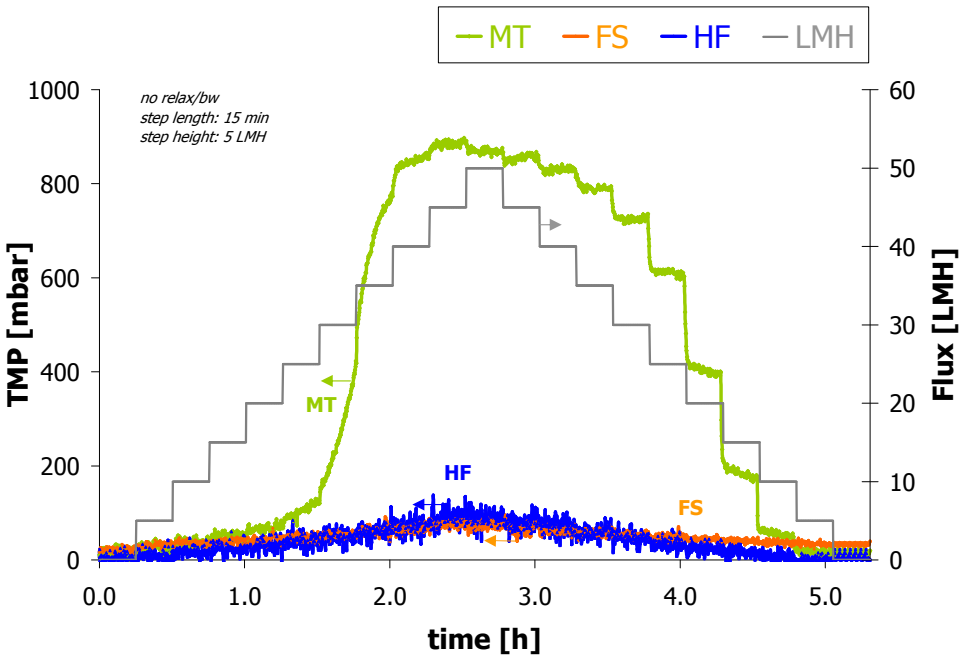

(a)

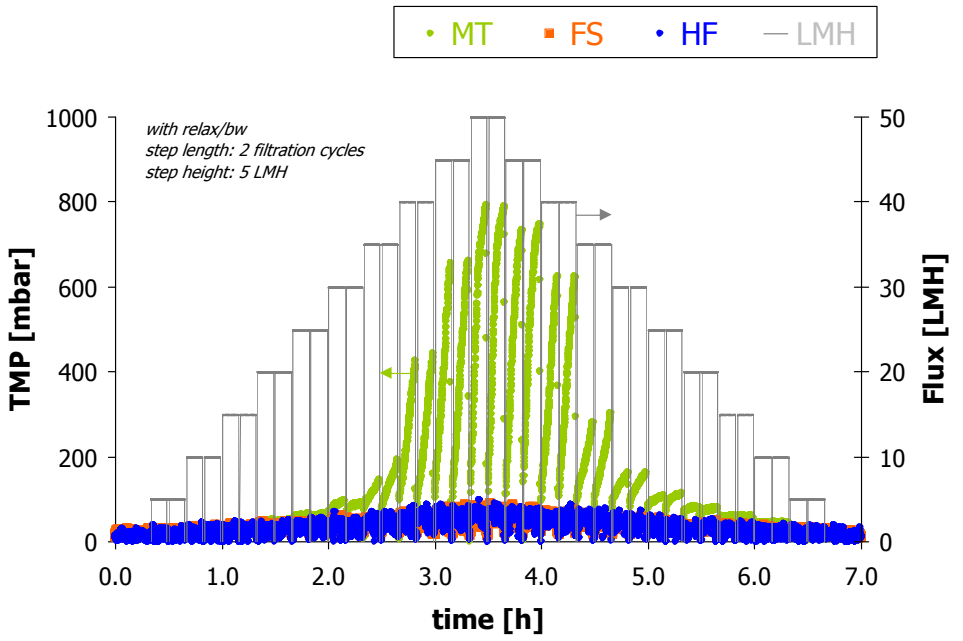

(b)

Figure 5.1.: Sample graph of critical flux determination (MLSS content 12g.L^{-1}): *(a)* classical filtration protocol without relaxation/backwash; *(b)* novel filtration protocol with 2 filtration cycles including relaxation/backwash.

(Please note that LMH curve represents the range of targeted fluxes based on clean water permeability. Actual LMH values may vary for each individual module due to difference in filtration performance.)

5.2. Comparison of critical flux trials with and without relaxation/backwash at MLSS 12 g.L^{-1}

5.2.1. Permeability

Permeability development during classical incremental flux step trials at fixed SADm rates and MLSS 12 g.L^{-1} revealed high deviations between the modules examined (average values and range for all trials illustrated in Figure 5.2a). This was observed especially for higher fluxes with J_{20} above 20 LMH; as for lower fluxes up to 20 LMH the determined transmembrane pressure P_{ave} of all modules remained below 40 mbar and permeability values exhibited insignificant variations.

Critical flux trials applying the novel flux step method, including backwash/relaxation, also revealed high variations in filtration performances between all three modules, with the highest deviation for the individual trials being observed for the MT module (average values and range for all trials illustrated in Figure 5.2c).

While the MT module revealed the highest deviation for measured permeability with maximum P_{ave} values varying from 400 to 800 mbar, the FS and HF modules showed less discrepancy between flux trials undertaken at different seasons. This was in fact similar to the classical flux step trials conducted without backwash though overall filtration performance was found to be better for relaxation and backwash protocol as it would have been expected.

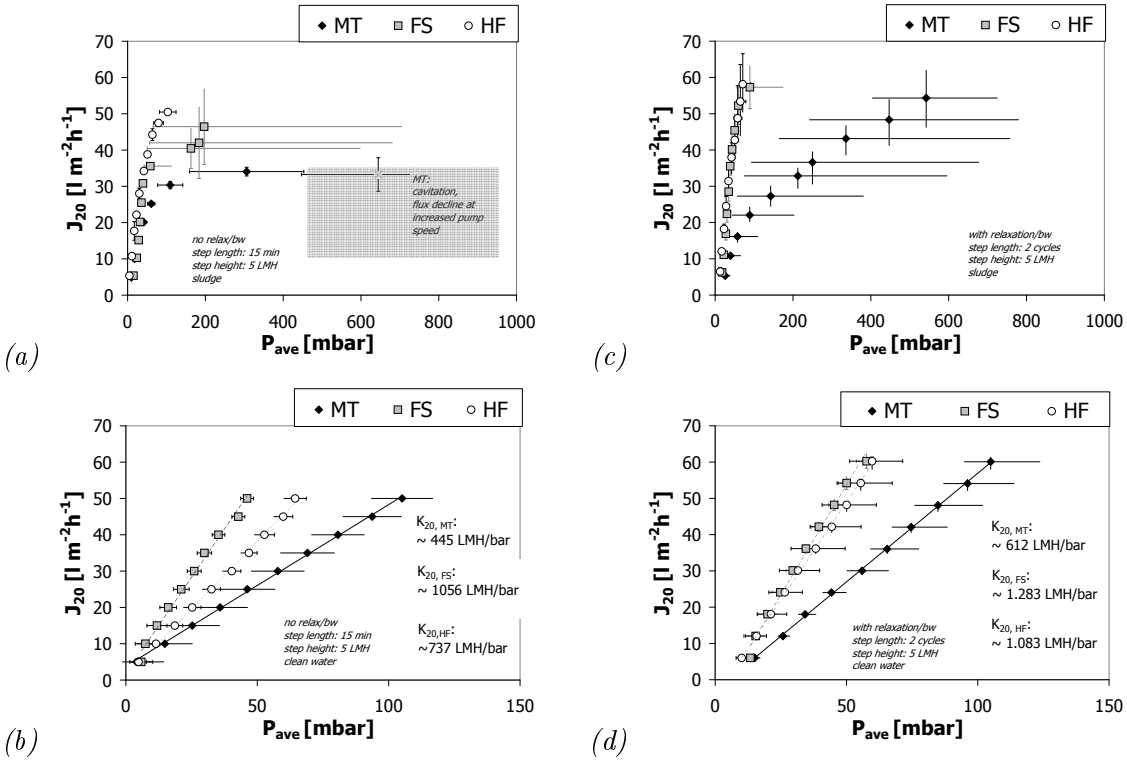

Figure 5.2.: Comparison of permeability curves of membrane modules at critical flux trials with and without backwash or relaxation (15min step length, 5 LMH step height, $n = 4, 6$) at biomass filtration trials (MLSS 12 g.L^{-1}; SAD$_m$= 1.0 (FS, HF) and 1.5 (MT) Nm^{3}m^{-2}h^{-1}) and post-sludge clean water trials: biomass trial *(a)* without and *(c)* with relaxation and/or backwash; post-sludge clean water trials *(b)* without and *(d)* with relaxation and/or backwash.

HF module

The **HF module** showed the most consistent filtration performance during biomass filtration, in comparison to the FS and MT module, at MLSS content of 12 g.L^{-1} (SAD$_m$= 1.0 Nm^{3}m^{-2}h^{-1}) for both critical flux protocols. During classical critical flux trials, the HF module revealed an average sub-critical permeability of 718 LMH.bar^{-1}, supra-critical of 594 LMH.bar^{-1}, whereas while applying the novel flux step protocol, average sub-critical permeability increased to 872 LMH.bar^{-1}, supra-critical to 842 LMH.bar^{-1} (Table 5.1). Permeability loss due to cake layer formation was determined with as little as 0.6% for the novel critical flux trial and 32.4% for the classical critical flux trial (Table 5.1).

For the classical critical flux trials, the average trans-membrane pressure, P$_{ave,HF}$, remained below 150 mbar for any flux exhibited (J$_{20,max}$ = 51 LMH, Figure 5.3*c*), while for critical flux trials applying the novel filtration protocol, the maximum P$_{ave}$ varied between 63 and 92 mbar only for fluxes up to 60 LMH (Figure 5.3*d*). During the classical filtration protocol, $P_{ave,HF}$ ranged between 39 mbar and 67 mbar at a flux of J$_{20}$ $\approx$ 40 LMH, with $P_{ave,HF}$ varying only between 59 mbar and 67 mbar for 5 out of 6 trials. Lowest fouling propensity for the HF module was hence observed during the classical filtration protocol for trial number (3), for which, however, the highest trans-membrane pressure increase including spacer/lumen clogging respectively, were found for the MT and the FS module (Figure 5.3*a,b*).

During the filtration trials applying backwash, limited fouling was generally observed for HF module for all trials with P$_{ave}$ remaining below 100 mbar for fluxes up to 65 LMH. However, more fouling was observed for test (3) than for test (2), and then test (1a) and (1b). To illustrate, a P$_{ave,HF}$ of 60 mbar was reached at fluxes of 65, 52, 43 and 41 LMH for the tests (1a), (1b), (2) and (3), respectively (Figure 5.3*f*). The apparent opposite outcome for test series number (3) showing best filtration performance during the classical critical flux step, but worst filtration performance during the novel filtration protocol, was suggested to have resulted from daily biomass fluctuation given the little differences which were determined between the different test series.

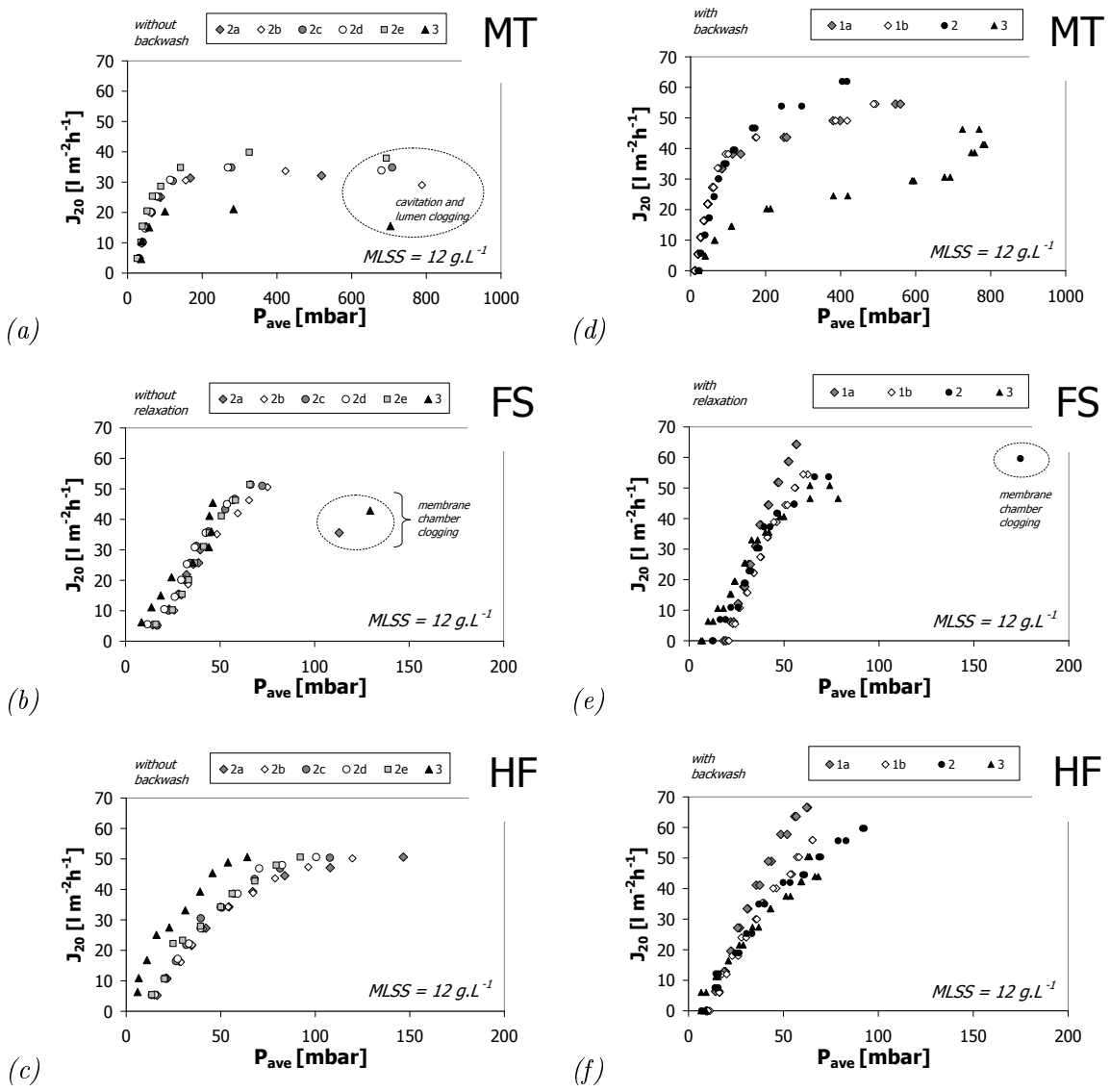

Figure 5.3.: Permeability curves for critical flux trials at $MLSS = 12\ gL^{-1}$; (a-c) classical critical flux protocol without backwash/relaxation: *(a)* MT module; *(b)* FS module; *(c)* HF module [trials undertaken in (2)=February and (3)=July]; (d-f) novel critical flux protocol with backwash/relaxation: *(d)* MT module; *(e)* FS module; *(f)* HF module [trials in chronological order (1)=May, (2)=February, (3)=July].

FS module

The **FS module** revealed a relatively stable filtration performance similar to that of the HF module for fluxes until 30 LMH with $P_{ave,FS} \leq 31$ mbar during the classical filtration protocol and with $P_{ave} \leq 48$ mbar for fluxes up to 40 LMH for the novel filtration protocol respectively. Above the determined transitional fluxes of 35 LMH for the classical filtration trials nad 40 LMH for the novel filtration trials respectively, a permeability decline with wide range during some tests could be observed (Figure 5.3*b,e*). During classical filtration trials, the high loss in permeability for the FS module at higher fluxes was indeed observed for two trials out of the six critical flux tests conducted. Trial 2a revealed module sludging for fluxes above 35 LMH, where a sudden TMP rise of $\approx$ 74 mbar from 30 mbar to 113 mbar was observed for J_{20}, increasing from 30 LMH to 35 LMH (Figure 5.3*b*). Trial number 3 also revealed clogging (sludging) of the FS vessel at a flux higher than 46 LMH with P_{ave} rising from 46 mbar to 126 mbar and the flux decreasing to 42 LMH, even with increasing pump speed.

During the critical flux trials applying relaxation, P_{ave} continued to increase linearly for all the flux tested for test number (1a) and (1b), demonstrating that the critical flux was not reached (Figure 5.3*e*) with maximum determined P_{ave} remaining between 56 mbar and 74 mbar for fluxes above 50 LMH. For test number (2), a rapid increase of P_{ave} was observed for fluxes above 50 LMH with characteristics of critical conditions. Indeed, P_{ave} increased from 73 mbar at 53 LMH to 174 (and even 418 mbar) at 60 LMH. It should be noted that again sludging/clogging of the membrane vessel was observed in this test which explains the significant difference with the other tests. For the final test (3), a deviation from the sub-critical linear increase of P_{ave} was observed for fluxes above 45 LMH.

During classical critical flux trials, the FS module revealed an average sub-critical permeability with 713 LMH.bar^{-1}, supra-critical with 625 LMH.bar^{-1}, whereas while applying the novel flux step protocol average sub-critical permeability increased to 866 LMH.bar^{-1}, supra-critical to 839 LMH.bar^{-1} (Table 5.1). Though overall filtration performance was found to be less in comparison to the HF module, permeability loss due to cake layer formation was determined less for the FS module with 0.5% for the novel critical flux trial and 18.1% for the classical critical flux trial (Table 5.1).

This phenomenon might be resulting from the fact that the HF module tended to absorb more potential foulants to the membrane surface than the FS module, which was in fact suggested in a study by Torres *et al.* (2008). Furthermore, it might be concluded that the differences in filtration mode between both module configurations is becoming more apparent with the HF module's permeability loss decreasing from 32.4% to 0.6% while applying relaxation and backwash mode to the flux step trials (Table 5.1, page 94). The FS module still seemed to benefit from applying a relaxation mode, whereas significance decreased in comparison to the HF module. In fact, the differences between both filtration modes for the FS module mainly

seemed to result from membrane vessel sludging problems. Membrane vessel sludging was found to have been reduced due to the relaxation mode allowing a better biomass circulation up to a threshold value of 50 LMH at the given short-term test with MLSS content of approx. 12 g.L^{-1} and SAD$_m$= 1.0 Nm^{3}m^{-2}h^{-1}.

MT module

The **MT module** was found to have exhibited high average permeability losses for fluxes above 25 LMH for classical critical flux trials. For instance, P$_{ave,HF}$ was determined 40 mbar, 60 mbar, 109 mbar, 306 mbar for fluxes of 20 LMH, 25.2 LMH, 30.3 LMH and 34.1 LMH. For fluxes higher than 35 LMH, P_{ave} rose above 600 mbar and the permeate pump displayed cavitation effects with no further increase in flux with an increasing pump speed. A highest average MT permeability was measured for fluxes below 15 LMH with 300 LMH.bar^{-1}, while average permeability for fluxes above 35 LMH dropped to below 100 LMH.bar^{-1} (Figure 5.3a). Due to observed lumen clogging, the range of fluxes tested did not reach values for J$_{20}$ higher than 38 LMH, even with increasing permeate pump rates. While the trials 2a-2e revealed linearity in permeability until a flux of 25 LMH with P$_{ave,MT}$ varying between 66 mbar (trial 2e) and 89.6 mbar (trial 2b), permeability (K$_{ave,MT}$) for trial number 3 was found to decrease dramatically for fluxes higher than 15 LMH. Sub-critical average permeability for the MT module was determined with 261 LMH.bar^{-1}, supra-critical with 117 LMH.bar^{-1} (Table 5.1).

For the critical flux test series applying back flush mode, the average trans-membrane pressure (P$_{ave,MT}$) increased linearly for fluxes up to 40 LMH for the tests (1a), (1b) and 2 (Figure 5.3d). Interestingly, although the same critical flux of 40 LMH was found for these three tests, more fouling with higher P$_{ave}$ was observed for the tests (1a) and (1b) (both identical) than for the test (2). Indeed, at a flux of approximately 50 LMH, P$_{ave}$ was approximately 240 and 400 mbar for tests (2) and (1a) and (1b) respectively. Significantly more fouling was recorded for test (3) with the MT module. Indeed, a critical flux of only 10 LMH was found with P$_{ave}$ reaching approximately 800 mbar for a flux of only 40 LMH.

Sub-critical average permeability for the MT module was determined with 344 LMH.bar^{-1}, supra-critical with 206 LMH.bar^{-1} for the novel flux step protocol (Table 5.1). Clean water permeability losses after biomass filtration reduced from 38.2% to 15.0% comparing the critical flux trials without backflush mode to critical flux trials with backflush mode, respectively. Compared to the FS and HF module, the MT module exhibited mostly lumen clogging even at lower fluxes, which indicates the difference between the two filtration modes *inside-out* to *outside-in*, and suggests that the MT module would require significant higher aeration rates to eliminate the risk of lumen sludging/clogging for higher MLSS content and higher permeate fluxes as long as the set up is limited to air-lift, to control cross-flow velocity. For the majority of multi-tubular membrane systems in full scale applications, cross-flow velocity is usually

controlled by cross-flow pumping including membrane aeration where necessary. Companies like Norit, Berghof and consequently Wherle are applying more and more low energy air-lift configurations with reduced pump energy, which are usually recommended for low COD concentrations (<1g.L^{-1} COD) and lower MLSS content (8-12 g.L^{-1}) (Judd, 2011). Typical SAD$_m$ rates for multitubular modules tested at Beverijk wastewater treatment plant were reported with 0.3 to 0.6 Nm^{3}m^{-2}h^{-1} at MLSS rate of 8 g.L^{-1} and typical flux of 15 - 50 LMH (Judd, 2006).

Table 5.1.: Comparison of permeability values, permeability loss per module for critical flux trials (with and without backwash/relaxation) at fixed SAD$_m$ and MLSS 12 g.L^{-1}

Module	**K$_{20}$ - virgin membrane material (clean water)**	**K$_{20}$ - biomass filtration**	**K$_{20}$ - post-sludge (clean water)**	**K$_{20}$ loss [%]**
classical critical flux trial - without backwash or relaxation				
MT	720 *(20)*		445 *(85)*	**38.2**
sub-critical $< 20 LMH$		261 *(73)*		63.7
supra-critical $> 20 LMH$		117 *(54)*		83.8
FS	1290 *(40)*		1056 *(58)*	**18.1**
sub-critical $< 30 LMH$		713 *(79)*		44.8
supra-critical $> 30 LMH$		625 *(306)*		51.6
HF	1090 *(32)*		737 *(65)*	**32.4**
sub-critical $< 38 LMH$		718 *(305)*		34.1
supra-critical $> 38 LMH$		594 *(166)*		45.5
novel critical flux protocol - with backwash and/or relaxation				
MT	720 *(20)*		612 *(52)*	**15.0**
sub-critical $< 27 LMH$		344 *(145)*		52.2
supra-critical $> 27 LMH$		206 *(136)*		71.4
FS	1290 *(40)*		1283 *(109)*	**0.5**
sub-critical $< 45 LMH$		866 *(177)*		32.9
supra-critical $> 45 LMH$		839 *(280)*		34.9
HF	1090 *(32)*		1083 *(92)*	**0.6**
sub-critical $< 48 LMH$		872 *(146)*		20.0
supra-critical $> 48 LMH$		843 *(176)*		22.7

Notation: 1290 *(161)*: 1290 = K$_{20}$ in LMH.bar^{-1}, *(161)* = standard deviation of sample range in LMH.bar^{-1}; permeability loss rate referenced to initial membrane material permeability

5.2.2. Fouling rates - dP/dt

Fouling rates calculated according the classical dP/dt resulted in major differences between the individual modules ranging in all modules from 0.06 mbar.min^{-1} to 26 mbar.min^{-1} for classical critical flux trials, and from 0.05 mbar.min^{-1} to 78 mbar.min^{-1} for the novel critical flux trails, with the highest dP/dt measured for the MT module during both filtration protocols (Figure 5.4 and Table 5.2).

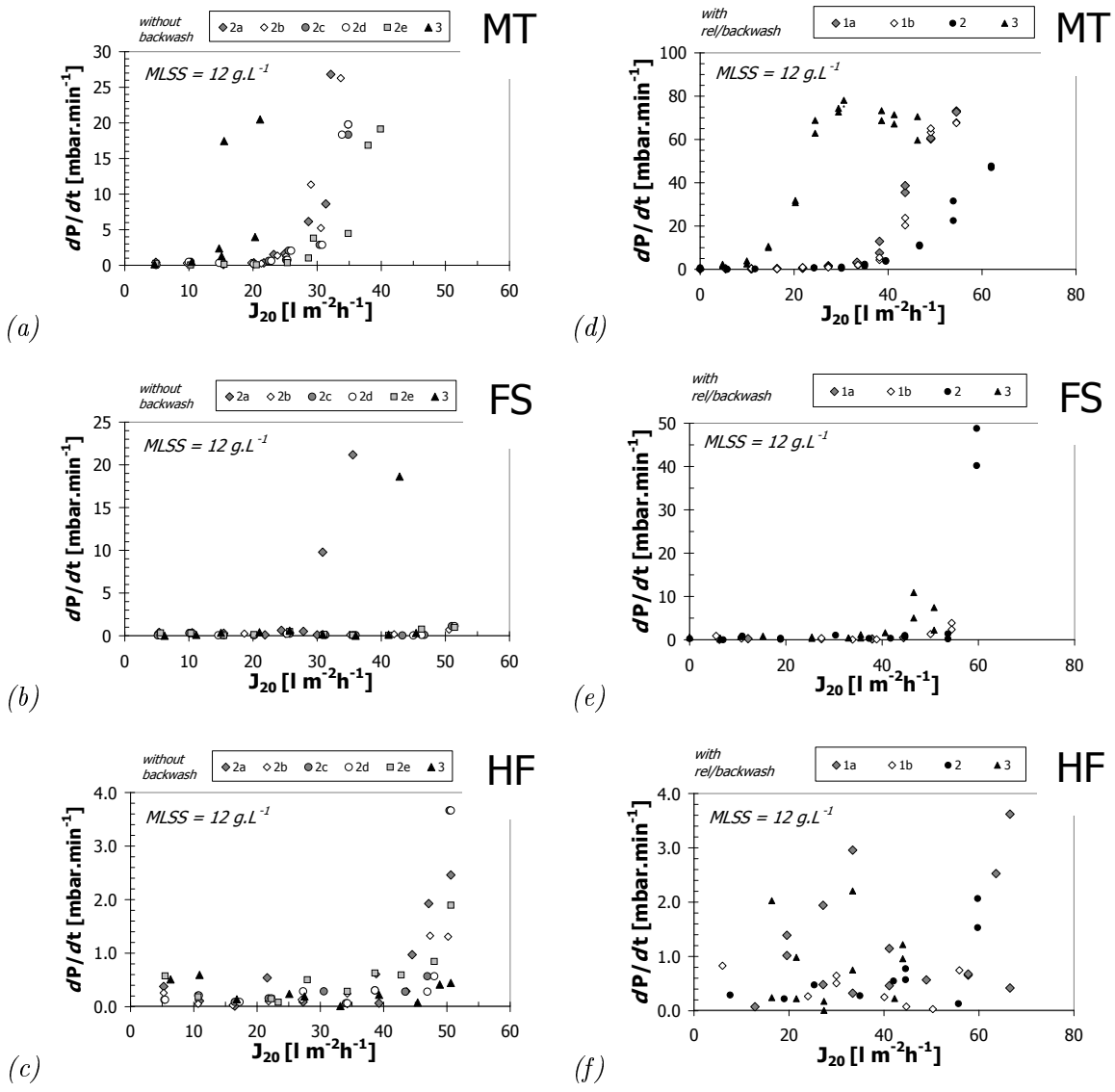

Figure 5.4.: dPdt curves for critical flux trials at $MLSS = 12\ gL^{-1}$ - comparison without backwash/relaxation *(a,b,c)* and with backwash/relaxation *(d,e,f)*: *(a,d)* MT module; *(b,e)* FS module; *(c,f)* HF module.

Table 5.2.: Comparison of average classical fouling rates dP/dt for different critical flux trials (n=4,5,6) at fixed SAD_m and MLSS 12 g.L^{-1}

MT			**FS**			**HF**		
dP_{MT}/dt	J_{20}	$P_{ave,MT}$	dP_{FS}/dt	J_{20}	$P_{ave,FS}$	dP_{HF}/dt	J_{20}	$P_{ave,HF}$
classical critical flux trial - without backwash or relaxation								
0.179 *(0.145)*	5	31 *(4)*	0.222 *(0.159)*	5	15 *(2)*	0.331 *(0.189)*	6	15 *(1)*
0.318 *(0.202)*	10	38 *(2)*	0.318 *(0.033)*	10	23 *(2)*	0.227 *(0.190)*	11	21 *(1)*
0.430 *(0.447)*	15	49 *(6)*	0.113 *(0.107)*	15	28 *(2)*	0.085 *(0.056)*	18	27 *(2)*
0.859 *(1.528)*	20	68 *(17)*	0.131 *(0.072)*	20	32 *(2)*	0.213 *(0.169)*	23	33 *(2)*
4.22 *(7.98)*	**25**	114 *(83)*	0.308 *(0.115)*	26	36 *(2)*	0.249 *(0.149)*	28	40 *(1)*
6.35 *(6.04)*	28	225 *(236)*	0.130 *(0.049)*	**31**	39 *(2)*	0.123 *(0.114)*	34	52 *(2)*
16.591 *(10.66)*	31	418 *(260)*	4.301 *(9.43)*	36	58 *(31)*	0.356 *(0.221)*	**39**	61 *(5)*
						0.416 *(0.319)*	44	74 *(7)*
						0.942 *(0.580)*	48	89 *(12)*
						2.244 *(1.29)*	51	113 *(21)*
novel critical flux protocol - with backwash and/or relaxation								
0.464 *(0.790)*	5	27 *(9)*	0.231 *(0.194)*	6	20 *(5)*	0.785 *(0.456)*	6	14 *(3)*
0.891 *(1.085)*	11	39 *(17)*	0.397 *(0.308)*	11	24 *(4)*	0.663 *(0.072)*	12	17 *(3)*
2.872 *(5.165)*	16	57 *(35)*	0.564 *(0.325)*	17	28 *(4)*	0.586 *(0.429)*	18	24 *(3)*
8.125 *(15.11)*	22	89 *(76)*	0.300 *(0.146)*	22	30 *(4)*	0.337 *(0.167)*	25	28 *(2)*
17.953 *(33.91)*	**27**	154 *(177)*	0.385 *(0.106)*	29	34 *(3)*	0.378 *(0.161)*	31	36 *(4)*
20.299 *(36.05)*	33	209 *(255)*	0.244 *(0.171)*	36	38 *(2)*	0.810 *(0.462)*	38	43 *(7)*
25.058 *(35.597)*	37	260 *(288)*	0.326 *(0.196)*	40	44 *(2)*	0.331 *(0.316)*	43	50 *(9)*
34.746 *(25.344)*	43	338 *(276)*	0.621 *(0.430)*	**45**	51 *(3)*	0.533 *(0.340)*	**49**	59 *(8)*
54.375 *(21.756)*	48	447 *(231)*	1.759 *(2.225)*	52	59 *(6)*	0.893 *(1.171)*	53	65 *(11)*
61.735 *(11.193)*	54	558 *(152)*	14.678 *(22.959)*	57	152 *(178)*	1.585 *(1.432)*	58	71 *(15)*

Notation: dP/dt in $mbar.min^{-1}$; J_{20} in LMH; P_{ave} in $mbar$

0.179 *(0.145)*: 0.179 = mean dP/dt of sample range, *(0.145)* = standard deviation of sample range

MT module

As the overall filtration performance of the **MT module** was determined to be generally lower than for the HF or FS module, the fouling rates determined illustrate the critical flux at filtration rates lower than 20 LMH for classical critical flux trials (figure 5.4*a*) and lower than 27 LMH for the backwash critical flux trials (Figure 5.4*d*). Below a flux of 20 LMH, dP/dt remained on average below 0.5 mbar.min^{-1} during classical critical flux trials, whereas above 20 LMH dP/dt increased significantly to an average of 4.22 mbar.min^{-1} and above a flux of 28 LMH to 16.6 mbar.min^{-1} (Table 5.2). During classical critical flux trials, the highest fouling rates with dP/dt of 26.6 mbar.min^{-1}, 26.8 mbar.min^{-1} respectively, were determined for tests 2a and 2b at a flux of 32 LMH. During critical flux trials applying backwash mode, the MT module fouling rates, however, reached values as high as 78 mbar.min^{-1} for the range of fluxes tested (figure 5.4*b*), while average trans-membrane pressure was 558 ($\pm$152) mbar at the corresponding flux step of 54 LMH (Table 5.2).

Even though the fouling rates determined were considered quite high especially at lower fluxes for both flux step protocol and for higher fluxes for the novel flux step protocol, they were found to be in range with fouling rates reported in literature. For instance, for critical flux trials of PVDF tubular membrane (0.03 μm; filtration length 1m) using the classical filtration protocol with a step length of 15 minutes and a step height of 2 LMH at a fixed air rate of 6 L.min^{-1} , Brookes (2005) determined a transitional flux of 12 LMH with fouling rates of 0.179 mbar.min^{-1} below J_{trans} and of 0.327 mbar.min^{-1} above J_{trans} respectively (see also Table 5.3, page 103). Average trans-membrane pressure for the transitional flux of 12 LMH was indicated with 79.8 ($\pm$17.2) mbar, whereas the highest fouling rate at a MLSS content of 12 g.L^{-1} was found with 0.618 ($\pm$0.27) mbar.min^{-1} with corresponding P_{ave} of 118.5 ($\pm$31.1) mbar at the highest tested flux of 16 LMH (Brookes, 2005). During this study, the average transitional critical flux for the classical filtration protocol for the MT module at MLSS content of 12 g.L^{-1} was 15 LMH, critical flux 20 LMH with average dP/dt of 0.43 mbar.min^{-1} at J_{trans} (Table 5.2).

On the other hand, during a study conducted at a MLSS content of 8 g.L^{-1} by Alvarez-Vazquez (2005), critical fluxes for two different types of membrane modules (PVDF 0.03μm and ceramic membrane module) were reported to be 36 LMH with dP/dt above J_c ranging from 0.37 to 12.6 mbar.min^{-1} for the polymeric membrane module, whereas no critical flux could be determined for the ceramic module with fluxes tested up to 60 LMH (Table 5.3, page 103). During this work, such high differences were also observed between pilot scale and bench-scale data, though differences between different tubular membrane material and the pilot plant resulted from the set up rather than from membrane material. Whilst the pilot scale trials were limited to air-lift to create cross-flow, the single-tube bench-scale trials were conducted using a constant high cross-flow pump rate of approx. 1 m.s^{-1}. Trials conducted

at a MLSS content of 12 g.L^{-1} hence revealed a critical flux of 25 LMH for the classical flux step protocol with dP/dt ranging from 0.15 to 25.4 mbar.min^{-1} from fluxes above 25 LMH to 60 LMH, whereas while applying the novel flux step protocol, no critical flux could be determined for fluxes tested up to 50 LMH. Classical fouling rates (dP/dt) for the latter test were determined in a range of 0.1 to 0.28 mbar.min^{-1} (Table 5.3).

FS module

During classical critical flux trials, the **FS module** revealed dP/dt values ranging between 0.05 and 0.498 mbar.min^{-1}, apart from trial (2a) and trial (3) where clogging/sludging of the FS occurred. For the two trials where a sludging phenomenon was observed, sudden dP/dt jumps up to 22 mbar.min^{-1} could be observed (Figure 5.4*b*). Interestingly, the dP/dt fouling rates determined generally did not show to increase with increasing flux as opposed to the observation made for the MT module. To illustrate, dP/dt varied for trial 2e from 0.054, 0.324, 0.066, 0.078, 0.246, 0.09 mbar.min^{-1} for fluxes of 5.1, 10.1, 15.4, 20.1, 25.7, 31.3 LMH respectively. Apart from trial (2a) and (3) this could be observed for all trials for fluxes up to 42 LMH. The overall average dP/dt ranges for those trials remained below 0.338 for any fluxes up to 50 LMH. The sequence of overall averaged fouling rates (dP/dt) of these trials resulted subsequently in 0.245, 0.312, 0.166, 0.230, 0.282, 0.140, 0.086, 0.090, 0.338 mbar.min^{-1} for overall average fluxes of 5.4, 10.3, 15.2, 20.2, 25.5, 30.8, 35.6, 43.4, 46.4 LMH respectively, which illustrates again the absence of an increase of dP/dt with increasing flux. The averaged dP/dt values, including the two trials where membrane vessel sludging was observed, resulted in significantly higher fouling rates for dP/dt values for fluxes above 30 LMH (Table 5.2) which therefore determined the overall critical flux with J_c = 30 LMH. During critical flux trials, including relaxation, the fouling rates for the FS module remained below 1.6 mbar.min^{-1} for fluxes up to 45 LMH and then generally below 11 mbar.min^{-1} for fluxes above 45 LMH (Figure 5.4*b*).

Even though the obtained critical fluxes for the pilot scale module were within range of what is reported in literature, the determined fouling rates were considered high, especially for lower fluxes. For instance, Guglielmi *et al.* (2008) conducted a critical flux study at a large pilot scale plant equipped with flat sheet PE 0.4μm membranes (classical critical flux trials at an aeration rate of SAD$_m$ 0.94 Nm^{3}m^{-2}h^{-1} with a step length of 15 minutes and a step height of 5 LMH; MLSS content around 20 g.L^{-1}) and observed fouling rates from 0.036 to 0.005 mbar.min^{-1} until the critical flux of 38 LMH was reached. Above that critical flux, dP/dt values were determined with 0.112 to 0.662 mbar.min^{-1} for fluxes ranging from 44.4 to 62.9 LMH.

Interesting to note is, critical flux trials conducted in parallel at bench-scale revealed much lower critical fluxes than the pilot scale module within this study. In fact, while average

J_c was 31 LMH and 45 LMH for the two filtration protocols in pilot scale, J_c dropped to 9 LMH, 12 LMH respectively for bench-scale trials (Table 5.3, page 103). In contrast, the determined fouling rates were found to be much lower for the bench-scale than for the pilot scale module, with ranges from 0.009 to 0.21 mbar.min^{-1} and 0.13 to 0.78 mbar.min^{-1} for the bench-scale and pilot scale trials respectively. This contradiction in results is assumed to derive from the different filtration patterns, with the horizontal bench-scale set-up limiting an even hydrodynamic flow along the membrane surface and creating a higher risk to sludging than the vertical air-lifted pilot scale module. This restriction of up-scaling results from bench to pilot scale has already been addressed by other authors (Guglielmi *et al.*, 2007a; Kraume *et al.*, 2008). Furthermore, it has to be mentioned that the biomass was exposed to much higher shear stress during bench-scale trials due to the cross-flow pump and due to higher rates of biomass circulation, which has also been found to lower membrane filtration performance (Wisniewski and Grasmick, 1998).

Summarising, it can be concluded for the FS pilot scale module, that major differences between both filtration protocol in terms of fouling rates and filtration performance at the given MLSS content were a significant reduction in membrane vessel sludging for the relaxation protocol and hence a higher determined critical flux due to lower biomass accumulation inside the membrane vessel, especially at higher fluxes.

HF module

The **HF module** exhibited the lowest fouling rates with dP/dt ranging between 0.012 mbar.min^{-1} and 3.668 mbar.min^{-1} amongst all three modules and for all trials conducted (Figure 5.4*c*). Similar to the FS module, no trend of an overall increase of dP/dt could be observed for increasing fluxes. In fact, the lowest overall fouling rate was determined for a flux of 18 LMH for the HF module and 15 LMH for the FS module respectively (Table 5.2). A steady increase of dP/dt for the HF module was found to occur for fluxes above 40 LMH for the classical critical flux trials, which therefore lead to an overall critical flux of $J_c = 40$ LMH. During critical flux trials applying backwash and relaxation, values for dP/dt were found to be more scattered making a definite determination of a certain critical flux impossible (Figure 5.4). For example, in the case of the HF module and trial number 1a, even if the rapid increase of determined fouling rates could lead to the assumption of indicating critical conditions, a critical flux in its weak form could not be observed up to a flux of 60 LMH according to the permeability curve (Figure 5.3*f*, page 91). In contrast to the relatively good filtration performance, fouling rates of more than 1.0 mbar.min^{-1}, considered high, were monitored at a flux of 20 LMH (Figure 5.4*f*, page 95). In one study, Guglielmi *et al.* (2007a) investigated critical fluxes under different aeration rates at a large scale HF pilot plant (PVDF 0.04μm, classical flux step, step length 15min, step height 5 LMH). At a MLSS content of $\approx$ 10 g.L^{-1} and an

aeration rate of 1.0 Nm^{3}m^{-2}h^{-1} SAD$_m$, J$_c$ was 31 LMH with a corresponding fouling rate of below 0.15 mbar.min^{-1}. The fouling rate at a flux step of 50 LMH was indicated to reach 1.0 mbar.min^{-1} (Guglielmi *et al.*, 2007a), which emphasises the relatively high fouling rates determined within this study. For lower aeration rates (0.3 Nm^{3}m^{-2}h^{-1} SAD$_m$), Guglielmi *et al.* (2007a) reported fouling rates of 4.01 mbar.min^{-1} at the final flux step of 55 LMH (Table 5.3, page 103).

5.2.3. Residual fouling rates - $dP_{p,s}/dt$

Residual fouling rates, calculated as peak-step fouling rates $dP_{p,s}/dt$ (Table 4.6, page 65), also revealed a broad range between the membrane module tested with the highest deviation being determined for the MT module (Figure 5.5).

For all modules, $dP_{p,s}/dt$ remained below 0.3 mbar.min^{-1} below critical fluxes. Above the determined critical flux, $dP_{p,s}/dt$ reached values up to $\approx$ 17 mbar.min^{-1} for the MT module, whereas residual foulings within negative range were determined for the FS and HF module at higher fluxes.

While a negative range of $dP_{p,s}/dt$ for the MT and HF module could be expected and explained by the effects of the applied backwash, a negative range for the FS module was not expected. However, Wu *et al.* (2008b) resumed that positive implication of relaxation were found to be as effective as the positive implication of backwash. Furthermore, in another publication the authors stated that a higher initial flux followed by a lower filtration flux resulted in much better overall performances (Wu *et al.*, 2008). The combination of the aforementioned two effects might be an explanation for the observed residual fouling rates within this study - as negative residual fouling rates were mainly observed for higher fluxes. Furthermore, it might be postulated that negative residual fouling rates for the FS module at higher fluxes be indicative that cake layer fouling for that step is a result of from clogging with the relaxation step subsequently reducing the biomass accumulation. However, further investigations would be needed to fully explain and understand the mechanisms.

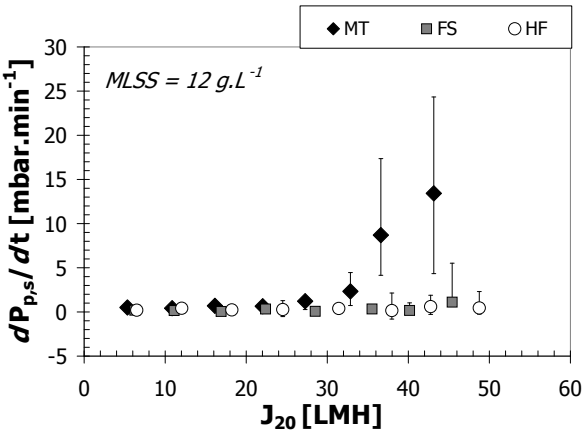

Figure 5.5.: Residual fouling rates: $dP_{p,s}/dt$ for critical flux trials at $MLSS = 12\ gL^{-1}$

5.3. Summary

Numerous different filtration protocols for short-term tests and fouling behaviour are reported within literature. Fouling trends are quite often controversially reported, which might not solely be due to the complexity of the system (membrane vs. biomass), but also dependent on the fact that studies are commonly undertaken with one set-up and hence limited in comparison of configuration. A direct comparison of fouling behaviour between different membrane configurations applied in MBR was therefore one of the main focuses of this study while using a filtration protocol similar to a full scale filtration mode.

A comparison of results for both filtration protocols in literature data revealed that average fouling rates could be considered high, though filtration performance significantly improved for the novel filtration protocol (Table 5.3). Fouling rates before and after critical flux revealed higher fouling rates for the backwash protocol than the classical incremental flux step, though determined critical fluxes were found to be higher for the novel filtration protocol. This phenomenon was anticipated, and results are in accordance with other studies (Germain, 2004; van der Marel *et al.*, 2009).

A side-by-side filtration experiment for bench-scale material (single-tube and flat sheet material analogue being the pilot scale membrane materials) disclosed further significant differences in filtration performance due to the different set-up. The bench-scale trials for flat sheet materials on the cross-cell consistently resulted in lower critical fluxes than the pilot scale module, whereas the lab scale trials on the multi-tubular materials showed higher critical fluxes for the single-tube test cell (Table 5.3). To illustrate, while applying the novel critical flux protocol, no critical flux during the filtration trial at MLSS content of 12 $g.L^{-1}$ was determined for the bench-scale single-tube (pumped cross-flow and no aeration; $J_c > 50$ LMH). The same experiment conducted using the classical critical flux protocol without relaxation mode revealed a critical flux of 25 LMH at bench-scale, while the pilot scale module tested in parallel revealed critical fluxes of 20 LMH (classical flux step) and 27 LMH (novel flux step) respectively (Table 5.3).

This was explained by the different hydrodynamic conditions between the different tests and configurations. While the single-tube module extracted permeate similar to that of the pilot scale module and benefited furthermore from higher cross-flow velocity than the pilot scale module, tests undertaken with the flat sheet cross-cell showed complete different flow patterns to those of the pilot scale module. Due to the set-up of the flat sheet cross-cell, the cross-flow along the membrane and furthermore the type of permeate extraction would generate higher solid accumulations on the bench-scale membrane surface than for the pilot scale module.

Table 5.3.: Comparison of critical flux fouling rates

System	Scale	Type	Material; Pore Size	MLSS [g.L^{-1}]	J_c [LMH]	dP/dt before J_c [mbar.min^{-1}]	dP/dt after J_c [mbar.min^{-1}]	Reference
asMBR	lab	MT	PVDF 0.03μm	8	36	0.09 - 0.14	0.37 - 12.6	Alvarez-Vazquez 2005
asMBR	lab	MT	ceramic	8	>60	0.39 - 0.49	-	Alvarez-Vazquez (2005)
asMBR	lab	MT	PVDF 0.03μm	12	12*	0.007 - 0.18	0.33 - 0.6	Brookes (2005)
asMBR	pilot	MT	PVDF 0.03μm	12	20	0.17 - 0.86	5.2 - 16.5	*this study (no bw)*
asMBR	pilot	MT	PVDF 0.03μm	12	27	0.7 - 8.1	16.7 - 64.8	*this study (bw)*
cross-cell	lab	MT	PVDF 0.03μm	12	>50	0.01 - 0.28	-	*this study (bw)*
cross-cell	lab	MT	PVDF 0.03μm	12	25	0.001 - 0.084	0.15 - 25.4	*this study (no bw)*
iMBR	lab	FS	PE 0.4μm	6	25	<0.1	0.1-1.2	Ndinisa *et al.* (2006)
iMBR	pilot	FS	PE 0.4μm	20	38	<0.005	0.112-0.662	Guglielmi *et al.* (2008)
asMBR	pilot	FS	PVDF 0.08μm	12	31	0.13 - 0.31	4.3-0.8	*this study (no rel)*
asMBR	pilot	FS	PVDF 0.08μm	12	45	0.23 - 0.78	1.79 - 14.7	*this study (rel)*
cross-cell	lab	FS	PVDF 0.08μm	12	9	0.009 - 0.0023	0.004 - 0.1	*this study (no rel)*
cross-cell	lab	FS	PVDF 0.08μm	12	12	0.15 - 0.21	0.5 - 6.1	*this study (rel)*
iMBR	pilot	HF	PVDF 0.04μm	10	27	0.09 - 0.15	0.49 - 4.01	Guglielmi *et al.* (2007a)
asMBR	pilot	HF	PES 0.04μm	12	39	0.085 - 0.416	1.2 - 2.24	*this study (no bw)*
asMBR	pilot	HF	PES 0.04μm	12	49	0.331 - 2.83	0.89 - 3.58	*this study (bw)*

(* sustainable flux; asMBR = air-lift side-stream MBR; iMBR = submerged MBR; bw = backwash; rel = relaxation)

Notwithstanding the general discussion within literature that reports that fouling rates for lab or pilot scale modules are up to a magnitude higher than those occurring in full scale application (Drews (2010); Kraume *et al.* (2008), Table 5.4: typical fouling values for full scale application), the bench-scale trials exhibited lower fouling rates ($d\mathrm{P}/d\mathrm{t}$) than the pilot scale trials. This is most interesting for the comparison of the flat sheet material, where critical flux at bench-scale was found to be much lower than the pilot scale module (Table 5.3). The lower fouling rates determined for the cross-flow bench-scale were attributed to the smaller flux step height which had to be used for the critical flux tests of the cross-cell due to the generally observed lower filtration performance. This is again an indication of the necessity to set up any laboratory scale applications (bench or pilot scale) as closely as possible to configurations used in full scale applications as postulated already in literature (Kraume *et al.*, 2008).

Residual fouling rates $d\mathrm{P}_{p,s}/d\mathrm{t}$ were also found to be in higher ranges than reported for full scale applications, but for some trials $d\mathrm{P}_{p,s}/d\mathrm{t}$ values were also determined in negative range, especially at higher fluxes (Table 5.4). This phenomenon was attributed to the efficiency of the applied relaxation/backwash mode, which was reducing the overall cake fouling.

Table 5.4.: *(a)* Typical fouling rates from full scale application (Drews, 2010),
(b) range of fouling rates from pilot plant results - MLSS 12 g.L^{-1}; fixed aeration rate

(a)

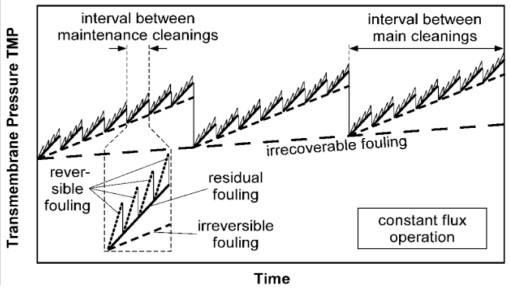

Category	Fouling rate in mbar.min-1	time frame
Reversible fouling (cake filtration)	0.1 ... 1	10 min
Residual fouling	0.01 ... 0.1	1-2 weeks
Irreversible fouling	0.001 ... 0.01	6-12 years
Irrecoverable fouling	0.0001 ... 0.001	years

(b)

		MT	FS	HF
Reversible fouling (cake filtration) [mbar.min-1]	**dP/dt**	0.11 - 78.1	0.10 - 48.8	0.007 - 3.62
Residual fouling [mbar.min-1]	**$dP_{p,s}/dt$**	0.30 - 16.26	-1.02 - 21.81	-0.45 - 1.04
Cake layer resistance [10^{12} m^{-1}]	**R_{cl}**	0.0016 - 30.6	0.037 - 2.66	0.003 - 1.03
TMP [mbar]	**P_{ave}**	18 - 710	15 - 330	11 - 86
Permeability [LMH.bar^{-1}]	**K_{20}**	100 - 495	227 - 1140	364 - 1188

6. Results and Discussion: Comparison of critical fluxes at varying MLSS concentration

6.1. Scope

The concentration of suspended solids of the biomass has been discussed contrastingly in literature. Positive effects on membrane permeability were observed with higher MLSS concentration (Brookes, 2005; Defrance *et al.*, 2000; Le-Clech *et al.*, 2003b), but also a decrease of filtration performance has been reported with increasing MLSS (Bottino *et al.*, 2009; Germain, 2004; Madaeni, 1999). Other studies determining different threshold values above or below MLSS content were found to have a significant impact (Schwarz *et al.*, 2007; Wu and Huang, 2009). Conversely, Rosenberger and Kraume (2002) reported no effect of suspended solids concentration on the filterability of activated sludge deriving from different MBR plants.

To identify the possible impact of MLSS content on the filtration performance of each module within this study, critical flux trials were repeated at three different MLSS contents ($\approx$ 3-4 g.L^{-1}, $\approx$ 6-7 g.L^{-1}, $\approx$ 12 g.L^{-1}). Biomass characterisation was undertaken for each experiment to examine the potential impact of biomass properties on the overall filtration performance and results will be discussed in Chapter 8.1. Furthermore, bench scale trials were undertaken in parallel to assess the potential impact of membrane material.

6.2. Comparison of critical trials with and without relaxation/backwash at varying MLSS concentration

6.2.1. Permeability

Filtration performances of the MT module (Figure 6.1*a*) were found to be very similar for the trials at MLSS contents of 3-4 and 12 g.L^{-1}. To illustrate, P_{ave} of 89 mbar at a flux of 22 and 23 LMH and 250 and 260 mbar at a flux of 37 and 39 LMH for MLSS of 12 and 3-4 g.L^{-1}, respectively. In these conditions, the deviation from the linear evolution of an average trans-membrane pressure (P_{ave}), indication of the critical flux, was found for a flux of about 20 LMH. Alternatively, with a MLSS concentration of 7 g.L^{-1} the critical flux was found to be 30 LMH demonstrating less fouling in the HF module in this condition.

Differences in filtration performance for different MLSS contents were most significant for the FS module (Figure 6.1*b*). Indeed, critical fluxes of 13, 23 and 40 LMH were determined for the trials at suspended solids contents of 3-4, 7 and 12 g.L^{-1}, respectively.

For the HF module tested with a MLSS concentration of 12g.L^{-1}, P_{ave} increased fairly linearly for the range of fluxes tested suggesting that the critical flux was above the highest flux tested of 60 LMH (Figure 6.1*c*). However, it should be noted that a slight decline of the permeability can be observed for fluxes above 42 LMH and consequently a more conservative critical flux of 43 LMH can be determined. As for the FS module, more fouling was then observed for the lower MLSS concentrations with critical fluxes of 31 and 18 LMH for the trials with solids contents of 7 and 3-4 g.L^{-1}, respectively.

From these results it can then be established that the FS and HF modules performed better with higher MLSS concentrations. Alternatively, filtration performance was found to be better at a medium MLSS content for the MT module (Table 6.1). As observed previously, higher critical fluxes were generally observed for the HF and FS modules than for the MT module (Table 6.1). Overall, the HF module was found to be the one performing the best during the short-term critical flux test. Differences in filtration performance for the two critical flux trials applied will be discussed within the next section.

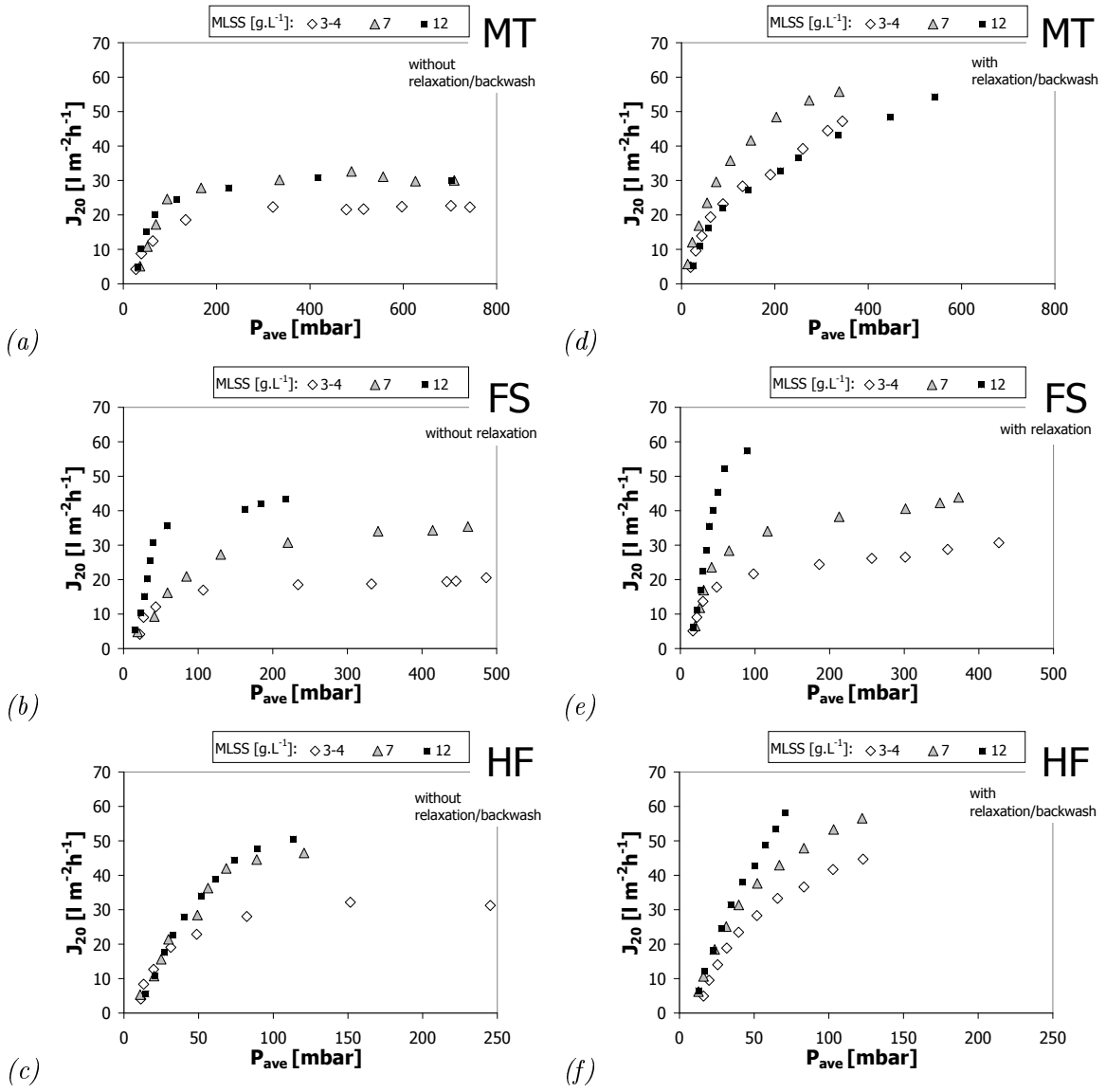

Figure 6.1.: Comparison of permeability curves for different critical flux protocols at varying MLSS content and constant SAD_m rates (a-c: without relaxation and/or backwash; d-f: with relaxation/backwash): *(a,d)* MT module; *(b,e)* FS module; *(c,f)* HF module.

6.2.2. Fouling rates dP/dt and $dP_{p,s}/dt$

Comparing the different fouling rates dP/dt and $dP_{p,s}/dt$ determined from both flux step protocols, emphasized the importance of the chosen 2 cycle filtration system for each flux step (Figure 6.2, Figure 6.3 and Figure 6.4).

To illustrate, the MT disclosed for the two types of critical flux protocols conducted a similar fouling rate for the classical dP/dt with values being around 5.0 mbar.min^1 at a flux of LMH 20, which would have resulted in a similar J_c between both protocols in case J_c would have been determined from the dP/dt vs J_{20} plot. However, as J_c in its weak form determined from the permeability curve was significantly higher for the backwash protocol, the residual fouling rate $dP_{p,s}/dt$ proved to provide a better basis when assessing critical flux from the dP/dt vs. J_{20} plot (Figure 6.2). So, for instance, J_c at MLSS 4 g.L^{-1} for the MT module was observed at fluxes around 19 LMH with $dP_{p,s}/dt$.

Moreover, the efficiency of the fouling control backwash regime, and hence the reversibility of cake layer formation could be assessed from the residual fouling parameter $dP_{p,s}/dt$. To illustrate, while the cake layer resistance (bw) was steadily increasing up to a value of 40 mbar.min^{-1} at a flux of 40 LMH (Figure 6.2*a*), the residual fouling parameter increased from a flux of 20 LMH up to a flux of 30 LMH with values ranging from 0.1 mbar.min^{-1} up to 4.0 mbar.min^{-1} and decreased again after fluxes of $\approx$ 33 LMH, which consequently suggests that higher backwash fluxes provide better fouling control.

For all trials conducted, dP/dt of the classical flux step protocol remained more or less within similar range compared to dP/dt of the relaxation protocol for the FS module (Figure 6.3). Moreover, the residual fouling rate, $dP_{p,s}/dt$, also presented similar ranges for MLSS content 6 g.L^{-1} and 12 g.L^{-1}, whereas significant differences were only observed for the trials conducted at 3 g.L^{-1}, which again suggests the importance of comparing fouling rates within the fouling control filtration scheme applied during full scale applications.

The HF module revealed much higher cake layer fouling rates, dP/dt, values for the backwash protocol than for the classic incremental flux step protocol, which was most obvious for trials conducted at low MLSS range (Figure 6.4). As described previously, this was, in fact, somewhat expected as similar observations were made within another study conducted on a HF pilot scale MBR (Germain, 2004). Nevertheless, the residual fouling rate $dP_{p,s}/dt$, also revealed the efficiency of the cleaning regime by applying relaxation and backwash, as for instance, $dP_{p,s}/dt$ increased for fluxes up to 33 LMH to a value of $\approx$ 2.0 mbar.min^{-1} and remained stable thereafter despite an increasing cake layer fouling rate (Figure 6.4 *a*).

Interesting to note is that the cake layer fouling rate was much higher for the backwash protocol only at 3 g.L^{-1} MLSS for the HF module, which might provide a basis to assume that particle transport towards the membrane surface at lower suspension density is higher if applying relaxation/backwash protocols. Hence, at lower suspension density, drag forces on fine particles are more likely to create higher cake layer resistances at higher fluxes in case of absence of an initial fouling layer. This could also be observed for the FS layer, and more or less for the MT module. In contrast to the FS and HF modules, the MT module showed higher cake layer fouling resistances for trials conducted at higher MLSS contents, which then might furthermore show the impacts of the difference in filtration mode (in-to-out and out-to-in).

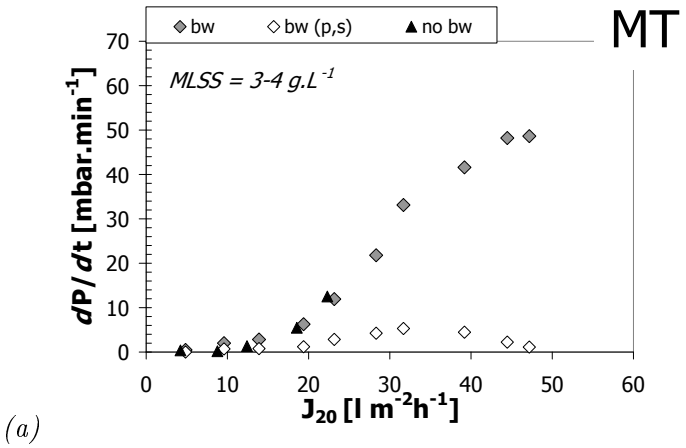

(a)

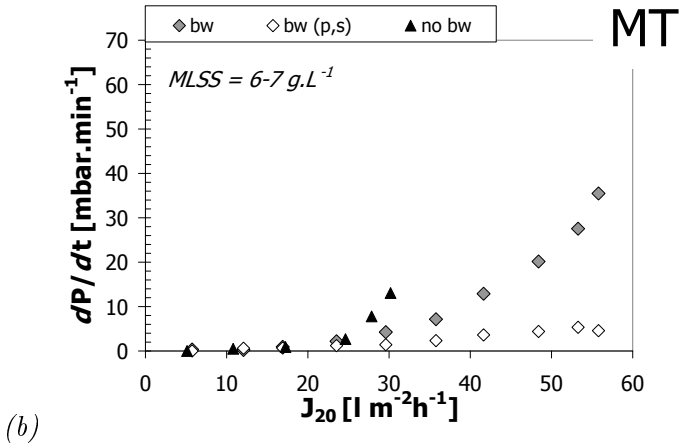

(b)

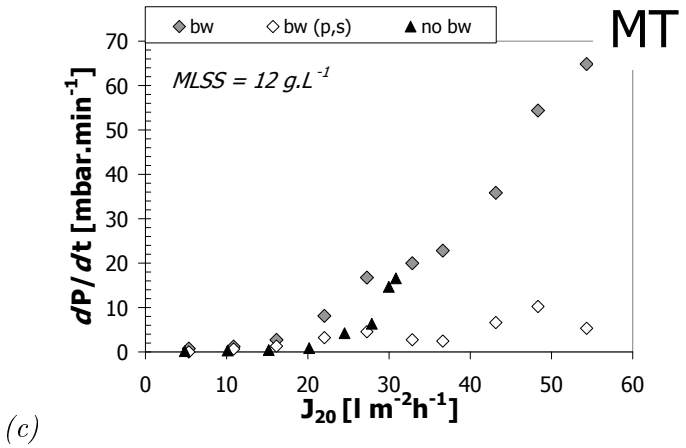

(c)

Figure 6.2.: Comparison of determined fouling rates dP/dt and $dP_{p,s}/dt$ for the two different flux step protocols - MT module: *(a)* MLSS 3-4 g.L^{-1} ; *(b)* MLSS 7 g.L^{-1}; *(c)* MLSS 12 g.L^{-1}.

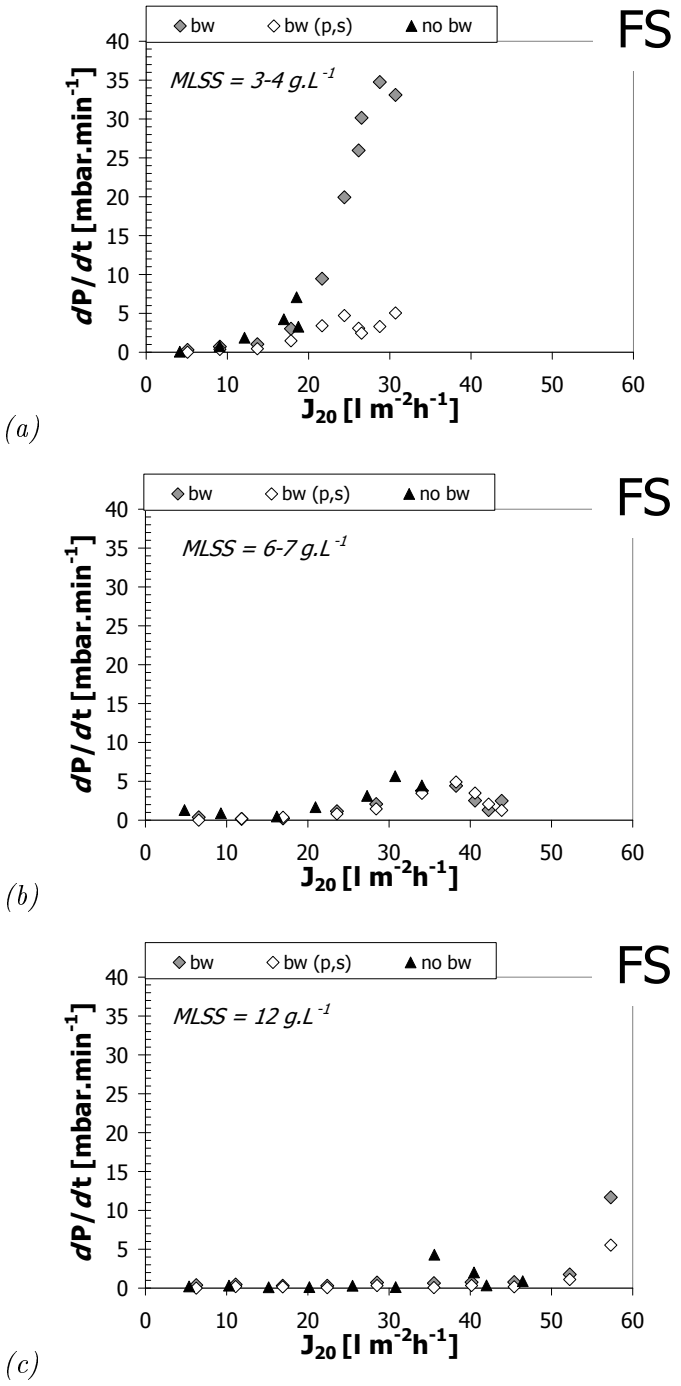

Figure 6.3.: Comparison of determined fouling rates dP/dt and $dP_{p,s}/dt$ for the two different flux step protocols - FS module: *(a)* MLSS 3-4 g.L^{-1} ; *(b)* MLSS 7 g.L^{-1}; *(c)* MLSS 12 g.L^{-1}.

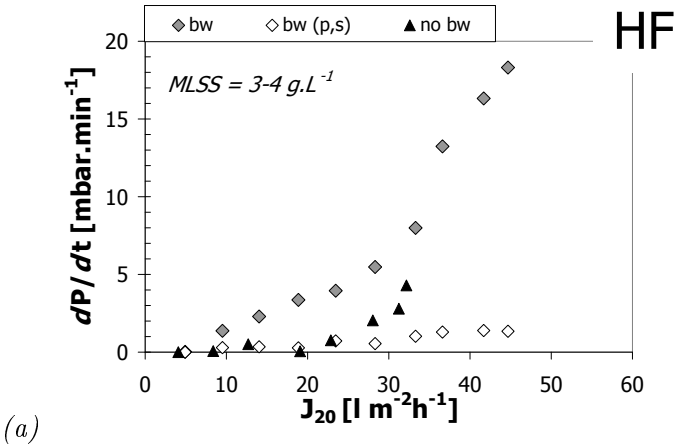

(a)

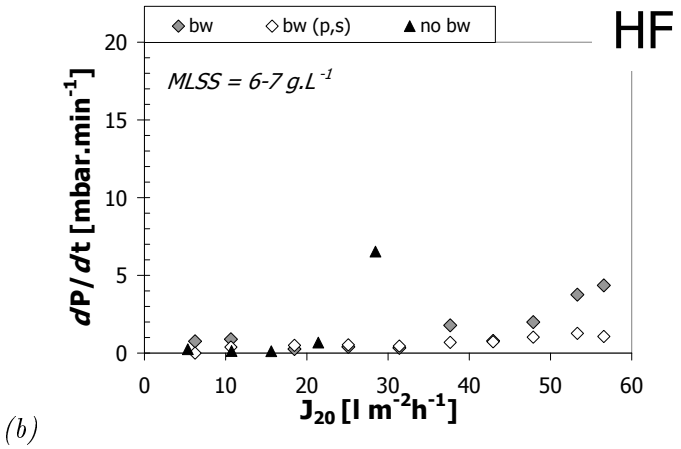

(b)

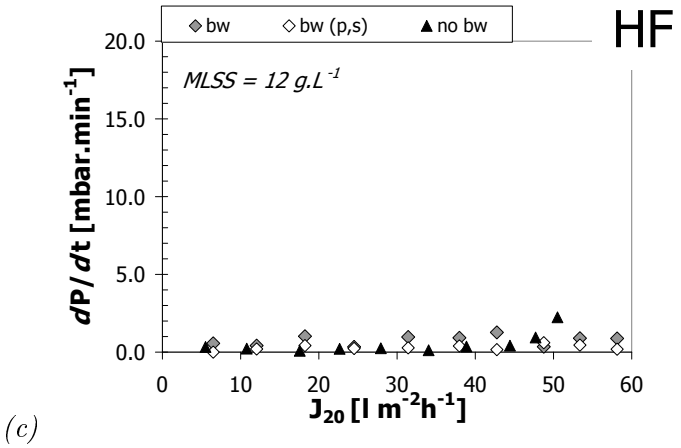

(c)

Figure 6.4.: Comparison of determined fouling rates dP/dt and $dP_{p,s}/dt$ for the two different flux step protocols - HF module: *(a)* MLSS 3-4 g.L^{-1}; *(b)* MLSS 7 g.L^{-1}; *(c)* MLSS 12 g.L^{-1}.

6.2.3. Cake layer resistance R_{cl}

To estimate the difference in cake layer development for the different filtration protocols, comparison trials on two consecutive days were compared for the cake layer resistance, which was determined from the total resistance minus the intrinsic membrane resistance prior to the test and the clean water resistance after the test (Figure 6.5).

Surprisingly, the development of cake layer resistance was found to be very similar for both filtration protocols with regards to the flat sheet membrane module (Figure 6.5*b*). Overall, R_{cl} was found to remain below 2.0 $\cdot 10^{12}$ m^{-1} for a MLSS content of 12 $g.L^{-1}$ increased up to $8.0 \cdot 10^{12}$, $10.0 \cdot 10^{12}$ m^{-1} respectively during the MLSS trial of 7 $g.L^{-1}$ and reached a maximum of 15.0 $\cdot 10^{12}$ m^{-1} during the MLSS trial at 3 $g.L^{-1}$.

Contrary to the flat sheet module, a very different pattern for the development of R_{cl} during the two different filtration protocols was determined for the HF and MT modules (Figure 6.5*a*,6.5*c*). During the backwash trial, R_{cl} of the HF module remained below $0.6 \cdot 10^{12}$ m^{-1} throughout all tests, but reached a maximum value of $5.5 \cdot 10^{12}$ m^{-1} for the trial applying the classic incremental flux step method at a MLSS content of 3 $g.L^{-1}$. R_{cl} was found below $2.0 \cdot 10^{12}$ m^{-1} for the MT module applying the backwash filtration protocol, whereas while using the non-backwash protocol, R_{cl} rose up to $19 \cdot 10^{12}$ m^{-1} for the trial undertaken at 3 $g.L^{-1}$.

These findings emphasised the need to undertake short-term trials by using a test protocol which can reflect the membranes filtration specifications, because applying backwash cycles to multi-tube and hollow fibre membranes are crucial fouling control parameters for these configurations and were found in this study to reduce the cake layer resistance significantly compared to the flat sheet membrane module. Furthermore the results obtained for cake layer resistance also suggests that the parameter *resistance (R)* provides better comparability between tests undertaken at different tests conditions, e.g. filtration protocols, than the frequently used parameter *fouling rate (dP/dt)*.

Interesting to note is also that during low filtration flux, R_{cl} is found to be higher than for the moderate flux at 10 LMH. This might either indicate that the cake layer resistance is compressible to a certain extent providing less resistance under moderate fluxes, or that under very low permeate flow a different cake layer is created which provides higher filtration resistance.

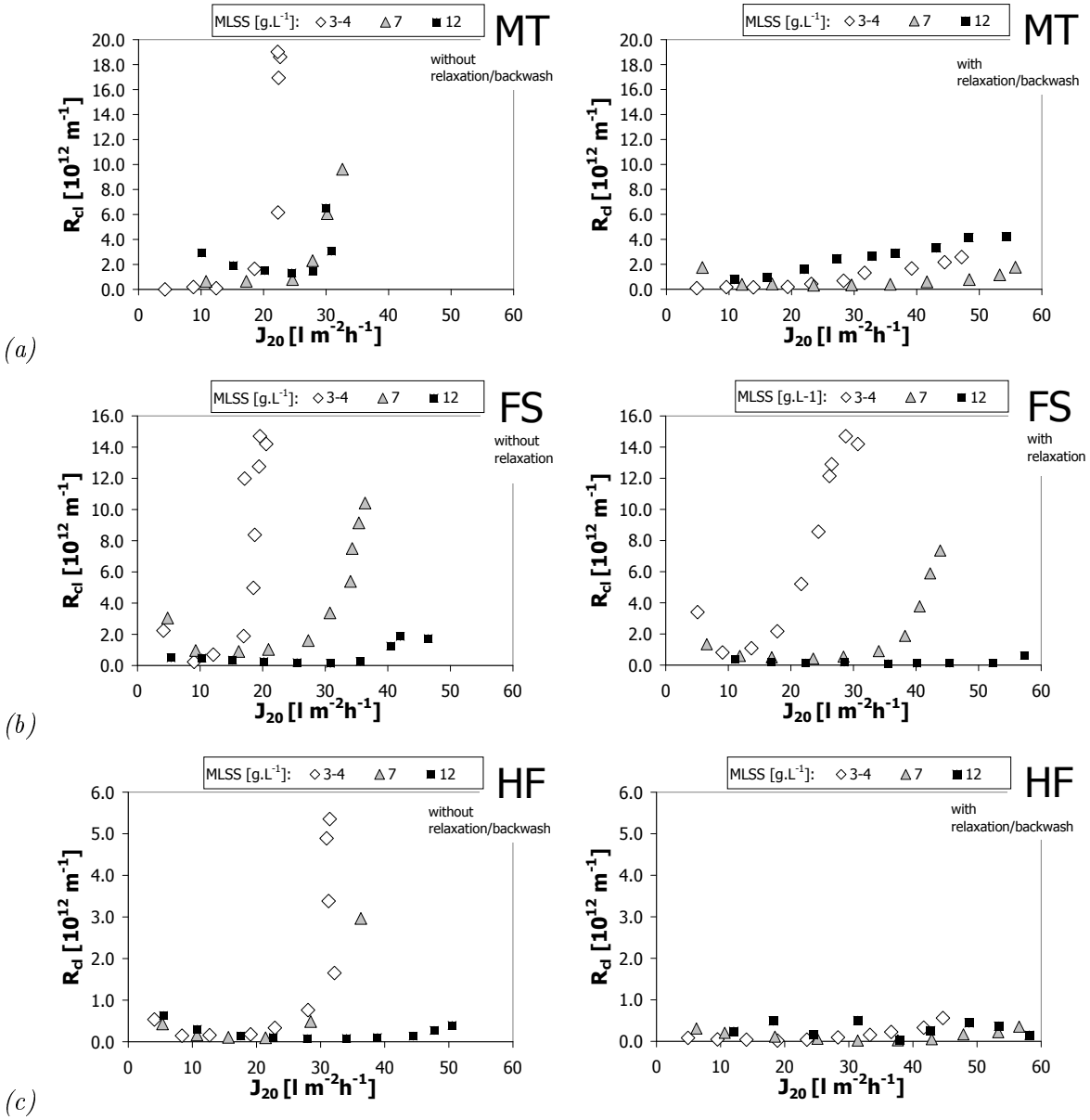

Figure 6.5.: Comparison of cake layer resistance R_{cl} of critical flux trials (constant aeration rate, different MLSS, trials on 2 consecutive days) for *(left)* non backwash and *(right)* relaxation/backwash trials: *(a)* MT; *(b)* FS; *(c)* HF.

6.2.4. Summary

A comparison of critical flux trials at varying MLSS contents revealed a general increase of J_c with increasing MLSS content of biomass for the HF and FS module. Comparing the classical incremental flux step method with the novel filtration protocol J_c ranged from 13 LMH to 39 LMH, from 19 LMH to 49 LMH for the HF module, and from 9 LMH to 31 LMH and 14 LMH to 45 LMH for the FS module (Figure 6.6). The MLSS content of the biomass revealed a significant impact on the overall filtration performance for these two membrane modules. The MT module on the other hand, showed the highest critical flux at MLSS content of 7 $g.L^{-1}$ with $J_c \approx 36$ LMH, with a difference of 11 LMH determined between backwash and non-backwash trials (Figure 6.6). Results will be discussed further in section 6.5 (page 122).

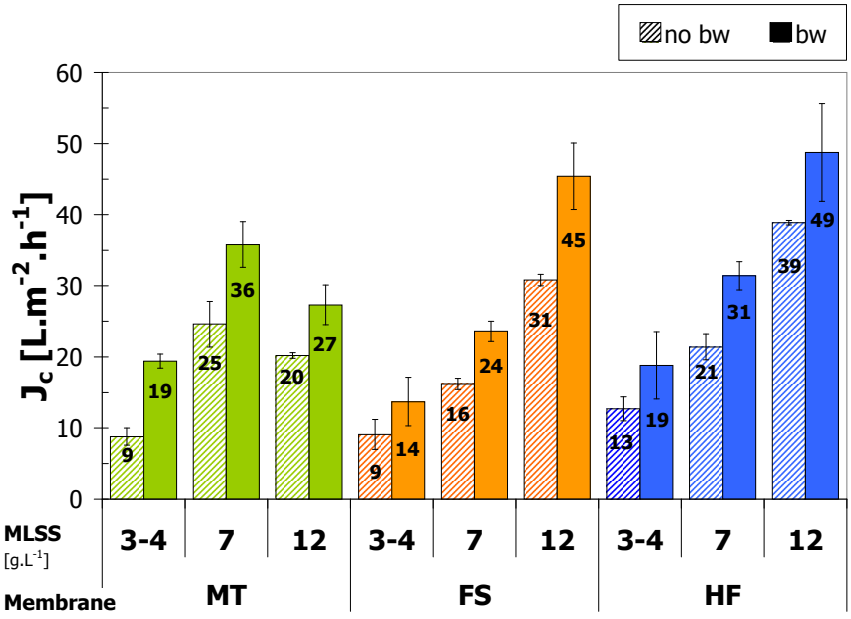

Figure 6.6.: Comparison of critical fluxes determined at varying MLSS content and different filtration protocols

Permeability values for the novel flux protocol varied widely for the different modules tested with the MT module revealing a permeability of 358 $LMH.bar^{-1}$ at J_c for the optimum MLSS range of 7 $g.L^{-1}$, while the HF and FS module showed the highest permeability values for MLSS of 12 $g.L^{-1}$ with 863 $LMH.bar^{-1}$ and 912 $LMH.bar^{-1}$ respectively. Permeability values for J_c determined for the classical incremental flux step method were found to be 50 to 100 $LMH.bar^{-1}$ lower for the MT module, 101 to 236 $LMH.bar^{-1}$ for the FS module and 47 to 225 for the HF, respectively (Table 6.1).

Table 6.1.: Overview of results for critical flux filtration tests with different critical flux protocol and at varying MLSS content (fixed SAD_m)

membrane	***MLSS*** *g.L^{-1}*	**MT**		**FS**		**HF**	
		bw	**no bw**	**bw**	**no bw**	**bw**	**no bw**
J_c (numer of flux step)	3-4	4	2	3	2	4	3
	7	**6**	**4**	4	3	5	4
	12	5	**4**	**8**	**6**	**8**	**7**
J_c (J_{20}) [LMH]	3-4	19.4 *1.0*	8.8 *1.2*	13.7 *3.4*	9.1 *2.1*	18.8 *4.7*	12.7 *1.7*
	7	**35.8** *3.2*	**24.6** *3.2*	23.6 *1.4*	16.2 *0.75*	31.4 *2.0*	21.4 *1.8*
	12	27.3 *2.8*	**20.2** *0.4*	**45.4** *4.7*	**30.8** *0.8*	**48.8** *6.9*	**38.9** *0.3*
P_{ave}(J_c) [mbar]	3-4	57 *13*	36 *16*	30 *29*	26 *19*	32 *40*	20 *14*
	7	**100** *45*	**89** *43*	42 *20*	49 *5*	39 *50*	30 *50*
	12	75 *22*	**65** *4*	**50** *35*	**39** *14*	**56** *31*	**61** *2*
K_{20} (J_c) [LMH.bar^{-1}]	3-4	342 *80*	245 *73*	455 *119*	348 *111*	590 *117*	637 *122*
	7	**358** *71*	**276** *75*	568 *69*	332 *145*	800 *40*	717 *36*
	12	365 *127*	309 *106*	**912** *135*	**783** *59*	**863** *221*	**638** *133*
overall $K_{20,ave}$ [LMH.bar^{-1}]	3-4	283 *105*	105 *59*	281 *134*	144 *51*	491 *82*	386 *88*
	7	**362** *74*	**162** *62*	484 *261*	223 *109*	659 *96*	562 *45*
	12	264 *102*	174 *74*	**754** *145*	**605** *107*	**820** *214*	**581** *77*

6.3. Critical Flux at pilot scale - Comparison to consecutive filtration runs and sub-critical long-term fouling

6.3.1. Critical Flux Trials under Consecutive Filtration

To compare the possible fouling history of the membrane, repetitive critical flux trials were conducted (MLSS 5.5 - 5.8 g.L^{-1}; HRT = 8h) consecutively with a relaxation period of half an hour between each test, but with no further cleaning. To illustrate the results, the classical fouling rates determined as $d\mathrm{P}/d\mathrm{t}$ are represented hereafter (Figure 6.7).

The MT module revealed overall a very stable filtration performance with only little changes for trial number 3, which lead to the suggestion that the difference could not have been attributed to membrane fouling history and that the filtration protocol provided full reversibility. The FS module on the other hand, presented the best results for critical flux trial number (2), but also revealed an increase in fouling resistance between trial (2) to (4).

The HF, however, considering the overall good performance this module revealed during the short-term sampling campaign, seemed to be affected the most by the fouling history. In fact, while for the other two modules, dP/dt shifts did not exceed 10 mbar.min^{-1}, the fouling rates for the HF module rose from trial (2) to (3) with $\approx$ 12 mbar.min^{-1} and furthermore increased for another 12 mbar.min^{-1} from trial number (3) to (4) (Figure 6.7). These results emphasised the importance of membrane fouling history on overall assessment of the filtration trial.

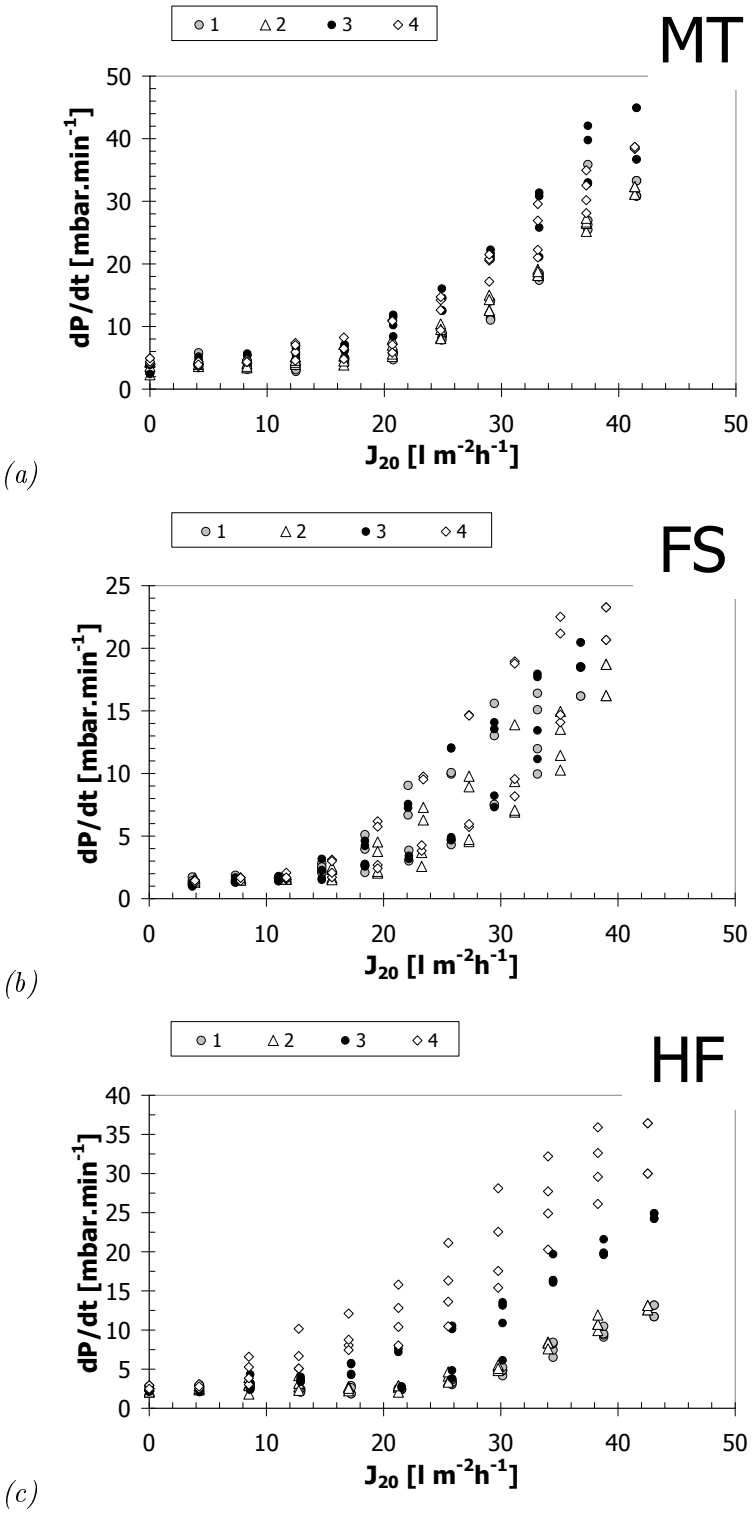

Figure 6.7.: Fouling rates dP/dt for consecutive critical flux trials - without cleaning between trials: *(a)* MT; *(b)* FS; *(c)* HF.

6.3.2. Sub-critical continuous filtration

A number of continuous trials were conducted at different moderate fluxes (6 to 27 LMH), which were however limited to one week and therefore did not reveal any significant fouling pattern. However, during the continuous filtration trial at MLSS 6 $g.L^{-1}$, the flat sheet module exhibited very characteristic slopes of residual fouling which seemed, however, to be reversible (Figure 6.8). These up-and-downs were assumed to derive from biomass changes to which the flat sheet module has shown to interact sensibly with during the critical flux trials.

For another trial, conducted at biomass content of 12 $g.L^{-1}$ and a flux of 27 LMH for FS, which would have been expected to be within sustainable range according to the overall good filtration performance exhibited by the FS module, the FS module suddenly (around 2 hours after initial start) showed a TMP increase from 125 mbar previously up to 750 mbar, while the MT and HF module remained a moderate filtration performance. The reason for this sudden TMP increase was, in fact, another clogging phenomenon, where biomass had accumulated within the side-stream vessel of the flat sheet module and the air-lift applied was not sufficient enough to lift the thickened biomass. No such effect was observed during the same period of time for the HF module being operated at the same flux of 27 LMH. Due to the outcome of the critical flux trials, the MT module was operated at 18 LMH and presented a stable filtration performance for the timescale documented (Figure 6.8).

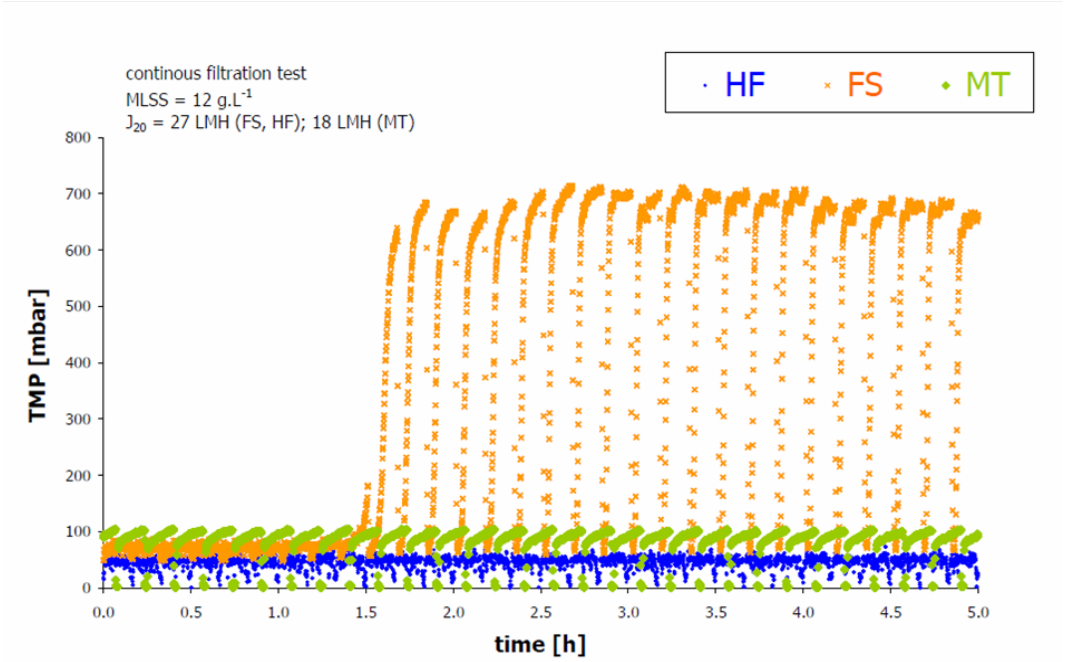

(a)

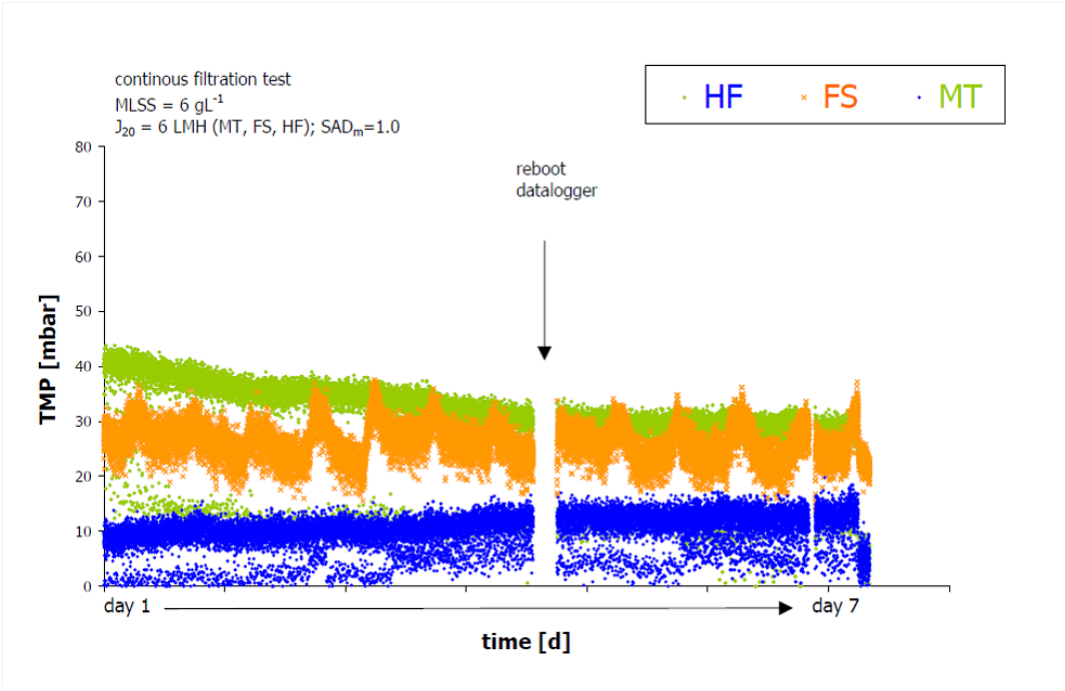

(b)

Figure 6.8.: Continuous filtration trials using relaxation/backwash protocol: *(a)* MLSS 6 g.L^{-1}; *(b)* MLSS 12 g.L^{-1}.

6.4. Critical flux of different membrane materials at varying MLSS - Bench-scale trials

To compare possible impacts of membrane material on the overall filtration performance, different membrane materials were chosen and critical flux trials were undertaken in parallel to the pilot scale study on a bench-scale cross-cell and a single-tube test cell device respectively. Membrane materials tested consisted of flat sheet membranes included polymeric membranes made of PVDF, PES, PS and PE with varying pore sizes, and tubular membranes made of PES and PVDF respectively with varying inner diameters for single tube trials (Table 4.1, page 43). Amongst the different bench-scale materials, the flat sheet material made of PVDF with a nominal pore size of 0.08 μm represented the material the pilot scale module was made of, for the multi-tubular membrane the material MT04 was made of PVDF with a nominal pore size of 0.03 μm.

Critical fluxes for the bench-scale **flat sheet material** varied between 9 LMH and 18 LMH, which was much lower than J_c determined for the pilot scale module. The bench scale flat sheet material tests furthermore did not reveal a consistent trend towards MLSS content (Table 6.3), as opposed to the pilot scale module. For instance, J_c for the PVDF 0.08 μm membrane material (the bench-scale material identical to the pilot scale module material) was lower with higher MLSS content, whereas the FS pilot scale module presented best filtration performance at 12 g.L^{-1}.

The different findings between bench and pilot scale flat sheet results were assumed to be caused by the set-up themselves, with the pilot scale being an aerated system, while the bench-scale biomass was non-aerated and exposed to further shear stress due to the additional circulation pump. Also, the retentate and permeate flow direction was different between the two scales, leading to a higher risk of biomass material accumulation on the membrane surface for the bench-scale material. These findings were supported by additional experiments undertaken to assess the impact of particle size distribution, which are reported in Chapter 8.

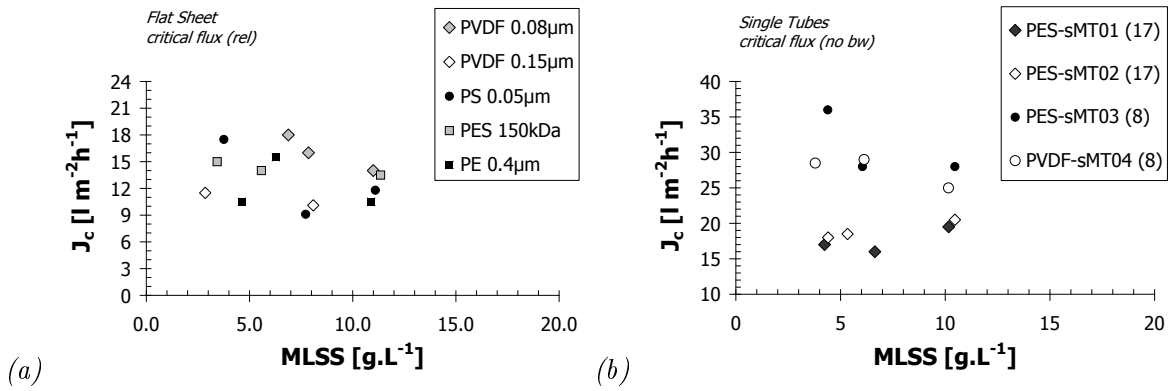

Figure 6.9.: Comparison of J_c to MLSS content of *(a)* flat sheet material and *(b)* single-tube

Filtration performances between all four **tubular membrane materials** varied widely, with critical fluxes ranging from 16 LMH for sMT01 and up to 36 LMH for sMT03. The most consistent filtration performance with the lowest total membrane resistance was found in the sMT04 membrane sample, which might indicate it as the optimal material choice for the multi-tubular membrane module. The highest total filtration resistance with the highest determined irreversible fouling resistance was found in the sMT02 membrane material. No direct correlation was observable between J_c and the MLSS content of the biomass for the range of materials tested (Figure 6.9).

6.5. Summary

As previously established in Chapter 5, permeability changed significantly per module tested. Filtration protocols without backwash were found in general to result in lower permeability compared to critical flux tests including relaxation/backwash step, which had been expected. However, the range of permeabilities determined within each repetition series was found to be very broad and emphasising the importance of replication. It furthermore emphasised the impact of membrane history, which can not be neglected even if a cleaning procedure re-establishes a permeability close to the original permeability. The deviation range of replicated tests was found to be much higher for the non-backwash trials for all three membrane configurations tested.

In this section, critical fluxes obtained through short-term tests were compared at MLSS concentration ranging from 3 to 12 g.L^{-1} with opposing results gained for the different membrane pilot scale module configurations, and moreover also for the different bench scale material (Table 6.2). To investigate the potential impact of scale on the experiments conducted, pilot scale and bench-scale were run in parallel during this study. Surprisingly different trends were reported, not only between different membrane module configurations in pilot scale, but also between the different scales of experiments; hence between bench and pilot scale of the same membrane material and configuration. For instance, while the MT pilot scale module showed best filtration behaviour at MLSS content of 7 g.L^{-1}, which was furthermore confirmed by the lab scale single tube module of same material, the lab scale modules made of PES revealed a completely different filtration behaviour.

When comparing the MLSS content measured at the retentate lines of each individual module with the critical flux determined at the novel flux step protocol, a direct correlation was evident for the FS and HF modules (FS: R^2=*0.6917*; HF: R^2=*0.8214*) but not for the MT module (MT: R^2=*0.031*, Figure 6.10). Indeed, with the FS and HF modules the permeability clearly improved when the MLSS concentration increased with permeabilities of about 300 LMH.bar^{-1} at a MLSS concentration of 4 g.L^{-1} up to 900 LMH.bar^{-1} at 15 g.L^{-1}. For the MT module, no clear correlation of the permeability with the MLSS could be found.

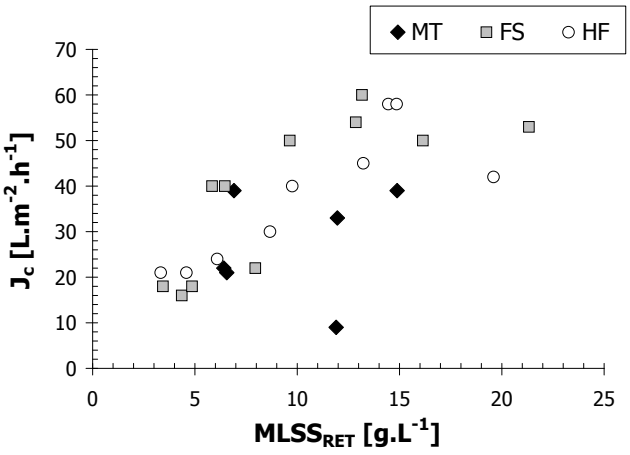

Figure 6.10.: Correlation of J_c with MLSS content of retentate lines ($MLSS_{RET}$) at constant aeration rates.

While the best filtration performance of the MT membrane module within this work was found for an MLSS content of 7 g.L^{-1} with permeability decreasing for higher MLSS, studies conducted at the same pilot hall revealed the best filtration performance was at the highest MLSS content for flux step tests undertaken with MT membrane modules (Brookes, 2005; Le-Clech, 2002). For instance, Le-Clech (2002) reported no difference between MLSS content of 4-8 g.L^{-1}, whereas critical flux significantly increased with MLSS increasing to 12 g.L^{-1}. Brookes (2005) on the other hand reported the highest transitional flux at the highest MLSS content tested (18 g.L^{-1}) (Table 6.2).

For a large pilot scale submerged HF membrane module, Germain (2004) observed a sustainable flux of 16.5 LMH. Below the sustainable threshold value, the filtration performance of the membrane module seemed independent of biomass make-up parameters, whereas above permeability was reported to deteriorate with increasing MLSS content and increasing bound EPS. Bouhabila *et al.* (1998) reported for a small lab scale HF, the lowest critical flux at MLSS of 8 g.L^{-1} gave no differences in critical flux for tests at MLSS 15 or 4 g.L^{-1}. Bottino *et al.* (2009) on the other hand, compared three different membrane materials in submerged HF lab-scale mode to identify critical flux at varying MLSS content and reported a decrease of J_c with increasing MLSS. Howell *et al.* (2004) carried out flux step tests at varying biomasses (5.4 to 21.1 g.L^{-1}) and also observed the lowest fouling rates at MLVSS 12.5 g.L^{-1}, whereas the highest fouling rate was observed at MLVSS 5.14 g.L^{-1}. Howell *et al.* (2004) furthermore indicated that history dependent fouling is a complex phenomenon that is difficult to quantify, and that membrane fouling models might be fitting well to the experiment they were developed from, but due to the complex interaction of membrane history it is almost impossible to apply to further tests, which is also indicated in this current work during the repetitive trials.

Table 6.2.: Comparison of impacts of MLSS on critical fluxes - literature data and this study

conf		scale	material	feed	MLSS	aeration	J_c	observation	Reference
					$g.L^{-1}$	1, (2), [3]	LMH		
sub	MT	lab	PES 0.01μm - 0.1μm	mun.	4 to 12	0.07; 0.22	16 - 121	no difference of J_c for MLSS 4-8 g.L^{-1}; but significant increase of J_c at 12g.L^{-1}	Le-Clech *et al.* (2003b)
sub	MT	lab	PVDF 0.03μm	synth.	6 to 18	-	8 - 14	transitional flux higher at highest MLSS	Brookes (2005)
ss*	MT	pilot	PVDF 0.03μm	mun.	3 to 12	0.02-0.09 [0.5 - 2.0]	7 - 50	highest J_c at MLSS 6 g.L^{-1}	this study (bw)
ss*	MT	pilot	PVDF 0.03μm	mun.	3 to 12	0.02 - 0.1 [1.5]	19 - 36	highest J_c at MLSS 6 g.L^{-1}	this study (bw)
ss*	MT	pilot	PVDF 0.03μm	mun.	3 to 12	0.02 - 0.05 [1.5]	9 - 25	highest J_c at MLSS 6 g.L^{-1}	this study (no bw)
ss	MT	lab	PVDF 0.03μm	mun.	4 to 10	-	25 - 29	highest J_c at MLSS 6 g.L^{-1}	this study (no bw)
			PES (0.117 ID)	mun.	4 to 10	-	16 - 20.5	highest J_c at highest MLSS	
			PES (0.08 ID)	mun.	4 to 10	-	28 - 36	highest J_c at lowest MLSS	
sub	HF	n.a.	PE		3 to 14	constant at 3.0 L/min	13.8 to 4.9	decrease of J_c with increasing MLSS	Bottino *et al.* (2009)
sub	HF	lab	PS 0.2-0.4μm	synth.	4 to 15	20 l/h ($\approx$ 1.25)	$\approx$ 10 to 20	lowest J_c for MLSS 8; similar range for MLSS 15 and MLSS 4	Bouhabila *et al.* (1998)
sub	HF	pilot	PVDF 0.04μm	mun.	4 to 13	0.07 to 0.13	$\approx$ 16-22	transitional flux, above that fouling increases with increasing MLSS	Germain *et al.* (2005)
sub	HF	pilot	PVDF 0.04μm	mun.	8 to 26	-	$\approx$ 12-42	max J_c around MLSS 21, but no obvious impact of MLSS.	Fan *et al.* (2006)
ss*	HF	pilot	PES 0.04μm	mun.	3 to 12	0.002-0.02 [0.5 - 2.0]	20 - 58	increasing J_c with increasing MLSS	this study (bw)
	HF	pilot	PES 0.04μm	mun.	3 to 12	0.003-0.02 [1.0]	19 - 49	increasing J_c with increasing MLSS	this study (bw)
	HF	pilot	PES 0.04μm	mun.	3 to 12	0.003-0.006 [1.0]	13 - 39	increasing J_c with increasing MLSS	this study (no bw)

x[1] = superficial gas velocity u_air in m.s^{-1}; (x)[2] = superficial liquid velocity u_lq in m.s−1; [x][3] specific aeration demand in N m^{3}m^{2}h^{-1}; +cross cell;

Table 6.3.: Comparison of impacts of MLSS on critical fluxes - literature data and this study

confi		scale	material	feed	MLSS	aeration	J_c	observation	Reference
					$g.L^{-1}$	1, (2), [3]	LMH		
ss^{+}	FS	lab^{+}	(HVLP) 0.45μm	mun.	1 to 10	(0.5-1.5)	$\approx$ 30-78	decreased J_c with higher MLSS; increased J_c with higher CFV	Madaeni (1999)
ss^{+}	FS	lab^{+}	PVDF 0.2μm		8 to 10	0.02-0.07 (0.2-0.4)	$\approx$ 8 to 18	decreasing J_c with slight increasing cross-flow velocity; trend consistent for range of MLSS	Prieske *et al.* (2008)
ss*	FS	pilot	PVDF 0.08μm	mun.	3 to 12	0.0006 - 0.02 [0.5 - 2.0]	16 - 60	increasing J_c with increasing MLSS	this study (bw)
	FS	pilot	PVDF 0.08μm	mun.	3 to 12	0.001 - 0.01 [1.0]	14 - 45	increasing J_c with increasing MLSS	this study (bw)
	FS	pilot	PVDF 0.08μm	mun.	3 to 12	0.0006 - 0.006 [1.0]	9 - 31	increasing J_c with increasing MLSS	this study (no bw)
ss^{+}			PVDF 0.08μm	mun.	7 to 11	-	18 - 14	highest J_c at lowest MLSS (7 g.L^{-1})	this study (bw)
			PE 0.4μm	mun.	4 to 10	-	10 - 16	highest J_c at MLSS 6 g.L^{-1}	
			PES 150kDa	mun.	3 to 11	-	13 - 15	highest J_c at lowest MLSS	
			PVDF 0.15μm	mun.	3, 8	-	11, 10	highest J_c for lower MLSS	

x^{1} = superficial gas velocity u_air in m.s^{-1}; (x)^{2} = superficial liquid velocity u_lq in m.s-1; [x]^{3} specific aeration demand in N m^{3}m^{2}h^{-1}; $^{+}$cross cell;

Generally, little is reported in literature about clogging events in MBR systems. This might be due to the usual set-up being a submerged system, where distinguishing between membrane fouling and clogging of membrane spacer/membrane lumen is almost impossible. In this study, the clogging phenomenon could be well observed due to the set-up as air-lift side-stream mode with the membrane chamber being made of Plexiglas. Sudden TMP increases, which are regularly reported in literature as a final detrimental fouling step (Brookes, 2005; Guglielmi *et al.*, 2007a; Judd, 2006; Zhang *et al.*, 2006) with fouling rates increasing exponentially with flux, were attributed to a number of models (Judd, 2011), but nonetheless to clogging. However, rapid increases in TMP with increasing flux in this study was found not only to be attributed to the fouling phenomenon, for instance, as observed at lower MLSS content for the FS module, but also to the clogging phenomenon especially at higher MLSS content and long-term filtration. Data should therefore be analysed for both phenomenon, clogging and fouling, when describing the positive or negative impact of MLSS on membrane filtration performance.

7. Results and Discussion: Fouling control by air scouring

7.1. Scope

Membrane scouring caused by an increase of aeration has been identified an effective technique for improving membrane filtration performance due to a reduction of particle deposition on the membrane surface (Judd, 2006; Stephenson *et al.*, 2000; Wintgens *et al.*, 2003). However, the advantage of increased aeration was reported in several studies to be effective only up to a certain threshold value where above a further increase in aeration does not reveal further improvements in filtration performance (Bouhabila *et al.*, 2001; Le-Clech *et al.*, 2003b; Ueda *et al.*, 1997). Whilst reducing membrane fouling is lowering maintenance costs, such as membrane cleaning and membrane replacement, applying aeration to control membrane fouling is one of the main cost parameters for wastewater treatment in full scale MBRs (Brepols *et al.*, 2010). Hence, optimised aeration rates during membrane filtration are essential for a cost-effective membrane operation.

Within this study, three different membrane modules (MT, FS, HF) were investigated for their fouling potential during different aeration scenarios using short-term critical flux tests. For the trials, MLSS concentration and HRT were maintained at chosen values and the filtration of the three modules was assessed for a range of specific aeration demands (SAD_m). Due to the set-up as an air-lift side-stream operation and the subsequently required relatively high gas hold-up to create an effective cross-flow, the minimum possible aeration rate for side-by-side comparison of all three modules was 0.5 $Nm^3m^{-2}h^{-1}$ SAD_m, which is higher compared to the lowest full scale aeration rates, but within range of typical pilot scale data (Table 7.1).

Table 7.1.: Typical aeration rates [SAD_m in $N.m^3m^{-2}h^{-1}$]

typical aeration rates SAD_m [$Nm^3m^{-2}h^{-1}$]	MT	FS	HF
full scale *(Judd 2011)*	0.3 - 0.6 [additional CVF: 2-4 $m.s^{-1}$]	0.5 - 0.8	0.1 - 0.3
pilot scale *(Judd 2011)*	0.3 - 1.2	0.35 - 1.5	0.2 - 0.6
this study	**0.5 - 2.0**	**0.5 - 2.0**	**0.25 - 2.0**

For the aeration rates applied within the current study, the resulting cross-flow velocities (CFV measured as air-liquid-solid three-phase cross flow velocity) were determined between 0.0007 $m.s^{-1}$ to 0.019 $m.s^{-1}$ for the FS module, 0.0038 $m.s^{-1}$ to 0.022 $m.s^{-1}$ for the HF module and 0.0167 $m.s^{-1}$ to 0.0936 $m.s^{-1}$ for the MT (Figure 7.1). The flux step tests were chosen to be run under similar filtration patterns than full scale operations using a filtration cycle of 10 minutes with 540 second on, 60 second relaxation including 10 seconds backwash where configuration permitted with a step height of 5 LMH (Table 4.6). Overall, the membrane modules were tested for three different MLSS concentrations between 3 and 12 $g.L^{-1}$.

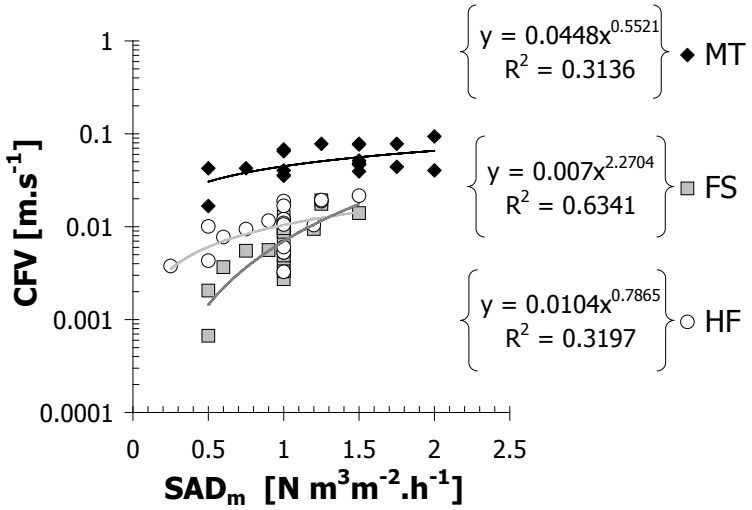

Figure 7.1.: Resulting CFV from chosen SAD_m rates for different module configurations and varying MLSS content.

Intensive membrane aeration was reported to not only intensify the shear rates on the membrane surface, but also on the MBR biomass, reducing floc size and releasing colloidal particles and SMP, which in turn was reported to increase pore blocking and colloidal fouling of the membranes (Menniti *et al.*, 2009; Stricot *et al.*, 2010; Wisniewski and Grasmick, 1998). Biomass parameters were therefore not only monitored for the aeration tank, but also for the retentate line of each membrane module.

Results for biomass impact are reported in Chapter 8. Furthermore, a study to investigate the changes of sludge filterability due to side-stream operation was conducted in parallel, applying the Delft Filtration Method (DFC_m), with results being reported summarised in Section 7.4 (page 143) and explained in detail in Appendix A.

7.2. Permeability Development of Critical Flux Trials at different SAD_m and MLSS content

The results obtained during varying aeration scenarios indicated, similarly to the observation reported in the previous chapter, that filtration performance varied significantly depending on the membrane module tested (Figure 7.2 to Figure 7.7).

7.2.1. MT module

Limited fouling was observed for the multi-tubular module for lower MLSS concentrations ($\approx$ 3-4 $g.L^{-1}$) with P_{ave} up to approximately 160 mbar at a flux (J_{20}) of 45 LMH (Figure 7.2*a*). In these conditions, an increased SAD_m had only a limited effect on the membrane performance. Moreover, an amelioration in the filtration performance was observed for SAD_m, decreasing from 1.0 $Nm^3m^{-2}h^{-1}$ to 0.5 $Nm^3m^{-2}h^{-1}$, whilst the best permeability values were measured for a SAD_m rate of 1.5 $Nm^3m^{-2}h^{-1}$. Membrane fouling of the MT module was found to progressively increase when MLSS content increased to 7 $g.L^{-1}$ and then to 12 $g.L^{-1}$ with P_{ave} of above 400 mbar and above 650 mbar respectively.

With a MLSS content of 7 $g.L^{-1}$ (Figure 7.2*b*), similar trends compared to MLSS 3-4 $g.L^{-1}$ were observed for the range of SAD_m tested (0.5 $Nm^3m^{-2}h^{-1} \leq SAD_m \leq$ 2.0 $Nm^3m^{-2}h^{-1}$) and for fluxes (J_{20}) up to approximately 32 LMH with a linear evolution of P_{ave}. Above that flux, fouling was found to increase with decreasing SAD_m. For example, at a flux of about 50 LMH, P_{ave} values of 120, 145, 190 and 230 mbar were measured for SAD_m of 2.0, 1.25, 1.0 and 0.5 $Nm^3m^{-2}h^{-1}$. This was expected as more scouring of the membrane surface was likely to be achieved with higher air flow rates.

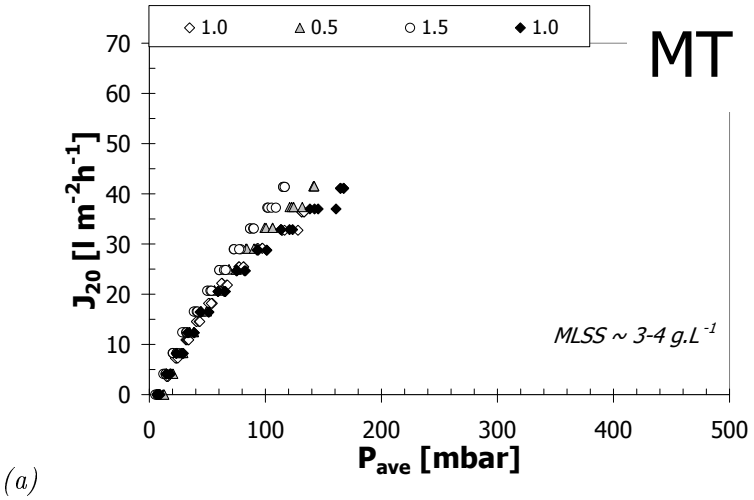

(a)

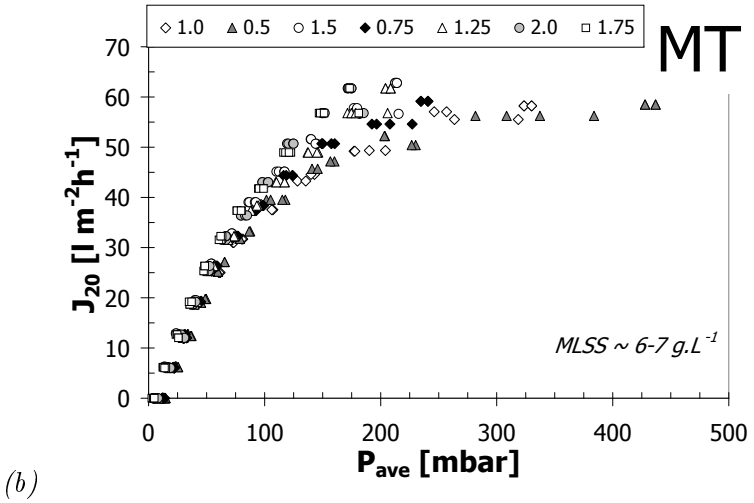

(b)

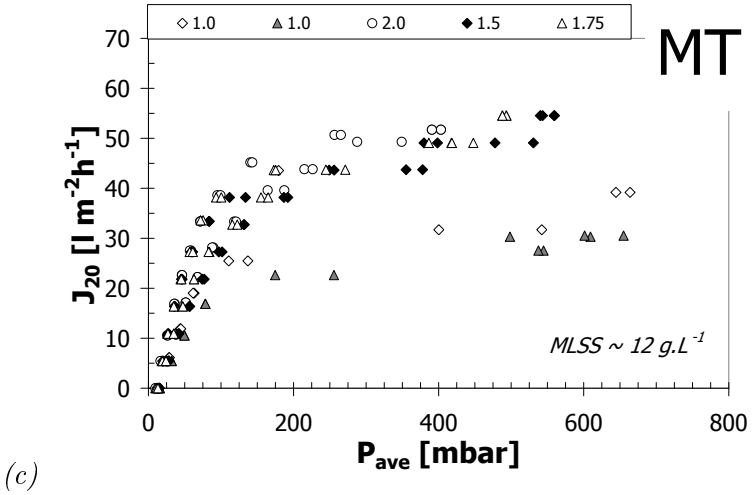

(c)

Figure 7.2.: Permeability curves for critical flux trials at different aeration rates and varying MLSS content - MT module: *(a)* MLSS 3-4 $g.L^{-1}$; *(b)* MLSS 6-7 $g.L^{-1}$; *(c)* MLSS 12 $g.L^{-1}$.

While the best filtration performance was determined for the highest aeration rates (SAD_m of 1.75 and 2.0 $Nm^3m^{-2}h^{-1}$), no further increase in permeability could be observed between both SAD_m rates, revealing a threshold value above which no further increase in filtration performance could be observed, as reported in literature (Bouhabila *et al.*, 2001; Le-Clech *et al.*, 2003b; Ueda *et al.*, 1997).

Similar behaviour was also observed at a MLSS content of 12 $g.L^{-1}$, where significant fouling of the membrane was observed for SAD_m below 1.5 $Nm^3m^{-2}h^{-1}$ (Figure 7.2*c*). In fact, critical flux trials at MLSS 12 $g.L^{-1}$ and SAD_m rates of 1.0 $Nm^3m^{-2}h^{-1}$ had to be stopped at a flux step of 35 LMH (Figure 7.2*c*) due to re-occurring lumen clogging, resulting in a significant increase of the TMP up to 700 mbar at fluxes above 20 LMH.

Due to the results gained for SAD_m = 1.0 $Nm^3m^{-2}h^{-1}$, no further trials were undertaken for aeration rates below 1.0 $Nm^3m^{-2}h^{-1}$ as an even poorer membrane performance was expected. For SAD_m of 1.5, 1.75 and 2.0 $Nm^3m^{-2}h^{-1}$ at this MLSS concentration, P_{ave} was found to increase linearly up to a flux of approximately 35 LMH. For P_{ave} at higher fluxes for these different SAD_m, hysteresis revealed better filtration performance with increasing aeration rates, so P_{ave} at J_{20} of approximately 50 LMH was to be 256 mbar for SAD_m =2.0 $Nm^3m^{-2}h^{-1}$ and 379 mbar, 386 mbar for SAD_m = 1.5, 1.75 $Nm^3m^{-2}h^{-1}$ respectively.

The best filtration performance observed for the MT module was for a lower MLSS content and more commonly for SAD_m values at 1.5 $Nm^3m^{-2}h^{-1}$ or above. The data obtained for the MT module revealed linearity between SAD_m and J_c analogues as reported in literature for the FS module (Guglielmi *et al.*, 2008) and MT module (Le-Clech *et al.*, 2003b), which was however, in opposition to observations for the FS and HF modules in the current study (see Figure 7.5, page 135 and Figure 7.6, page 136).

The impact of increased aeration intensity on J_c for the MT module was found to be higher with a higher MLSS content (Figure 7.3). This could be attributed to the effect of higher aeration lowering the susceptibility to lumen clogging at a higher MLSS content. The higher the aeration intensity, the lower the difference was found between J_c of the MT module at varying MLSS contents (Figure 7.3).

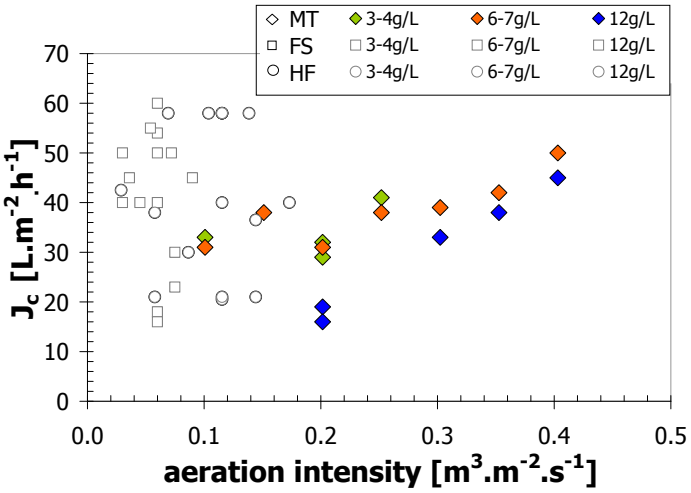

Figure 7.3.: Comparison of determined critical flux J_c and applied aeration intensity at varying MLSS contents - MT module

7.2.2. FS module

Overall, the FS module revealed unexpected results, where better filtration performances were most commonly observed for lower SAD_m values. Moreover, this effect was found to be intensified for the lower MLSS contents (Figure 7.4).

For critical flux trials at a MLSS content of 3-4 $g.L^{-1}$, the measured P_{ave} at the lowest aeration rate of 0.5 $Nm^3m^{-2}h^{-1}$ increased linearly and remained below 75 mbar for fluxes up to 40 LMH, whilst at the same flux P_{ave} increased above 115 mbar for any trials at higher aeration rates ($SAD_m \geq 1.0$ $Nm^3m^{-2}h^{-1}$; Figure 7.4*a*). Indeed, critical fluxes of approximately 18 and 23 LMH were found for SAD_m of 1.0 and 1.25 $Nm^3m^{-2}h^{-1}$. The lowest filtration performance was observed for both critical flux trials at SAD_m = 1.0 $Nm^3m^{-2}h^{-1}$ (maximum $P_{ave,FS}$ = 330 mbar, 418 mbar respectively). The hysteresis effect observed for the decreasing fluxes for the duplicate tests at a SAD_m of 1.0 $Nm^3m^{-2}h^{-1}$ suggested that irreversible fouling had occurred.

The maximum $P_{ave,FS}$ for the highest flux step of critical flux trials undertaken at MLSS $\approx$ 6-7 $g.L^{-1}$ varied from 67 mbar (J_{20} = 61 LMH for SAD_m = 0.5 $Nm^3m^{-2}h^{-1}$) to 412 mbar (J_{20} = 51 LMH; SADm = 1.0 $Nm^3m^{-2}h^{-1}$) with the filtration performance clearly showing to decrease over experimental period (Figure 7.4*b*). The lowest resistance to filtration was found for the first two trials (SAD_m = 1.0 and 0.5 $Nm^3m^{-2}h^{-1}$), with P_{ave} increasing linearly for fluxes up to 60 LMH . Interestingly, P_{ave} increased linearly up to a critical flux of 38 LMH for the rest of the tests with SAD_m ranging from 0.75 to 1.5 $Nm^3m^{-2}h^{-1}$, where a better filtration performance was observed for an aeration rate of 0.75 $Nm^3m^{-2}h^{-1}$ than for higher aeration rates applied thereafter. The suspected decline in sludge filterability could be observed for the duplicate tests carried out at a SAD_m of 1.0 $Nm^3m^{-2}h^{-1}$, with one test revealing no fouling for the range of fluxes tested whereas the other fouled rapidly with the hysteresis curve indicating irreversible fouling. This decline in sludge filterability could, in fact, be confirmed during a study conducted in parallel applying the Delft Filtration method (see a detailed description in Appendix A) with the FS module found to be highly impacted by changes in sludge filterability, as opposed to the MT module.

At a MLSS of 12 $g.L^{-1}$ (Figure 7.4*c*), the best filtration performance for the FS module were monitored. Apart from one critical flux trial at a SADm of 0.6 $Nm^3m^{-2}h^{-1}$, where clogging occurred at fluxes above 45 LMH, the maximum $P_{ave,FS}$ were found to remain below 67 mbar for fluxes (J_{20}) up to 60 LMH. For all the trials with SAD_m ranging from 0.9 to 1.2 $Nm^3m^{-2}h^{-1}$, P_{ave} increased linearly for fluxes up to 60 LMH. Indeed, for the trials with a SAD_m of above 0.6 $Nm^3m^{-2}h^{-1}$, very limited changes in membrane fouling could be observed with no obvious impact of the increased aeration rate.

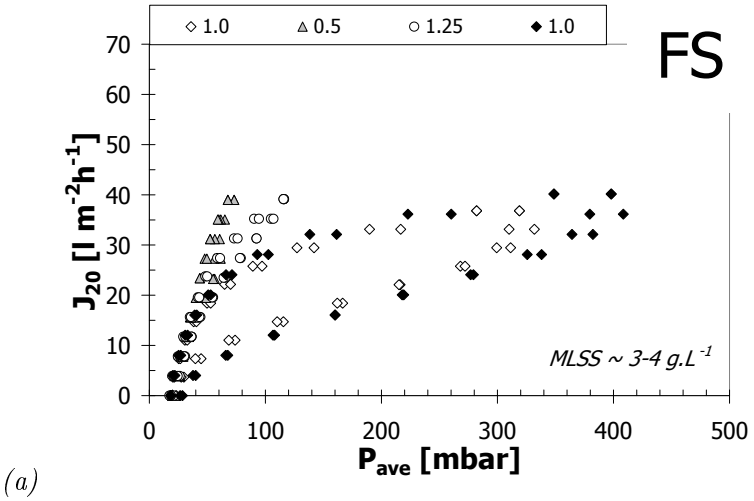

(a)

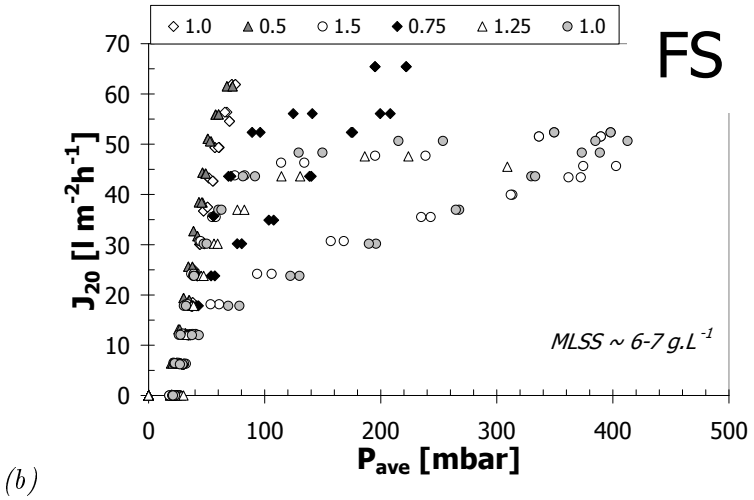

(b)

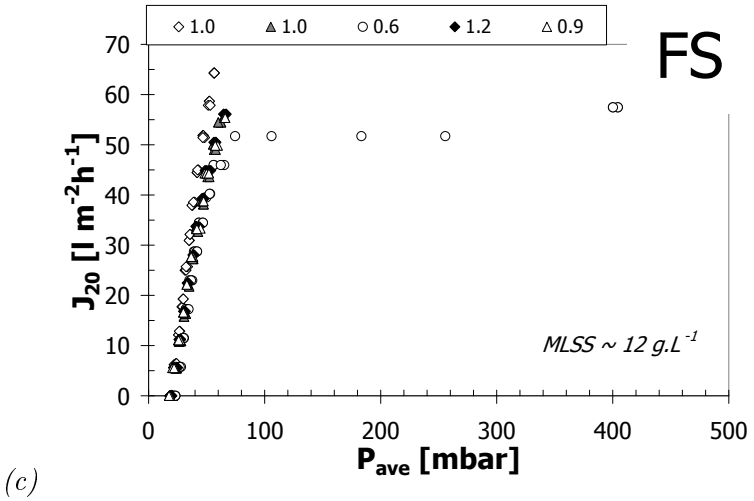

(c)

Figure 7.4.: Permeability curves for critical flux trials at different aeration rates and varying MLSS content - FS module: *(a)* MLSS 3-4 g.L^{-1}; *(b)* MLSS 6-7 g.L^{-1}; *(c)* MLSS 12 g.L^{-1}.

Overall, the determined critical fluxes for the FS module varied between 12 and 60 LMH for the air-rates and MLSS ranges tested (Figure 7.5). In contrast to the MT module and to previously mentioned studies reported in literature (Guglielmi *et al.*, 2007a, 2008; Le-Clech *et al.*, 2003b), no linearity between SAD_m rates and J_c could be observed. In fact, for lower aeration rates at lower MLSS contents, higher critical fluxes were determined (Figure 7.5). This phenomenon could be attributed to changes in sludge filterability due to dewatering of the biomass during the side-stream passage and will be further discussed in Section 7.4 (page 143).

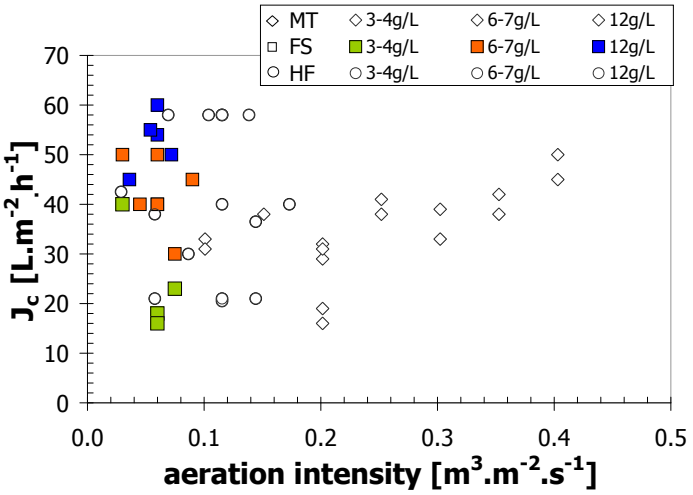

Figure 7.5.: Comparison of determined critical flux J_c and applied aeration intensity at varying MLSS content - FS module

7.2.3. HF module

Overall, the HF module displayed less susceptibility to fouling than the other modules tested. Indeed, for all of the conditions tested $P_{ave,HF}$ remained below 120 mbar (Figure 7.7). Variations of SAD_m were also found to have limited impact on the overall filtration performance of this membrane module (Figure 7.7). For instance, at MLSS 3-4 $g.L^{-1}$ the best permeability values were determined for the highest SAD_m applied (SAD_m = 1.25 $Nm^3m^{-2}h^{-1}$) with the maximum $P_{ave,HF}$ measured at 74 mbar and a difference in maximum $P_{ave,HF}$ to others applied, SADm remained as little as 15 mbar (Figure 7.7*a*). On the other hand, at MLSS 6-7 $g.L^{-1}$ the best filtration performance was observed for the lowest SAD_m rate of 0.25 $Nm^3m^{-2}h^{-1}$ with $P_{ave,HF}$ = 83 mbar at a flux (J_{20}) of 63 LMH. The highest average trans-membrane pressure was determined for a SAD_m of 0.5 $Nm^3m^{-2}h^{-1}$ with $P_{ave,HF}$ = 102 mbar at a similar flux (J_{20} = 65 LMH).

Similarly to the FS module an increase in permeability was observed with increasing MLSS.

For example, at a flux of 30 LMH and the range of SAD_m, $P_{ave,HF}$ of about 55, 38 and 35 mbar were observed for MLSS contents of 4-5, 6-7 and 12 $g.L^{-1}$, respectively. The best overall filtration performance was indeed observed at a MLSS concentration of 12 $g.L^{-1}$ where the critical flux was not reached for fluxes up to 65 LMH even for a SAD_m as low as 0.6 $Nm^3m^{-2}h^{-1}$.

Linearity between J_c and aeration intensity was not evident for this membrane module. In fact, the higher the MLSS content, the lower the impact of varying aeration intensity, which was clearly in opposition to the MT module. For the lower MLSS content, J_c slightly increased with decreasing aeration intensity, which was similar to the FS module, though evidence was less significant (Figure 7.6).

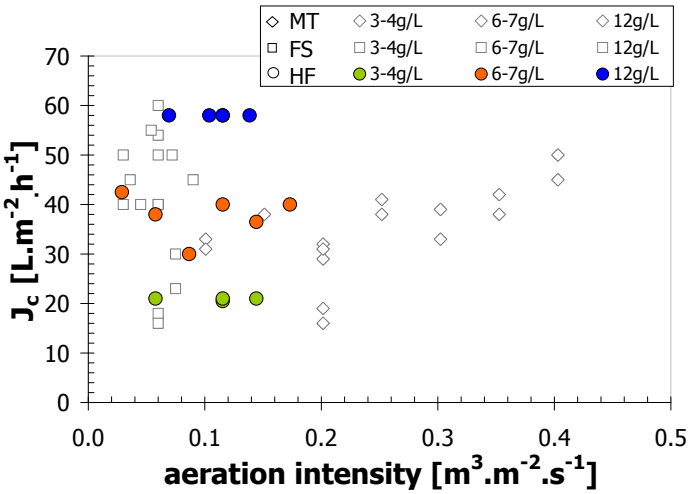

Figure 7.6.: Comparison of determined critical flux J_c and applied aeration intensity at varying MLSS content - HF module

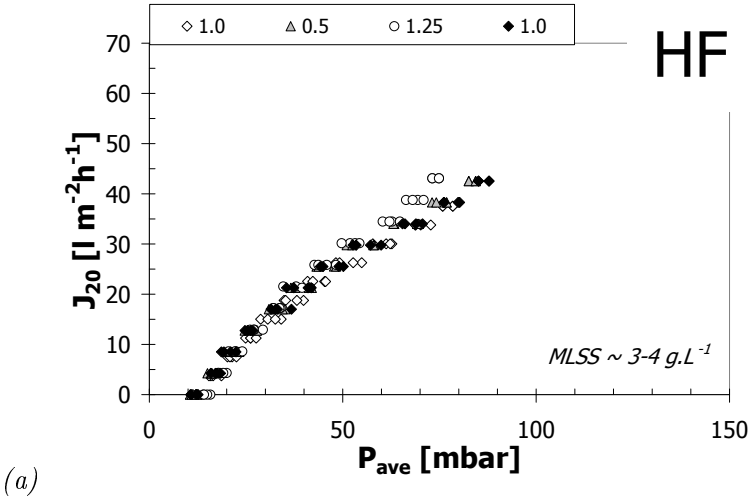

(a)

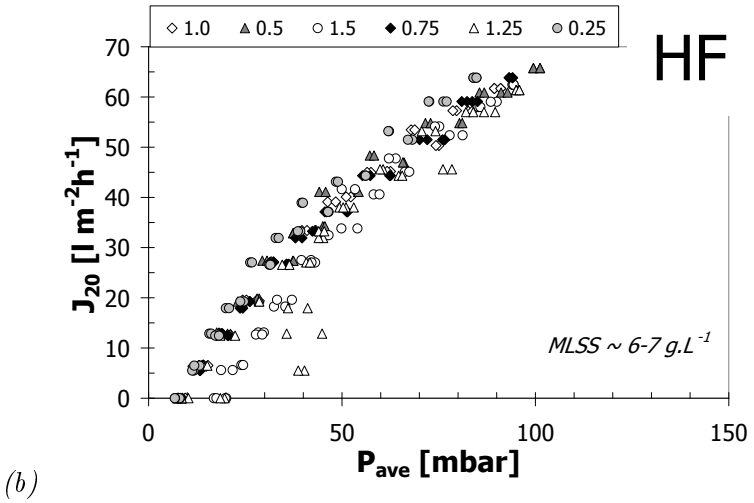

(b)

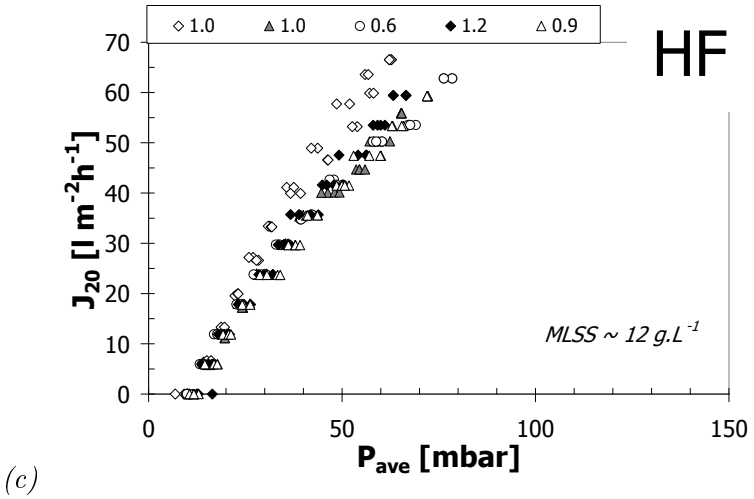

(c)

Figure 7.7.: Permeability curves for critical flux trials at different aeration rates and varying MLSS content - HF module: *(a)* MLSS 3-4 g.L^{-1}; *(b)* MLSS 6-7 g.L^{-1}; *(c)* MLSS 12 g.L^{-1}.

7.3. Fouling rates - dP/dt, $dP_{p,s}/dt$

Values determined for fouling rates of cake layer (dP/dt) and residual peak fouling ($dP_{p,s}/dt$) varied widely for the individual modules tested and ranged up to 75.0 mbar.min^{-1} dP/dt and 25.0 mbar.min^{-1} $dP_{p,s}/dt$ for the MT module, 33.0 mbar.min^{-1} dP/dt and 20.0 mbar.min^{-1} $dP_{p,s}/dt$ for the FS module, and 5.1 mbar.min^{-1} dP/dt and 1.1 mbar.min^{-1} $dP_{p,s}/dt$ for the HF module respectively (Figure 7.8 to Figure 7.10).

7.3.1. MT module

The **MT module** showed a significant increase in both dP/dt and $dP_{p,s}/dt$ with increasing MLSS content. While the maximum determined dP/dt was 13 mbar.min^{-1} at MLSS 3 g.L^{-1} for the test conducted at SAD$_m$ 1.0 Nm^{3}m^{-2}h^{-1}, the maximum dP/dt for the same aeration rate reached 28 mbar.min^{-1} at MLSS 7 g.L^{-1} and more than 70 mbar.min^{-1} at MLSS 12 g.L^{-1}, respectively.

Similar high ranges were found for $dP_{p,s}/dt$ with maximum values being 5 times higher at the peak step for MLSS 7 g.L^{-1} and 10 times higher at the peak step for MLSS 12 g.L^{-1} than at MLSS 3 g.L^{-1}. Most importantly to note is that fluxes varied significantly and thus, for instance, at a flux of 30 LMH the MT module exhibited a fouling rate of 4.5 mbar.min^{-1} at MLSS 3 g.L^{-1}, 1.6 mbar.min^{-1} at MLSS 6 g.L^{-1} and 25 mbar.min^{-1} at 12 g.L^{-1} MLSS respectively for the aeration trial at SAD$_m$ 1.0 Nm^{3}m^{-2}h^{-1}. $dP_{p,s}/dt$ for the same filtration rate trial were found to vary from 1.2, 0.8 and 18 mbar.min^{-1} for MLSS 3, 6 and 12 g.L^{-1}, respectively. The high fouling rate determined at 12 g.L^{-1} was attributed to the clogging phenomenon which was observed at the lowest aeration rate at that MLSS series (Figure 7.8).

7.3.2. FS module

The **FS module** exhibited the lowest fouling rate at MLSS 12 g.L^{-1}, with dP/dt and $dP_{p,s}/dt$ remaining below 4.0 and 1.5 mbar.min^{-1} respectively, except for the clogging event where the fouling rate rose up to 28 mbar.min^{-1} dP/dt at a flux of 50 LMH and up to 23 mbar.min^{-1} $dP_{p,s}/dt$ at 55 LMH (Figure 7.9).

For trials at the lowest MLSS content, it was again very interesting to note that the lowest dP/dt and $dP_{p,s}/dt$ were determined for the lowest SAD$_m$ trial of 0.5 Nm^{3}m^{-2}h^{-1}, with dP/dt remaining below 2.0 mbar.min^{-1} for dP/dt and below 0.8 mbar.min^{-1} $dP_{p,s}/dt$, respectively. The highest fouling rates were determined at that MLSS content for both aeration trials at SAD$_m$ 1.0 Nm^{3}m^{-2}h^{-1} with dP/dt reaching 25 mbar.min^{-1} at a flux of 35 LMH and $dP_{p,s}/dt$ 5 mbar.min^{-1} at the same flux. On the example of the trial conducted at a SAD$_m$ rate of 1.0 Nm^{3}m^{-2}h^{-1}, $dP_{p,s}/dt$ was found to provide a good indication for the reversibility of the

filtration protocol with values reaching up to -3 mbar.min^{-1} for the descending flux of 20 LMH.

Similar to the test at MLSS 3 g.L^{-1}, the lowest fouling rates of the test series conducted at MLSS 7 g.L^{-1} were also determined at the lowest aeration rates of SAD_m 0.5 Nm^{3}m^{-2}h^{-1} with $dP/dt \leq 2.5$ mbar.min^{-1} and $dP_{p,s}/dt \leq 1.0$ mbar.min^{-1}.

In fact, during the study conducted in parallel applying the DFC_m method, this phenomenon could be linked to an increase of MLSS content during the passage of the side-stream vessel, which resulted in an amelioration of sludge filterability and will be further discussed in Section 7.4 (page 143).

7.3.3. HF module

The **HF module** exhibited the least variation in both, dP/dt and $dP_{p,s}/dt$, with a maximum fouling rate of 5.75 mbar.min^{-1} for dP/dt and 1.1 mbar.min^{-1} for $dP_{p,s}/dt$, respectively.

Overall, it was found that the distribution of determined fouling rates was very scattered throughout the varying aeration rates, fluxes and MLSS concentration, which made a clear determination of critical flux based on fouling curve plots (dP/dt or $dP_{p,s}/dt$ vs. flux) impossible, also at logarithmic scale (Figure 7.10).

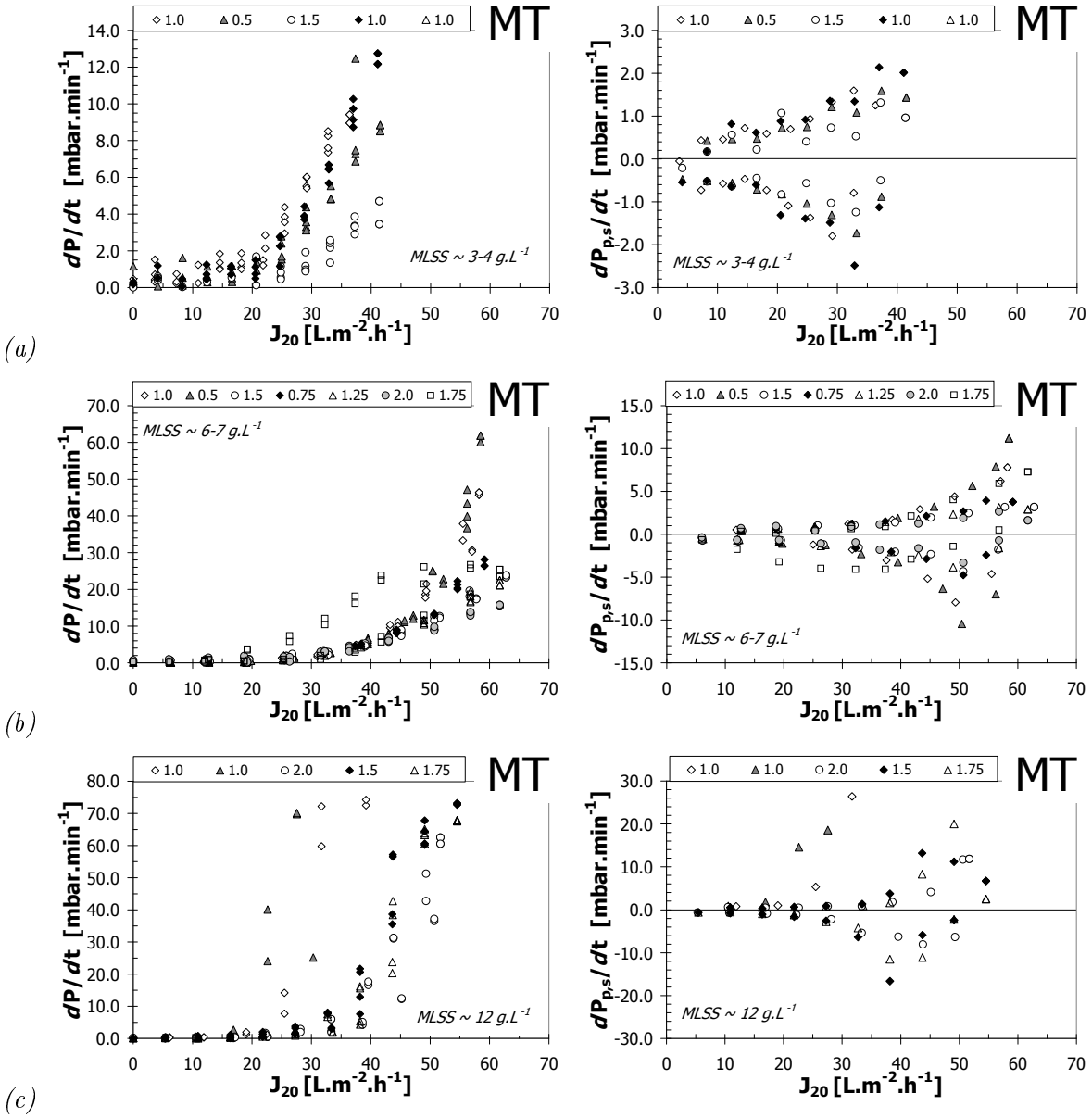

Figure 7.8.: Fouling rates (classical $d\mathrm{P}/d\mathrm{t}$ vs. peak fouling $d\mathrm{P}_{p,s}/d\mathrm{t}$) for critical flux trials at different aeration rates and varying MLSS content - MT module: *(a)* MLSS 3-4 g.L^{-1}; *(b)* MLSS 6-7 g.L^{-1}; *(c)* MLSS 12 g.L^{-1}.

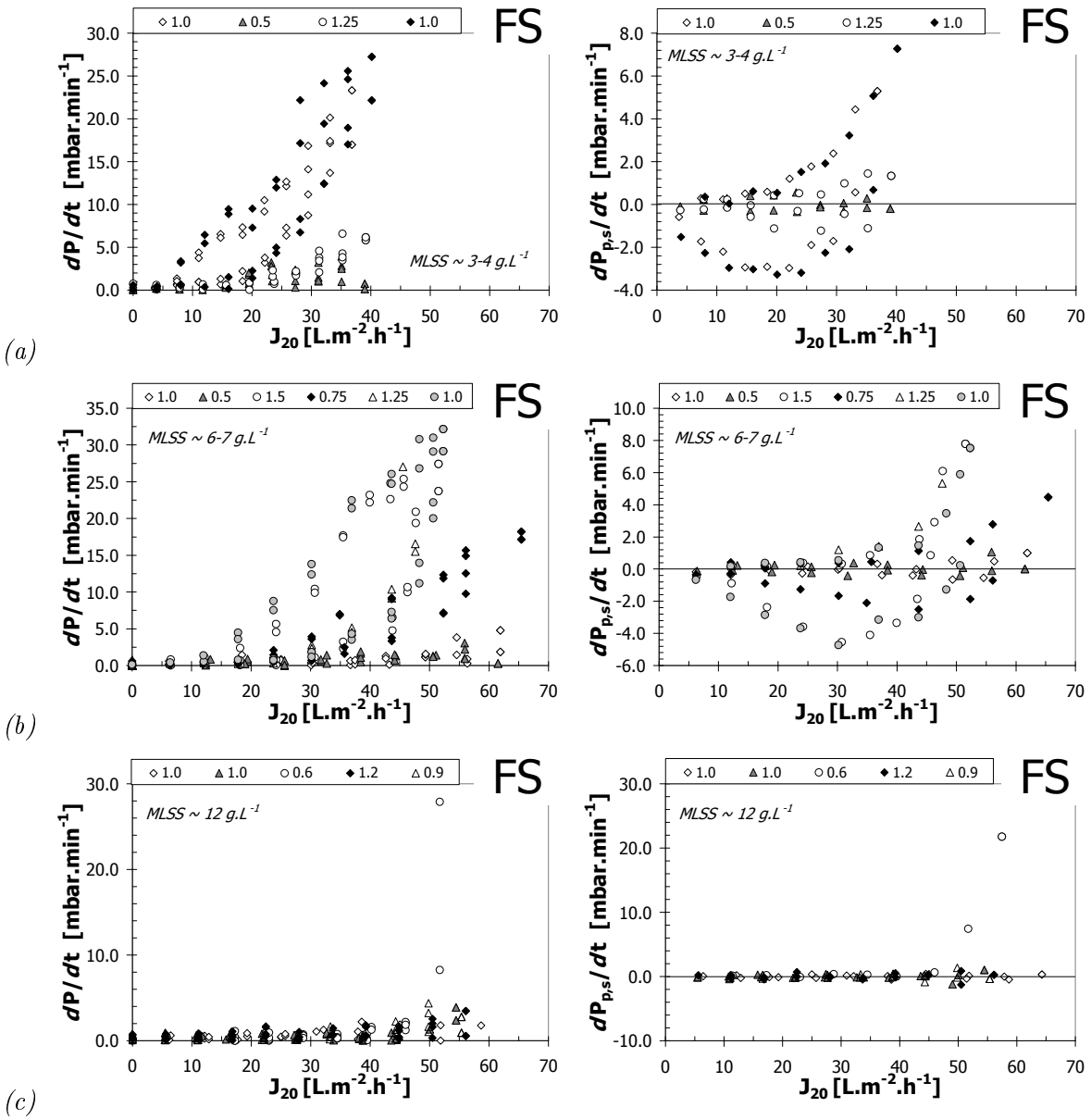

Figure 7.9.: Fouling rates (classical dP/dt vs. peak fouling $dP_{p,s}/dt$) for critical flux trials at different aeration rates and varying MLSS content - FS module: *(a)* MLSS 3-4 g.L^{-1}; *(b)* MLSS 6-7 g.L^{-1}; *(c)* MLSS 12 g.L^{-1}.

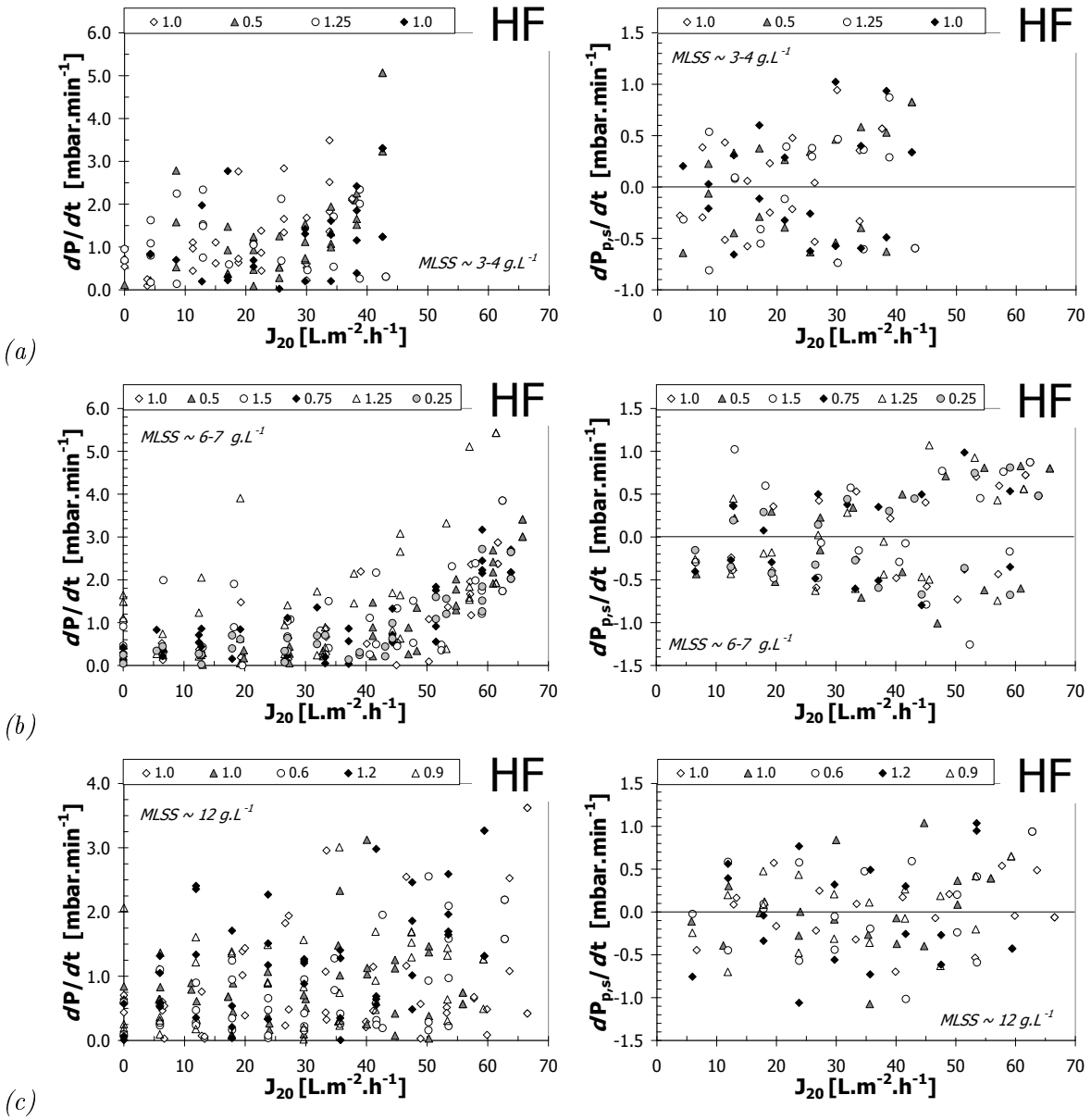

Figure 7.10.: Fouling rates (classical $d\mathrm{P}/d\mathrm{t}$ vs. peak fouling $d\mathrm{P}_{p,s}/d\mathrm{t}$) for critical flux trials at different aeration rates and varying MLSS content - HF module: *(a)* MLSS 3-4 g.L^{-1}; *(b)* MLSS 6-7 g.L^{-1}; *(c)* MLSS 12 g.L^{-1}.

7.4. The positive effects of low membrane aeration

Aeration intensities have been reported to have a negative impact on membrane permeability if they are too low, causing an insufficient removal of membrane foulants and hence increasing cake layer resistance, but were also reported to have a negative impact if aeration intensities are too excessive, causing floc break up and releasing membrane foulants which in turn lead to permeability decline (Meng *et al.*, 2009).

Whilst the MT module revealed the expected higher filtration performance during increased aeration rates, the FS and the HF modules have shown decreased permeability with increasing aeration intensity during the previously reported aeration studies. This may have led to the conclusion that the applied aeration rates may have caused floc damage leading to detrimental sludge properties decreasing filtration performance for the FS and HF modules.

However, during a simultanous study applying the Delft Filtration Method at a MLSS content of 6-7 g.L^{-1}, it became clearly evident that after the passage of the side-stream vessels, the biomass exhibited a significant amelioration in resistance of sludge filterability (ΔR_{20}, section A.5, page 233). This was mostly obvious for the FS module and the HF module. The enhanced sludge filterability of the biomass after the passage of the side-stream vessel could also be related to the positive effects on the filtration performance of the individual side-stream module.

This amelioration of increased sludge filterability could be related to an up-concentration of the biomass during the side-stream vessel passage, which became higher the lower the aeration rate and the higher the flux of the membrane module. The parameter involved was found to be the *dewatering* of the biomass within the side-stream vessel, which is a function of flux and cross-flow velocity, and the effective cross-sectional area of the membrane filtration unit, hence a function of flux and the effective SRT of the sludge during the filtration process.

The positive effect of the *dewatering* was not only found for lower aeration rates, but also for trials at constant aeration rates and with changing fluxes (see section A.5, page 233). A further improvement of sludge filterability due to higher *dewatering* could also be confirmed during the flux step tests for steps at higher LMH rates. Due to the different configurations, the parameter *dewatering* was found to be higher for the FS and HF modules at the same SAD$_m$ rate and flux than for the MT module. Assessing the parameter for all critical flux trials conducted at varying aeration rates, it became evident that the previously observed higher filtration performances of the FS and HF modules at lower aeration rates could be linked to the effect of sludge up-concentration due to the dewatering of the biomass (Figure 7.11). No such effects were observed for the MT module, which emphasised the difference between the two filtration modes, *out-to-in* and *in-to-out*, with the latter clearly benefiting from higher cross-flow velocities.

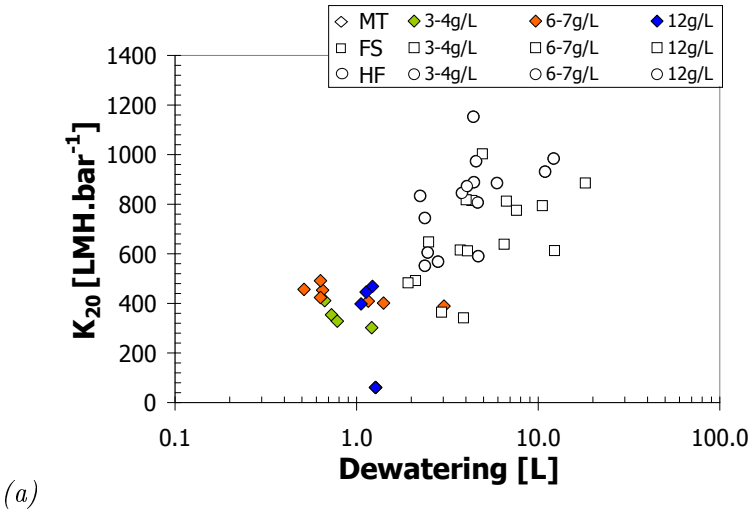

(a)

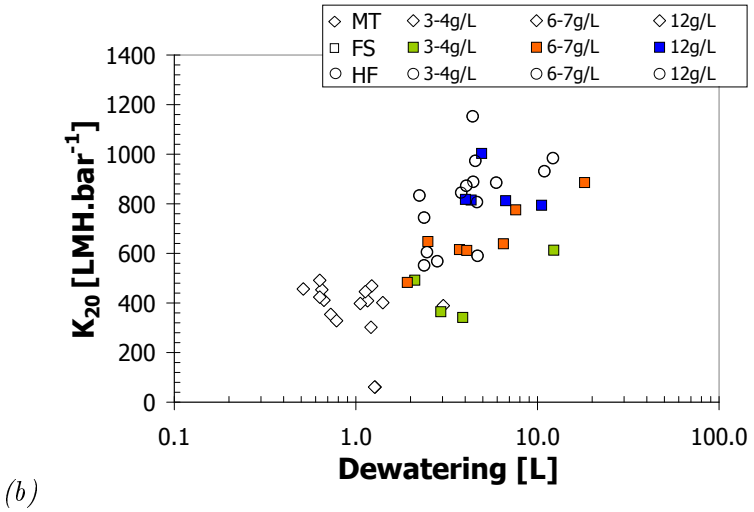

(b)

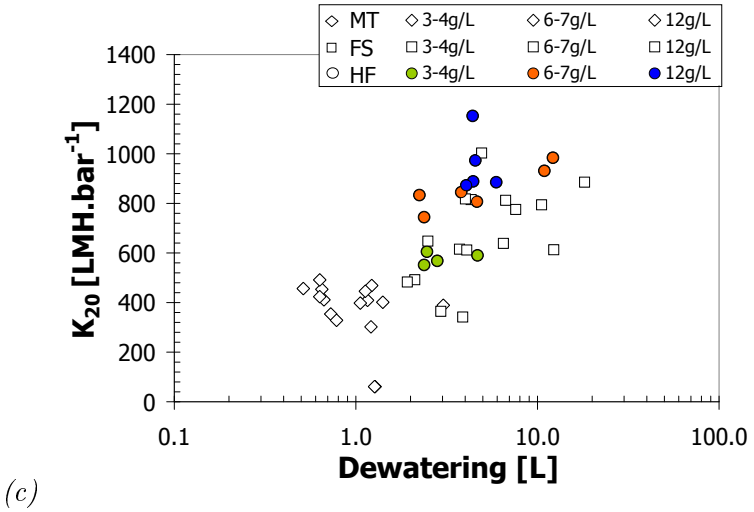

(c)

Figure 7.11.: Permeability values at 30 LMH step vs. dewatering of the individual sidestream module: *(a)* MT module; *(b)* FS module; *(c)* HF module.

7.5. Summary

As previously observed during the different critical flux trials, determined J_c varied widely and did not necessarily reveal the correlation pattern expected. For instance, the FS and HF membrane modules both presented a significant increase of J_c with increasing MLSS content of the biomass (Figure 7.12). The lowest J_c was determined for the flat sheet module at MLSS 3 g.L^{-1} with 16 LMH and the highest at MLSS 12 g.L^{-1} with 60 LMH. The HF revealed an almost constant J_c of 20 LMH at MLSS 3 g.L^{-1}, which increased up to 58 LMH at MLSS 12 g.L^{-1}. The MT module on the other hand, did not reveal such a pattern, but J_c was shown to increase with increasing aeration rates and a maximum was determined for an MLSS content of 6 g.L^{-1} with almost 50 LMH, compared to 29 LMH at MLSS 3 g.L^{-1} and 7 LMH at 12 g.L^{-1}, respectively (Figure 7.12).

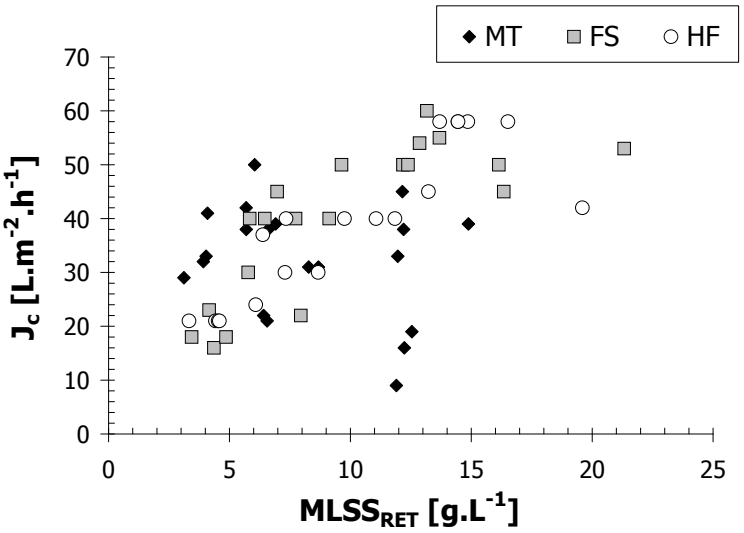

Figure 7.12.: Comparison of determined critical flux J_c for different aeration rates at varying MLSS content.

The positive effects of air scouring on the MT membrane resulted in a linear relationship between J_c and the applied aeration intensity, which became more significant the higher MLSS content and which were furthermore found to be in accordance with what has been reported in literature (Guglielmi *et al.*, 2007a, 2008; Le-Clech, 2002). The absence of such a correlation for the HF and FS modules emphasised the findings within this study, that air scouring was not effective in providing better membrane performances for the latter two types of membrane modules below a certain MLSS level. In fact, due to the results obtained during the sludge filterability measurements, it became evident that for lower MLSS concentrations of the biomass (3-7 g.L^{-1} during the current work), operating the FS and HF at lower air rates

(and/or higher fluxes) increased MLSS concentration next to the membrane surface, which in turn ameliorated the permeability of the respective membrane module.

However, at an MLSS range more typical for a full scale MBR operation (12 g.L^{-1}), the critical flux development under different aeration scenarios was found to be similar to other studies reported in literature (Guglielmi *et al.*, 2007a, 2008; Le-Clech, 2002) for all three membrane modules (Figure 7.13). For instance, at a biomass concentration of 12 g.L^{-1} the critical flux was found to have increased for the flat sheet module up to a threshold of 0.06 m.s^{-1}. Above that threshold value, no further increase of J_c could be observed, which was in accordance with observations made by Guglielmi *et al.* (2007a) for a large FS pilot plant.

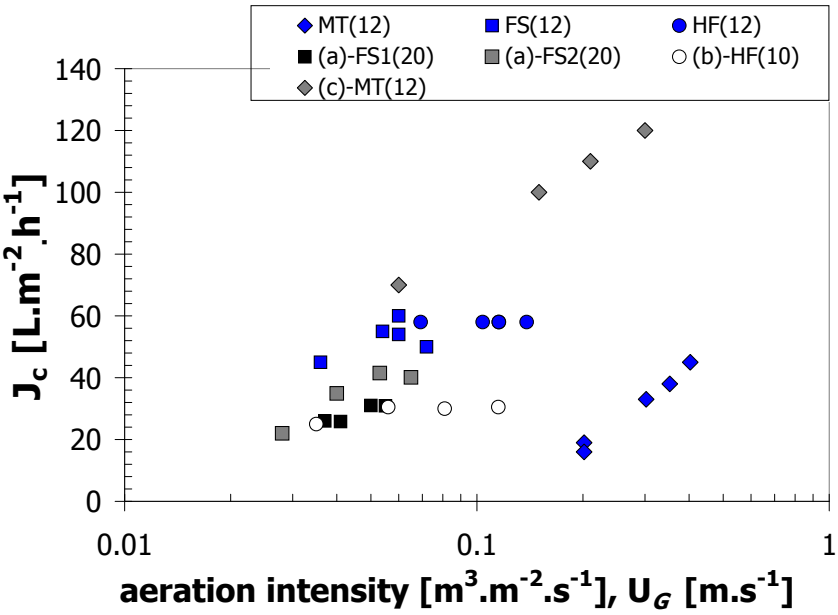

Figure 7.13.: Comparison of determined critical flux J_c and aeration intensity. *(MT(12), FS(12), HF(12)*: results within this study for the three pilot scale modules at MLSS content 12 g.L^{-1}; *(a)-FS1(20), (a)-FS2(20), (b)-HF(10)*: pilot scale data taken from Verrecht *et al.* (2008), adapted from Guglielmi *et al.* (2007a, 2008) - FS at 20 g.L^{-1} MLSS; HF at 10 g.L^{-1} MLSS; *(c)-MT(12)*: MT lab scale results adapted from Le-Clech (2002) at 12 g.L^{-1} MLSS)

Due to the insights gained during the sludge filterability measurements (DFCm), it was postulated that due to the dewatering of the biomass during the passage of the side-stream vessel, a sludge amelioration was achieved, which in turn was also positively impacting the filtration performance of the respective side-stream membrane module (see Section A.5, page 233; Figure A.11, Figure A.13). While the effects were significant for the flat sheet and hollow fibre modules, the multi-tubular module remained almost unaffected (Figure A.11, Figure A.13, page 233, Figure A.13). In contrast to the flat sheet and hollow fibre modules, the multi-

tubular module presented the expected increase in permeability with an increasing air-flow rate up to a certain threshold level and depending on the MLSS content of the biomass.

However, amongst others, some researches found that applying aeration, to a certain extent significantly improved membrane filtration performance (Bouhabila *et al.*, 1998; Germain *et al.*, 2005; Howell *et al.*, 2004; Ueda, 2001). Prieske *et al.* (2008) on the other hand, also observed a decrease of J_c with increasing cross-flow velocity of a flat sheet test cell. This trend was consistent for a range of MLSS tested. It is most likely that the observed sludge filtration amelioration due to the dewatering of sludge as a result of lower sidestream passage, might have had an impact on the findings. In fact, Monclus *et al.* (2010) tested three submerged modules individually and could observe a slightly higher J_c for the middle module, which might also be attributed to the effects observed during the sludge filterability measurements. The membrane module placed in the middle row would therefore have benefited from the dewatering of the passing biomass through the surrounding modules.

Furthermore, Ueda *et al.* (1997) and Ueda (2001) suggested that fouling amelioration could be achieved with a higher packing density due to the greater effective cross-flow velocity. This conclusion is in accordance with Liu *et al.* (2000), who reported ideas regarding the optimised design for a submerged MBR module.

Considering the observations made within the current work it might, however, be assumed that a higher packing density would lead to fouling amelioration regardless of the greater effective cross-flow velocity, as the ameliorating effect would arise from the higher sludge dewatering which would increase with a higher packing density. An increase in aeration would then subsequently be used to avoid biomass accumulation between the flat sheet and fibre bundles, respectively. Higher aeration rates would therefore be applied to the prevention of *clogging* rather than *fouling*. However, further impact factors still need to be considered which were not intensively studied during this work. For instance, Guglielmi *et al.* (2007a) suspected feed water characteristics to be the most important factor in the sub-critical fouling rate. A high susceptibility to biomass changes was also observed during the DFCm filtration trials, especially for the FS module.

Furthermore, it needs to be mentioned, that despite the fact that the DFCm measurements could be clearly correlated to permeability data of the membrane modules within this current work, a further comparison by Delft University researchers, revealed a lack in correlation of sludge filterability measurements with permeability data of other pilot and full scale plants investigated (Moreau *et al.*, 2009). It was concluded that reliable correlations were obtainable if membranes are close to virgin membrane conditions, e.g. cleaned on a regular basis. This is in accordance with the limitations manifested by Howell *et al.* (2004), who excluded the effects of membrane history to be predictable and would also explain the good fitting within this study, as membranes were thoroughly cleaned prior each measurement.

Table 7.2.: Comparison of effects of aeration on critical flux - MT

Conf		Scale	Material	Feed	MLSS	Aeration	J_c	Observation	Reference
					$g.L^{-1}$	a, (b), [c]	LMH		
ss	MT	LS (45L)	PES 0.01 μm	municipal	4 - 12	0.07; 0.22^a	37 - 109	increased J_c with increased aeration	Le-Clech *et al.* (2003*b*)
ss	MT		PES 0.1μm		4 - 12	0.07; 0.22^a	16 - 121	highest J_c for highest MLSS	
sub	MT	LS (45L)	PES 0.2μm	municipal	3	0 - 0.25^a	6 - 26	increased J_c with increased aeration	Le-Clech *et al.* (2005)
ss	MT		PES 0.2μm			0.05-0.55^a	10.5 - 16	for both configuration; fouling rate for sidestream general higher than for submerged system	
ss	MT	LS (40L)	PES 0.03μm	municipal	7	0.16-0.28^a	24 - 36	increased J_c with increased aeration	Alvarez-Vazquez *et al.* (2008)
			ceramic				>60	no impact of changes in aeration observable	
ss	MT	LS (34L)	ceramic 150kDa	grey water	8.8	0.73-1.95^a	>70	no impact observable	Pidou (2006)
ss	MT		ceramic 300kDa		8.8	0.73-1.22^a	>70	J_c always above 70 LMH	
ss*	MT	pilot 2 m^2	PVDF 0.03μm	municipal	3 - 12	(0.016-0.09)^b [0.5-2.0]^c	16 - 50	increased J_c with increased aeration	*this study (bw)*

Aeration data as: x^a = superficial gas velocity u_air in m.s^{-1}; (x)^b = superficial liquid velocity u_lq in m.s^{-1}; [x]^c specific aeration demand in N m^{3}m^{2}h^{-1}

Table 7.3.: Comparison of effects of aeration on critical flux - FS

Conf		Scale	Material	Feed	MLSS	Aeration	J_c	Observation	Reference
					$g.L^{-1}$	a, (b), [c]	LMH		
sub	FS	lab (3.5L)	PE 0.4 μm	synthetic wastewater	17	0.025-0.21[a]	≈10 - 23	increasing Jc with increasing aeration - limitation to aeration at 0.2 to exceed further increase of J_c than 23LMH	Howell *et al.* (2004)
ss*	FS	test cell	PVDF 0.2μm	sludge from synthetic fed MBR	8 - 10	0.02[a] (0.2-0.4)[b] 0.07[a] (0.2-0.4)[b]	≈6 - 11 ≈19 - 23	decreasing J_c with slight increasing cross-flow velocity;trend consistent for range of gas flow velocity, J_c in general higher for superficial gas velocity of 0.07	Prieske *et al.* (2008)
sub	FS	pilot	PE 0.04μm	municipal	20	[0.5-1.0][c]	21.0 - 40.0	J_c increased with increasing aeration rate; threshold value of 0.88; 0.94 N $m^3m^2h^{-1}$	Guglielmi *et al.* (2008)
ss*	FS	pilot 2 m^2	PVDF 0.08μm	municipal	3 - 12	(0.002-0.02)[b] [0.5-2.0][c]	16 - 60	decreased J_c with increased aeration	*this study (bw)*

Aeration data as: x[a] = superficial gas velocity u_air in $m.s^{-1}$; (x)[b] = superficial liquid velocity u_lq in $m.s^{-1}$; [x][c] specific aeration demand in N $m^3m^2h^{-1}$

Table 7.4.: Comparison of effects of aeration on critical flux - HF

Conf		Scale	Material	Feed	MLSS	Aeration	J_c	Observation	Reference
					$g.L^{-1}$	a, (b), [c]	LMH		
sub	HF	pilot	PVDF 0.04μm	municipal	4 - 13	0.07 - 0.13[a]	$\approx$ 16 - 22	transitional flux between 16 and 22 LMH, below which fouling remained low regardless aeration (or MLSS); higher MLSS and higher fluxes required higher aeration to maintain performance	Germain (2004)
sub	HF	lab (2.5L)	PS 0.2-0.4μm	synthetic wastewater	4 - 15	[$\approx$1.25-50][c]	$\approx$ 10 - 30	Increasing J_c with increasing aeration; highest shift from lowest SAD_m 1.5 to SAD_m 25 above that little change was observed	Bouhabila *et al.* (1998)
sub	HF	pilot	PVDF 0.04μm	municipal	10	0.029; 0.048-0.097 [a] [0.3; 0.5-1.0][c]	24.9; 30.0 - 31.0	lowest aeration rate with lowest J_c of 24.9 LMH; aeration rates above did not reveal much difference	Guglielmi *et al.* (2007a)
ss*	HF	pilot 2 m^2	PES 0.03μm	municipal	3 - 12	(0.003-0.02)[b] [0.25-2.0][c]	21 - 60	little impact evident for aeration rates on J_c , decreased J_c with increased aeration at MLSS content 6-7, no impact of aeration intensity on J_c at highest MLSS concentration	*this study (bw)*

Aeration data as: x[a] = superficial gas velocity u_air in m.s^{-1}; (x)[b] = superficial liquid velocity u_lq in m.s-1; [x][c] specific aeration demand in N m^{3}m^{2}h^{-1}

8. Results and Discussion: Biomass Properties and their potential impact on filtration performance

8.1. Scope

Membrane fouling is one of the most contradictory discussed topics in membrane research. The parameters which have been antithetically discussed are (beside operational parameters, such as solid retention time, organic loading and MLSS content), *soluble microbial products (SMP); particle size distribution* and *colloids*.

To assess the potential impact of the biomass parameter on the different membrane module filtration performances, statistical analyses have been applied by using STATISICA and in order to quantify the significance of the individual parameters, Pearson's correlation factor was determined.

The parameters assessed included amongst others:

- pH; Temp, DO
- MLSS; TSS, VSS, VTS and the ratio
- soluble microbial products as $mg.L^{-1}$, $mg.g.SS^{-1}$ in activated sludge tank, retentate line and permeates
- particle size, floc rupture expressed as particle fractionation, for activated sludge tank and retentate lines
- retention and rejection of the individual membrane modules and the suspected foulants
- the mass of SMP within the feed flow passing the membrane modules

The membrane filtration performance was therefore assessed by correlating the above parameters to the membrane permeability, the different fouling rates (dP/dt, $dP_{p,s}/dt$, $dP_{i,s}/dt$), the determined critical flux, the slope of the determined fouling curve of the critical flux, the cake layer resistance, and the cake layer velocity of the different membrane modules - for the different tests conducted. As this resulted in various parameters, only the most significant ones will be discussed during the following section.

8.2. Overall biomass characteristics and effluent quality of the pilot plant

With installation of the submerged HF module, the HRT of the pilot plant varied between 24.0 to 8.0 hours and hence treated influent increased from 2.0 to 6.0 $m^3.d^{-1}$. To reach those HRT values, the flux of the submerged HF module was regulated between 4.75 and 14.2 LMH. The submerged HF ran continuously at constant flux without any periodical relaxation or backwash regime. Cleaning was undertaken when necessary with the duration of the cleaning regime being kept to a minimum. Throughout a run-time of approximately 1.5 year, the submerged module was cleaned in-situ every three to four months and an intensive ex-situ cleaning became necessary once. Permeability of the HRT control module dropped from initially 420 LMH.bar^{-1} to 30 LMH.bar^{-1} prior to the intensive ex-situ cleaning. Permeability was found to be on average approximately 80 LMH.bar^{-1}, with the trans-membrane pressure being kept below 200 mbar and only reaching at its highest stress period 350 mbar.

Within this study, influent concentration of COD was generally found to be of lower average strength with measured soluble COD concentrations of around 335 mg.L^{-1}, resulting in average loading rates for organic and sludge loading of 0.550 kg $COD_{soluble}.m^{-3}.d^{-1}$ and 0.091 kg.$COD_{soluble}$.kg $MLSS^{-1}.d^{-1}$, respectively, with HRT being kept between 8 hours and 24 hours. This was, in fact, comparable to other studies for MBR pilot plants, as for instance Germain (2004) investigated membrane fouling of an MBR pilot plant with loading rates varying from 0.381 to 0.666 kg $COD_{soluble}.m^{-3}.d^{-1}$ and between 0.047 to 0.100 kg$COD_{soluble}$.kg $MLSS^{-1}.d^{-1}$ for a hydraulic retention time of 11.5 hours. A compilation of published pilot plant research data of aerobic MBRs treating municipal/domestic wastewater by Stephenson *et al.* (2000), revealed average loading rates of 0.07 to 1.76 kg COD.$kg^{-1}.d^{-1}$ and 0.49 to 5.78 kg COD.$m^{-3}.d^{-1}$, respectively.

Effluent concentration values for the permeate of the HRT control module were on average 24.2 mg.L^{-1} COD, 1.2 mg.L^{-1} NH_4-N and 31.8 mg.L^{-1} NO_3-N resulting in an overall removal of 92.7% for the chemical oxygen demand and 96.2% for ammonium (Table 8.2). Throughout this study, the effluent quality of the pilot plant met throughout this study regulations for small wastewater treatment plants in terms of COD removal with a maximum c_{COD} determined of 108 mg.L^{-1} (design limit for COD effluent: 150 mg.L^{-1}).

Suspended solids within the aeration tank (MLSS) varied between 3.0 and 14.4 g.L^{-1}, with no specific HRT run being attributed to a definite range of MLSS content (Table 8.1). Sludge waste was only intended to obtain the targeted MLSS content and resulted, due to varying influent strength and due to three occasions of unexpected biomass loss, in an MBR operation with no sludge disposal other than for biomass sampling throughout the study. To avoid false interpretation of the potential impact arising from steadily increased sludge age but, due to

the nature of the experiment, likely being attributed to HRT, it was subsequently chosen to intermittently change HRT from low to high and high to low.

The ratio of MLVSS/MLSS is regarded to be one important parameter to assess the degree of biomass stabilization with biomass being regarded as stabilised if MLVSS/MLSS remains above 0.8 (Lyko *et al.*, 2008b). Throughout this study the determined ratio for MLVSS/MLSS did not drop below 0.8, even though the pilot plant suffered from a total of three occurrence of biomass losses. Due to the constant relationship, only the parameter MLSS was used as a referencing parameter and will be considered hereafter.

Particle size (expressed as $d_{0.5}$) of the biomass flocs of the aeration tank changed throughout this study in high variations from 17 μm and 91 μm, where no significant impact of MLSS content on the floc size could be observed. In fact, while only a slight trend was seen for decreasing particle size with increasing MLSS content, overall the measured particle sizes seemed to decrease throughout this study and the decrease in floc size could rather be attributed to an alteration of the sludge age of the biomass than to an alteration in HRT or MLSS content (Figure 8.1).

Concentrations determined for **soluble microbial products (SMP)** within the supernatant varied widely from 12.1 to 139 mg.L^{-1} for DOC, 2.8 to 68.3 mg.L^{-1} for proteins and 5.0 to 483 mg.L^{-1} for carbohydrates (Table 8.1). Throughout this study, concentrations of soluble microbial products, determined as proteins, carbohydrates and DOC of the supernatant, could not be linked in overall to a specific MLSS content or particle size (Figure 8.2). Variations within concentration of SMP were also found to change significantly within one set of experimental trials at fixed biomass operation mode (same HRT and SRT tests run on consecutive days). Highest variations were found for concentration of carbohydrates with, for instance, a reduction in SMP concentration of over 50% from 44 mg.L^{-1} to 20 mg.L^{-1} during 2 consecutive days of operation (Figure 8.2).

Concentrations of SMP within the permeate of the submerged HF module were found to vary between 4.2 and 11.6 mg.L^{-1} for DOC, 2.7 to 27.0 mg.L^{-1} for proteins and 1.9 to 56.3 mg.L^{-1} for carbohydrates. Turbidity of the bulk phase of the aeration tank varied overall from 0.512 to 13.2 NTU, whereas turbidity within the permeate line of the HRT-control module was measured from 0.101 to 1.099 NTU.

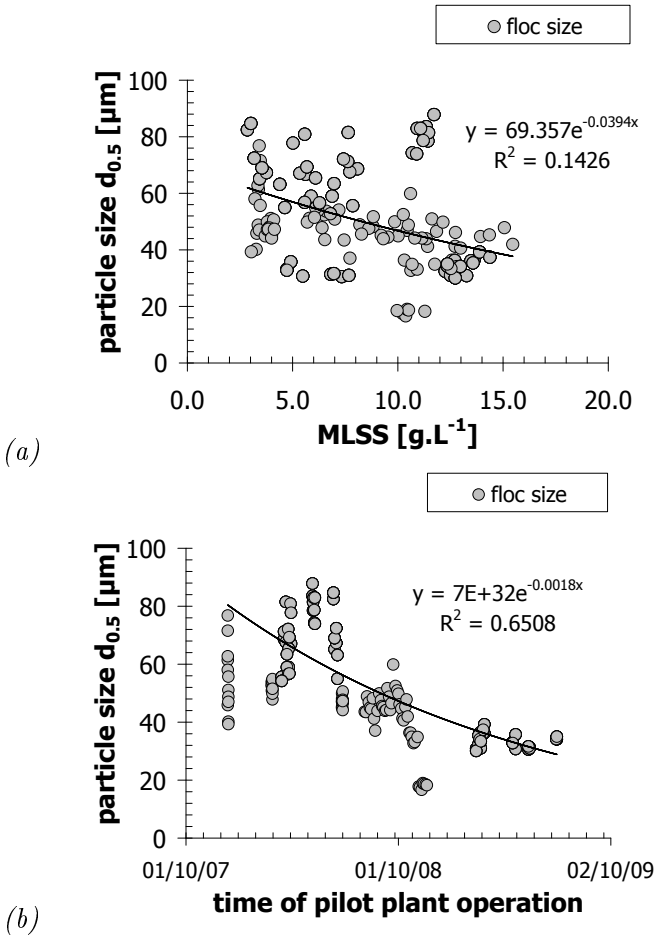

Figure 8.1.: Floc size distribution within the 2.2 m^3 membrane aeration - overall variation within this study *(a)* vs MLSS content *(b)* vs time of plant operation.

The observed retention for the submerged HF module resulted on average in 78.0% for DOC, 45.8% for proteins and 70.1% for carbohydrates (Table 8.2). Interestingly, as observed for the side-stream HF module, measured carbohydrates resulted in negatively observed retention for the submerged HRT control module measured at HRT 8, 10 and 16 with a maximum value of -30.9% S_{Carbs}. The observed retention, S_{Carbs}, also resulted in the highest observed value with 92.4%, whereas S_{DOC} remained most consistently around 78.0% with a minimum observed retention of 59.8% and a maximum of 88.9%. The observed retention for proteins, S_{Prots}, varied between 10.3% and 91.4%.

The most relevant parameters for biomass make-up of the pilot plant and effluent quality of the HRT-control module are summarised in Table 8.1 and Table 8.2.

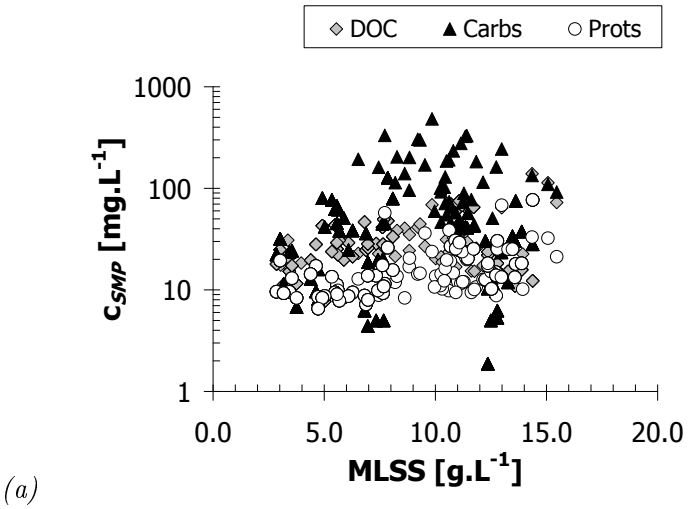

(a)

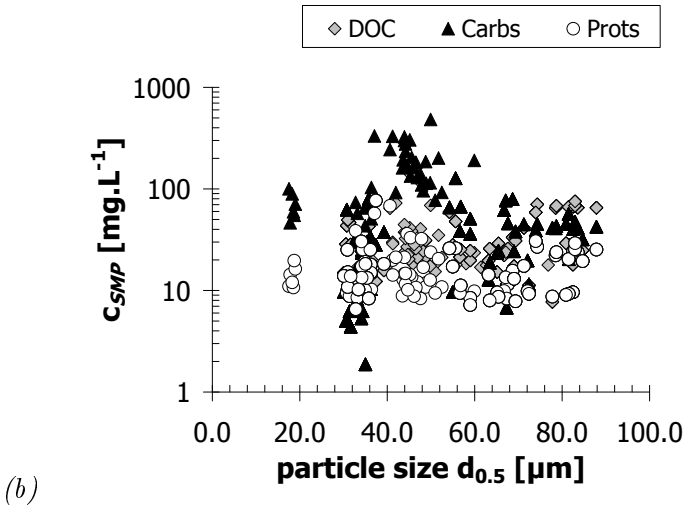

(b)

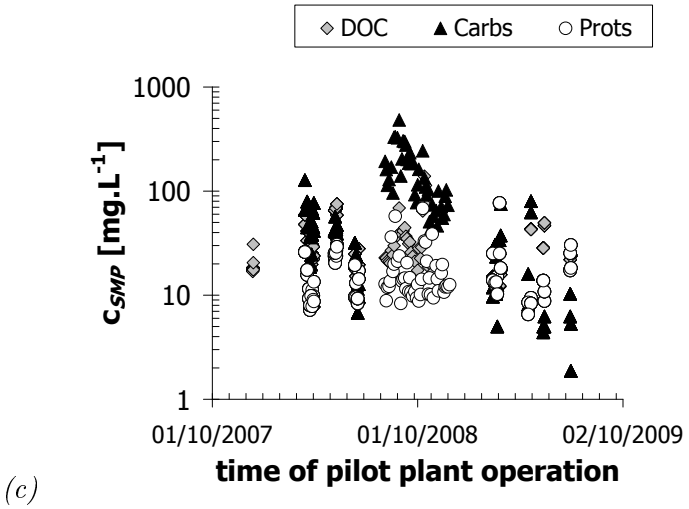

(c)

Figure 8.2.: Variation of SMP throughout this study vs *(a)* MLSS content, *(b)* particle size and *(c)* time of pilot plant operation.

Table 8.1.: Biomass and supernatant parameters throughout this study - classified according to operated HRT

	operational parameters and biomass properties								supernatant		
	COD removal *(c_{Inf})*	**NH_4 removal** *(c_{Inf})*	**organic load**	**sludge load**	**MLSS**	**VSS**	**$d_{0.5}$ particle size**	**turb.**	**c_{DOC}**	**c_{Prots}**	**c_{Carbs}**
	%, $(mg.L^{-1})$	%,$(mg.L^{-1})$	$kgCOD.m^{-3}.d^{-1}$	$kgCOD.kg^{-1}.d^{-1}$	$g.L^{-1}$	%	μm	NTU	$mg.L^{-1}$	$mg.L^{-1}$	$mg.L^{-1}$
HRT 8.0											
average	91.8 *(229)*	98.6 *(31.3)*	0.613	0.130	4.7	89.0	53.5	1.349	18.2	11.2	15.6
min	80.0 *(120)*	99.4 *(20.3)*	0.295	0.067	3.0	87.2	44.2	0.739	11.5	8.3	6.8
max	96.3 *(340)*	94.7 *(34.5)*	0.912	0.265	11.4	90.4	84.7	2.065	28.0	17.2	23.5
HRT 10.0											
mean	94.0 *(337)*	94.7 *(33.5)*	0.726	0.071	10.8	90.2	40.1	3.115	36.5	17.5	159
min	76.7 *(171)*	74.3 *(9.8)*	0.368	0.035	7.4	88.3	16.7	0.512	15.3	2.8	43
max	97.7 *(603)*	100.0 *(59.7)*	1.297	0.217	15.5	91.5	59.9	8.590	139.2	68.3	483
HRT 12.0											
mean	91.7 *(227)*	97.9 *(33.4)*	0.407	0.064	6.4	89.8	52.2	1.349	103.2	15.4	26.0
min	81.2 *(150)*	99.5 *(18.3)*	0.269	0.043	5.7	86.8	47.9	0.739	95.2	13.7	15.9
max	96.7 *(320)*	93.8 *(28.5)*	0.574	0.093	7.2	92.8	90.8	2.065	106.7	18.4	57.4
HRT 16.0											
mean	96.3 *(402)*	96.8 *(27.9)*	0.576	0.063	10.8	88.6	34.2	6.4	22.2	17.3	21.6
min	91.5 *(244)*	87.5 *(4.0)*	0.346	0.027	4.7	85.6	30.1	2.7	12.1	8.5	5.0
max	99.4 *(580)*	99.9 *(42.3)*	0.834	0.131	14.4	93.2	39.3	13.2	46.5	30.4	75.0
HRT 24.0											
mean	90.0 *(479)*	92.8 *(32.7)*	0.430	0.127	3.4	81.5	54.9	4.730	19.1	14.4	15.1
min	73.7 *(410)*	84.7 *(12.4)*	0.368	0.093	3.0	78.7	39.3	2.680	16.9	13.7	9.7
max	95.7 *(637)*	96.4 *(48.7)*	0.571	0.173	4.0	84.9	76.8	6.850	30.9	15.2	17.0

Table 8.2.: Effluent quality of MBR pilot plant throughout this study - classified according to operated HRT

Determined permeate quality for submerged HF module (HRT-control module) - effluent of pilot plant										
	$\mathbf{c}_{COD}$ *(removal)*	$\mathbf{c}_{NH_4-N}$ *(removal)*	$\mathbf{c}_{NO_3-N}$	**turbidity**	$\mathbf{c}_{DOC}$	$\mathbf{S}_{DOC}$	$\mathbf{c}_{Prots}$	$\mathbf{S}_{Prots}$	$\mathbf{c}_{Carbs}$	$\mathbf{S}_{Carbs}$
	$mg.L^{-1}$,(%)	$mg.L^{-1}$,(%)	$mg.L^{-1}$	*NTU*	$mg.L^{-1}$	%	$mg.L^{-1}$	%	$mg.L^{-1}$	%
HRT 8.0										
average	18.8 *(91.8)*	0.4 *(98.6)*	36.9	0.433	6.6	72.2	7.7	39.9	3.6	69.5
min	12.4 *(80.0)*	0.1 *(99.4)*	24.4	0.330	4.2	63.3	2.7	13.9	1.9	-5.2
max	24.0 *(96.3)*	1.8 *(94.7)*	49.3	0.661	9.4	72.6	14.8	62.7	5.0	78.7
HRT 10.0										
average	20.3 *(94.0)*	1.8 *(94.7)*	31.8	0.212	6.6	79.0	7.9	45.9	33.9	70.3
min	13.9 *(76.7)*	0.0 *(74.3)*	8.9	0.101	4.2	59.8	5.3	12.3	18.8	-30.9
max	39.8 *(97.7)*	2.5 *(100.0)*	55.3	0.936	9.4	88.3	12.1	91.4	56.3	92.4
HRT 12.0										
average	18.9 *(91.7)*	0.7 *(97.9)*	28.4	0.678	10.6	85.4	6.5	52.9	12.8	73.3
min	10.4 *(81.2)*	0.1 *(99.5)*	7.5	0.201	9.6	70.9	4.5	28.8	4.0	74.9
max	28.2 *(96.7)*	1.8 *(93.8)*	43.3	1.024	11.2	88.5	13.1	74.3	24.8	91.6
HRT 16.0										
average	14.9 *(96.3)*	0.5 *(96.8)*	29.8	0.464	6.4	74.1	18.2	47.6	13.8	74.4
min	3.2 *(91.5)*	0.0 *(87.5)*	5.5	0.205	4.8	60.5	4.8	10.3	5.0	-10.9
max	20.8 *(99.4)*	0.9 *(99.9)*	40.8	1.090	8.9	80.8	27.0	89.7	43.8	85.3
HRT 24.0										
average	48.0 *(90.0)*	1.9 *(92.8)*	32.2	0.542	5.4	79.2	9.4	42.8	4.8	62.8
min	27.5 *(73.7)*	1.8 *(84.7)*	4.3	0.371	4.8	70.4	4.0	71.0	3.1	0.0
max	107.8 *(95.7)*	2.3 *(96.4)*	52.8	1.099	5.9	88.9	15.8	89.1	6.9	82.1
Overall Average										
average	24.2 *(92.7)*	1.2 *(96.2)*	31.8	0.6	7.1	78.0	9.9	45.8	13.8	70.1

8.3. Soluble microbial products and their potential impact on the filtration performance

Measured soluble microbial products during the different aeration trials showed no correlation for carbohydrates to MLSS content, whereas proteins and DOC concentration within the supernatant were found to increase with increasing MLSS content (Figure 8.3). As best filtration performance was observed for the FS and HF module at the highest MLSS content, the high concentration of DOC and proteins were therefore not expected and the concentrations were found to be unsuitable in explaining fouling mechanism. Overall, carbohydrate concentration varied between 6 mg.L^{-1} and 77 mg.L^{-1}, proteins between 7 mg.L^{-1} and 30 mg.L^{-1} and DOC between 11 mg.L^{-1} and 71 mg.L^{-1} for the range of MLSS concentrations tested.

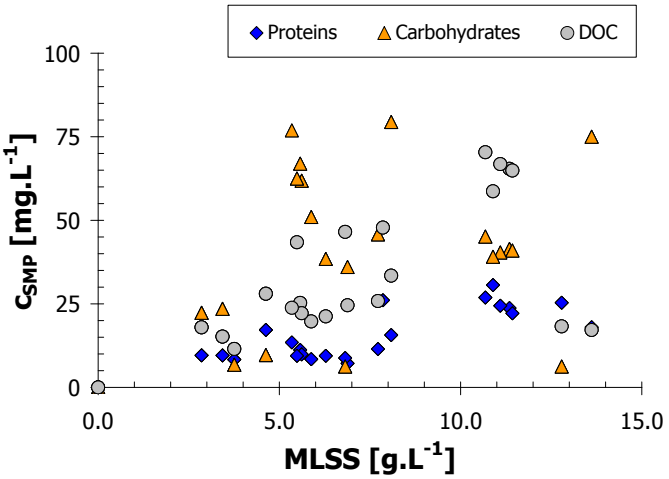

Figure 8.3.: Concentration of soluble microbial products per varying MLSS content of biomass for critical flux trials at varying aeration rates.

Furthermore, no overall correlation could be observed between soluble microbial product content (normalised in the graphs provided to g.VSS^{-1}) and the filtration performance of the individual membrane modules (Figure 8.4). This was also observed for rejection rates or observed retention rate of the individual side-stream module.

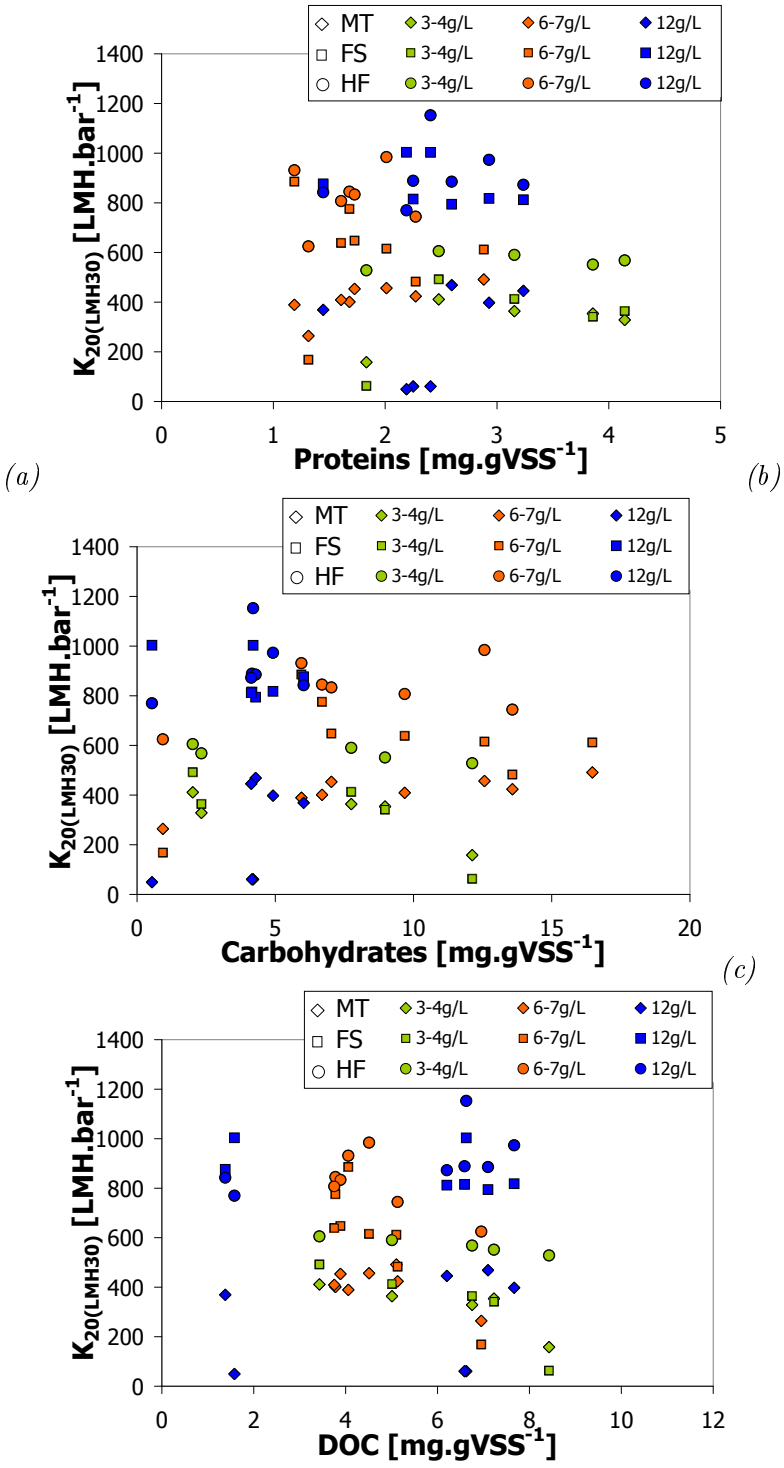

Figure 8.4.: Impact of soluble microbial product concentration on permeability development - critical flux trials at different aeration rates and varying MLSS content: *(a)* Protein content per g.VSS; *(b)* Carbohydrate content per g.VSS; *(c)* DOC content per g.VSS.

Most interestingly, while plotting the SMP content per individual test run (MLSS test trials), high DOC content at low MLSS content was found to have had an adverse effect on membrane permeability of all three modules with R^2 ranging from 0.89 to 0.54 (HF), 0.58 to 0.47 (FS) and 0.50 to 0.35 (MT) at MLSS 3-4 and 6-7 $g.L^{-1}$, respectively. While carbohydrates concentrations were not found to have an adverse impact on permeability values at higher MLSS; a likely adverse impact was assumed to have happened at a lower MLSS concentration. No evident impact was observable for protein concentration.

In order to include potential influences from hydrodynamics, the **load of soluble microbial products** passing the membrane surface during side-stream passage was calculated (as $mg.s^{-1}$) and correlated to the determined fouling parameters. While protein load passing the membrane surface again did not reveal any evidence for impacting membrane permeability; the carbohydrate load was found to significantly correlate with permeability at the lowest MLSS content. For MLSS content from 6 to 12 $g.L^{-1}$, results were insignificant or in opposition of what would have been expected. DOC mass seemed to have impacted permeability rates again only at the lowest MLSS content with the highest significant impact found for the MT module and the FS module (R^2=0.76, 0.73 respectively). At an MLSS content of 6-7 $g.L^{-1}$, the DOC load passing the membrane surface seemed to have impacted the FS module and, with less significance, the HF module. No significant correlation was observed for the highest MLSS content investigated.

The difference between each module configuration and the complexity of potential biomass impact was furthermore indicated by Pearson's correlation matrix for individual membrane module and different filtration performance parameters. From those correlation matrixes, the following main results were suggested:

Impact of MLSS on critical flux was highest for the HF module (*R=0.8410, p=0.0*), followed by the FS module (*R=0.7532, p=0.0*), whereas no significant impact was found on the MT module (*R=-0.30, p=0.187*). While the critical flux value *per se*, had no correlation to MLSS content for the MT module, overall permeability however indicated lower permeability at a higher MLSS content. This was previously related to effective aeration on the one hand and higher susceptibility to lumen clogging at higher MLSS content on the other hand.

Cake layer resistance, R_{cl}, was furthermore found to be affected by biomass properties, whereas trends were opposing between the membrane module configurations. While the cake layer resistance of the MT was found to be slightly impacted by MLSS concentration, but furthermore did not show any overall correlation to other biomass parameters, R_{cl} of the flat sheet module seemed to be negatively impacted by DOC content of the bulk phase and the COD of the sludge. An affinity to a higher R_{cl} with a higher DOC content was also found for the HF module.

The **residual fouling parameter ($d\mathbf{P}_{p,s}/d\mathbf{t}$)** showed a slight correlation to DOC content for the flat sheet module (*R=0.5347, p=0.015*), and to COD of the sludge (*R=0.597, p=0.031*) and sum of SMP content (*R=0.5259, p=0.021*) for the HF module, whereas no statistical significance was observed for $d\mathrm{P}_{p,s}/d\mathrm{t}$ and any biomass parameter for the MT module.

Another parameter interesting to mention is the **ratio of protein to carbohydrates (P/C)** within the bulk phase of the retentate line. The correlation of ratio P/C with the determined cake layer resistance for each individual module, revealed a significant impact of P/C on the flat sheet module for MLSS content of 6-7 g.L^{-1}, whereas no impact was obvious at 3 and 12 g.L MLSS. The development of cake layer resistance for the hollow fibre module, however, presented a significant correlation to P/C ratio at 6 and 12 g.L^{-1} MLSS content, whereas no such correlation could be found for the lowest MLSS content of 3 g.L^{-1}. The cake layer resistance of the MT module was found to not have not been impacted by the ratio of P/C in the side-stream bulk phase. A correlation was observed at an MLSS content of 6-7 g.L^{-1}, but this correlation was due to one outstanding value than the determined series of results. Presumably, these findings might indicate the different impact of changes in sludge filterability as observed during the DFCm filtration trials. During those tests, an increase of the ratio P/C ratio was found to increase resistance to sludge filterability (see Figure A.14, page 236).

8.4. Particle size

Particle size varied widely with surprisingly high daily variations at young SRT (SRT = 30d). Average particle size seemed to be uninfluenced by higher interactions created due to higher MLSS content, but particle size changed significantly during this study with increasing sludge age. However, it has to be noted that sludge age was not controlled and biomass loss happened three times during the overall study. Conversely, apart from the initiation sludge seeding, no further biomass inoculation took place and biomass growth happened quickly. Furthermore, the ratio of MLSS/VSS did not drop below 0.8 for all tests conducted.

After two years of operation, floc size had decreased down to 35 μm, compared to 90 μm microns at the time of biomass inoculation. It has to be considered however, that during 2-hourly biomass monitoring, the shift in determined average particle size was found to be as high as 39 to 80 μm during one day only. Daily floc dynamic was found to be highest during winter trials at lower temperature, higher HRT and lower SRT. However, the effects of the latter parameter on floc size were not investigated systematically within this study. Nevertheless, Masse *et al.* (2006) and Stricot *et al.* (2010) also reported decreased particle size with increased solid retention time. Furthermore, it might be assumed that the higher permeability losses during colder temperatures might be related to higher floc dynamic. Higher floc dynamic was also observed to create higher fluctuations in SMP and colloidal organic carbon (determined as DOC).

The decrease in particle size could not be clearly linked to higher permeability losses, however a slight trend could be observed, especially for fractionation of a smaller particle range for the FS and HF module, whereas the MT module seemed to remain unaffected. For the flat sheet bench scale, the shifts in mainly sheared particle size and hence released SMP were assumed to furthermore contribute to higher observed attachments at lower MLSS.

The impact of particle fractionation (as a fraction between the retentate line and the biomass tank) was however not found to be substantial to explain the permeability changes determined (Figure 8.5). This might however also result from the observation made during the floc size monitoring that occasionally particle sizes were found to increase during side-stream passage regardless of the additional shear exhibited.

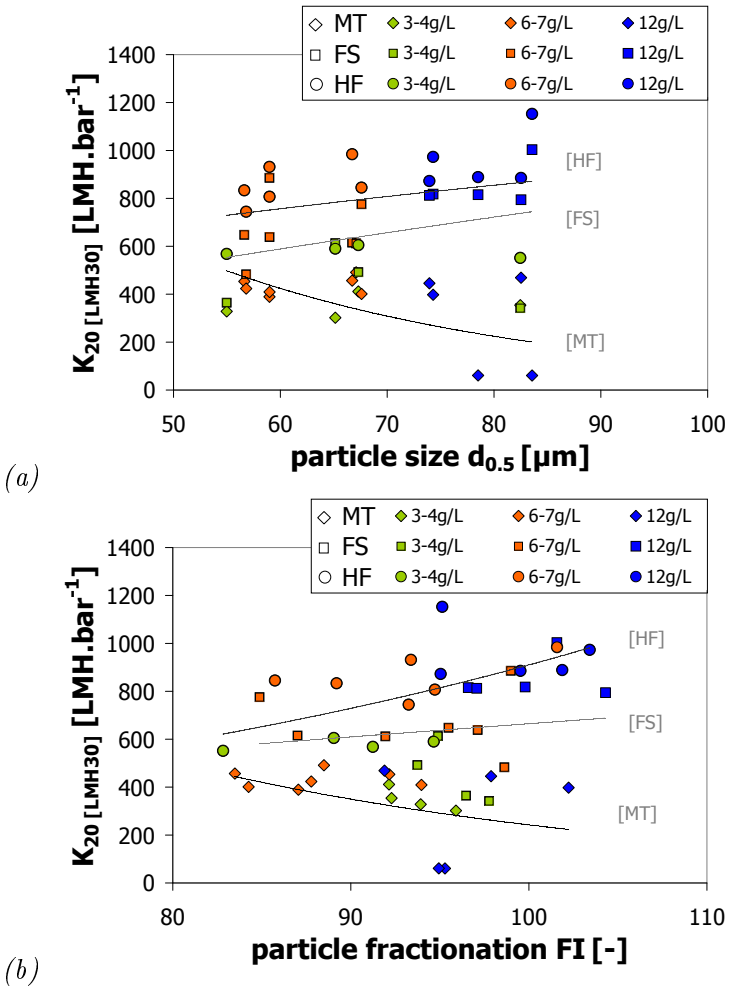

Figure 8.5.: Permeability per changing MLSS content of biomass for critical flux trials at varying aeration rate vs. *(a)* particle size; *(b)* particle fractionation;

A poor sludge dewatering deriving from higher proportion of supra-colloids was observed by Karr and Keinath (1978). Karr and Keinath (1978) furthermore assumed that particles in supra-colloidal range would blind the sludge cake and thus create a larger resistance to filtration. Within the model by Altmann and Ripperger (1997), this could furthermore be attributed to the higher drag force being exhibited on smaller particles and hence resulting in a higher attachment at membrane surfaces, especially at lower permeate fluxes. This is also in accordance with the observation made by Drews *et al.* (2010). A lower flux at low MLSS content can thus be assumed to create higher irreversible fouling. This was in accordance to the observation made during the bench-scale resistance fractionation (Chapter 9).

8.5. Floc rupture - SMP release, SMP retention and HPSEC profiles

Throughout the side-stream passage, apart from few occasional samples, microbial flocs were generally found to decrease in size due to shear exhibited from the aeration and side-stream vessel passage. Soluble microbial release, observed retention and rejection values were calculated and correlated to the determined different filtration performance parameters.

Similarly to the soluble microbial products and the particle size determination, no obvious impact was observed between the retention and rejection of potential foulants and the membrane module performance.

Due to the exhibited shear, turbidity of the bulk phase increased within the retentate lines. This increase in turbidity was found to statistically correlate to the permeability of the flat sheet and the hollow fibre module, showing a decrease in filtration performance the higher the turbidity of the bulk phase. The higher the release of turbidity from the biomass, the higher the permeability decline for the FS module (R= *-0.5759,* p= *0.008*), followed by the HF module (R= *-0.5209,* p= *0.022*). In opposition, no such correlation was found for the MT module.

These findings could be repeated while assessing the filterability of a small submerged flat sheet membrane with biomass being exposed to lower or higher shear rates. Two Hach-Lange filtration units, with additional separation panels having the same separation distance as the full scale module, were equipped with the sample material of the pilot scale module (PVDF 0.08 m) and run in parallel to the flat sheet pilot scale module and the cross flow test cell. While one Hach-Lange filtration module was placed in an aerated bench-scale tank, the other one was placed in the tank also feeding the cross-flow test cell. The biomass of the latter was therefore experiencing higher pump shear rates. The critical flux revealed almost no difference between the aerated submerged bench-scale module and the pilot scale module (J_c = 26, 25 LMH at MLSS 10 g.L^{-1}), whereas a significant loss in permeability was observed for the

cross-flow test cell and furthermore also for the submerged bench scale module filtering the high shear rated biomass. J_c dropped for both bench-scale membranes to 16 and 19 LMH, respectively.

The biomass was furthermore analysed for the effects of floc rupture resulting from cross-flow pumping of the test cell device, which yielded overall in biomasses with much lower particle size (23 μm to 50 μm, Figure 8.6) and significantly higher SMP values within the supernatant. The same analyses conducted for all bench scale trials revealed significantly higher SMP values within the supernatant with DOC ranging from 33 to 204 mg.L^{-1}, proteins from 8 to 132 mg.L^{-1} and carbohydrates from 7.5 to 244 mg.L^{-1} (Table 8.3).

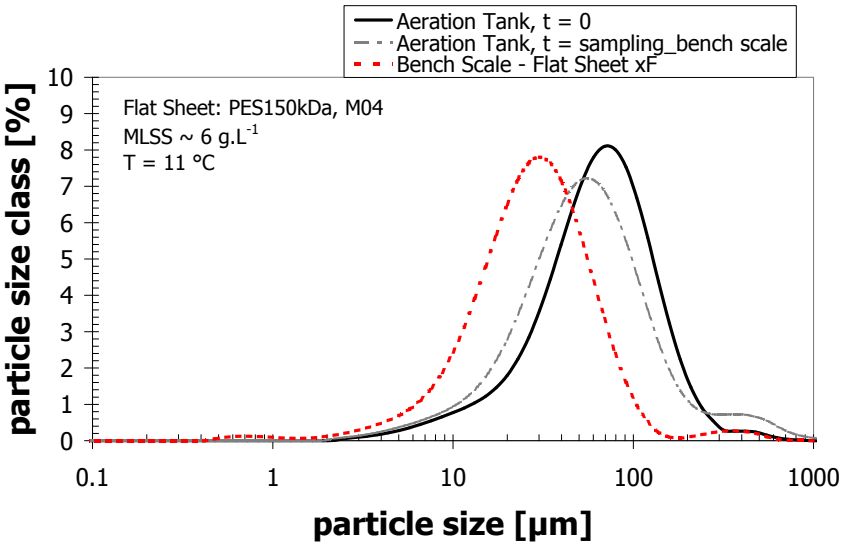

Figure 8.6.: Impact of pump shear rate on floc size development Example of floc size development between biomass taken from aeration tank (AT) and bench-scale cross-flow of flat sheet test cell device

Table 8.3.: Biomass and SMP parameter for critical flux trials of different flat sheet membrane material

Sample trial	MLSS [g.L^{-1}]	VSS [%]	TS [g.L^{-1}]	Particle size [μm]	NTU	DOC [mg.L^{-1}]	Prots [mg.L^{-1}]	Carbs [mg.L^{-1}]	P/C
Biomass deriving from MBR aeration tank									
Comparison (1): March 2008; HRT 12h - *Membranes tested: T06, T07, B03, M04, P03, K07*									
average	6.9	88.1	7.1	60.7	2.183	33	13	35	0.40
min	4.9	87.1	5.6	55.6	1.015	10	8	19	0.21
max	8.1	88.6	8.4	68.7	3.895	59	26	66	0.50
Comparison (2): May 2008; HRT 8h - *Membranes tested: T08, P05, M05, K08*									
average	11.1	86.1	11.8	79.6	12.05	74	28	45	0.61
min	10.9	84.8	11.6	74.0	6.81	65	25	42	0.60
max	11.4	87.0	12.3	83.6	16.40	89	31	50	0.63
Comparison (3)*: June 2008; HRT 8h - *Membranes tested: B04, P06, M06, K09*									
average	3.7	88.7	4.2	67.5	1.405	18	14	20	0.77
min	2.9	87.2	3.5	55.0	0.567	11	9	11	0.54
max	4.6	89.7	5.1	82.5	1.910	25	19	32	1.12
Parameters of Retentate line - sheared biomass									
(1) ave	6.6	88.0	6.7	32.4	6.3	60.9	17.5	244.5	0.1
min	4.5	87.7	4.8	28.9	2.6	33.1	8.6	179.0	0.0
max	8.0	88.3	8.3	36.9	9.6	105.7	22.2	341.4	0.1
(2) ave	10.5	86.8	11.8	47.2	43.3	174.3	121.5	85.2	1.4
min	10.3	86.4	11.3	45.5	37.4	159.0	111.1	84.8	1.3
max	11.1	87.2	12.7	50.1	48.0	204.6	132.5	86.1	1.6
(3) ave	4.5	89.6	5.1	26.5	18.3	43.8	41.5	34.0	1.3
min	1.9	88.1	2.8	23.0	1.7	20.0	12.4	7.5	0.3
max	9.9	91.6	10.9	30.1	58.0	71.5	119.8	63.0	2.6
Permeate values at J$_{max}$= 21 LMH									
(1) ave	-	-	-	-	1.18	19.6	3.1	4.8	0.7
min	-	-	-	-	0.49	3.3	1.3	2.2	0.3
max	-	-	-	-	1.87	57.3	5.5	8.5	1.3
(2) ave	-	-	-	-	0.69	29.8	14.0	8.4	1.8
min	-	-	-	-	0.39	11.3	8.7	4.2	1.3
max	-	-	-	-	0.87	54.4	18.2	13.8	2.1
(3) ave	-	-	-	-	1.08	7.9	5.5	6.5	0.9
min	-	-	-	-	0.38	4.7	1.0	3.0	0.1
max	-	-	-	-	2.11	11.1	9.8	8.5	1.5

* low MLSS content due to previous biomass loss; experiment on 5 consecutive days, 14 days after biomass loss occasion

Assessing the supernatant release occurring during floc rupture due to the pump shear, an increase in cake layer resistance, R_{cl}, was observed with increasing SMP release of carbohydrates (*R = 0.5606, p=0.037, n=14*). However, no such impact could be found for other SMP constituents, such as proteins or DOC. Furthermore, the cake layer resistance presented a significant increase with decreasing fractionation of either $d_{0.1}$, $d_{0.2}$ or $d_{0.5}$ of the sludge particles (*R = -0.6526, p=0.016, n=13*). An increased SUVA of the retentate line was also found to correlate with an increasing biomass resistance (*R = 0.8980, p=0.039, n=8*). It has to be noted that the release of carbohydrates during floc rupture was found to correlate to particle fractionation.

In general, these observations lead to the assumption that floc rupture occurring during the side-stream passage had a significant impact on the overall filtration performance of all of the tested membranes with higher cake layer formation, the higher the floc rupture, which is in accordance to other studies (Stricot *et al.*, 2010; Wisniewski and Grasmick, 1998).

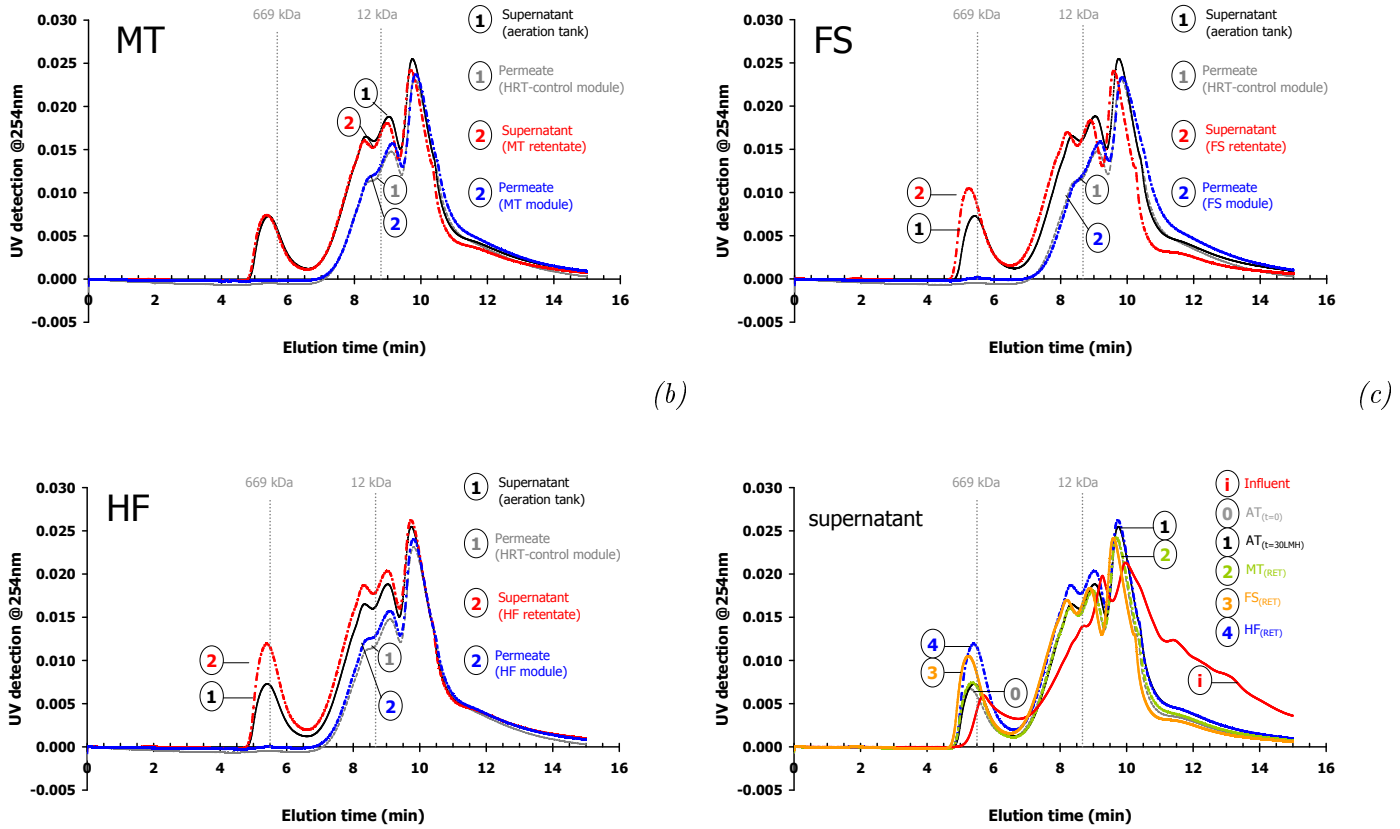

Figure 8.7.: Sample of changes in supernatant molecular composition during sidestream operation and retention due to membrane filtration - HPSEC profiles: *(a)* MT; *(b)* FS; *(c)* HF; *(c)* supernatant comparison.

8.6. Summary

Soluble microbial products are frequently reported as potential major foulants in MBR systems. Overall, carbohydrate concentrations varied between 6 mg.L^{-1} and 77 mg.L^{-1}, proteins between 7 mg.L^{-1} and 30 mg.L^{-1} and DOC between 11 mg.L^{-1} and 71 mg.L^{-1} for the range of MLSS concentrations and critical flux tested, and were found within range of many pilot trials studied, but also show elevated levels for carbohydrates and DOC concentration (Table 8.4).

While no obvious direct impact between module filtration performance and biomass parameters was found, a higher concentration of SMP at lower MLSS content was found to have adversely impacted the membrane, moreover the reversible/irreversible membrane resistance. This was not only observed in pilot scale, but also for the flat sheet bench-scale where the higher amount of SMP was found to have attached to the membrane surface the lower the MLSS.

This might be furthermore supported by the observed correlation of bulk ratio P/C to the sludge filterability development. Arabi and Nakhla (2008) also observed higher fouling rates and increased cake filtration resistances with increase P/C ratio in the influent. Houghton *et al.* (2001) furthermore found a relationship between sludge filterability and the ratio of protein to carbohydrates of the biomass giving an indication of hydrophobicity of the biomass. Though the trend was not found to be consistent for the entire data gained during this study, it is worth mentioning that, for example, during the flat sheet material trials, highest biomass resistances were determined when the ratio of protein to carbohydrate of the bulk phase was above 1.0.

Data therefore suggested that the impact of SMP on membrane fouling is a complex interaction between MLSS content, membrane configuration and SMP composition. Generally, for HF and FS it could be assumed that the lower MLSS content, the more likely is the attachment, pore penetration respectively, of carbohydrates and DOC. Moreover, the determined DOC measurements, *which could be assumed to represent colloidal matter due to the analyses through a 1.25 μm glass fibre filter*, were also found overall to statistically interrelate with the cake layer resistance of the HF and FS module.

This is in accordance with Itonaga *et al.* (2004), who reported no clear correlation between measured dissolved organic matter (DOC, carbohydrates, proteins) and membrane fouling on two parallel run HF submerged MBRs, whereas colloidal fractions within the supernatant seemed to play an important role in membrane fouling (Itonaga *et al.*, 2004). Furthermore, Fan *et al.* (2006) also reported colloidal TOC being the main fouling parameter with J_c decreasing with increasing colloidal TOC, whereas no clear relationship could be drawn to MLSS content which varied from 7 to 21 g.L^{-1}. Furthermore, J was reported to decrease with increasing soluble carbohydrates and increasing EPS, whereas EPS was directly related to colloidal TOC. Humic substances and proteins showed less impact.

Lyko *et al.* (2008b) suggested that DOC would provide an alternative to more complex and costly measurements of soluble EPS to predict sludge filterability, whereas no proteins, carbohydrates or DOC measurements were found to be usable *stand-alone-parameters* in order to predict changes in filtration performance on a reliable basis.

Important to note is that HF, FS and MT modules presented correlations between determined permeability and the estimated load of carbohydrates passing the membrane surfaces during the lowest MLSS content. The load of DOC during the lowest MLSS was also statistically significant for MT and FS, whereas no significant correlation could be determined for the HF module. However, the DOC content per mg.VSS was found to show correlation to all three membrane configurations at a low MLSS content. It should, however, be mentioned at this point that during this study some contradicting correlations were observed with very high statistical significance.

Exhibited shear on flocs was observed to lead to floc rupture with carbohydrate and turbidity release causing a higher cake layer resistance. This phenomenon was observed for both bench and pilot scale experiments and is in accordance with literature (Stricot *et al.*, 2010; Wisniewski and Grasmick, 1998).

Retention of potential foulants was monitored, but was not found to have had an impact on the overall filtration performance. HPSEC profiles showed the complete retention for higher molecular species for all membranes applied. Similar results were obtained by Al-Halbouni *et al.* (2008). Furthermore, Lyko *et al.* (2008a) stated a clear relationship between permeate flux and the concentration of larger macromolecules in permeates with an increase in flux increasing retention of soluble macromolecule causing subsequently a higher fouling rate.

While most studies concentrate on fouling deriving from SMP and EPS, potential scaling foulants are generally neglected. However, during a monitoring of a full scale activated sludge plant, Lyko *et al.* (2007) observed no impact of calcium and magnesium on the fouling behaviour, whereas complexes formed with iron were suspected to contribute to pore clogging.

Table 8.4.: Examples of data from literature - soluble microbial products (SMP), particle sizes - part 1

Conf.	Material	Feed	MLSS	Particle	Proteins		Carbohydrates		DOC		Reference
			[g.L^{-1}]	Size [μm]	[mg.L^{-1}]	[mg.g^{-1} MLSS]	[mg.L^{-1}]	[mg.g^{-1} MLSS]	[mg.L^{-1}]	[mg.g^{-1} MLSS]	
full-scale plants (tank volume > 100 m^3)											
iHF	PVDF 0.04μm	mun.	11-12	-	2-11	0.17-0.95	1-18	0.08-1.6	5-27	0.4-2.4	Lyko *et al.* (2008*b*)
iHF	PVDF 0.04μm	mun.	10-14	-	3.6 $\pm$2.9	$\approx$ 0.3-0.5	2.4 $\pm$4.1	$\approx$ 0.2-0.6			Lyko *et al.* (2007)
diff	diff	diff.	12-20	58.4-111	-	0 - 3.8	-	0.25-0.7	-	1.5-11.4	Brookes *et al.* (2003)
iFS	PVDF 0.4μm	mun.	12-18	25-275	0-200	-	10-180	-	-	-	Reid (2005)
iFS	PVDF 0.4μm	mun.	17-23	44.5-76.8	4.2-7.8	0.25-1.0	2.1-4.9	0.18-0.25	8.1-19.1	0.5-1.48	*this study*
pilot-scale plants (0.2 m^3 < tank volume $\leq$ 20.0 m^3)											
iHF	PVDF 0.04μm	mun.	5-9	68.0-128	0.13-11.0	0.01-1.9	6.0-12.0	0.97-2.1	-	-	Germain (2004)
iHF	PE, PVDF 0.4μm	mun.	11	-	5-35	0.5-3.2	4-11	0.3-1.0	0-17*	0-1.5*	Yamato *et al.* (2006)
iHF	PVDF 0.1μm	mun.	3.0-15.4	16.7-90.8	2.8-68.3	0.8-6.4	5.0-159.0	0.2-16.3	11.5-139.2	1.1-8.7	*this study*

(* different fractionation of SMP; ** ΣSMP; asMBR = air-lift side-stream MBR; iMBR = submerged MBR; mun. = municipal; syn. = synthetic)

Table 8.5.: Examples of data from literature - soluble microbial products (SMP), particle sizes - part 2

Conf.	Material	Feed	MLSS	Particle	Proteins		Carbohydrates		DOC		Reference
			[g.L^{-1}]	Size [μm]	[mg.L^{-1}]	[mg.g^{-1} MLSS]	[mg.L^{-1}]	[mg.g^{-1} MLSS]	[mg.L^{-1}]	[mg.g^{-1} MLSS]	
pilot-scale plants (0.02 m^3 < tank volume ≤ 0.2 m^3)											
iHF	PE 0.4μm	mun.	15	-	2.0-7.0	≈ 0.47	0.0-2.5	≈ 0.17	2.5-11.0	≈ 0.73	Itonaga *et al.* (2004)
iMT	PES 0.01μm	mun.	3-12	≈ 75	7.5-19.2	0.7-1.7	0	0	≈ 20-25		Le-Clech (2002)
asMT	PES 0.01μm	mun.	4-12	≈ 75	21-32	2.3-7.0	0	0			Le-Clech (2002)
diff	diff	mun.	4-12	38.8 - 88.6	-	0-4.5	-	0.5-10.0	-	0-37.3	Brookes *et al.* (2003)
iMT, asMT	PVDF 0.03μm	syn.	6-17	75-105	11.4-22.7	1.3-1.8	18.7-48.5	2.8-3.0			Brookes (2005)
iHF	PS 0.08μm	syn.	4 -14*	60-75	50-400**	25-28**	50-400**	25-28**	-	-	Khongnakorn *et al.* (2007)
lab-scale plants (tank volume ≤ 0.02 m^3)											
iFS	ceramic, 0.08μm - 0.3μm	mun.	5	-	14-73	2.8-14.6	7-18	1.4-3.6	-	-	Jin *et al.* (2009)

(* different fractionation of SMP; ** ΣSMP; asMBR = air-lift side-stream MBR; iMBR = submerged MBR; mun. = municipal; syn. = synthetic)

9. Results and Discussion: Impact of membrane material properties

9.1. Scope

An adequate membrane morphology is expected to contribute significantly to the overall process optimisation. Within the *'road map of fouling'* postulated by Zhang *et al.* (2006), membrane material properties such as pore size distribution, hydrophilicity, surface roughness and surface charge are indicated as major criteria for the selection of membranes in terms of fouling prevention.

Different commercially available membranes were tested for their surface characteristics and filtration performances. Membrane materials tested included polymeric membranes made of PVDF, PES, PS and PE with varying pore sizes (Table 9.1, page 181).

While membrane material and pore sizes were given by the supplier, this study investigated further virgin material membrane properties, such as ultrapure water permeability (K_{20}), intrinsic membrane resistance (R_m), RMS surface roughness (AFM) and contact angle of several wetting liquids to determine the membrane's surface tension parameters and the surface free energy (Table 4.5, page 62).

To complete the study, high resolution pictures were taken on a scanning electron microscope for visual comparison of the membrane surfaces, for example, for the homogeneity of pore size distribution (Figure 9.2 and Figure 9.1).

9.2. Membrane Surface Characterisation

From the SEM images, the most obvious difference is the **pore size distribution** of the micro-porous; the PE 0.4μm, membrane material. This membrane is a so-called symmetric membrane, meaning the membrane is approximately unified across the membrane depth with no additional supporting layer and, hence, the separation and filtration performance would presumably be similar at either side of the membrane surface.

The nano-filtration membrane, the PES 150kDa membrane, and the PS 0.05μm did not reveal much difference regarding their active layer appearance. The PVDF membranes, deriving from two different manufacturers, with indicated pore sizes of 0.08μm and 0.15μm respectively, revealed an arbitrarily arranged pore size distribution with the PVDF 0.15μm membrane showing a wide range of differently shaped pores (Figure 9.1 *a-d*).

PVDF 0.15 μm

(a) 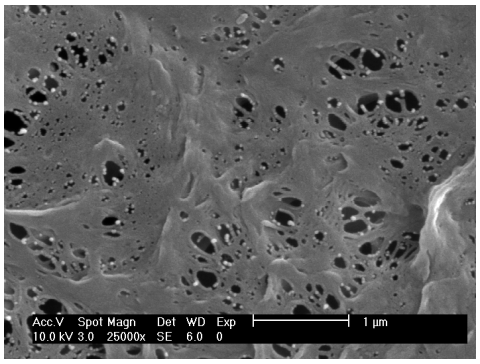

(b) 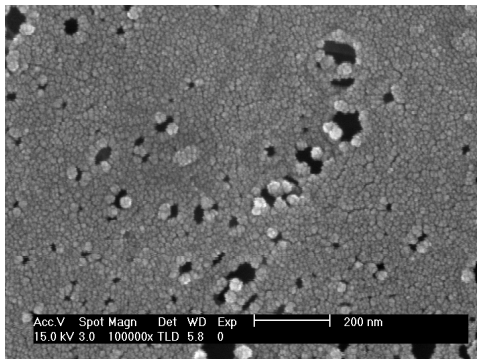

PVDF 0.08 μm

(c) 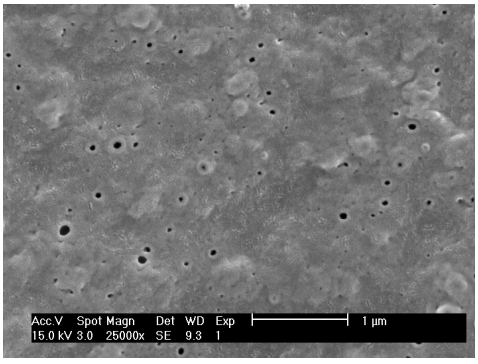

(d) 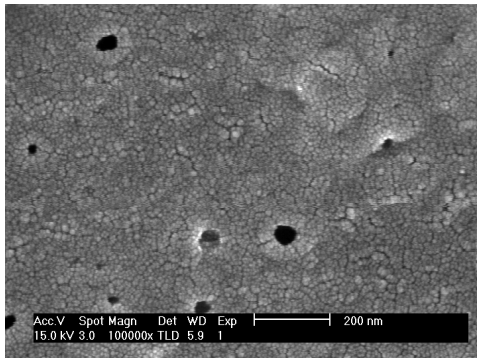

Figure 9.1.: Scanning electron microscope - Selection of pictures of PVDF membrane samples (virgin material) at varying magnitudes:
PVDF 0.15 μm at magnitude of *(a)* 25,500 and *(b)* 100,000
PVDF 0.08 μm at magnitude of *(c)* 25,500 and *(d)* 100,000.

PE 0.4 μm

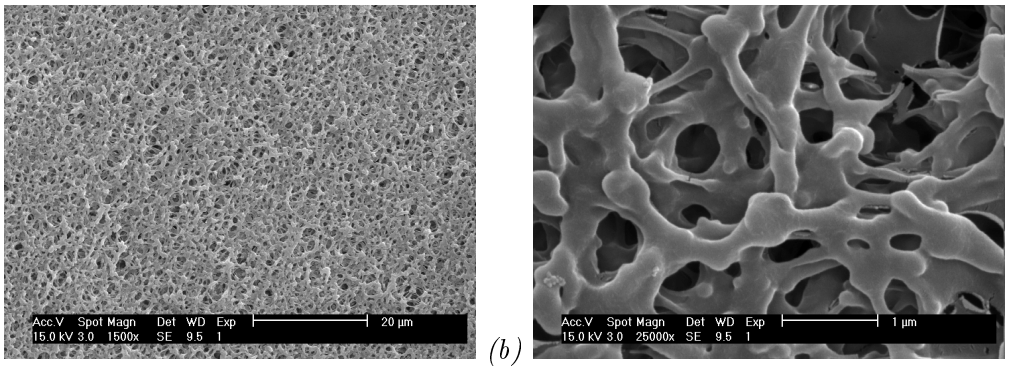

(a) *(b)*

PES 150 kDa

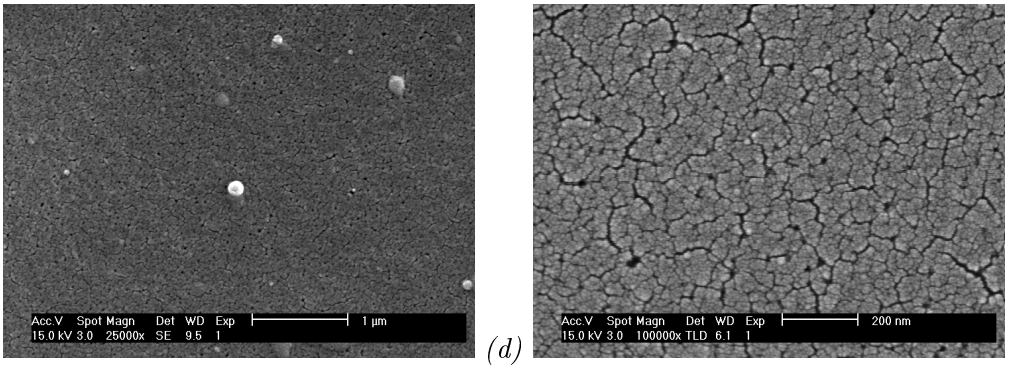

(c) *(d)*

PS 0.05 μm

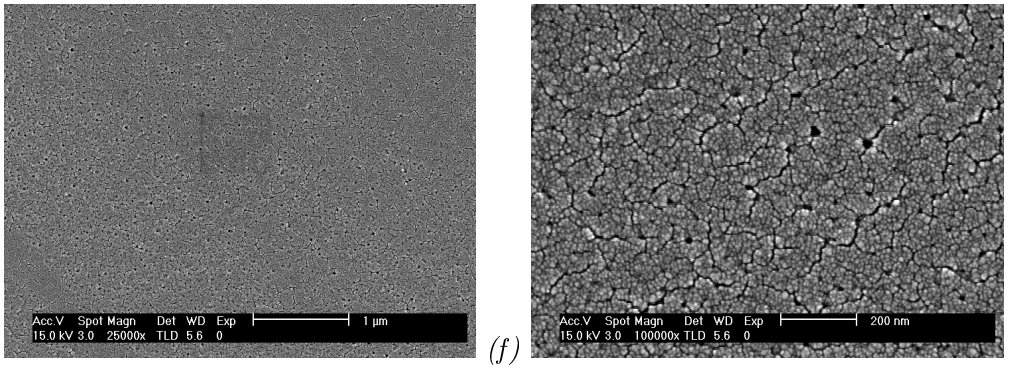

(e) *(f)*

Figure 9.2.: Scanning electron microscope - Selection of pictures of different membrane samples (virgin material) at varying magnitudes:
PE 0.4 μm at magnitude of *(a)* 1,500 and *(b)* 25,000
PES 150 kDa at magnitude of *(c)* 25,500 and *(d)* 100,000
PS 0.05 μm at magnitude of *(e)* 25,000 and *(f)* 100,000.

Ultrapure water permeability revealed a high difference between the different types of membranes tested and, surprisingly, also between individual membrane samples made from the same material (K_{20} and R_m in Table 9.1). The lowest permeability with an average of only 153 LMH.bar^{-1} was found for the PVDF 0.15μm membrane, followed by an average of 326 LMH.bar^{-1} for the PS 0.05μm membrane, while the range of permeabilities determined included, for instance, values of up to 5300 LMH.bar^{-1} for the 0.08μm PVDF membrane resulting in an average permeability of 2237 LMH.bar^{-1} for the range of samples tested.

The comparison of both PVDF membrane materials emphasised the importance of material properties other than the polymer they are made from, for their overall filtration performance. While the PVDF 0.08μm membrane material always revealed permeability values for clean water above 900 LMH.bar^{-1}, some of the sample material of the PVDF 0.15μm membrane had to be omitted for further research trials as a clean water flux could not be achieved even after thorough sampling pre-treatment as described by the manufacturer. The PE 0.4μm membrane and the PES 0.4μm membrane revealed on average permeabilities of 2667 LMH.bar^{-1} and 889 LMH.bar^{-1}, respectively.

The corresponding **intrinsic membrane resistances (R_m)** varied between 0.091 $\cdot 10^{12}$ m^{-1} and 1.904 $\cdot 10^{12}$ m^{-1} for the PE 0.4μm membrane and the PVDF 0.15μm membrane respectively (R_m in Table 9.1). Again, very different results have been obtained for the different PVDF membrane materials.

The results for **surface roughness** (Figure 9.4 and Figure 9.3) and contact angle measurements (Figure 9.5) also showed wide variations across individual membrane samples. For instance, surface roughness RMS for PS 0.05μm membrane material revealed a deviation of 39.7 nm for an average RMS value of only 56.1 nm. The highest average RMS was determined for the micro porous PE 0.4μm membrane with 186.9 nm, indicating a trend for higher surface roughness measurements based on membrane pore size. According to the values obtained for the two PVDF membrane samples, pore size distribution and surface homogeneity seemed to be a further crucial parameter for surface roughness. Furthermore, it has to be noted that the surface roughness data represented hereafter (Figure 9.3) was evaluated from samples taken with the Veeco Explorer under tapping mode with an image spectrum size of 10 μm and with the type of cantilever tip as described during Chapter 4.3.1. This distinction had to be made, as significant differences were determined when comparing samples analysed from the two different Veeco instruments, from the same Veeco instrument but with a different cantilever and, mostly important, the highest deviations were observed between samples analysed on the same sample but with a different image spectra.

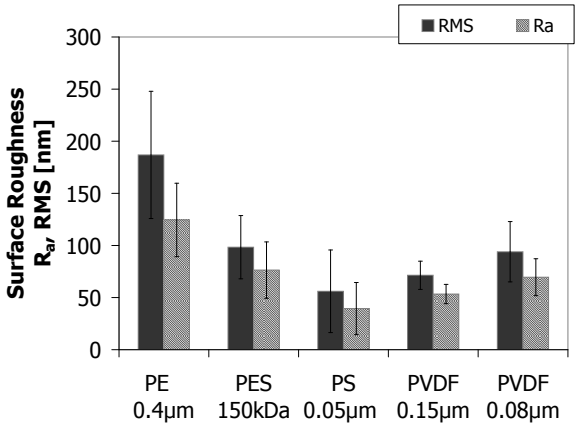

Figure 9.3.: Determined surface roughness (RMS and R_A) for different flat sheet membrane material

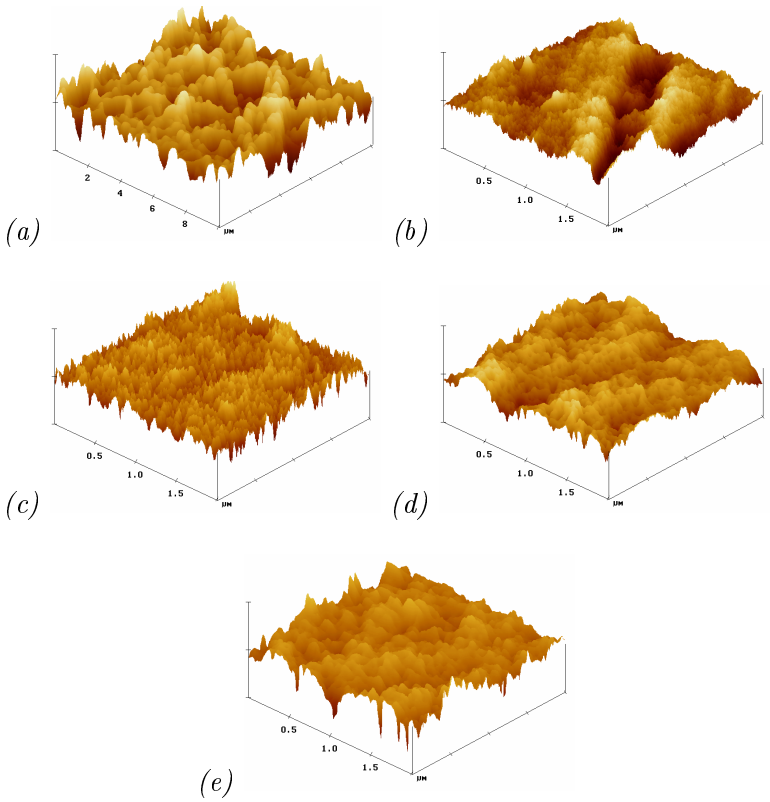

Figure 9.4.: Atomic force microscope - Sample of AFM pictures of different membrane samples (virgin material, image spectrum for (a) 10x10 μm, (b)-(e) 2x2 μm):
(a) PE 0.4 μm , *(b)* PES 150 kDa, *(c)* PS 0.05 μm, *(d)* PVDF 0.15 μm, *(e)* PVDF 0.08 μm.

Contact angle measurements undertaken on non-prepared samples with ultrapure water identified two membranes with complete wettability (PE 0.4μm, PVDF 0.08μm), while complete wettability on prepared samples (see Section 4.3.1.1) was only achieved for the PVDF 0.08μm. This led to the suggestion that surface properties of the PE 0.4μm changed dramatically due to the wetting-drying action, while the PVDF 0.08μm remained less impacted. In fact, it is common procedure to never let membranes run dry due to the high property changes this would create. However, within this research all analyses were taken on previously wetted and then air-dried membranes for the purpose of simple comparison.

As previously mentioned determined contact angles varied widely for the different membrane materials and also across the membrane surfaces, which was assumed to be a result of the different pore size distribution. For instance, the contact angle of the wetting liquid diiodmethane varied from 0° to 21° for the PES 150kDa membrane material and for the PVDF 0.15μm membrane material from 0° to 52°. Furthermore, in contrast to the other membrane materials tested, the PVDF 0.08μm membrane material showed complete wettability to all wetting liquids applied, except for glycerol. The contact angle measured for glycerol varied between 42° and 70°.

The high deviations found across the membrane surface of each material were consequently also affecting the overall determination of the surface tension parameters and subsequently led to the suggestion that it is either very difficult to obtain reliable results by the techniques applied, or that the wide range of results is a representative picture of different surface properties prevailing across the membrane with some parts being more hydrophobic than others. Furthermore, it has to be noted that the type of determination method of the respective surface energy parameter may also impact the overall results (Bargir, 2007).

For instance, the component for γ_S^{LW} (apolar) surface free energies varied between 13 and 262 mJ.m^{-2} for the PE 0.4 μm membrane material, showing changes from a very low surface energy to a very high surface energy indicating a surface with weak and strong apolar binding forces. Similar high deviations were found for the PS 0.05 μm membrane material (10 and 182 mJ.m^{-2}) and for the PVDF 0.08 μm membrane (10 and 148 mJ.m^{-2}). On average, γ_S^{LW} varied between 44.5 and 71.5 mJ.m^{-2} across the sample of different membrane materials.

The polar components, γ_S^+ and γ_S^-, with the PE 0.4μm membrane and the PVDF 0.08μm membrane materials both showing the highest average values for γ_S^+, also revealed high deviations for these two materials ranging from 0.001 to 145 mJ.m^{-2} and 0.002 to 147.5 mJ.m^{-2}, respectively. Values for γ_S^+ varied between 0.6 to 20.2 mJ.m^{-2} for the PES 150kDa and PE 0.4 μm membrane and γ_S^- between 4.1 to 66.1 mJ.m^{-2} for the PE 0.4 μm and PVDF 0.08 μm membrane, respectively. The surface energy parameter γ_S showed values between 50.9 mJ.m^{-2} and 88.7 mJ.m^{-2} for the PES 150kDa and the PVDF 0.08 μm membrane, respectively. The total interfacial free energy of interaction between surfaces immersed in water (ΔG_{iwi}*, van Oss, 2003) varied between -243.8 mJ.m^{-2} (PES 150kDa) and -488.4 mJ.m^{-2}

(PVDF 0.08μm) would then indicate a high hydrophobic attraction of the respective membrane surfaces to water. The interfacial surface tension between membrane material and water (γ_{SL}) was determined with -10.3 mJ.m^{-2} for the PVDF0.08 μm membrane material. While this membrane exhibited on average a negative value for γ_{SL}, the other tested membrane materials were found to have positive values with the PE 0.4μm membrane material showing the highest average γ_{SL} of 31.6 mJ.m^{-2}. This would then suggest that the PVDF 0.08 μm tends to show hydrophilic attraction, while the other membrane materials would be commonly showing hydrophobic attraction (van Oss, 2003).

Overall, it should be noted that due to the wide variations obtained, it was decided to use not only average values, but also minimum and maximum results for statistical analyses. As this resulted in a huge matrix with enormously different parameters, only data with relevant outcomes will be mentioned within the next sections. Parameters not discussed can therefore generally be assumed as not having had shown any statistical significance.

Correlating the determined contact angle to the given nominal pore size, did not disclose any statistical significance, whereas amongst the determined surface tension parameters the apolar parameter γ_S^{LW} (gslw), and the polar constituent γ_S^+ (g+) presented an increase with increasing pore size, with *R^2=0.6319 (p=0.001)* and *R^2=0.4682 (p=0.003)* respectively. Furthermore, an increase of interfacial surface tension between membrane and water, γ_{SL}, could be observed with increasing pore size, though correlation obtained was less significant with *R^2=0.384 (p=0.000)*. As expected a significant linear correlation was observed with the determined surface roughness RMS *(R^2=0.7156 p=0.000)*.

The intrinsic membrane resistance R_m did not reveal any statistically significant correlation to pore size, surface tension or surface energy parameter, which was somewhat expected given the fact that R_m is supposed to be directly dependent on pore size distribution and membrane thickness (or active filtration layer thickness) and only indirectly dependent on the parameters determined. However, for the membranes investigated, it could be observed that even though the linear correlation of surface roughness to intrinsic membrane resistance was less than *R^2 = 0.2919*, a multiple correlation of pore size, R_m and RMS revealed a strong statistically significant correlation with R^2 = 0.9461. This could also be observed for the interfacial surface tension γ_{SL} with linear correlation to R_m of *R = 0.1865*, where the significance increased for the multiple correlations (*R = 0.6970*).

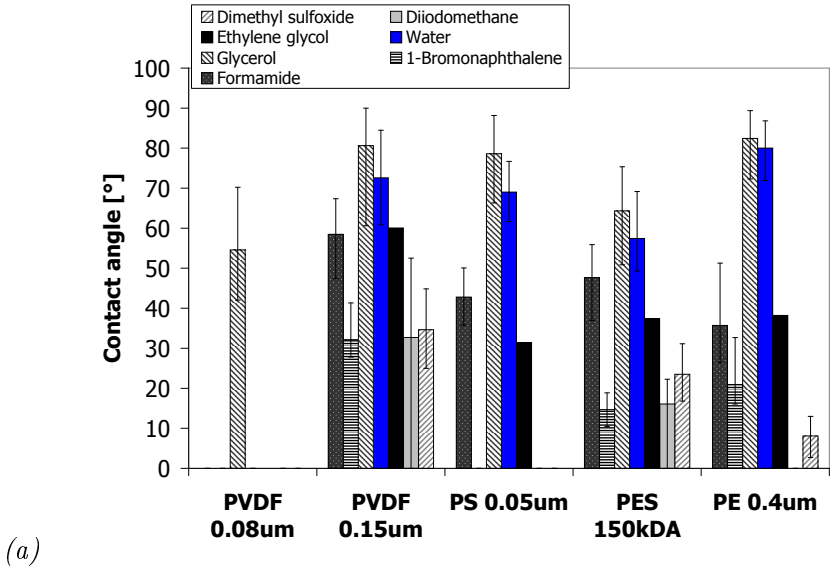

(a)

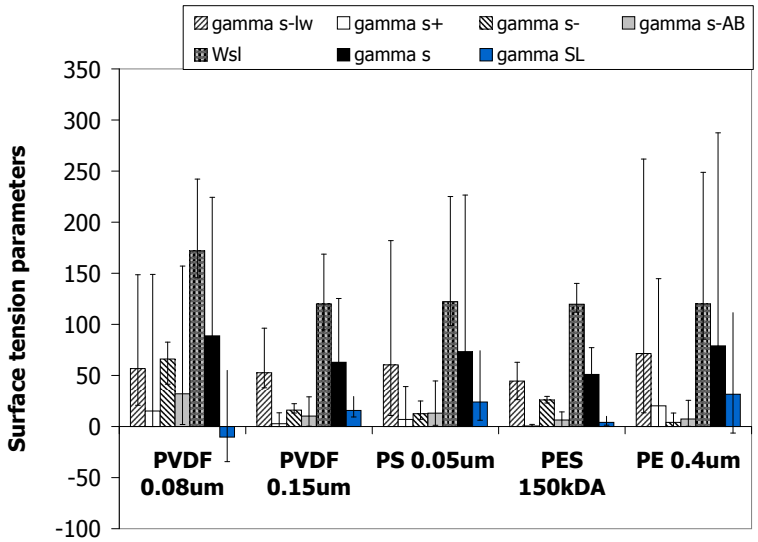

(b)

Figure 9.5.: Determination of *(a)* contact angle ° for different flat sheet membrane materials and varying wetting liquids and *(b)* the resulting surface tension parameters in $mJ.m^{-2}$

Table 9.1.: Summary of determined membrane material characterisation parameters

Comparison of different Flat Sheet Membrane Material					
Membrane ID	**K01-K09**	**M01-M04**	**P01-P05**	**B01-B05**	**T01-T10**
Membrane material	PE	PES	PS	PVDF	PVDF
Nominal pore size	0.4 μm	150 kDa	0.05 μm	0.15 μm	0.08 μm
Filtration Performance					
K_{20} [$Lm^{-2}h^{-1}.bar^{-1}$]	2667 ±1175	889 ±186	326 ±38	153 ±10	2237 ±1010
R_m [$\cdot 10^{12}$ m^{-1}]	0.091 ±0.04	0.272 ±0.069	0.746 ±0.014	1.904 ±0.162	0.115 ±0.087
Contact Angle [°]					
Dimethyl sulfoxide	8.1 (3/13)	23.5 (17/31)	0.0 (0/0)	34.6 (25/444)	0.0 (0/0)
Diiodomethane	0.0 (0/0)	16.1 (0/22)	0.0 (0/0)	32.7 (0/52)	0.0 (0/0)
Ethylene glycol	38.2 (30/45)	37.4 (29/49)	31.4 (24/39)	60.1 (48/72)	0.0 (0/0)
Water	80.0 (72/88)	57.4 (45/66)	69.0 (53/83)	72.6 (60/88)	0.0 (0/0)
Glycerol	82.4 (72/89)	64.3 (51/75)	78.6 (66/88)	80.6 (61/90)	54.6 (42/70)
1-Bromonaphthalene	20.9 (16/33)	14.7 (11/19)	0.0 (0/0)	32.2 (28/41)	0.0 (0/0)
Formamide	35.7 (26/51)	47.6 (37/56)	42.8 (36/50)	58.5 (47/67)	0.0 (0/0)
Surface tension and energy parameters [$mJ.m^2$]					
γ_S^{LW}	71.5 (13/262)	44.5 (26/63)	60.3 (10/182)	52.7 (38/96)	56.7 (21/148)
γ_S^+	20.2 (0/145)	0.6 (0/2)	6.9 (0/39)	2.7 (0/13)	15.2 (0/148)
γ_S^-	4.1 (0/13)	26.0 (23/29)	12.6 (7/25)	16.0 (13/23)	66.1 (41/82)
γ_S^{AB}	7.4 (0/26)	6.4 (0/14)	13.1 (1/45)	10.2 (0/29)	32.0 (2/157)
γ_S	78.9 (18/287)	50.9 (40/77)	73.4 (33/227)	62.9 (38/125)	88.7 (46/224)
W_{sl}	120 (85/249)	119 (112/140)	122 (99/225)	119 (95/169)	172 (146/242)
γ_{SL}	31.6 (-67/111)	4.0 (1/10)	24.0 (7/74)	15.8 (7/29)	-10.3 (-26/55)
ΔG_{iwi}*	-298.6	-243.8	-283.0	-256.3	-488.4
AFM - surface roughness [nm]					
RMS	186.9 ±61.0	98.3 ±30.4	56.1 ±39.7	71.4 ±13.5	94.0 ±28.9
R_A	124.5 ±35.2	76.4 ±27.0	39.5 ±25.0	53.4 ±9.3	69.6 ±17.7

* according to van Oss (2003);

notation: 71.5 (13/262) = average (minimum/maximum); 186.9 ±61.0 = average±stdev.

9.3. Membrane Filtration Resistances - R_t, R_m, R_{cl}, R_{rev}, R_{irrev}

The determination of resistance according to the resistance in-series model revealed significant differences between the individual membrane materials tested (Figure 9.6).

The lowest average total resistances (R_t) were determined for the PES 150kDa and the PVDF 0.08μm membrane material with R_t values of 2.39 $\cdot 10^{12}$ and 2.66 $\cdot 10^{12}$ m^{-1} respectively. The highest average total resistance was determined for the PVDF 0.15 μm membrane material with 6.84 $\cdot 10^{12}$ m^{-1}, which emphasised again the enormous difference in filtration performance between the two PVDF membrane materials tested.

The PE 0.4μm membrane module presented the highest variations in determined total resistance with values ranging from 3.55 $\cdot 10^{12}$ m^{-1} to 8.90 $\cdot 10^{12}$ m^{-1}, followed by the PS 0.05μm membrane material with variations from 2.16 $\cdot 10^{12}$ m^{-1} to 7.36 $\cdot 10^{12}$ m^{-1} (Figure 9.6).

The overall average cake layer resistance was 2.19 $\cdot 10^{12}$ m^{-1} for all membranes tested with the highest R_{cl} for the PE μm membrane material (K09, R_{cl} = 5.02 $\cdot 10^{12}$ m^{-1}) and the lowest for the PVDF 0.08μm membrane material (T06, R_{cl} = 0.55 $\cdot 10^{12}$ m^{-1}).

Reversible fouling resistance was determined on average with 1.35 $\cdot 10^{12}$ m^{-1} and the highest values were found for the filtration trial of sample K09 with 3.59 $\cdot 10^{12}$ m^{-1} R_{rev}. The lowest values for R_{rev} were determined for the membrane samples T07, P06 and M06, with similar values of R_{rev} = 0.07 $\cdot 10^{12}$ m^{-1}, where it has to be noted that these similar values were measured during different test series and with different biomass parameters.

Irreversible fouling (R_{irrev}) was found to vary between 0.07 $\cdot 10^{12}$ m^{-1} and 1.77 $\cdot 10^{12}$ m^{-1}, for the PVDF 0.08μm membrane material and PVDF 0.15μm membrane material respectively. Overall, the irreversible fouling represented $\approx$ 12.5% of the total fouling resistance R_t. The cake layer resistance was found to be on average 54.4% of R_t, while the reversible fouling was on average one third of R_t (33.3%).

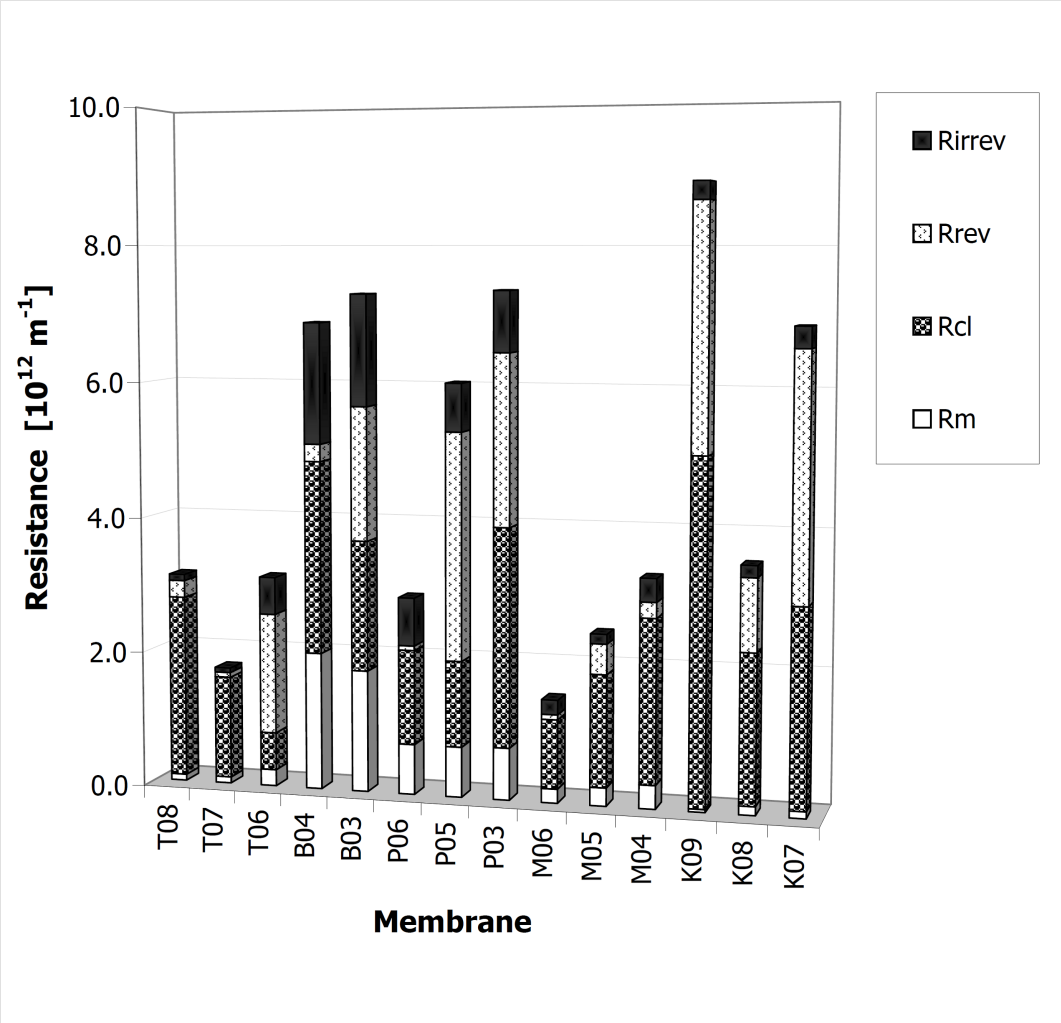

Figure 9.6.: Determined filtration resistances according to resistance-in-series method for different flat sheet membrane materials

As one might have expected, the determined resistance for cake layer and reversible fouling showed a significant increase with the increasing total resistance of the filtration trial, with *R=0.8012 (p=0.001)* for R_{rev} and *R=0.7109 (p=0.004)* for R_{cl}. In contrast, the intrinsic membrane resistance and the resistance for irreversible fouling did not show any significant correlation to R_t, R_{cl} or R_{rev}. This led to the assumption that cake layer resistance and reversible fouling resistance are parameters influenced by biomass make-up and are independent of the intrinsic membrane resistance. Interestingly, the irreversible resistance, R_{irrev} showed a very strong correlation to the determined intrinsic membrane resistance *R=0.9774, p=0.000*, which led to the conclusion that a low intrinsic membrane resistance is a crucial parameter for avoiding irreversible fouling during MBR filtration processes.

9.4. Fractionation of potential membrane foulants

Potential foulants extracted from the mechanical cleaning step and from the alkaline cleaning step surprisingly revealed patterns evidently different to what was expected from the determined fouling resistance factors for each individual membrane material (Figure 9.7).

In fact, having shown a notably high fouling resistance (reversible and irreversible) for the PVDF 0.15μm membrane, the extracted potential foulants within those layers revealed a significantly lower concentration than, for example, the PVDF 0.08μm membrane. The PVDF 0.08μm membrane, in contrast, was measured to have a very low filtration resistance compared to all other membranes, whereas the amount of extracted potential foulants from the surface of the PVDF 0.08μm membrane was by far the highest compared to all other membrane materials tested (see visual comparison of R_b, expressing the filtration resistance of the biomass as $R_b = R_{irrev} + R_{rev} + R_{cl}$ in Figure 9.7).

For instance, the DOC content within the mechanical cleaning layer of the PVDF 0.08μm membrane (T07) was as high as 1325 mg.m^{-2} membrane surface, but only 42 mg.m^{-2} for the PVDF 0.15μm membrane (B04, Table 9.2). The total extracted DOC content within the mechanical cleaning step was approximately 247 mg.m^{-2} for all tests conducted within a minimum value of 40 mg.m^{-2} (M06, PES 150kDa) and a maximum value of 1325 mg.m^{-2} (T07, PVDF 0.08μm). Extracted proteins were found to be on average of 27 mg.m^{-2} with a minimum value of 8 mg.m^{-2} and a maximum of 73 mg.m^{-2} for the PS 0.05μm membrane material (P06 and P05 respectively). The maximum extracted amount for carbohydrates was found for the K07 sample (PE 0.4μm) with 275 mg.m^{-2} and a minimum value for the PES 150kDa sample, M06, with 16 mg.m^{-2}.

In general, more potential foulants were removed from the membrane surfaces during the mechanical cleaning step than during the alkaline cleaning step, with the sum of DI extracted SMP values representing a maximum of 13 fold of the sum of extracted SMP during the alkaline cleaning step (K06). On average, the amount of DI extracted SMP was 4.64 fold higher than during the alkaline cleaning step. However, four samples (K09, M06, P06, B04) presented a higher content of extracted SMP during the alkaline cleaning with a ratio of on average 0.64 of the sum of SMP extracted during the mechanical cleaning. Surprisingly, this was observed during the same test series, hence the same type of biomass, which had, with $\approx$ 3.7 g.L^{-1}, the lowest MLSS content compared to the other trials of 6.9 g.L^{-1} and 11.1 g.L^{-1} MLSS respectively. The maximum values for NaOH extracted SMP did not necessarily coincide with the low MLSS trials, apart from the DOC content of sample K09 with 180 mg.m^{-2}, compared to an average of 73 mg.m^{-2}. However, the overall extraction of proteins, carbohydrates and DOC was slightly higher for the lower MLSS trials, with 84 mg.m^{-2} DOC, compared to 49 mg.m^{-2}; 31 mg.m^{-2} Proteins, compared to 19 mg.m^{-2} and 19 mg.m^{-2} Carbohydrates, compared to 15 mg.m^{-2}.

Overall, the measured content of DOC during the alkaline cleaning extraction was approximately 73 mg.m^{-2}. Proteins were detected with 25.4 mg.m^{-2} on average and carbohydrates with 18.1 mg.m^{-2} (Table 9.2). Despite the aforementioned observation made for the adsorbed amount during low MLSS values, no correlation could be statistically verified for the MLSS content and the amount of extracted SMP on the membrane surfaces.

Table 9.2.: Amount of extracted potential foulants from membrane material challenged with MBR biomass

	Extracted Potential Foulants from membrane material [X_F mg.m^2]					
	Mechanical Cleaning (DI)			**Alkaline Cleaning (NaOH)**		
Membrane	**DOC$_{DI}$**	**Prots$_{DI}$**	**Carbs$_{DI}$**	**DOC$_{NaOH}$**	**Prots$_{NaOH}$**	**Carbs$_{NaOH}$**
PE 0.4μm						
K07	183 ± 0.0	33 ± 1.3	275 ± 21.0	18 ± 0.3	14 ± 4.1	5 ± 1.4
K08	236 ± 0.2	41 ± 5.7	178 ± 3.8	37 ± 0.3	20 ± 3.1	28 ± 2.7
K09	47 ± 0.6	10 ± 1.3	18 ± 2.1	180 ± 4.6	37 ± 6.2	11 ± 1.9
PES 150kDa						
M04	43 ± 0.1	24 ± 3.3	35 ± 3.0	7 ± 0.1	3 ± 0.4	8 ± 0.6
M05	72 ± 3.3	9 ± 1.4	53 ± 3.6	26 ± 1.3	38 ± 5.9	17 ± 2.6
M06	40 ± 0.3	11 ± 1.7	16 ± 2.7	18 ± 0.8	23 ± 2.9	28 ± 1.6
PS 0.05μm						
P03	55 ± 1.0	32 ± 1.2	45 ± 1.0	10 ± 0.6	9 ± 2.1	0 ± 0.0
P05	300 ± 2.3	73 ± 4.2	188 ± 28.0	38 ± 1.7	50 ± 1.8	7 ± 0.5
P06	40 ± 1.3	8 ± 0.6	27 ± 2.4	80 ± 1.4	40 ± 3.4	14 ± 1.9
PVDF 0.15μm						
B03	52 ± 0.3	21 ± 0.9	42 ± 2.4	11 ± 0.6	6 ± 1.5	0 ± 0.2
B04	42 ± 0.2	15 ± 2.4	28 ± 3.7	59 ± 1.2	22 ± 1.9	22 ± 3.2
PVDF 0.08μm						
T06	751 ± 0.5	49 ± 4.4	103 ± 2.8	103 ± 0.4	25 ± 1.3	28 ± 1.7
T07	1325 ± 2.3	29 ± 3.3	18 ± 0.7	129 ± 0.6	12 ± 0.6	17 ± 0.8
T08	359 ± 1.6	24 ± 4.2	31 ± 5.0	111 ± 0.6	15 ± 2.0	37 ± 4.0

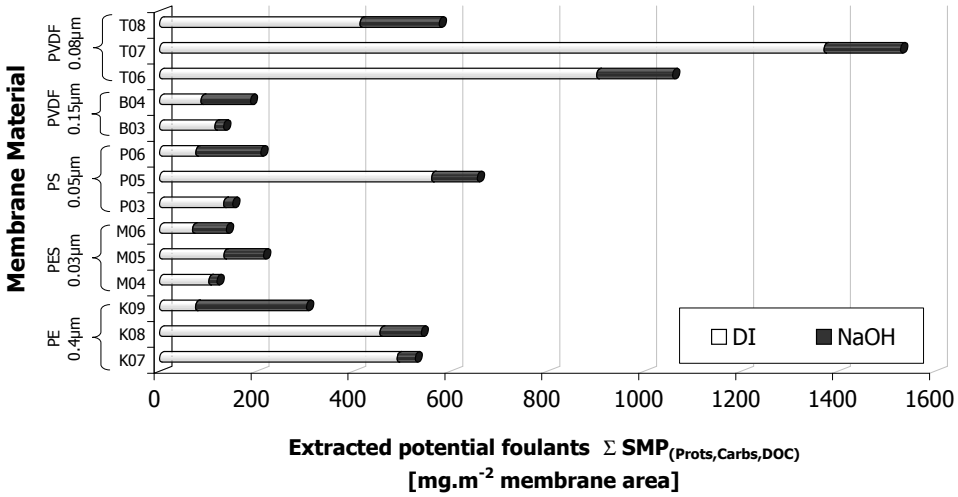

(a)

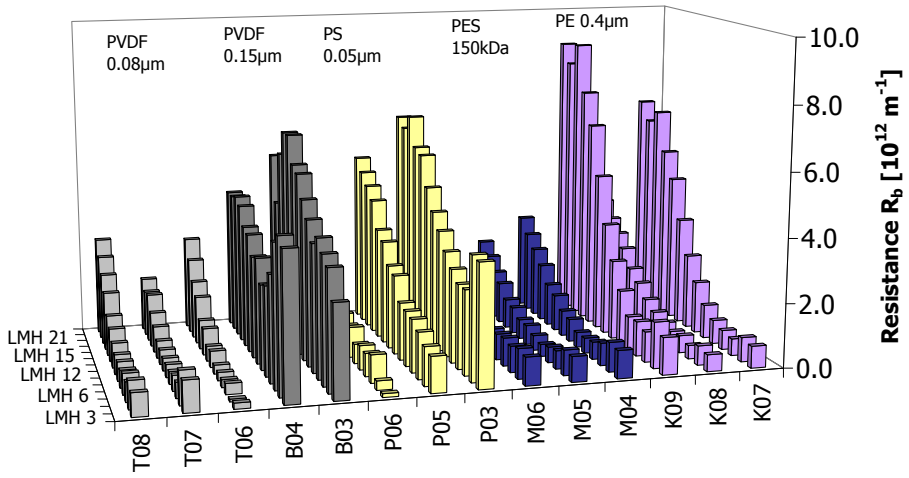

(b)

Figure 9.7.: Comparison of attached potential foulants and biomass resistance: *(a)* Sum of extracted potential foulants per membrane area (mechanical cleaning = DI, alkaline cleaning = NaOH) *(b)* Development of biomass resistances R_b over the critical flux trials from flux 0 to flux 21.

However, as the adsorbed amount of potential foulants was without a doubt expected to be influenced by the total amount of the filtered volume, the amount of SMP within the bulk phase and the SMP retention of the membrane, the following calculation (equation 9.1) was introduced:

$$A_{XF(DI,NaOH)} = \frac{c_{XF}}{c_{bulk} - c_{perm}} \cdot 100 \tag{9.1}$$

$$\text{with } c_{XF} = \frac{X_F}{\Sigma V_{Filt}} \tag{9.2}$$

where

$A_{XF(DI,NaOH)}$ = *the observed attachment of the respective potential foulant (%)*

c_{XF} = *the concentration of extracted foulants from membrane surface normalised to filtered volume* ($mg.L^{-1}$)

c_{bulk} = *the concentration within the bulk phase* ($mg.L^{-1}$)

c_{perm} = *the concentration within the permeate* ($mg.L^{-1}$)

X_F = *the amount of extracted foulants from the membrane surface* ($mg.m^{-2}$)

ΣV_{filt} = *the sum of filtered volume* ($m^3.m^{-2}$)

The percentage of observed attachment (A_x) varied widely for the different trials conducted. The PVDF 0.08μm membrane material presented an overall variation for DOC attached during the complete filtration process and extractable due to mechanical cleaning from 6% to 54%, with DOC also representing the major component of the extracted foulants. Variations were found to be less for the other membranes tested, with an overall observed attachment for DOC of 8.8%, proteins 3.1% and carbohydrates 2.4%. While the major component for the PVDF 0.08μm membrane was found to be a material consisting of DOC, it varied for the other membranes tested; for instance, membrane M04 (PES 150kDa) presented proteins with 12.4% to be the main component and in contrast P06 (PS 0.08μm) revealed carbohydrates with 13.5%. The percentage of attachment removed during the alkaline cleaning procedure was commonly less than for the mechanical cleaning and varied for DOC between 0.5% and 7.7%, for proteins between 0.3% and 12.0% and for carbohydrates between 0% and 6.8%.

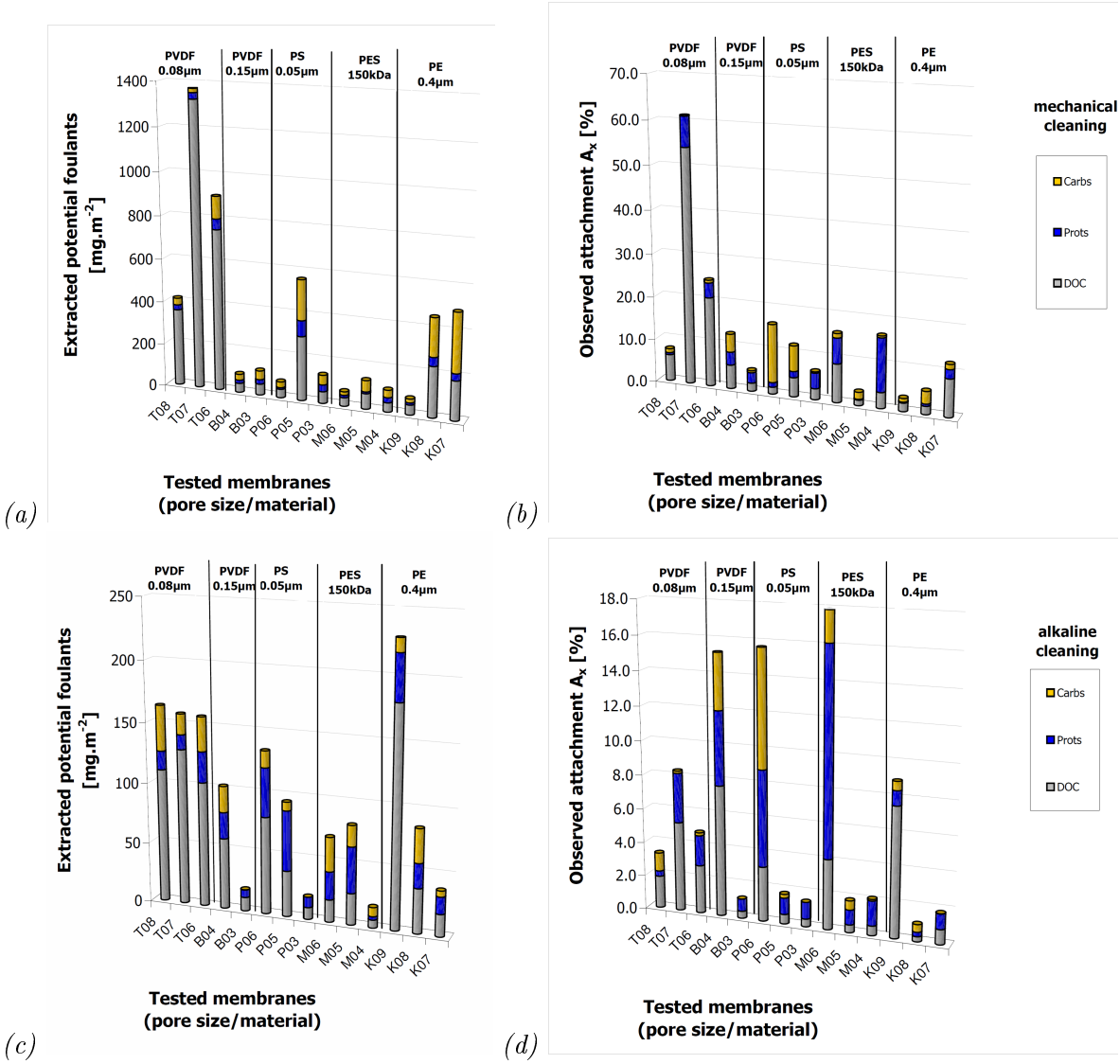

Figure 9.8.: Extracted potential foulants from membrane materials - amount of extracted foulants per membrane surface for *(a)* mechanical cleaning and *(c)* alkaline cleaning; percentage of observed attachment for *(b)* mechanical cleaning and *(d)* alkaline cleaning

While no significant impact of MLSS concentration could be shown by only comparing MLSS and the amount of extracted foulants, an impact became evident with the observed attachment. For instance, the four membrane samples (B04, P06, M06, K09) having shown a higher amount of foulants removed during the alkaline cleaning than during the mechanical cleaning, were also revealed to have on average the highest observed attachment during the alkaline cleaning. Comparing the observed attachment for DOC, proteins and carbohydrates to the MLSS content presented a significant impact of the MLSS content on the observed attachment

during the alkaline cleaning for DOC (R^2=*0.4879, p= 0.054*) and Proteins (R^2= *0.6319, p= 0.003*). Less interrelation was observed for Carbohydrates (*R=0.4879, p=0.054*) and no statistical significance could be shown overall for any observed attachments which were removed during the mechanical cleaning.

Interestingly, it has to be noted that while overall no correlation could be drawn for $A_{DOC,DI}$ and $A_{Prots,DI}$, individual membrane materials presented opposing trends. For instance, while there was no impact of MLSS on $A_{DOC,DI}$ and $A_{Prots,DI}$ for the PE 0.4μm membrane, a similar trend as that for $A_{DOC,NaOH}$ and $A_{Prots,NaOJ}$ was evident for the PVDF 0.08μm and the PES 150kDa. The PS 0.05μm membrane material, in contrast, did not reveal any trend for $A_{Prots,DI}$ vs MLSS, but $A_{DOC,DI}$ was observed to increase with increasing MLSS.

9.5. Comparison of Attached Foulants on Membrane Materials after biomass filtration from MBR full scale plant

To assess potential differences between the adsorption potential of activated sludge from the pilot plant, short term filtration tests were undertaken with biomass deriving from a full scale plant. Furthermore, fouled membrane samples from a full scale MBR plant were investigated for their attached foulants, applying the same membrane material as the flat sheet pilot scale module (PVDF 0.08μm), which was operated for approximately one year.

A comparison between different fouled samples of the PVDF 0.08μm membrane material suggested different fouling patterns between full-scale and pilot scale biomass. The membrane derived from from full-scale application after one year of operation, showed the highest accumulated amount of carbohydrates removable by the alkaline cleaning step. Similar high contents were removed from the short-term fouled membrane samples with full-scale MBR sludge. The pilot plant samples, however, presented very high amounts of detachable potential foulants during the mechanical cleaning, but a smaller amount of adsorbed carbohydrates during the alkaline cleaning procedure (see Table 9.3). This might suggest that the pilot plant biomass had a higher affinity to attach to the membrane surface, hence resulting in higher mechanical removable foulants, but on the other hand, helping to reduce pore penetration.

Furthermore, it has to be noted that the long-term fouled full-scale samples were derived from the sample module, representing sections of one membrane panel. With regards to the obtained results, this highlights the potential inhomogeneity being prevalent within membrane filtration processes.

Table 9.3.: Comparison of extracted foulants from PVDF 0.08μm flat sheet membrane material - short-term vs. long-term fouling

Sample Material	DOC_{DI} [$mg.g^{-2}$]	$Carbs_{DI}$ [$mg.g^{-2}$]	$Prots_{DI}$ [$mg.g^{-2}$]	DOC_{NaO} [$mg.g^{-2}$]	$Carbs_{NaO}$ [$mg.g^{-2}$]	$Prots_{NaO}$ [$mg.g^{-2}$]	R_t [$10^{12}m^{-1}$]	R_{vm} [$10^{12}m^{-1}$]	R_{cl} [$10^{12}m^{-1}$]
Long-term fouling - Full-Scale Membrane Material Sample									
LT-FS-01	6.8 *(0.10)*	8.6 *(0.21)*	0.8 *(0.01)*	83.4 *(1.71)*	73.0 *(1.52)*	5.4 *(0.11)*	N/A	N/A	0.38
LT-FS-02	15.6 *(0.31)*	14.8 *(0.30)*	0.7 *(0.01)*	54.2 *(1.12)*	48.7 *(1.07)*	N/A *(-)*	N/A	N/A	0.34
Short-term fouling - Full-Scale Biomass									
ST-MBR-01	67.2 *(1.31)*	6.9 *(0.12)*	n.d *(-0.1)*	101.1 *(2.01)*	47.1 *(0.90)*	3.7 *(0.11)*	0.81	0.17	0.56
ST-MBR-02	127.2 *(0.74)*	7.3 *(0.12)*	n.d *(-)*	89.3 *(4.21)*	38.7 *(0.71)*	2.9 *(0.22)*	0.79	0.19	0.61
Short-term fouling - Pilot-Plant Biomass									
ST-PP-01	751 *(0.51)*	49 *(4.42)*	103 *(2.81)*	103 *(0.42)*	25 *(1.32)*	28 *(1.71)*	3.12	0.24	0.55
ST-PP-02	1325 *(2.3)*	29 *(3.3)*	18 *(0.7)*	129 *(0.6)*	12 *(0.6)*	17 *(0.8)*	1.74	0.09	1.51
ST-PP-03	359 *(1.6)*	24 *(4.2)*	31 *(5.0)*	111 *(0.6)*	15 *(2.0)*	37 *(4.0)*	3.12	0.09	2.68

9.6. Summary

Within this study, five different commercially available flat sheet membrane materials for use in MBRs were analysed for their filtration performance, but also for their **surface characteristics**. An investigation of membrane materials at bench-scale revealed very different behaviours for the range of materials tested. The best filtration performances were observed with the PE 0.4 μm and PVDF 0.08μm. However, these trials did not allow a clear selection of a most favourable material, as for example, the membrane PVDF 0.15μm displayed a much lower filtration performance than the PVDF 0.08μm, suggesting that fouling is not only linked to the type of material but also to other parameters such as pore size and material preparation. A more detailed analysis of the materials would then be needed to fully understand the mechanisms occurring.

A membrane surface characterisation of the different membrane materials commercially available for application in MBRs revealed significant differences between the individual materials, but also between membrane samples of the same material analysed. In terms of material, extaordinarily high differences were discovered for the PVDF membrane material samples. Whilst one material sample presented overall a very good filtration performance, the other membrane material with higher pore size performed very poorly and proved to be unsuitable for MBR application. For instance, some sample sheets of the PVDF 0.15 μm membrane were found to have very limited water percolation and had to be excluded from further analyses. In terms of surface characterisation, high deviations were furthermore observed between aliquot analyses of the same membrane sample. This is in accordance with other data from literature (Jönsson and Jönsson, 1995) and provides an indication for inhomogeneity of surface characteristics across the membrane as observed by other researchers (Buetehorn *et al.*, 2009).

The high difference in material characterisation of the two tested PVDF membranes amplified the importance of optimised membrane manufacturing. Even though both membranes were made of similar polymeric compositions, the membrane with the higher pore size revealed the least preferred performance characteristics for membranes used within wastewater filtration (much lower permeability, lower wettability, higher surface roughness). Within this study, R_m was found to be a crucial parameter for reversible fouling for the flat sheet trials, which was also observed by Le-Clech (2002) for tubular membrane materials. R_{cl} was found to be the predominant parameter of R_t which was also observed by Khan *et al.* (2009). The strong correlation between intrinsic membrane resistance and irreversible fouling resistance was also reported by Khan *et al.* (2009), with a correlation rate of $R^2 = 0.991$, using the same type of membrane module throughout a test series with different shear rates applied.

Generally, MBR pilot plant sludge has been found to show lower filterability than full scale biomass, which was also confirmed during the Delft Filtration Method trials (Moreau *et al.*, 2009). The reasons for this are still unclear, but are generally presumed in literature to be

related to SMP foulants, such as carbohydrates, DOC and/or the ratio of P/C. Furthermore, the F/M ratio and probably also the microbiological diversity could play an important role. Carbohydrates within this pilot plant were found to be higher than in biomass from full scale plant, but no direct correlation between measured content of SMP and increase of filterability could be drawn.

Extracts from membrane samples fouled by either pilot or full scale sludge presented opposing trends to what was expected from the resistance in series determination of the individual membrane sample. For instance, the PVDF 0.08 μm membrane material was found to have the highest amount of potential foulants attached on the membrane surface, while exhibiting the lowest total membrane resistance during biomass filtration, and also post-sludge filtration. This was effective for flat sheet membrane materials having been challenged with pilot and full scale biomass and furthermore for multi-tubular membrane materials after pilot plant filtration trials and is in agreement with the data in literature (Yamato *et al.*, 2006; Lyko *et al.*, 2008a; Al-Halbouni *et al.*, 2008; Kimura *et al.*, 2009). The results gained during this study suggest that adsorbed foulants on membrane surfaces do not directly relate to the performance of the membrane during biomass filtration and furthermore it is likely that other parameters must be involved in permeability reduction.

Chen and Lee (2006) investigated the composition of fouling layers of membranes using a confocal laser scanning microscope and no correlation of the composition of the fouling layer to the membrane filtration behaviour could be determined.

The comparison conducted for one membrane material with a different biomass, however, presented higher adsorbed foulants on the membrane surface for pilot plant biomass samples than for full scale biomass samples, but again no direct correlation could be drawn between the values determined.

In general, membrane fouling is expected to be higher for hydrophobic membranes than for hydrophilic due to possible hydrophobic interactions between the membrane surface and components of the biomass, such as microbial cells, sludge flocs and solutes (Le-Clech *et al.*, 2006). Furthermore, it is expected that biomass' affinity to attach onto the membrane's surface and hence increasing the cake layer resistance will rise with increasing surface roughness. Within this study, a slight increase in biomass resistance and cake layer resistance was observed with increasing pore size, which was related to increased surface roughness. Furthermore, an increase in interfacial surface tension presented a slight tendency to increase reversible fouling resistance and, in general, a tendency to higher biomass filtration resistance.

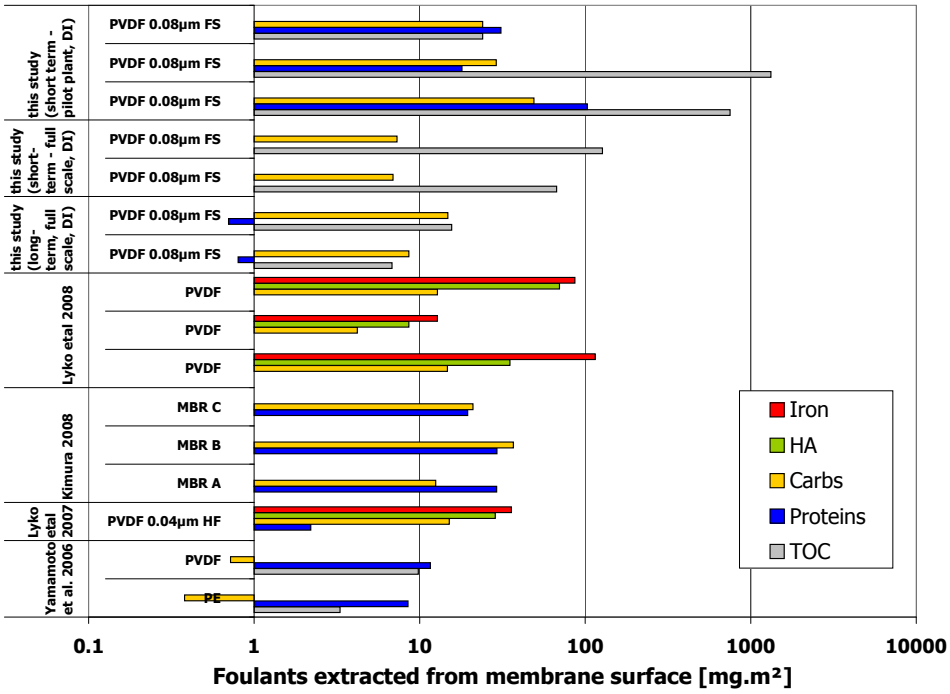

Figure 9.9.: Comparison of extracted foulants from membrane surface in this study to literature.

Jin *et al.* (2009) concluded that the membrane with the biggest pore size exhibited the highest fouling potential, while fouling potential was observed at its least for the membrane with the smallest pore size. Clean water permeability was not stated. Fouling potential of EPS, SMP could not be observed. For SMP, protein values were around 13 $mg.L^{-1}$, carbohydrates 32 to 46 $mg.L^{-1}$ and MLSS at 5 $g.L^{-1}$. In general, it was found difficult to assess an observed correlation between fouling and hydrophilicity, as changes in hydrophilicity have also been reported to occur with other membrane surface modifications such as pore size and morphology (Le-Clech *et al.*, 2006).

Important to note is that Lyko *et al.* (2007) detected SMP in ranges within the supernatant significantly lower than that of the usual pilot and lab scale of 3.6 $mg.L^{-1}$ carbohydrates, 2.4 $mg.L^{-1}$ and humic acid 24.8 $mg.L^{-1}$. This was, in fact, already discussed by other researchers as the up-scaling of lab and pilot scale results will most likely become difficult if not impossible (Drews, 2010; Kraume *et al.*, 2008).

10. Overall Summary

In this study, critical fluxes obtained through short-term tests at two different flux step protocols were compared at varying MLSS concentrations ranging from 3 to 12 g.L^{-1}, with opposing results gained for the different membrane pilot scale module configurations, and moreover also for the different bench-scale materials. Results were completed by assessing the impact of varying aeration rates during different MLSS concentration. Furthermore, bench-scale membrane materials were investigated for the attached foulants.

In the trials at fixed aeration rates (SAD$_m$ 1.0; 1.5 Nm^{3}m^{-2}h^{-1}) at 12 g.L^{-1}, the FS and HF modules were found to have better performances than the MT module (**Chapter 5**). Repeating trials at fixed aeration rates (SAD$_m$ 1.0; 1.5 Nm^{3}m^{-2}h^{-1}) but varying MLSS content revealed that the FS and HF modules had better performances with increasing MLSS concentrations. Alternatively, the MT module exhibited a better performance at a concentration of 7 g.L^{-1} (**Chapter 6**). This was then confirmed in the trials with different aeration rates as the FS and HF modules displayed better filtration performances at high MLSS contents with clear correlations between the critical flux and permeability, and the MLSS concentration of the retentate line (**Chapter 7**).

However, in all cases no overall correlation could be found between the MLSS concentration, the fouling observed and the typical biomass characteristics, such as concentration of SMP (**Chapter 8**). Nonetheless, filtration under low MLSS content was found to significantly increase the observed attachment of foulants on the membrane surface (**Chapter 9**). Furthermore, solutes (SMP) and colloids of the biomass were found to adversely impact permeability during MLSS content as low as 3 g.L^{-1}. Overall, at the more typical MLSS concentration of 12 g.L^{-1} for the operation of membrane bioreactors, the HF module was found to show best filtration performances, according to the short term trials conducted in this current study.

To investigate the potential impact of scale on the experiments conducted, pilot scale and bench-scale trials were run in parallel during this study. Surprisingly, different trends were observed not only between the different membrane module configurations in pilot scale, but also between the different scale of experiments, hence between bench and pilot scale of the same membrane material and configuration. For instance, while the MT pilot scale module showed best filtration behaviours at MLSS content of 7 g.L^{-1}, which was furthermore confirmed by the lab scale single-tube module of same material, the tubular lab scale modules made of PES

revealed a completely different filtration behaviour. Furthermore, much lower critical fluxes were determined for the flat sheet bench-scale trials than for the pilot scale trials, which was attributed to the different hydrodynamic conditions of the set-ups. Additionally, high shear rates exhibited on the biomass due to the cross-flow pump of the bench-scale trial were found to decrease filtration performance of the membrane materials tested at the bench-scale cross-cell. Overall, these opposing results poses the question which has been postulated by Kraume *et al.* (2008) already; *'What use are lab investigations for full scale operation?'* and moreover, place reasonable doubts in the practicability when comparing results reported in literature which do not only derive from different biomass feed sources, but also from varying set-ups and scales.

One further crucial observation made during this study was the effect of lumen or vessel clogging during membrane filtration, leading to exponential trans-membrane pressure development and indicating significant differences in operating the different configurations. For instance, while the multi-tubular membrane module was prone to lumen clogging at higher MLSS content even at short-term trials at high fluxes and low aeration rates, which also led to the lower J_c with higher MLSS, an extreme increase of trans-membrane pressure became evident for the FS module due to sludge accumulation within the membrane vessel at low aeration rates and higher MLSS content and furthermore at moderate aeration rates and long-term filtration at higher MLSS.

On the other hand, operating the FS and HF module at lower MLSS level with higher fluxes and lower aeration rates was shown to significantly improve the sludge filterability of the biomass passing through the membrane chamber. This amelioration in sludge filterability was furthermore found to significantly improve the filtration performance of the membrane module.

The assessment of filtration performance of the FS module and HF module was hence impacted by two different flux decline scenarios:

1. **fouling due to biomass properties** and
2. **clogging due to insufficient cross-flow**

Moreover, the clogging phenomenon at long-term filtration was preceded by an amelioration of sludge filterability due to the dewatering during side-stream passage, as observed during the Delft Filtration Method Trials. This consequently suggested that the better filterability due to dewatering is only beneficial up to a certain threshold value, above which the solid accumulation due to the dewatering causes rapid flux decline and spacer/lumen clogging. These findings hence lead to the assumption that the frequently reported threshold value for MLSS content, up to which permeability improvement with increasing MLSS was observed, may indicate the threshold value to spacer clogging due to sludge accumulation.

11. Conclusions

Pilot Scale Trials

- Filtration performance of different membrane module configurations under identical biomass and confined hydraulic boundary conditions (same SAD_m, same membrane filtration path length, operation as air-lift side-stream) resulted in opposing trends for the modules investigated in this study.
- Aeration applied to create air scouring created a positive effect on the fouling behaviour on the MT module, whereas the FS and HF module revealed lower critical fluxes with higher aeration rates.
- Increased MLSS concentration resulted in lower critical fluxes for the MT module, where the FS and HF module revealed significantly higher critical fluxes, especially with higher solid content within the retentate line.
- While the hollow fibre and flat sheet modules were more prone to biomass make-up changes, with the flat sheet module having shown to be highly impacted, the limitations to higher permeate suction was found to be lumen clogging for the multi-tubular module. This phenomenon was shown to be mainly effective for short-term studies.
- During a long-term filtration trial, however, the FS module exhibited excellent cake layer filtration performances at higher sustainable fluxes and MLSS of 12 $g.L^{-1}$, whereas a sudden TMP increase from 100 to 700 mbar after only 1.5 hours of filtration was linked to spacer clogging of the module vessel. This part of fouling was reversible and could probably be avoided by introducing longer relaxation periods within the filtration cycle of that module.
- Dewatering of the sludge was found to have a positive effect on overall filtration performances for FS and HF modules, whereas the dewatering is a function of flux and cross-flow-velocity, and an effective cross-sectional area of the membrane filtration unit, hence a function of flux and the effective SRT of the sludge during the filtration process.
- Counterpart to the ameliorating sludge filterability effect is clogging, which occurred when the up-lift of sludge particles became insufficient due to an insufficient cross-flow (aeration) and /or an insufficient time for relaxation, and hence, material built up within the cross-section of the membrane separation channels.

Bench scale testing and membrane surface characterisations and extracted foulants suggested:

- Filtration performance is highly impacted by different materials. Filtration performance may also vary widely between samples of the same material due to uneven production mode.
- A strong correlation between the intrinsic membrane resistance R_m, and the irreversible fouling resistance, R_{irrev}, (r = -0.9731, r=0.03) showed a membrane performance less prone to irreversible fouling with lower intrinsic membrane resistance, which revealed the importance of membranes operating at low trans-membrane pressure for avoiding irreversible pore blocking. This was observable for flat sheet bench scale trials, whereas the correlation was less significant for the single tubular trials.
- Floc rupture as occurring during side-stream pumping presented a high release in fine particles and macro molecular substances increasing, hence, the SMP within the bulk phase.
- Floc rupture and carbohydrate release could be shown to correlate to the biomass resistance exhibited on all of the flat sheet membrane samples. No such correlation could be drawn from the initial SMP of the supernatant.
- Fractionation of the attached biomass onto the membrane samples presented a pattern evidently different from the biomass filtration resistance. The amount of extracted foulants could furthermore not be related to biomass parameter.
- The percentage distribution of attached foulants on the membrane surface - *removable by alkaline cleaning* - could clearly be linked to MLSS content, with increased observed attachment at lower MLSS. This approved the benefits of higher solid content within the bulk phase providing gel layer formation preventing pore penetration.
- Biomass deriving from pilot and full scale plants exhibited different fouling patterns.
- Comparison of filtration experiments undertaken at different set-ups is generally very difficult, if not impossible. Reference measurements are hence inevitable in normalising the results. To be able to compare lab scale data to full scale data, hydrodynamic conditions in lab scale should be as close as possible to full scale. Important parameters to be considered are, besides others, direction of flow and potential impact of gravity.

12. Future Aspects

- Critical flux trials at different aeration rates did not exhibit the expected growth with increasing air-flow rate for the HF and FS module. In fact, a lower aeration increased the sludge filterability of the biomass circulating along the membrane surface, increasing in turn the permeability of the membrane module. This was suggested to be an effect of the sludge dewatering, which was found to exhibit positive effects during short-term tests, but led to clogging phenomenon during long-term test.

  It is therefore assumed that permeability of membrane module is, *to a certain extent*, manipulative by an effective sludge dewatering due to the membrane itself. Further investigation might help to find an optimum range between the SRT of the biomass within the membrane module (due to aeration), the MLSS content of the biomass and the applied flux to achieve lowest fouling and lowest aeration costs on the one hand, but avoid clogging on the other. These optimum boundary conditions should be determined in long-term studies.

- Further research needs to be undertaken to understand the phenomenon of fouling as an interaction of membrane surface and biomass make-up. As none of the conducted parameters seemed to correlate to fouling propensity of the biomass, different parameters need to be investigated. The phenomenon of clogging should also be included into the research, as the effects of fouling need to be strictly distinguished from the channel clogging phenomenon to be able to understand biomass impact on membrane surfce.

- Generally, membrane research lacks the ability to reliably compare results. Standard procedure for measuring sludge filterability should be set up in order to be able to compare results from different locations/different set-ups/research groups. The DFCm method did provided a good example for easy use and quick validation for the data of this study, however provided limitations to others.

- Filtration performance of same material but on various bench-scale set-ups could be investigated to understand the differences between the varying fouling/clogging phenomena occurring due to the different hydrodynamics. This could then help to interpret the different research results. Investigations should be undertaken in defined model solutions, but also with biomass derived from MBR plants, whereas attention has to be paid that set-ups are tested in parallel to avoid biomass changes.

- **Suggestions based on the data of this work**

  By the outcome of this research, it was furthermore assumed that the optimum condition for sludge filterability seem to be able to be manipulated to a certain extent by sludge dewatering.

  The current findings then promote the suggestion of running membranes in external MBR tanks, with low to moderate void volume of the membrane tank and benefit from two effects:

  1. being able to run the aeration tank decoupled from the membrane process at moderate MLSS concentration and hence save aeration costs due to lower required alpha values, and
  2. benefit from the amelioration of the sludge dewatering for the membrane filtration performance while also saving energy due to lower membrane coarse aeration.

  This current suggestion is, however, limited to the outcome of this research and therefore requires further verification. For instance long-term trials are inevitable to assess under which conditions the threshold value to clogging is reached.

References

Agfa-Gevaert NV (2010), 'A new generation flat sheet membrane module', company product information leaflet, IFAT 2010; www.agfa.com. 21

Ahmed Z, Cho J, Lim B R, Song K G and Ahn K H (2007). Effects of sludge retention time on membrane fouling and microbial community structure in a membrane bioreactor, *Journal of Membrane Science* **287**, 211–218. 29

Al-Halbouni D, Traber J, Lyko S, Wintgens T, Melin T, Tacke D, Janot A, Dott W and Hollender J (2008). Correlation of EPS content in activated sludge at different sludge retention times with membrane fouling phenomena, *Water Research* **44**, 14751488. 169, 192

Altmann J and Ripperger S (1997). Particle deposition and layer formation at the crossflow microfiltration, *Journal of Membrane Science* **124**, 119–128. 9, 10, 33, 163

Alvarez-Vazquez H (2005), Membrane bioreactors for sewage and stabilised leachate treatment, PhD thesis, Cranfield University, Cranfield, UK. 97, 103

Alvarez-Vazquez H, Pidou M, Holdner J and Judd S J (2008). Character of Extracellular Polymeric Substances and Soluble Microbial Products and Their Effect on Membrane Hydraulics During Airlift Membrane Bioreactor Applications, *Water Environment Research* **80**(12), 2193–2201. 30, 148

APHA, ed. (1998). *Alpha Standard Methods for Examination of Water and Wastewater*, 20 edn, American Public Health Association. 80, 81

Arabi S and Nakhla G (2008). Impact of protein/carbohydrate ratio in the feed wastewater on the membrane fouling in membrane bioreactors, *Journal of Membrane Science* **324**, 142–150. 28, 29, 168

Atkinson S (2006). Research studies predict strong growth for MBR markets, *Membrane Technology* **2006**(2), 8–10. 1

Babock Jr. R, Huang T, Chanthawornsawat Y and Debroux J C (2007). Pilot test comparison of six different membrane bioreactors, *World Environment and Water Resources Congress 2007; Restoring our Natural Habit. Tampa, Florida, USA* . 30, 31

Bacchin P, Aimar P and Field R (2006). Critical and sustainable fluxes: Theory, experiments and applications, *Journal of Membrane Science* **281**, 42–69. 11, 63, 85

Bae T and Tak T (2005). Interpretation of fouling characteristics of ultrafiltration membranes during the filtration of membrane bioreactor mixed liquor, *Journal of Membrane Science* **264**, 151–160. 66

Baker R (2004). *Membrane Technology and Applications*, 2 edn, John Wiley & Sons, West Sussex, England. 13, 14, 16, 17

Bargir S M (2007), Nanoscale Investigations of Surface Phenomena in the Water Treatment Industry using the Atomic Force Microscope, PhD thesis, School of Applied Science, Centre for Water Science, Microsystems and Nanotechnology Centre, Cranfield University, UK. 178

Baumgarten S (2007), Membranbioreaktoren zur industriellen Abwasserreinigung, PhD thesis, Fakultät für Bauingenieurwesen, Rheinisch-Westfälischen Technischen Hochschule Aachen, RWTH Aachen, Germany. xv, xxi, 12, 35

Belfort G, Davis R and Zydney A (1994). Review: The behaviour of suspensions and macromolecular solutions in crossflow microfiltration, *Journal of Membrane Science* **96**, 1–58. 8

Bemberis I, Hubbard P and Leonard F (1971). Membrane sewage treatment systems - potenital for complete wastewater treatment, *American Sciety of Agricultural Engineers - Winter Meeting* **71-878**, 1–28. 1

Bottino A, Capannelli G, Comite A and Mangano R (2009). Critical flux in submerged membrane bioreactors for municipal wastewater treatment, *Desalination* **245**(1-3), 748–753. 105, 123

Bouhabila E, Aim R B and Buisson H (2001). Fouling characterisation in membrane bioreactors, *Separation and Purification Technology* **22-23**, 123–132. 4, 127, 131

Bouhabila E, BenAim R and Buisson H (1998). Microfiltration of activated sludge using submerged membrane bioreactor with air bubbling, *Desalination* **118**, 315–322. 32, 123, 147, 150

Brannock M, Wang Y and Leslie G (2010). Evaluation of Full-Scale Membrane Bioreactor Mixing Performance & the Effect of Membrane Configuration, *Journal of Membrane Science* **350**(1-2), 101–108. 37

Brepols C, Dorgelohb E, Frechen F B, Fuchs W, Haider S, Joss A, de Korte K, Ruiken C, Schier W, van der Roest H, Wett M and Wozniak T (2008). Upgrading and retrofitting of municipal wastewater treatment plants by means of membrane bioreactor (MBR) technology, *Desalination* **231**, 20–26. 37

Brepols C, Schaefer H and Engelhardt N (2010). Consideration on design and financial feasibility of full scale membrane bioreactors for municipal applications, *Water Science & Technology* **61**(10), 2461–2468. 127

Brookes A (2005), Immersed Membrane Bioreactor for produced water treatment, PhD thesis, School of Applied Science, Centre for Water Science, Cranfield University, UK. 97, 103, 105, 123, 126, 171

Brookes A, Judd S, Germain E, Smith S, Alvarez H, Le-Clech P, Stephenson T, Turra E and Jefferson B (2003). Biomass characterisation in membrane bioreactors, *in Proceedings of the 5th International Membrane Science and Technology Conference (IMSTEC)*, November 10-14; Sydney, Australia. 170, 171

Buetehorn S, Kochan J, Koh C, Wintgens T, Volmering D, Vossenkaul K and Melin T (2009). Assessment principles for membrane and membrane module development: a case study, *in Final MBR-Network Workshop, 30 March to 1 April 2009, Berlin, Germany*, pp. 152–157. 20, 191

Busch J, Cruse A and Maquardt W (2007). Modeling submerged hollow-fiber membrane filtration for wastewater treatment, *Journal of Membrane Science* **288**, 94–111. 33

Chang I S, Clech P L, Jefferson B and Judd S (2002). Membrane Fouling in Membrane Bioreactors for Wastewater Treatment, *Journal of Environmental Engineering* **128**(11). 28

Chang I S, Gander M, Jefferson B and Judd S (2001). Low-cost membranes for use in submerged MBR, *Trans. IchemE.* **79**(Part B), 1183–188. 16

Chang M, Tzou W, Chunag S and Chang W (2003). Application of non-woven fabric material in membrane bioreactor processes for industrial wastewater treatment, *in Proceedings of the 5th International Membrane Science and Technology Conference (IMSTEC)*, November 10-14; Sydney, Australia. 16

Chen M Y and Lee D J (2006). Extracellular polymeric substances in fouling layers, *Separation Science and Technology* **41**, 1467–1474. 192

Cicek N, Dionysiou D, Suidan M, Ginestet P and Audic J (1999). Performance deterioration and structural changes of a ceramic membrane bioreactor due to inorganic abrasion, *Journal of Membrane Science* **163**(1), 19–28. 15

Coakley W and James C (1978). A simple linear transformation for the Folin-Lowry protein calibration curve to 1.0 mg/mL, *Analytical Biochemistry* **85**(1), 90–97. 76

Davis R and Sherwood J (1990). Similartiy solution for steady state crossflow microfiltration, *Chemical Engineering Science* **45**, 3204–3209. 8

De Wilde W, Richard M, Lesjean B and Tazi-Pain A (2007). Towards a standardisation of MBR technology?, *Desalination* **231**, 156–165. 37

Defrance L, Jaffrin M, Gupta B, Paullier P and Geaugey V (2000). Contribution of various constituents of activated sludge to membrane bioreactor fouling, *Bioresource & Technology* **73**, 105–112. 3, 4, 105

Drews A (2010). Membrane Fouling in Membrane Bioreactors - Characterisation, Contradictions, Causes and Cures, *Journal of Membrane Science* **363**, 1–28. 11, 27, 28, 83, 85, 104, 193

Drews A, Mante J, Iversen V, Vock M, Lesjean B and Kraume M (2007). Impact of ambient conditions on SMP elimination and rejection in MBRs, *Water Research* **41**, 3850–3858. 29

Drews A, Prieske H, Meyer E L, Senger G and Kraume M (2010). Advantageous and detrimental effects of air sparging in membrane filtration: Bubble movement, exerted shear and particle classification, *Desalination* **250**, 10831086. 33, 163

Dubois M, Gilles K, Hamilton J, Rebers P and Smith F (1956). Colorimetric method for determination of sugars and related substances, *Analytical Chemistry* **28**(3), 350–356. 77

Espinasse B, Bacchin P and Aimar P (2002). On an experimental method to measure critical flux in ultrafiltration, *Journal of Membrane Science* **146**, 91–96. 63

Evenblij H, Geilvoet S, van der Graaf J and van der Roest H (2005). Filtration characterisation for assessing MBR performance: three cases compared, *Desalination* **178**, 115–124. 217, 218

Fan F, Zhou H and Husain H (2006). Identification of wastewater sludge characteristics to predict critical flux for membrane bioreactor processes, *Water Research* **40**, 205–212. 30, 168

Fane A (1986). Ultrafiltration: factors influencing flux and rejection, *Progress in Filtration and Separation* **4**, 101–179. 8

Fane A, Fell C, Hodgson P, Leslie G and Marshall K (1991). Microfiltration of biomass and biofluids: Effects of membrane morphology and operating conditions, *Filtration & Separation* **28**(5), 332–340. 20

Field R, Wu D, Howell J and Gupta B (1995). Critical flux concept for microfiltration fouling, *Journal of Membrane Science* **100**, 259–272. 11, 63, 66, 85

Fletcher H, Mackley T and Judd S (2007). The cost of a package plant membrane bioreactor, *Water Research* **41**(12), 2627–2635. 36

Frølund B, Griebe T and Nielsen P (1995). Enzymatic activity in the activated-sludge floc matrix, *Applied Microbiology and Biotechnology* **43**, 755–761. 74, 76

Frølund B, Palmgren R, Keiding K and Nielsen P (1996). Extraction of extracellular polymers from activated sludge using a cation exchange resin, *Water Research* **30**, 1749–1758. 74

Fuchs W, Resch C, Kernstock M, Mayer M, Schoeberl P and Braun R (2005). Influence of operational conditions on the performance of a mesh filter activated sludge process, *Water Research* **39**, 803–810. 16

Futamura O, Katoh M and Takeuchi K (1994). Organic waste water treatment by activated sludge process using integrated type membrane separation, *Desalination* **98**, 17–25. 20

Gander M, Jefferson B and Judd S (2000). Aerobic MBRs for domestic wastewater treatment: a review with cost considerations, *Separation & Purification Technology* **18**(2), 119–130. 20

Garces A, De Wilde W, Thoeye C and De Gueldre G (2007). Operational cost optimisation of MBR Schilde, *Proceedings of the 4th IWA Membrane Conference, Membrane for Wastewater Treatment, 14-17 May, Harrogate, UK.* . 37

Gekas V and Hallström B (1990). Microfiltration membranes, cross flow transport mechanisms and fouling studies, *Desalination* **77**(1-3), 195–218. 20

Germain E A (2004), Biomass effects on Membrane Bioreactors operation, PhD thesis, School of Industrial and Manufacturing Science, School of Water Sciences, Cranfield University, UK. 79, 86, 102, 105, 108, 123, 150, 152, 170

Germain E, Stephenson T and Pearce P (2005). Biomass Characteristics and Membrane Aeration: Toward a Better Understanding of Membrane Fouling in Submerged Membrane Bioreactors (MBRs), *Biotechnology and bioengineering* **90**(3), 316–322. 147

Green G and Belfort G (1980). Fouling of ultrafiltration membranes: lateral migration and the particle trajectory model, *Desalination* **35**, 129–147. 8

Grelot A, Weinrich L, Tazi-Pain A, Lesjean B and Trouve E (2007). Evaluation of a novel flat sheet MBR filtration system, *Proceedings of the 4th IWA Membrane Conference, Membrane for Wastewater Treatment, 14-17 May, Harrogate, UK.* . 21, 32

Guglielmi G, Chiarani D, Judd S and Andreottola G (2007a). Flux criticality and sustainability in a hollow fibre submerged membrane bioreactor for municipal wastewater treatment, *Journal of Membrane Science* **289**, 241–248. 28, 99, 100, 103, 126, 135, 145, 146, 147, 150

Guglielmi G, Chiarani D, Judd S and Andreottola G (2008). Impact of chemical cleaning and air-sparging on the critical and sustainable flux in a flat sheet membrane bioreactor for municipal wastewater treatment, *Water Science and Technology* **57**(12), 1873–1885. 98, 103, 131, 135, 145, 146, 149

Günder B (2001). *The Membrane-coupled activated sludge process in municipal wastewater treatment*, 1 edn, Technomic Publishing Company, Lancaster. xv, 1, 6, 13, 15

Hai F I, Ymamoto K and Fukushi K (2005). Different fouling modes of submerged hollow-fiber and flat-sheet membranes induced by high strength wastewater with concurrent biofouling, *Desalination* **180**(1-3), 89–97. 30

Han S, Bae T, Jang G and Tak T (2005). Influence of sludge retention time on membrane fouling and bioactivities in membrane bioreactor system, *Process Biochemistry* **40**, 2393–2400. 4

He Y, Le-Clech P, Chen V and Fane A (2005b). Evolution of fouling during crossflow filtration of model EPS solutions, *Journal of Membrane Science* **264**, 190–199. 4

He Y, Li C and Zhang B (2005a). High-concentration food wastewater treatment by an anaerobic membrane bioreactor, *Water Research* **39**(17), 4110–4118. 4, 19

Hermia J (1982). Constant pressure blocking filtration laws: application to power-law non-newtonian fluids, *Trans Inst Chem Eng* **60**, 183–192. 8

Hilal N, Ogunibiyki O, Miles N and Nigmatullin R (2005). Methods Employed for Control of Fouling in MF and UF Membranes; A Comprehensive Review, *Separation Science and Technology* **40**(10), 1957–2005. 8, 27

Houghton J, Quarmby J and Stephenson T (2001). Municipal wastewater sludge dewaterability and the presence of microbial extracellular polymer, *Water Science & Technology* **44**(2-3), 373–379. 168

Howe K J, Marwah A, Chiu K P and Adham S S (2007). Effect of membrane configuration on bench-scale MF and UF fouling experiments, *Water Research* **41**, 3842–3849. 30

Howell J (1995). Sub-critical flux operation for microfiltration, *Journal of Membrane Science* **107**, 165–171. 63

Howell J, Chua H and Arnot T (2004). In situ manipulation of critical flux in a submerged membrane bioreactor using variable aeration rates, and the effects of membrane history, *Journal of Membrane Science* **242**, 13–19. 11, 30, 123, 147, 149

Huang X, Gui P and Qian Y (2001). Effect of sludge retention time on microbial behaviour in a submerged membrane bioreactor, *Process Biochemistry* **36**, 1001–1006. 4

Huang X, Liu R and Qian Y (2000). Behaviour of soluble microbial products in a membrane bioreactor, *Process Biochemistry* **36**, 401–406. 3

Hughes D and Field R (2006). Cross flow filtration of washed and unwashed yeast suspensions at constant shear under nominally sub-critical conditions, *Journal of Membrane Science* **280**, 89–98. 18

ItN Nanovation AG (2010), 'MBBR Sewage Treatment Container Plant', company product information leaflet, IFAT 2010; www.itn-nanovation.com. 21, 24

Itonaga T, Kimura K and Watanabe Y (2004). Influence of suspension viscosity and colloidal particles on permeability of membrane used in membrane bioreactor (MBR), *Water Science & Technology* **50**(12), 301–309. 28, 29, 30, 168

Iversen V, Mehrez R, Horng R, Cheng C, Meng F, Drews A, Lesjean B, Ernst M, M.Jekel and Kraume M (2009). Fouling mitigation through flocculants and absorbents addition in membrane bioreactors: comparing lab and pilot studies, *Journal of Membrane Science* **345**, 21–30. 31

Jaffrin M Y (2008). Dynamic shear-enhanced membrane filtration: A review of rotating disks, rotating membranes and vibrating systems, *Journal of Membrane Science* **324**, 725. 31

Jin L, Ng H Y and Ong S L (2009). Performance and fouling characteristics of different pore-size submerged ceramic membrane bioreactors (SCMBR), *Water Science & Technology* **59**(11), 2213–2218. 19, 193

Jönsson C and Jönsson A S (1995). Influence of the membrane material on the adsorptive fouling of ultrafiltration membranes, *Journal of Membrane Science* **108**, 79–87. 191

Judd S (2006). *The MBR book*, 1 edn, Elsevier, London, England. xv, xxi, 1, 3, 7, 8, 12, 13, 15, 16, 18, 21, 22, 23, 24, 27, 28, 37, 57, 85, 94, 126, 127

Judd S (2011). *The MBR book - Principles and Applications of Membrane Bioreactor for Water and Wastewater Treatment*, 2 edn, Elsevier, London, England. 94, 126

Karr P and Keinath T (1978). Influence of Particle Size on Sludge Dewaterability, *Water Pollution Control Federation* **50**(8), 1911–1930.
URL: *http://www.jstor.org/stable/25040372* 163

Khan S J, Visvanathan C and Jegatheesan V (2009). Prediction of membrane fouling in MBR systems using empirically estimated specific cake resistance, *Bioresource Technology* **100**, 61336136. 191

Khongnakorn W, Wisniewski C, Pottier L and Vachoud L (2007). Physical properties of acitvated sludge in a submerged membrane bioreactor and relation with membrane fouling, *Separation and Purification Technology* **55**, 125–131. 171

Kimura K, Hane Y, Watanabe Y, Amy G and Ohkuma N (2004). Irreversible membrane fouling during ultrafiltration of surface water, *Water Research* **38**, 3431–3441. 19, 22

Kimura K, Naruse T and Watanabe Y (2009). Changes in characterisation of soluble microbial products in membrane bioreactors associated with different solid retention times: relation to membrane fouling, *Water Research* **43**, 1033–1039. 192

Kimura K, Yamamura H and Watanabe Y (2006). Irreversible Fouling in MF/UF Membranes Caused by Natural Organic Matters (NOM) isolated from Different Origins, *Separation Science and Technology* **47**(7), 1331–1344. 19

Kimura S (1991). Japan's Aqua Renaissance '90 project, *Water Science & Technology* **23**(7-9), 1573–1582. 1

Kochan J, Wintgens T, Hochstrat R and Melin T (2009). Impact of wetting agents on the filtration performance of polymeric ultrafiltration membranes, *Desalination* **241**, 34–42. 20

Kochan J, Wintgens T, Wong J and Melin T (2009). Properties of polyethersulfone ultrafiltration membranes modified by polyelectrolytes, *Desalination* **250**, 1008–1010. 20

Kraume M, Wedi D, Schaller J, Iversen V and Drews A (2008). Fouling in MBR: What use are lab investigations for full scale operation?, *Desalination* **236**, 94103. 99, 104, 193, 196

Le-Clech P, Jefferson B, Cheng I and Judd S (2003c). Critical flux determination by the flux-step method in a submerged membrane bioreactor, *Journal of Membrane Science* **227**(1-2), 113–119. 63, 68, 69, 85

Le-Clech P, Jefferson B and Judd S (2003b). Impact of aeration, solids concentration and membrane characteristics on the hydraulic performance of a membrane bioreactor, *Journal of Membrane Science* **218**(1-2), 117–129. 3, 18, 32, 105, 127, 131, 135

Le-Clech P (2002), Process Configurations and Fouling in Membrane Bioreactors, PhD thesis, Cranfield University, Cranfield, UK. 47, 63, 123, 145, 146, 171, 191

Le-Clech P (2010). Membrane bioreactors and their uses in wastewater treatments, *Applied Microbiology and Biotechnology* **88**, 1253–1260. 27

Le-Clech P, Chen V and Fane A (2006). Fouling in membrane bioreactors used in wastewater treatment, *Journal of Membrane Science* **284**, 17–53. 2, 3, 18, 28, 192, 193

Le-Clech P, Jefferson B and Judd S (2005). A comparison of submerged and sidestream tubular membrane bioreactor configurations, *Desalination* **173**, 113–122. 30, 148

Lee J, Ahn W and Lee C (2001). Comparison of the filtration characteristics between attached and suspended growth microorganisms in submerged membrane bioreactor, *Water Research* **35**, 2435–2445. 3

Lee W, Kang S and Shin H (2003). Sludge characteristics and their contribution to microfiltration in submerged membrane bioreactor, *Journal of Membrane Science* **216**, 217–227. 29

Liu R, Huang X, Wang C, Chen L and Qian Y (2000). Study on hydraulic characteristics in a submerged membrane bioreactor process, *Process Biochemistry* **36**(3), 249–254. 147

Lowry O, Rosebrough N, Farr A and Randall R (1951). Protein measurement with the Folin phenol reagent, *Journal of Biological Chemistry* **193**, 365–375. 76

Lyko S, Al-Halboumi D, Wintgens T, Janot A, Hollender J, Dott W and Melin T (2007). Polymeric compounds in activated sludge supernatant - Characterisation and retention mechanisms at a full-scale municipal membrane bioreactor, *Water Research* **4**(17), 38943902. 169, 193

Lyko S, Wintgens T and Melin T (2008a). Comparative investigation on the impact of polymeric substances on membrane fouling during sub-critical flux operation of a municipal membrane bioreactor, *Water Science & Technology* **58**(2), 18491855. 169, 192

Lyko S, Wintgens T and Melin T (2005). Estrogenic trace contaminants in wastewater - possibilities of membrane bioreactor technology, *Desalination* **178**, 95–105. 2

Lyko S, Wintgens T, Al-Halbouni D, Baumgarten S, Tacke D, Drensla K, Janot A, Dott W, Pinnekamp J and Melin T (2008b). Long-term monitoring of a full-scale municipal

membrane bioreactor - Characterisation of foulants and operational performance, *Journal of Membrane Science* **317**, 7887. 28, 153, 168

Madaeni S (1999). The effect of operating conditions on critical flux in membrane filtration of latexes, *Process Safety and Environmental Protection* **75**(B4), 266–269. 105

Mallevialle J, Odendaal P and Wiesner M, eds (1996). *Water Treatment Membrane Processes*, McGraw-Hill, UK. 15

Marchese J, Ochoa M P N, Pradanos P, Palacio L and Hernandez A (2003). Fouling behaviour of polyethersulfone UF membranes made with different PVP, *Journal of Membrane Science* **211**, 1–11. 20

Masse A, Sperandio M and Cabassud C (2006). Effects of sludge retention time on membrane fouling and microbial community structure in a membrane bioreactor, *Water Research* **40**, 2405–2415. 29, 161

Melin T, Jefferson B, Bixio D, Thoeye C, Wilde W D, Koning J D, van der Graaf J and Wintgens T (2006). Membrane bioreactor technology for wastewater treatment and reuse, *Desalination* **187**, 271–282. 1, 13

Melin T and Rautenbach R (2004). *Membranverfahren - Grundlagen der Modul- und Anlagenauslegung*, 2 edn, Springer, Berlin, Germany. xv, 5, 6, 8, 12, 13, 21, 35, 61

Meng F, Chae S R, Drews A, Kraume M, Shin H and Yang F (2009). Recent advances in MBR: Membrane fouling and membrane material, *Water Research* **43**, 1489–1515. 28, 143

Meng F, Yang F, Shi B and Zhang H (2008). A comprehensive study on membrane fouling in submerged membrane bioreactors operated under different aeration intensities, *Separation and Purification Technology* **59**, 91100. 32

Meng F, Zhang H, Yang F, Zhang S, Li Y and Zhang X (2006). Identification of activated sludge properties affecting membrane fouling in submerged membrane bioreactors, *Separation and Purification Technology* **51**, 95–103. 28

Meng Z, Yang F and Zhang X (2005). Do non-wovens offer a cheaper option?, *Filtration Separation* pp. 28–30. 16

Menniti A, Kang S, Elimelech M and Morgenroth E (2009). Influence of shear on the production of extracellular polymeric substances in membrane bioreactors, *Water Research* **43**, 4305–4315. 129

Möbius C and A.Helble (2006). Membranbioreaktoren im Vergleich zu koneventionellen aeroben Abwasserreinigungsanlagen für Papierfabriksabwässer, *Vortrag ZELLCHEMING-Haptversammlung 29.06.2006 Wiesbaden* pp. 2–22. xv, 36

Moghaddam M A, Satoh H and Mino T (2002). Performance of coarse pore filtration activated sludge system, *Water Science and Technology* **46**(11-12), 71–76. 16

Monclus H, Zacharias S, Santos A, Pidou M and Judd S (2010). Criticality of Flux and Aeration for a Hollow Fiber Membrane Bioreactor, *Separation Science and Technology* **45**, 956961. 147

Moreau A, Krzeminski P, van Nieuwenhuijzen A and van der Graaf J (2009). Reversible fouling quantifications: any links with full-scale plant permeability?, *in Final MBR-Network Workshop, Berlin*, pp. 246–252. 147, 191

Mueller J and Davis R (1996). Protein fouling of surface-modified polymeric membranes, *Journal of Membrane Science* **116**(1), 47–60. 18, 19

Mulder M (1997). *Basic Principles of Membrane Technology*, 2 edn, Kluwer Academic Publisher, The Netherlands. 15, 16, 17

Ndinisa N, Fane A and Wiley D (2006). Fouling Control in a Submerged Flat Sheet Membrane System: Part I - Bubbling and Hydrodynamic Effects, *Separation Science and Technology* **41**, 1383–1409. 32, 103

Nguyen M T (2004), Deckschichtbildung in Kapillarmembrane bei der Querstrom-Mikrofiltration und ihre Beeinflussung durch polymere Flockungsmittel, PhD thesis, Technische Universität Dresden, Dresden, Germany. 8, 10

Nywening J P and Zhou H (2009). Influence of filtration conditions on membrane fouling and scouring aeration effectiveness in submerged membrane bioreactors to treat municipal wastewater, *Water Research* **43**, 3548–3558. 32

Ognier S, Wisniewski C and Grasmick A (2002). Influence of macromolecule adsorption during filtration of a membrane bioreactor mixed liquor suspension, *Journal of Membrane Science* **209**, 27–37. 3

Ozcan C and Hasirci N (2008). Evaluation of Surface Free Energy for PMMA Films, *Journal of Applied Polymer Science* **108**, 438446. 62

Pearce G (2008). Introduction to membranes - MBRs: Manufacturers comparison: part 1, *Filtration & Separation* **45**(2), 28–31. 13, 16, 17

Peeters J and Theodoulou S (n.d.). Membrane Technology treating oily wastewater for Reuse, *ZENON Environmental Inc.* . xv, 5

Persson K, Tragardh G and Dejmek P (1993). Fouling behaviour of silica on four different microfiltration membranes, *Journal of Membrane Science* **76**(1), 51–60. 20

Pidou M (2006), Hybrid membrane processes for water reuse, PhD thesis, Cranfield University, Cranfield, UK. 148

Pinnekamp J and Friedrich H (2006). *Membrane Technology for Wastewater Treatment*, 2 edn, FiW Verlag, Aachen, Germany. xv, xxi, 5, 6, 13, 14, 18, 23

Pollice A, Brookes A, Jefferson B, S. and Judd (2005). Sub-critical flux fouling in membrane bioreactors - a review of recent literature, *Desalination* **147**, 221–230. 29

Pollice A, Laera G, Saturno D and Giordano C (2007). Effects of sludge retention time on the performance of a membrane bioreactor treating municipal sewage, *Journal of Membrane Science* pp. xx–xx. 29

Prieske H, Meyer E L, Drews A and Kraume M (2008). Analysis of particle classification during the membrane filtration of activated sludge, *in Proceedings of Engineering with Membranes 2008*, May 2528, Algarve, Portugal. 33, 147, 149

Rautenbach R and Albrecht R (1989). *Membrane Processes*, 1 edn, John Wiley & Sons, Chichester, Great Britain. xv, 13, 14, 65

Reid E (2005), Salinity shocking and fouling amelioration in Membrane Bioreactors, PhD thesis, School of Industrial and Manufacturing Science, School of Water Sciences, Cranfield University, UK. 170

Ripperger S (1992). *Mikrofiltration mit Membranen: Grundlagen, Verfahren, Anwendungen*, VCH. 8

Romero C and Davis R (1990). Transient Model of crossflow microfiltration, *Chemical Engineering Science* **45**(4), 13–25. 8

Rosenberger S (2003). *Charakterisierung von belebtem Schlamm in Membranbelebungsreaktoren zur Abwasserreinigung*, VDI Reihe 3 Nr. 769 edn, VDI Verlag, Düsseldorf. 3, 8, 13, 18

Rosenberger S, Evenblij H, te Poele S, T.Wintgens and Laabs C (2005). The importance of liquid phase analyses to understand fouling in membrane assisted activated sludge processessix case studies of different European research groups, *Journal of Membrane Science* **263**, 113–126. 3

Rosenberger S and Kraume M (2002). Filterability of activated sludge in membrane bioreactors, *Desalination* **146**, 373–379. 3, 28, 105

Roudman A and DiGiano F (2000). Surface energy of experimental and commercial nanofiltration membranes: effects of wetting and natural organic matter fouling, *Journal of Membrane Science* **175**, 61–73. 20

Santos A and Judd S (2010). The commercial status of membrane bioreactors for municipal wastewater, *Separation Science and Technology* **45**, 850–857. xxi, 17, 26

Schwarz A, Rittmann B, Crawford G, Klein A and Daigger G (2007). Critical Review on the Effects of Mixed Liquor Suspended Solids on Membrane Bioreactor Operation, *Separation Science and Technology* **47**(1), 1489–1511. 28, 105

Seo G, Moon B, Lee T, Lim T and Kim I (2002). Non-woven fabric filter separation activated sludge system reactor for domestic wastewater reclamation, *Water Science & Technology* **47**, 133–138. 16

Smith C, di Gregorio D and Talcott R (1969). The use of ultrafiltration membranes for activated sludge separation, *in Proceedings 24th Annual Purdue Industrial Waste Conference, 1300-1310.*, pp. 1300–1310. 24

Stephenson T, Judd S, Jefferson B and Brindle K (2000). *Membrane Bioreactors for Wastewater Treatment*, 1 edn, IWA Publishing, London, England. xxi, 6, 7, 14, 15, 21, 23, 27, 85, 127, 152

Stricot M, Filali A, Lesage N, Sperandio M and Cabassud C (2010). Side-stream membrane bioreactors: Influence of stress generated by hydrodynamics on floc structure, supernatant quality and fouling propensity, *Water Research* **44**, 2113–2124. 129, 161, 166, 169

Sutton P (1997). *Membrane biological reactor systems: historical development and future needs and opportunities. Literature Review.*, Environmental Engineering Consultants. 24

Torres A, Santiago V and Borges C (2008). Performance Evaluation of Submerged Membrane Bioreactor Pilot Units for Refinery Treatment, *Environmental Progress* **27**(2), 189–194. 29, 92

Trussell R, Melo R, Hermanowicz S and Jenkins D (2007). Influence of mixed liquor properties and aeration intensity on membrane fouling in a submerged membrane bioreactor at high mixed liquor suspended solids concentration, *Water Research* **41**, 947–958. 28

Tyszler D, Zytner R, Batsch A, Bruegger A, Geissler S, Zhou H, Klee D and Melin T (2006). Reduced fouling tendency of ultrafiltration membrane in wastewater treatment by plasma modification, *Desalination* **189**, 119–129. 20

Ueda T (2001). Removal of Microorganisms from Wastwater with a Membrane Bioreactor, *Bulletin of the National Research Institute of Agricultural Engineering* **40**. 147

Ueda T, Hata K, Kikuoka Y and Seino O (1997). Effects of aeration on suction pressure in a submerged membrane bioreactor, *Water Research* **31**(3), 489–494. 32, 127, 131, 147

van der Marel P, Zwijnenburg A, Kemperman A, Wessling M, Temmink H and van der Meer W (2009). An improved flux-step method to determine the critical flux and the critical flux for irreversibility in a membrane bioreactor, *Journal of Membrane Science* **332**, 24–29. 102

van Oss C (2002). Use of the combined Lifshitzvan der Waals and Lewis acidbase approaches in determining the apolar and polar contributions to surface and interfacial tensions and free energies, *Journal of Adhesion Science & Technology* **10**, 669–667. 62

van Oss C (2003). Long-range and short-range mechanisms of hydrophobic attraction and hydrophilic repulsion in specific and aspecific interactions, *Journal of Molecular Recognition* **16**, 177–190. 61, 62, 178, 179, 181

Verrecht B, Judd S, Guglielmi G, Brepols C and Mulder J (2008). An aeration energy model for an immersed membrane bioreactor, *Water Research* **42**, 4761–4770. 37, 146

Wintgens T (2005), Modellierung von Membranbioreactoren für die Abwasserbehandlung unter Berücksichtigung endokrin wirksamer Substanzen, PhD thesis, RTWH Aachen, Aachen, Germany. 35

Wintgens T, Rosen J, Melin T, Brespols C, Drensla K and Engelhardt N (2003). Modeling of a membrane bioreactor sysrtem for municipal wastewater treatment, *Journal of Membrane Science* **216**, 55–65. 32, 127

Wisniewski C and Grasmick A (1998). Floc size distribution in a membrane bioreactor and consequences for membrane fouling, *Colloids Surface A: Physicochem. Eng. Aspects* **2138**, 403–411. 3, 99, 129, 166, 169

Wu J, Le-Clech P, Stuetz R, Fane A and Chen V (2008). Novel filtration mode for fouling limitation in membrane bioreactors, *Water Research* **42**(14), 3677–3684. 32, 100

Wu J, Le-Clech P, Stuetz R, Fane A and Chen V (2008b). Effects of relaxation and backwashing conditions on fouling in membrane bioreactor, *Journal of Membrane Science* **324**, 26–32. 100

Wu J and Huang X (2009). Effect of mixed liquor properties in fouling propensity in membrane bioreactors, *Journal of Membrane Science* **342**(1-2), 88–96. 28, 105

Yamato N, Kimura K, Miyoshi T and Watanabe Y (2006). Difference in membrane fouling in membrane bioreactors (MBRs) caused by membrane polymer materials, *Journal of Membrane Science* **280**, 911–919. 19, 192

Yildirim I (2001), Surface Free Energy Characterisation of Powders, PhD thesis, Mining and Minerals Engineering, Virginia Polytechnic Institute and State University, Blacksburg, Virginia, USA. 62

Yoon S, Kim H and Yeom I (2004). The optimum operational condition of membrane bioreactor (MBR): cost estimation of aeration and sludge treatment, *Water Research* **38**, 3746. 37

Zahid W and El-Shafai S (2011). Use of cloth filter media for membrane bioreactor treating municipal wastewater, *Bioresource Technology* **102**(3), 2193–2198. 16

Zhang J, Chua H, Zhou J and Fane A (2006). Factors affecting the membrane performance in submerged membrane bioreactors, *Journal of Membrane Science* **284**, 54–66. xv, 2, 3, 11, 18, 126, 173

Zhang S, Qu Y, Liu Y, Yang F, Zhang X, Furukawa K and Yamada Y (2005). Experimental study of domestic sewage treatment with a metal membrane bioreactor, *Desalination* **177**, 83–93. 15

Zhang X, Bishop P and Kinkle B (1999). Comparison of extraction methods for quantifying extracellular polymers in biofilms, *Water Science and Technology* **39**(7), 211–218. 74

Zydney A and Coloton C (1986). A concentration polarization model for the filtrate flux in cross flow microfiltration of particulate suspensions, *Chemical Engineering Communications* **47**, 1–21. 8

Appendix

A. Sludge Filterability - impact on membrane filtration performance

A.1. Scope

During a combined study with Delft University, the sludge filterability of the pilot plant was determined, applying the Delft Filtration Method (DFCm, Evenblij *et al.*, 2005) under two different scenarios:

1. Different permeate suction rates (run continuous with $J_{20} = 9\ LMH$, $J_{20} = 18\ LMH$) at a constant aeration rate
2. Different SAD_m rates with samples taken at the same permeate suction step (step $J_{20} = 30\ LMH$ and $J_{20} = 10\ LMH$ of the applied critical flux protocol)

where the focus was on the changes in sludge filterability during the passage of each retentate line and the potential impact on the TMP development of the individual side-stream module. For all trials, the same filtration protocol was applied (540s on/50s off/10s backwash (HF,MT) or 540s on/60s off (FS), see Table 4.6, page 65 and Table 4.7, page 66). Analyses were completed by monitoring changes in biomass parameters, such as pH, DO, TSS, MLSS, VSS, turbidity and SMP content for supernatant and permeate.

A.2. Measurements of resistance to filterability - ΔR_{20}

A.2.1. Aeration Tank (ΔR_{20AT})

During the first stage of the experiment, a baseline benchmarking was undertaken for the aerobic biological tank, analysing samples throughout the day from $8am$ till $9pm$. Daily variations of sludge filterability (expressed as filterability resistance ΔR_{20AT} in 10^{12} m^{-1}) seemed to follow an influent loading pattern, with obvious peaks of deteriorated sludge filterability during the morning and evening hours (Figure A.1: ΔR_{20AT} resistance starting with $4.1 \cdot 10^{12}$ m^{-1}, $3.9 \cdot 10^{12}$ m^{-1} respectively during the morning, decreasing to $3.2 \cdot 10^{12}$ m^{-1}, $2.8 \cdot 10^{12}$ m^{-1} respectively during the afternoon and increasing again to $3.5 \cdot 10^{12}$ m^{-1}, $3.3 \cdot 10^{12}$ m^{-1} respectively during the evening).

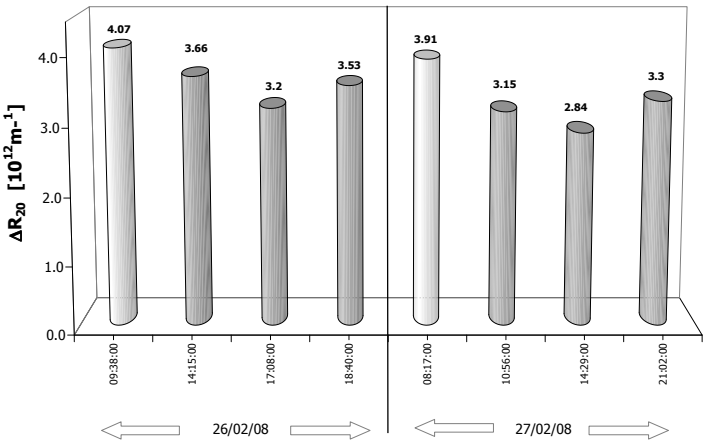

Figure A.1.: Sludge filterability (results of DFCm measurements) - Daily variations in sludge filterability during 2 days monitoring (DFCm flux: 30 LMH)

The sludge filterability of the biomass of the pilot plant showed immensely higher filtration resistances than MBR biomass analysed in previous studies with the DFCm method, where the usual flux applied to the DFCm unit was 80 LMH (Evenblij *et al.*, 2005). During this study, the flux applied to the DFCm measurement device had to be lowered to avoid an exposure of the DFCm membrane to TMP values above the recommended threshold value of 0.5 bar.

During the first stage of the experiment (February 2008, low to high flux trials), a flux of 30 LMH was adopted in the DFCm unit, whereas due to an overall amelioration of sludge filterability over time (February 2008 to March 2008) the DFCm unit was operated with J_{20} = 60 LMH during the second stage of the experiment (different SAD_m values) (Figure A.2).

Average values of ΔR_{20AT} varied between 2.2 and 3.6 $\cdot$ 10^{12} m^{-1} for the first batch of experiments (DFCm flux: 30 LMH) and between 2.2 and 2.8$\cdot 10^{12}$ m^{-1} for the varying SADm trials (DFCm flux: 60 LMH). Daily variations of ΔR_{20AT} were found to be commonly between 0.05 and 0.5$\cdot 10^{12}$ m^{-1}, with one extreme value of 1.1 for the first SAD_m 1.0 trial (Figure A.2).

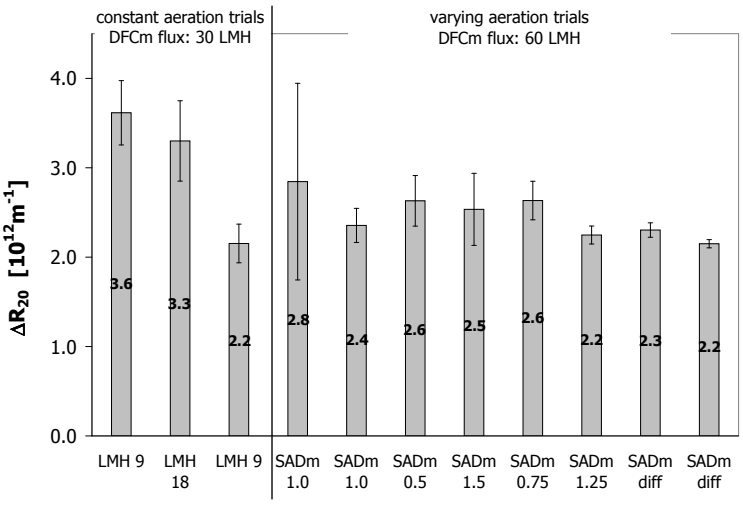

Figure A.2.: Sludge filterability (results of DFCm measurements): Daily average values (ΔR_{20AT}) of samples taken from the aeration tank

A.2.2. Retentate Lines of Air-lift Sidestream Modules (ΔR_{20Ret})

Due to the significant daily variations experienced in sludge filterability of samples taken from the aeration tank (Figure A.2), side-stream retentate line samples are compared as ratio $\frac{\Delta R_{20\ Ret}}{\Delta R_{20\ AT}}$ with ΔR_{20AT} being the time-interpolated value of samples from the aeration tank taken prior to and after the retentate line measurement.

Hence, a ratio value $\frac{\Delta R_{20\ Ret}}{\Delta R_{20\ AT}}$ of 1.0 represents no differences in sludge fouling propensity, whereas values below 1.0 are yielding from an increase in sludge filterability with a ratio of below 0.5 showing a significant amelioration of sludge filterability. $\frac{\Delta R_{20\ Ret}}{\Delta R_{20\ AT}}$ values above 1.0 arise from a decrease in sludge quality in terms of filterability due to changes exerted on the biomass during the passage of the sidestream vessels (Figure A.3*a* and A.3*b*).

A.2.2.1. Constant Aeration - Low to High Permeate Fluxes

During the trial, at constant aeration and low to high permeate fluxes, $\frac{\Delta R_{20\ Ret}}{\Delta R_{20\ AT}}$ did not reveal any significant changes in sludge fouling propensity for the MT module, with values around 1.0 (Figure A.3*a*).

FS and HF samples, however, exhibited an increased fouling propensity at low permeate fluxes and a lower fouling propensity at higher permeate fluxes with changes showing to be more significant for the HF module. While $\frac{\Delta R_{20\ Ret}}{\Delta R_{20\ AT}}$ was 1.11 and 1.13 at $J_{20} = 9\ LMH$ for the FS module, the HF module showed an increased ratio of 1.26 and 1.25. At higher fluxes ($J_{20} = 18$

LMH), $\frac{\Delta R_{20\ Ret}}{\Delta R_{20\ AT}}$ was around 0.9 for the FS module and dropped down to 0.7 for the HF module (Figure A.3*a*).

A.2.2.2. Varying Aeration - SAD_m trials

While the average fouling propensity within the aeration tank ($\Delta R_{20\ AT}$) varied between $2.1{\cdot}10^{12} m^{-1}$ and $2.88 \cdot 10^{12} m^{-1}$, the ratios $\frac{\Delta R_{20\ Ret}}{\Delta R_{20\ AT}}$ for all modules revealed an extended array of values with $\Delta R_{20\ Ret}$ ranging from $0.13{\cdot}10^{12} m^{-1}$ (*HF, SAD_m 0.5*) to $2.60{\cdot}10^{12} m^{-1}$ (*MT, SAD_m diff (1)*) (Figure A.15*b*) and, therefore resulted in ratios of 0.05 to 1.14 (Figure A.3*b*).

ΔR_{20} ratio for the HF module disclosed the highest variation (average: 0.54, deviation: 0.45) with a low-range of 0.05 and a high-range value of 1.14. A similar amplitude of ΔR_{20} ratios were found for the FS module with an average $\frac{\Delta R_{20\ Ret}}{\Delta R_{20\ AT}}$ of 0.72 (deviation: 0.39) and $\frac{\Delta R_{20\ Ret}}{\Delta R_{20\ AT}}$ ≥ 0.13 and ≤ 1.12. The MT module showed the least broadness with an average $\frac{\Delta R_{20\ Ret}}{\Delta R_{20\ AT}}$ of 0.86 and a deviation of 0.2. The highest ratio for the MT module during the varying SAD_m trials was 1.17, and the lowest 0.47.

Interestingly, $\frac{\Delta R_{20\ Ret}}{\Delta R_{20\ AT}}$ per module revealed at first glance a higher change with time/date shift than with changing aeration rates. Theoretically, ratios of $\frac{\Delta R_{20\ Ret}}{\Delta R_{20\ AT}}$ were expected to show a clear impact of aeration rates applied to the side-stream modules, but the experimental series revealed a sudden increase of all ratio values on day 4 of the sequence (25/03/08), the SAD_m trial of 1.5 $Nm^3 m^{-2} h^{-1}$.

Correlating $\frac{\Delta R_{20\ Ret}}{\Delta R_{20\ AT}}$ with SAD_m values and with the corresponding dates not only confirmed this observation, but also revealed some interesting aspects (Figure A.4). While both plots disclosed a slight correlation for the overall data trend-line between $\frac{\Delta R_{20\ Ret}}{\Delta R_{20\ AT}}$ and SAD_m (R^2 *= 0.47*),$\frac{\Delta R_{20\ Ret}}{\Delta R_{20\ AT}}$ and day of sequence (R^2 *= 0.46*) respectively, the FS module showed the strongest association with $\frac{\Delta R_{20\ Ret}}{\Delta R_{20\ AT}}$ to the date the analyses were undertaken (R^2 *= 0.91*, Figure A.4*b*) regardless of the applied aeration rate (R^2 *= 0.07*, Figure A.4*a*). The HF module, on the other hand, revealed the strongest correlation between $\frac{\Delta R_{20\ Ret}}{\Delta R_{20\ AT}}$ and the applied SAD_m (R^2 *= 0.73*, Figure A.4*a*) and no significant impact of the date of analyses on the $\frac{\Delta R_{20\ Ret}}{\Delta R_{20\ AT}}$ (R^2 *= 0.15*, Figure A.4*b*). The MT module showed a higher correlation to the date of analyses (R^2 *= 0.74*, Figure A.4*b*) than to the applied aeration rate (R^2 *= 0.4*).

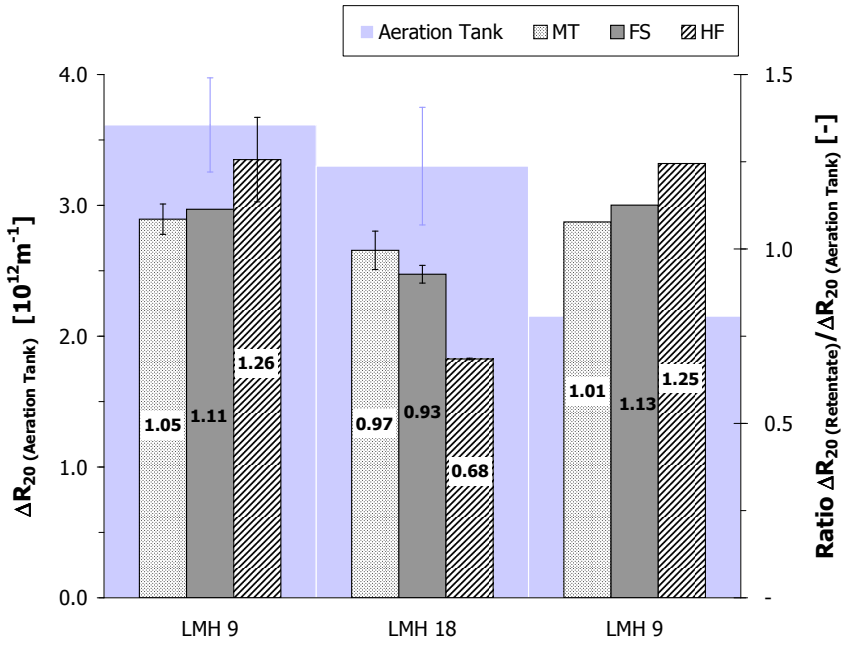

(a)

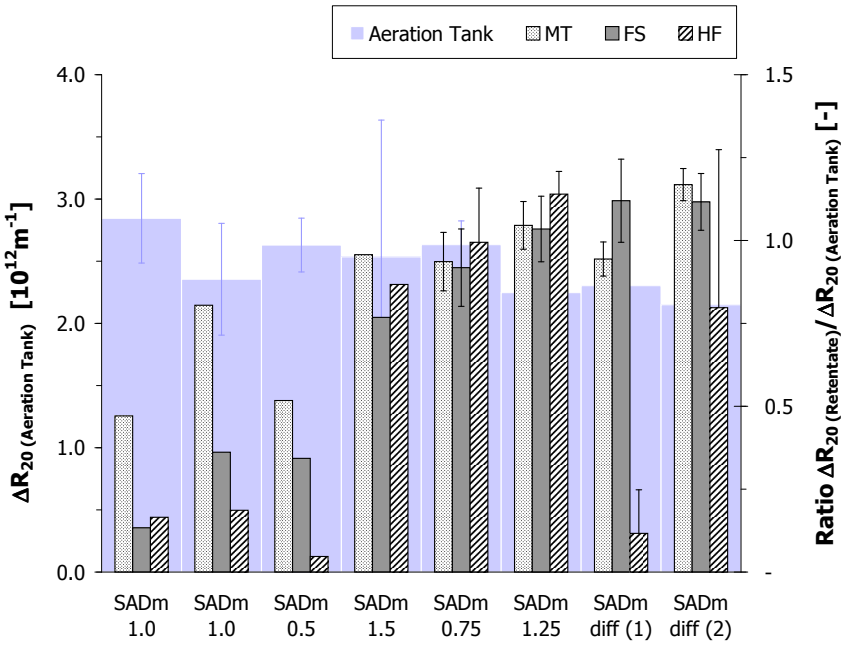

(b)

Figure A.3.: Sludge filterability (results of DFCm measurements) - comparison of ΔR$_{20}$ values for aeration tank and ratio of $\frac{\Delta R_{20\ Ret}}{\Delta R_{20\ AT}}$ - *(a)* first stage of experiment: constant aeration and low to high permeate fluxes; *(b)* second stage of experiment: critical flux trials with varying SAD$_m$ (corresponding graphs with $\Delta R_{20\ Ret}$ values see Figure A.15)

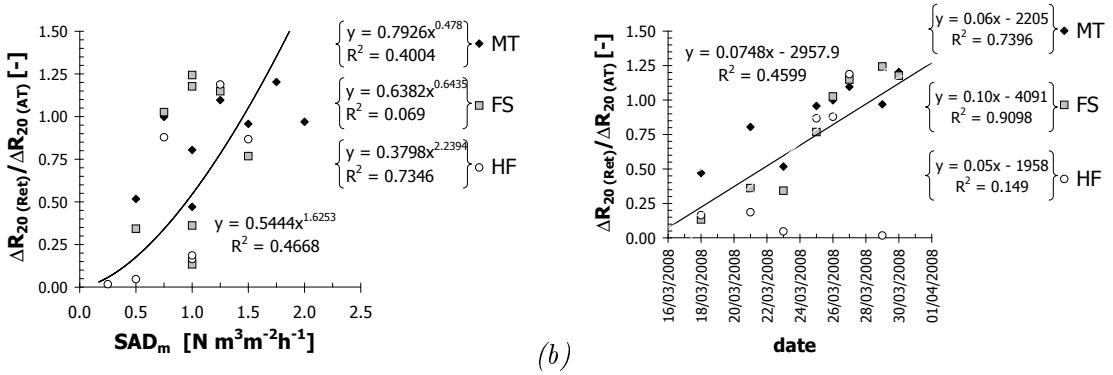

Figure A.4.: Sludge filterability (results of DFCm measurements) - Correlation of $\frac{\Delta R_{20\ Ret}}{\Delta R_{20\ AT}}$ with *(a)* SAD_m rates and *(b)* date; trend-line showing overall correlation, individual module trend-line in brackets (graphs showing individual module trendlines see Figure A.16)

A.3. Impact of biomass parameters on ΔR_{20} variations

A.3.1. Biomass parameters during critical flux trials at varying aeration rates (SAD_m trials)

Biomass parameters varied throughout this set of experiments, showing MLSS changes from to 5.5 to 6.6 $g.L^{-1}$ within the aeration tank and higher variations per side-stream vessel according to the aeration applied (Table A.1). MLLS content for retentate samples of side-stream vessels showed the highest increase for the FS (12.2 $g.L^{-1}$) and HF modules (11.9 $g.L^{-1}$) at the lowest SAD_m rates (SAD_m = 0.5 $Nm^3m^{-2}h^{-1}$, 0.25 $Nm^3m^{-2}h^{-1}$ respectively).

Measured pH values were found to be showing the highest average values for the HF retentate sample between 6.7 and 7.2, with a pH of 7.1. Conductivity showed limited changes from aeration tank to side-stream retentate with average values between ≈ 1,909 μS (AT, HF) and ≈ 1,937 μS (MT, FS).

The dissolved oxygen levels (DO) of aeration tank sludge samples exhibited on average a value of 0.6 $mg.L^{-1}$ DO with a lowest measured parameter of 0.2 $mg.L^{-1}$ and a highest of 1.8 $mg.L^{-1}$. Those low parameters were later attributed to one partially blocked plate of the aeration system installed in the main aeration tank, consequently leading to a scarce air supply at higher MLSS rates, and higher influent loading rates respectively. The dissolved oxygen levels increased (with the exception of one set of samples) during the passage of the side-stream vessels, showing an augmentation expressed as ratio $\frac{DO_{Ret}}{DO_{AT}}$ of 1.4 to 13.0 with an average DO concentration of 1.6 $mg.L^{-1}$.

Chemical oxygen demand of sludge samples showed high variations linked to changes in MLSS

and VSS respectively, with the lowest COD value of 6.4 $g.L^{-1}$ for the AT sludge sample and highest value of 17.6 $g.L^{-1}$ for the retentate sample of the FS vessel.

Particle size ($d_{0.5}$) of sludge flocs was found to be between 55.6 and 68.7 μm for the AT sludge samples with an obvious decrease in particle size during the passage of the side-stream vessels (Table A.1) with ratios of $\frac{d_{0.5\ Ret}}{d_{0.5\ AT}}$ lying between 0.76 and 0.98.

Soluble microbial products (SMP) determined as Proteins, Carbohydrates (*Polysaccharides*) and DOC concentrations revealed the highest deviations for measured Carbohydrates with AT values between 5.9 $mg.gVSS^{-1}$ and 16.5 $mg.gVSS^{-1}$. SMP_{Carb} content inclined invariably within retentate samples from $\frac{Carbs_{Ret}}{Carbs_{AT}} = 1.2$ to 4.0, with highest values of 28.1 $mg.gVSS^{-1}$ for the HF module and lowest values of 7.8 $mg.gVSS^{-1}$ for the FS module. Conversely, protein contents normalised to $gVSS$ did not show high variations, with average values remaining between 1.5 and 1.9 $mg.gVSS^{-1}$ and displaying on average (Proteins as $mg.gVSS^{-1}$) a decrease within the retentate samples. Dissolved organic carbon values also presented limited variations with average values of 4.3 $mg.gVSS^{-1}$ (AT) to 4.3 $mg.gVSS^{-1}$ (FS), 4.4 $mg.gVSS^{-1}$ (MT) and 4.0 $mg.gVSS^{-1}$ (HF) with the highest value measured for FS retentate sample (5.7 $mg.gVSS^{-1}$, see Figure A.5, Table A.1).

Turbidity of SMP samples also increased within the side-stream vessels, showing an average turbidity of AT samples of 1.790 NTU and 2.141 NTU (MT), 2.205 NTU (FS) and 2.392 NTU (HF). The highest SMP turbidity values were determined for the MT module with 5.035 NTU (Table A.1).

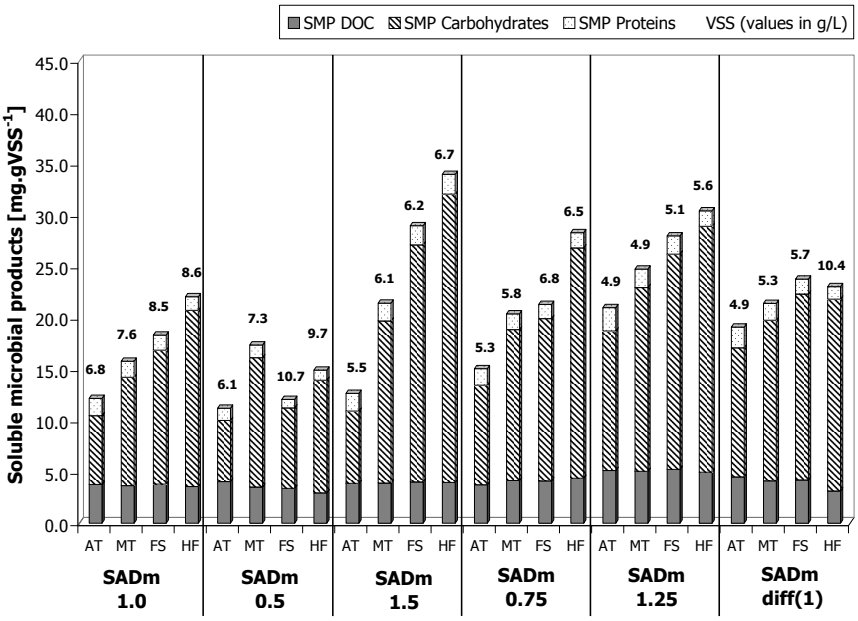

Figure A.5.: Sludge filterability (results of DFCm measurements) - SMP values of varying SADm trials: Proteins, Carbohydrates and DOC as $mg.gVSS^{-1}$ and values of VSS in $g.L^{-1}$

Table A.1.: Summary of biomass parameters during DFCm - SADm trial

Parameter		**AT**	**MT_{Ret}**	**FS_{Ret}**	**HF_{Ret}**
		BIOMASS			
Temperature	min	10.0	10.0	9.3	9.3
[°C]	max	16.6	14.5	14.9	14.9
	mean	12.2	12.0	12.0	11.9
DO	min	0.2	0.4	1.0	0.1
$[mgL^{-1}]$	max	1.8	2.6	4.0	3.5
	mean	0.6	1.5	2.0	1.4
pH	min	6.7	6.8	6.9	7.0
[-]	max	7.1	7.0	7.2	7.2
	mean	6.9	6.9	7.0	7.1
Conductivity	min	1,728	1,838	1,838	1,834
$[\mu S]$	max	2,070	2,060	2,060	2,040
	mean	1,909	1,937	1,936	1,908
MLSS (VSS)	min	5.4 *(87.1)*	5.7 *(86.7)*	5.8 *(87.5)*	6.4 *(87.4)*
$[gL^{-1}]$ *([%])*	max	8.1 *(89.5)*	9.8 *(88.7)*	12.2 *(88.5)*	11.9 *(91.6)*
	mean	6.6 *(88.2)*	7.3 *(88.0)*	8.4 *(88.0)*	9.2*(88.7)*
Particle Size	min	55.6	47.2	48.0	46.3
$d_{0.5}$ $[\mu m]$	max	68.7	59.3	61.7	67.8
	mean	61.7	53.8	56.9	54.9
COD_{sludge}	min	6,440	6,775	6,855	7,690
$[mgL^{-1}]$	max	11,760	14,589	17,648	16,686
	mean	8,489	9,715	10,710	12,120
		SMP			
Proteins	min	1.2 *(7)*	1.2 *(8)*	0.8 *(8)*	1.0 *(8)*
$mg.gVSS^{-1}(mgL^{-1})$	max	2.9 *(16)*	2.5 *(21)*	2.5 *(24)*	2.4 *(23)*
	mean	1.9 *(11)*	1.7 *(11)*	1.6 *(12)*	1.5 *(13)*
Carbohydrates	min	5.9 *(36)*	10.5 *(72)*	7.8 *(84)*	11.0 *(106)*
$mg.gVSS^{-1}(mgL^{-1})$	max	16.5 *(79)*	18.7 *(160)*	23.1 *(217)*	28.1 *(261)*
	mean	10.1 *(56)*	15.0 *(95)*	17.8 *(122)*	21.1 *(168)*
DOC	min	3.8 *(20)*	3.5 *(22)*	3.4 *(24)*	3.0 *(27)*
$mg.gVSS^{-1}(mgL^{-1})$	max	5.1 *(33)*	5.1 *(44)*	5.7 *(47)*	5.3 *(51)*
	mean	4.3 *(25)*	4.3 *(27)*	4.4 *(31)*	4.0 *(32)*
Turbidity	min	0.919	1.175	0.984	1.565
$[NTU]$	max	3.500	5.035	4.570	4.670
	mean	1.790	2.141	2.205	2.392

AT (Aeration Tank); MT (Multi Tubular Module); FS (Flat Sheet Module); HF (Hollow Fibre Module)

Amongst all monitored sludge and SMP parameters, the most significant correlations were found between MLSS content of sludge samples (TS and VSS content respectively) and ΔR_{20} (VSS: R^2=*0.8195*; Figure A.6*a*) with resistance to filterability decreasing with increasing VSS content. The measured chemical oxygen demand of the sludge samples also indicated a highly significant correlation to ΔR_{20} values (COD_{sludge}: R^2=*0.7288*; Figure A.6*c*), with COD_{sludge} also having shown to be interrelated to MLSS and VSS values respectively, and ΔR_{20} being lower for higher COD_{sludge}.

Particle size expressed as $d_{0.5}$ did not show any impact on ΔR_{20} values measured (R^2=*0.0025*; Figure A.6*b*), whereas pH values of the individual sludge samples seemed to have a slight impact on ΔR_{20} (R^2=*0.5175*; Figure A.6*d*) where lower pH values were attributed to higher resistance to filterability.

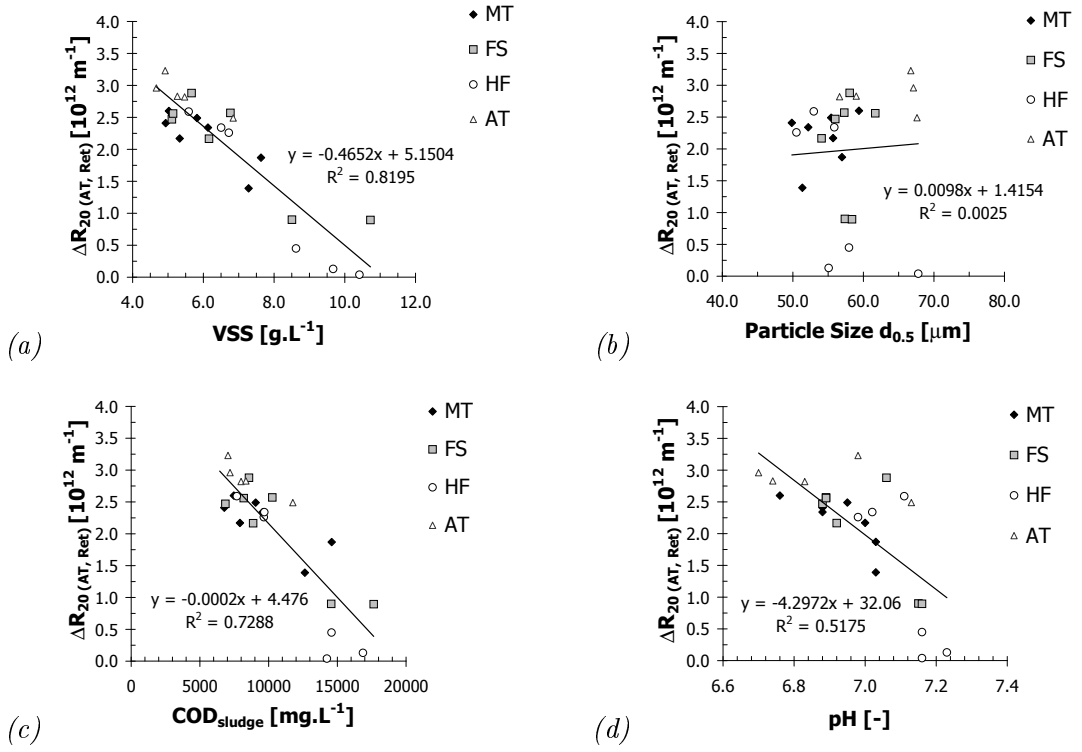

Figure A.6.: Sludge filterability (results of DFCm measurements) - Correlation of ΔR_{20} with *(a)* Volatile Suspended Solids; *(b)* Particle Size; *(c)* COD_{sludge}; *(d)* pH

No significant correlation could be observed between SMP content (ΣSMP) or Carbohydrates content and ΔR_{20} (Figure A.7*a* and A.7*d*). However, slight trends could be shown for Proteins (R^2=0.3575; Figure A.7*b*) and Dissolved Organic Carbon content (R^2=0.4346; Figure A.7*c*), where resistance to filterability improved with increasing Protein or DOC concentration per $gVSS$.

Overall, measured turbidity values did not indicate any impact on the determined resistance to filterability (Figure A.7*e* and A.7*f*).

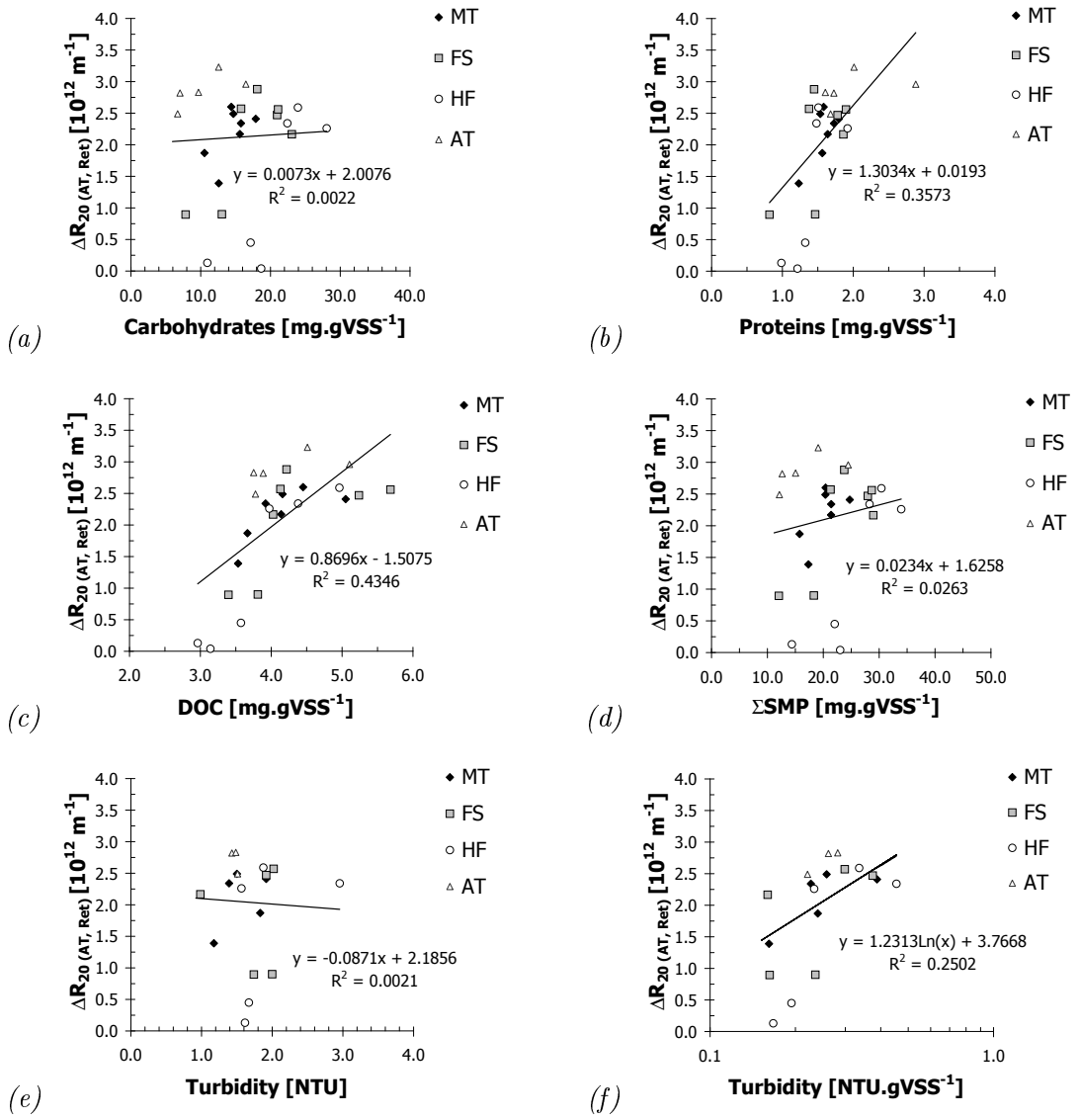

Figure A.7.: Sludge filterability (results of DFCm measurements) - Correlation of ΔR_{20} with *(a)* Carbohydrates per gVSS; *(b)* Proteins per gVSS; *(c)* DOC per gVSS; *(d)* Sum SMP per gVSS; *(e)* Turbidity in NTU and *(f)* in NTU per gVSS

A.3.2. Biomass parameters during constant aeration trials

As described previously, the filtration flux of the DFC_m unit had to be lowered to 30 LMH from the usual 80 LMH during the trials at constant aeration rate and was doubled again to 60 LMH during the SAD_m trials. Due to the different applied fluxes, it is impossible to directly compare the resulting values for sludge filterability. However, assessing biomass parameters measured during the constant aeration trials did not reveal significant differences to the biomass parameters determined during the subsequent SAD_m test series, apart from the amount of dissolved organic carbon, hereafter listed as DOC $mg.gVSS^{-1}$. While values varied between 3.0 and 5.7 mgDOC.$gVSS^{-1}$ during the SAD_m trials aeration trial (Table A.1, page 225), the amount of DOC was detected during the constant aeration trials as high as 20.5 mgDOC.$gVSS^{-1}$ with an average of 16.6 mgDOC.$gVSS^{-1}$ and at its lowest 13.6 mgDOC.$gVSS^{-1}$ while having the same range of MLSS content (Table A.2).

Table A.2.: Summary of biomass parameters during DFCm - Constant aeration trial

Parameter		**AT**	**MT_{Ret}**	**FS_{Ret}**	**HF_{Ret}**
		BIOMASS			
MLSS (VSS)	min	5.9 *(82.5)*	6.3 *(76.6)*	6.5 *(85.3)*	6.9 *(84.2)*
$[gL^{-1}]$ *([%])*	max	7.3 *(87.7)*	8.5 *(87.4)*	8.1 *(86.6)*	8.1 *(87.5)*
	mean	6.6 *(85.7)*	7.3 *(83.6)*	7.2 *(85.9)*	7.6 *(86.4)*
Particle Size	min	47.9	46.6	47.0	46.4
$d_{0.5}$ $[\mu m]$	max	73.5	69.3	61.2	68.0
	mean	55.6	50.5	50.2	51.1
COD_{sludge}	min	4,225	4,725	4,473	4,095
$[mgL^{-1}]$	max	7,890	8,354	8,090	8,960
	mean	5,170	5,709	5,817	6,065
		SMP			
Proteins	min	2.3 *(14)*	1.6 *(10)*	1.4 *(10)*	2.8 *(16)*
$mg.gVSS^{-1}(mgL^{-1})$	max	3.4 *(18)*	2.6 *(14)*	3.0 *(17)*	3.5 *(25)*
	mean	2.8 *(15)*	2.1 *(12)*	2.0 *(12)*	3.1 *(21)*
Carbohydrates	min	2.4 *(15)*	2.6 *(17)*	2.5 *(16)*	7.0 *(46)*
$mg.gVSS^{-1}(mgL^{-1})$	max	10.6 *(57)*	8.4 *(48)*	17.8 *(99)*	34.5 *(199)*
	mean	5.0 *(25)*	4.3 *(25)*	7.7 *(44)*	20.7 *(101)*
DOC	min	13.6 *(74)*	16.2 *(101)*	14.2 *(79)*	14.0 *(81)*
$mg.gVSS^{-1}(mgL^{-1})$	max	20.5 *(107)*	20.4 *(110)*	18.0 *(107)*	17.7 *(123)*
	mean	17.1 *(97)*	17.1 *(103)*	16.2 *(99)*	16.6 *(110)*

AT (Aeration Tank); MT (Multi-Tubular Module); FS (Flat Sheet Module); HF (Hollow Fibre Module)

Plotting the determined resistance to sludge filterability against the parameters measured as soluble microbial products within the respective supernatants emphasised this theory. While soluble carbohydrates and proteins did not show any significant correlation to ΔR_{20}, the amount of soluble DOC presented the same trend as observed during the SAD$_m$ trials. It should be mentioned that the particle size of sludge flocs and pH of the biomass did not prove any of the correlation determined during the SAD$_m$ trials to be true. The only value other than the amount of DOC which exhibited a similar trend during this type of experiment, was the determined concentration of COD of the biomass (Figure A.8).

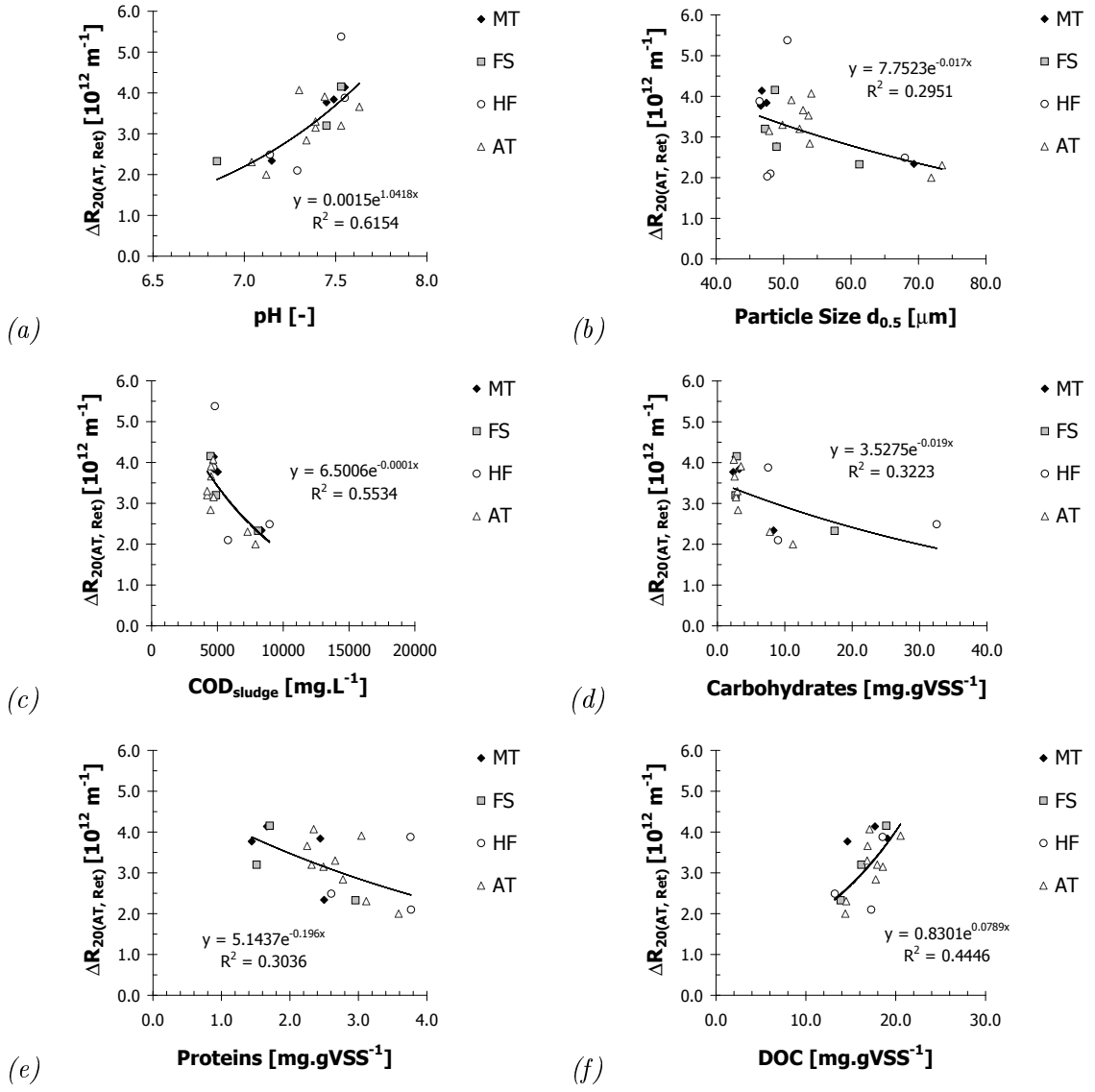

Figure A.8.: Sludge filterability (results of DFCm measurements) - Correlation of ΔR_{20} with *(a)* pH; *(b)* COD$_{sludge}$; *(c)* carbohydrates; *(d)* proteins ; *(d)* DOC; *(e)* particle size during constant aeration trials

A.4. Impact of operational parameters on ΔR_{20} ratios

A.4.1. Critical flux trials at varying aeration rates (SADm trials)

Throughout this study, changes in sludge filterability proved to be a direct effect of changes exhibited onto the biomass during the passage of the individual side-stream vessel, subject to module configuration. As previously indicated (Figure A.4, page 222) variations of $\frac{\Delta R_{20\ Ret}}{\Delta R_{20\ AT}}$ seemed dependent on either daily biomass changes (Figure A.4*a*) or applied aeration rates (SAD_m, Figure A.4*b*), where module configuration determined the significance of impact.

This proposition could be amplified by assessing changes of $\frac{\Delta R_{20\ Ret}}{\Delta R_{20\ AT}}$ and SAD_p, $SRT_{side-stream}$, cross-flow velocity (CFV) and sludge $dewatering_{side-stream}$ (Figure A.9*a* to A.9*d*). While the applied aeration rate (expressed as either SAD_p or SAD_m) showed no impact on $\frac{\Delta R_{20\ Ret}}{\Delta R_{20\ AT}}$ for the FS module (*R^2 = 0.07 and 0.2 respectively*), a significant impact could be observed for the HF module (*R^2 = 0.8178 and 0.7346 respectively*). Influences of SAD_p rates on $\frac{\Delta R_{20\ Ret}}{\Delta R_{20\ AT}}$ for the MT module were also found to be relevant (*R^2 = 0.59*, Figure A.9*a*).

Average air-lift cross flow velocities (CFV measured as air-liquid-solid three-phase flow velocity) resulting from different applied aeration rates (SAD_m) were, *due to configuration*, the highest for the MT module where CFV varied between 0.017 ms^{-1} and 0.094 ms^{-1}. On average, the lowest CFVs were measured for the FS module with values ranging from 0.002 to 0.019 ms^{-1}. The same SAD_m rates simultaneously applied to the HF module exhibited cross-flow velocities of 0.004 to 0.019 ms^{-1}. Compared to the correlation observed between SAD_m rates and changes in sludge filterability, CFVs showed a higher impact on $\frac{\Delta R_{20\ Ret}}{\Delta R_{20\ AT}}$ with the highest correlation found for the HF module (*R^2 = 0.81*, Figure A.9*c*). For all modules, sludge filterability improved with decreasing cross-flow velocity, which was, *due to sampling strategy*, also directly linked to sludge dewatering (Figure A.9*d*) and hence linked to an increase in mixed liquor suspended solids content (TS or VSS respectively) within each retentate line (see Figure A.6, page 226).

Highest ameliorations in sludge filterability ($\frac{\Delta R_{20\ Ret}}{\Delta R_{20\ AT}} \leq 0.5$) were found at 3 L sludge dewatering for the MT module (CFV < 0.02 $m.s^{-1}$), above 10 L sludge dewatering for the HF module and above 7.5 L sludge dewatering for the FS module (CFV for HF and FS < 0.004 $m.s^{-1}$). Sludge filterability increased the most for the HF module with $\frac{\Delta R_{20\ Ret}}{\Delta R_{20\ AT}} \leq 0.05$ for sludge dewatering $\geq$ 10.82 L (Figure A.9*d*).

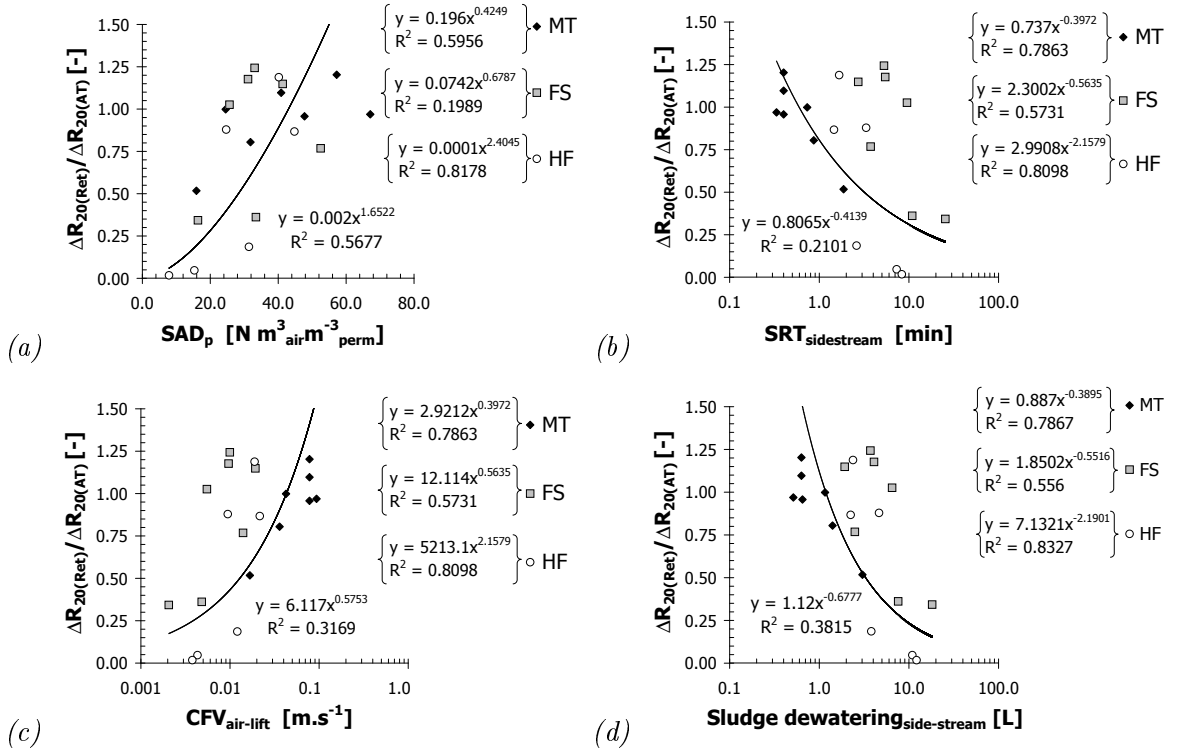

Figure A.9.: Sludge filterability (results of DFCm measurements) - Correlation of $\frac{\Delta R_{20\ Ret}}{\Delta R_{20\ AT}}$ with *(a)* SAD$_p$; *(b)* SRT$_{side-stream}$; *(c)* CFV; *(d)* Sludge Dewatering$_{side-stream}$. (Corresponding graphs showing individual module trend-lines, Figure A.17)

A.4.2. Continuous filtration at constant aeration rates

The change from low to high fluxes at constant aeration rate yielded in varying sludge dewatering for each side-stream module, which then also impacted on the sludge filterability (Figure A.3, page 221). Depending on the module configuration, and hence on the ratio of membrane area to void volume of the side-stream vessel and on the cross-flow velocity resulting from the fixed aeration rate, the sludge dewatering varied from $\approx 0.3\ L$ to $0.7\ L$ for the MT module, from $\approx 0.6\ L$ to $1.1\ L$ for the FS module and from $\approx 1.0\ L$ and $1.9\ L$ for the HF module for fluxes of 9 LMH and 18 LMH respectively. The positive effects on amelioration due to sludge dewatering during the side-stream passage could also be observed during the continuous filtration trials (Figure A.10a). The highest amelioration in sludge filterability ($\frac{\Delta R_{20\ Ret}}{\Delta R_{20\ AT}} \leq 0.7$), was again observed for the HF module, with sludge dewatering around $2\ L$ for the trial at flux of 18 LMH. For sludge dewatering around $1\ L$, therefore for the trial at a flux of 9 LMH, resistance to filterability increased during the side-stream vessel passage. This might be attributed to a complex interaction between the release of residual fouling due to shear exhibited onto the biomass during the side-stream passage and the MLSS content of the

biomass. For instance, an increase of total solids during the side-stream passage revealed an increase in sludge filterability only for $\frac{TS_{Ret}}{TS_{AT}}$ above 1.25 (Figure A.10b). A similar 'threshold' value of 1.25 $\frac{TS_{Ret}}{TS_{AT}}$ was observed for the FS module with sludge filterability increasing, with total solids of the retentate line being 1.25 times (or higher) than the total solid content of the aeration tank. Sludge filterability increased during the passage of the MT module with $\frac{TS_{Ret}}{TS_{AT}}$ $\leq$ 1.5 (Figure A.10b).

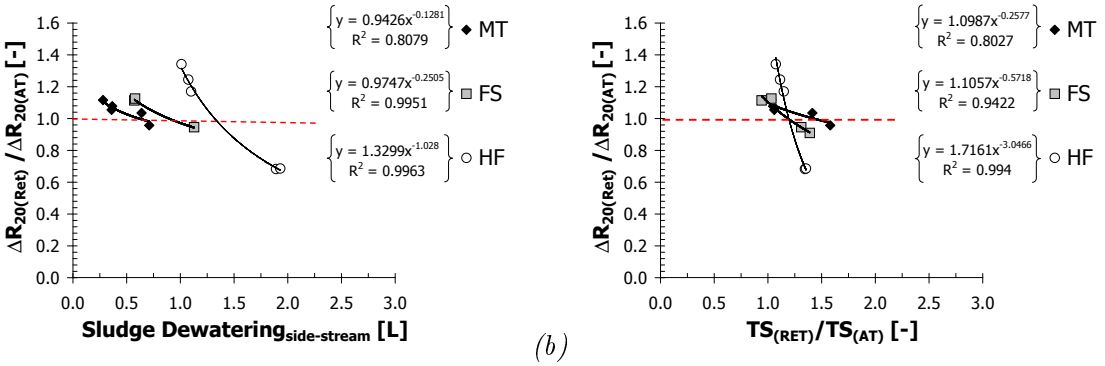

Figure A.10.: Sludge filterability (results of DFCm measurements) - $\frac{\Delta R_{20\ Ret}}{\Delta R_{20\ AT}}$ development during constant aeration trial vs *(a)* Sludge dewatering during the passage of the sidestream vessel; *(b)* Ratio of total solids (retentate line/aeration tank).

A.5. Membrane filtration performance and ΔR_{20} variations

The membrane filtration performance during the **constant aeration** trial and **continuous fluxes** (9 LMH and 18 LMH) did not reveal significant changes during the set of experiments and is therefore not discussed within this section.

Critical flux tests conducted under varying SAD$_m$ scenarios during this combined study suggested that, *depending on module configuration*, membrane fouling propensity was not only dependent on the aeration rate applied for membrane air scouring (see Chapter 7.2). In fact, the observed changes in sludge filterability ($\frac{\Delta R_{20\ Ret}}{\Delta R_{20\ AT}}$) were found to have had an interesting impact on the critical flux development for each configuration and supported explanations for antithetically apparent results.

While permeability at a given flux of J$_{20}$= 30 LMH indicated a decrease for FS and HF modules with increasing aeration rates and therefore opposing the expected ameliorating effects of air scouring, $\frac{\Delta R_{20\ Ret}}{\Delta R_{20\ AT}}$ measurements revealed that the increase in permeability was concomitant with altered sludge filterability (Figure A.11).

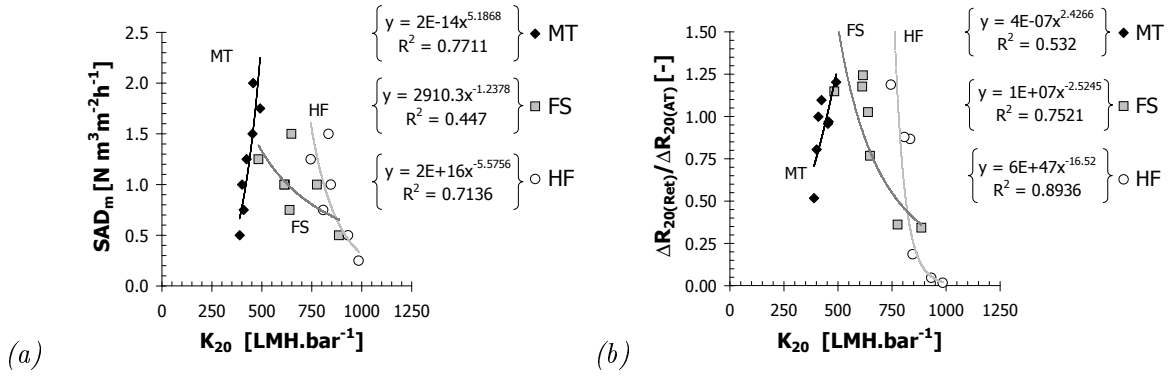

Figure A.11.: Sludge filterability (results of DFCm measurements) - Permeability of side-stream modules vs. *(a)* SAD$_m$; *(b)* $\frac{\Delta R_{20\ Ret}}{\Delta R_{20\ AT}}$.

The highest increase in permeability per 0.1 $\frac{\Delta R_{20\ Ret}}{\Delta R_{20\ AT}}$ was found for the FS module with 30 $LMH.bar^{-1}$. Overall, permeability increased from 615 $LMH.bar^{-1}$ to 886 $LMHbar^{-1}$ with a decrease in SAD$_m$ from 1.0 to 0.5 Nm^{3}m^{-2}h^{-1}, resulting in an overall increase of sludge filterability expressed as $\frac{\Delta R_{20\ Ret}}{\Delta R_{20\ AT}}$ from 1.24 to 0.34.

Sludge filterability increased the most for HF retentate samples with values of $\frac{\Delta R_{20\ Ret}}{\Delta R_{20\ AT}}$ dropping from 1.19 at a SAD$_m$ rate of 1.25 Nm^{3}m^{-2}h^{-1} down to $\frac{\Delta R_{20\ Ret}}{\Delta R_{20\ AT}} = 0.02$ at SAD$_m$ = 0.25 Nm^{3}m^{-2}h^{-1}. Membrane permeability of the HF module revealed an overall increase of K$_{20}$ = 240 $LMH.bar^{-1}$ with an incline of K$_{20}$ of 20 $LMH.bar^{-1}$ per 0.1 $\frac{\Delta R_{20\ Ret}}{\Delta R_{20\ AT}}$ drop.

The MT module on the other hand, showed an improvement in permeability with increasing membrane air scouring (R^2=*0.7711*, Figure A.11*a*) and hence an increase of permeability with decreasing sludge filterability, whereas less impact of changes in sludge filterability on the overall membrane performance could be observed (R^2= *0.532*, Figure A.11*b*).

Determined fouling resistances (R_f) revealed similar trends for the individual module configuration. While higher applied SAD_m values were associated with lower fouling resistances (R_f) for the MT module (R^2=*0.6239*, Figure A.12*a*), less significance was observed for decreasing sludge filterability (R^2=*0.4892*, Figure A.12*b*). The HF and FS modules, however, showed an increase in R_f with increased aeration rates (HF: R^2=*0.7163*, FS: R^2=*0.6992*; Figure A.12*a*), which were found to be quasi-simultaneous to decreased sludge filterability (HF: R^2=*0.7502*, FS: R^2=*0.6307*; Figure A.12*b*).

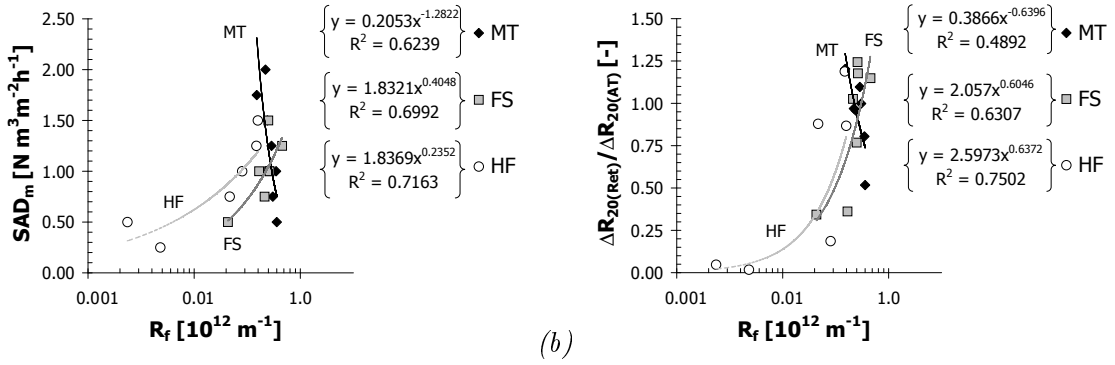

(a) *(b)*

Figure A.12.: Sludge filterability (results of DFCm measurements) - Module performance: fouling resistance R_f vs. *(a)* SAD_m; *(b)* $\frac{\Delta R_{20\ Ret}}{\Delta R_{20\ AT}}$

Fouling rates according to the classical dTMP/dt determination indicated having been insignificantly affected by either changing SAD_m rates or sludge filterability for the multi-tubular module (Figure A.13*a*, A.13*b*: R^2=*0.0742* (SAD_m), R^2=*0.1578* ($\frac{\Delta R_{20\ Ret}}{\Delta R_{20\ AT}}$)). dTMP/dt values increased for both HF and FS modules with increased aeration rates, which again could be linked to worsened sludge filterability. The significance for correlation remained similar for the FS module (R^2=*0.6373* (SAD_m), R^2=*0.6195* ($\frac{\Delta R_{20\ Ret}}{\Delta R_{20\ AT}}$)), whereas impact of SAD_m on dTMP/dt was found to be higher for the HF module than the impact of $\frac{\Delta R_{20\ Ret}}{\Delta R_{20\ AT}}$ changes (Figure A.13*a*,*b*; R^2=*0.7758* (SAD_m) , R^2=*0.5743* ($\frac{\Delta R_{20\ Ret}}{\Delta R_{20\ AT}}$)).

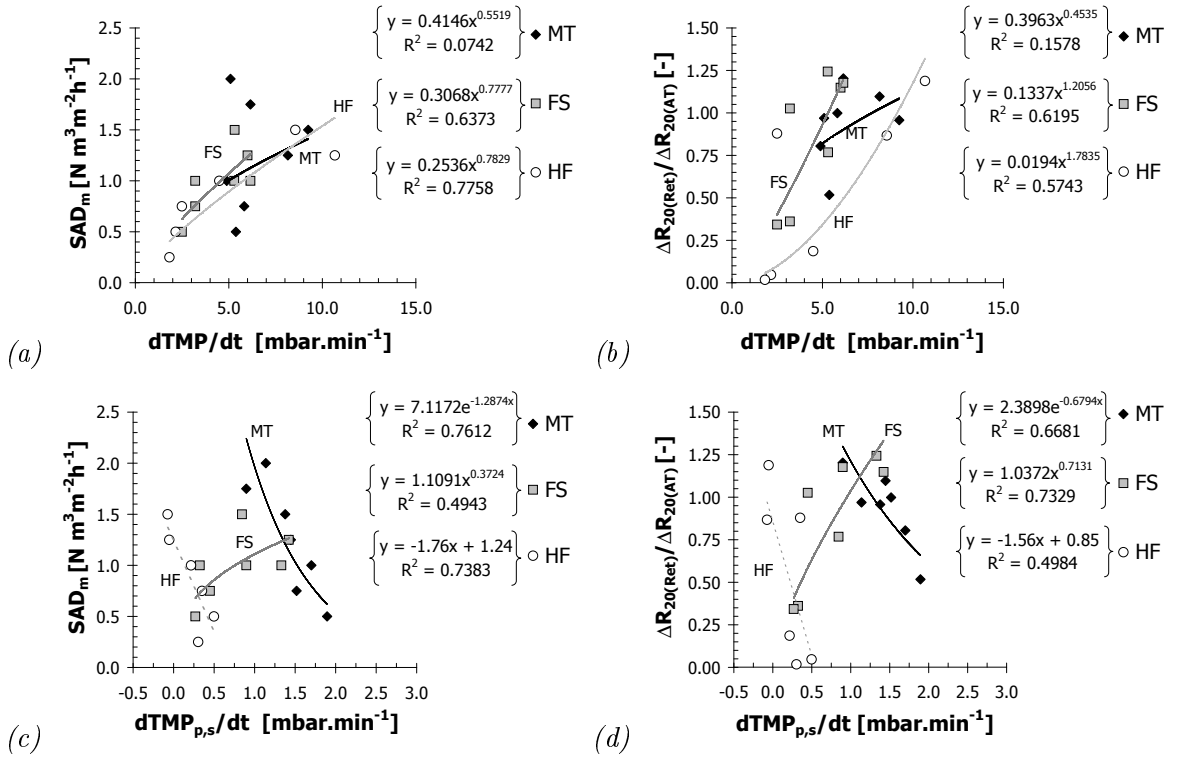

Figure A.13.: Sludge filterability (results of DFCm measurements) - Module filtration performance: *(a)* classical dTMP$/d$t vs SAD$_m$; *(b)* classical dTMP$/d$t vs $\frac{\Delta R_{20\ Ret}}{\Delta R_{20\ AT}}$ *(c)* peak-step dTMP$_{p,s}/d$t vs SAD$_m$; *(d)* peak-step dTMP$_{p,s}/d$t vs $\frac{\Delta R_{20\ Ret}}{\Delta R_{20\ AT}}$

Contrary to the classical dTMP$/d$t analysis, the trans-membrane pressure changes over time between both peaks per flux step (dTMP$_{p,s}/d$t), depleted with increasing aeration rates for the HF module (Figure A.13c). In fact, dTMP$_{p,s}/d$t showed slightly negative fouling rates ($dTMP_{p,s}/dt$ = *-0.05 and -0.07 mbar.min*$^{-1}$) for the HF module with aeration rates above SAD$_m$ = 1.0 Nm^{3}m^{-2}h^{-1}, which indicated that even though fouling rates during filtration periods increased with decreasing sludge filterability, the effects of air scouring during relaxation and backwash cycles had enormously positive effects on fouling prevention.

Whilst the multi-tubular module exhibited a significant decline of dTMP$_{p,s}/d$t with increasing aeration rates (Figure A.13c, R^2=*0.7612*) similar to the HF module, the dependency of filtration resistance between biomass and membrane modules remained unchanged for the FS module (Figure A.13d, R^2=*0.7329*). Therefore, between all three module configurations compated, only the FS module showed no amelioration during relaxation periods for higher applied air scouring rates; however sludge filterability showed to have the highest impact on filtration performance.

Comparing the trials conducted for fluxes of LMH 30 and LMH 60 of the DFCm unit, it might be concluded that besides having higher DOC values, the ratio between proteins and carbohydrates of the bulk phase might be a possible explanation for the much lower filterability of the sludge during the start of the experiment. Ratios of proteins to carbohydrates varied between 0.25 and 1.0 for trials at LMH 30, and P/C ratio was reduced from 0.36 to 0.09 during the trials where the DFCm unit could be operated with a flux of 60 LMH ($R^2 = 0.44$, Figure A.14). However, with a correlation of only $R^2 = 0.34$ during the SAD_m variation trials, this biomass parameter can not explain the entire phenomenon of ameliorated sludge filterability occurring from the indirect effects of the side-stream operation.

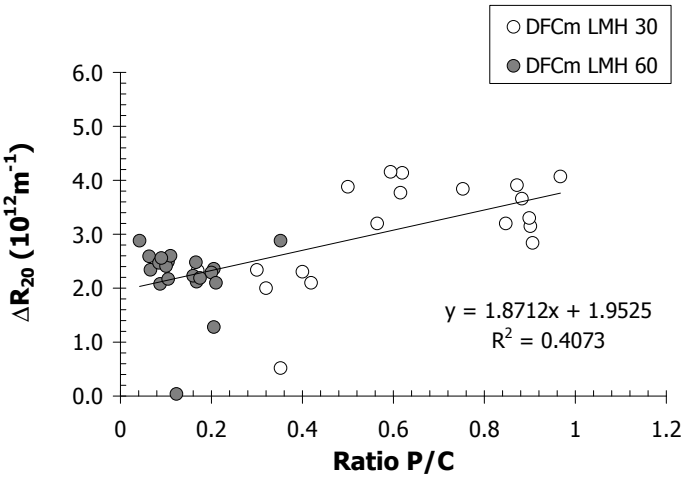

Figure A.14.: Correlation of DFCm resistance to filtration measurement and ratio of P/C for bulk phase of the biomass sample.

A.6. ANNEX: DFCm filtration trials - Correlation Graphs

A.6.1. Corresponding graph to Figure A.3

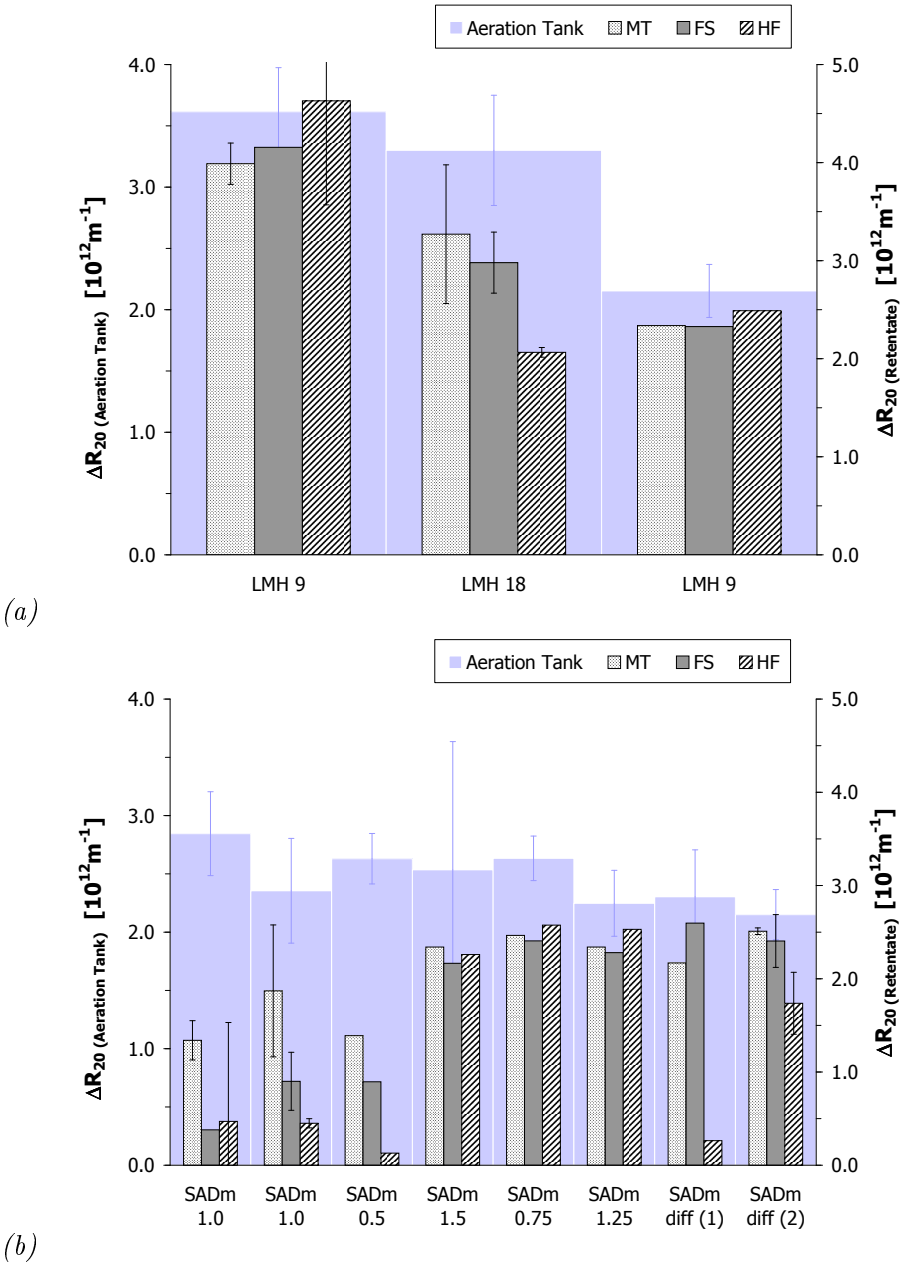

Figure A.15.: Sludge filterability (results of DFCm measurements) - comparison of ΔR_{20} values aeration tank and retentate lines - *(a)* 1^{st} stage of experiment: constant aeration and low to high permeate fluxes; *(b)* 2^{nd} stage of experiment: critical flux trials with varying SADm; corresponding graphs indicating the $\frac{\Delta R_{20\,Ret}}{\Delta R_{20\,AT}}$ ratio, Figure A.3, page 221

A.6.2. Corresponding graph to Figure A.4

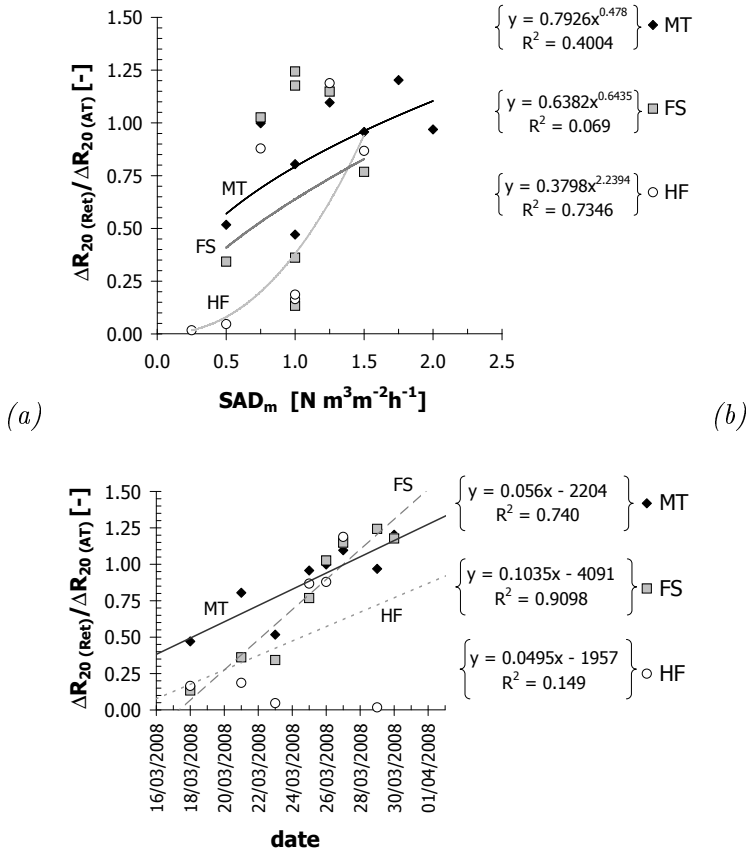

Figure A.16.: Sludge filterability (results of DFCm measurements) - Correlation of $\frac{\Delta R_{20\ Ret}}{\Delta R_{20\ AT}}$ with *(a)* SADm rates and *(b)* date; trendline showing individual module correlation (Overall trendline and text see Figure A.4, page 222)

Figure A.17.: Sludge filterability (results of DFCm measurements) - Correlation of $\frac{\Delta R_{20\ Ret}}{\Delta R_{20\ AT}}$ with *(a)* SAD$_p$; *(b)* SRT$_{side-stream}$; *(c)* CFV; *(d)* Sludge Dewatering$_{side-stream}$: showing individual module trendlines. (Overall trend-line graph and text see Figure A.9, page 231)

B. Biomass Parameter - Summary of overall process operation

B.1. Monitoring of biomass changes during constant HRT

Changes in soluble microbial products (SMP) are often linked to changes in operational parameters, such as HRT and SRT and changing MLSS content, which are then in turn related to membrane fouling. It was therefore of interest to elucidate possible changes in SMP concentration for a period with constant operational parameters. Besides the monitoring during critical flux trials, two different types of experiments were conducted:

- intensive monitoring over a period of three months at constant HRT (HRT = 10 hours) without operation of the side-stream modules, and
- a daily monitoring on a 2-hourly basis during three different HRT trial periods without and with side-stream module operation.

Most relevant results of both types of experiments are presented hereafter and were, where considered necessary, compared to the overall results of biomass characterisation.

B.1.1. Monitoring of overall biomass and SMP changes at constant operation without side-stream operation

During the 3 months monitoring period (HRT 10 hours), the concentration of soluble microbial products determined in the supernatant of the aeration tank varied widely, showing the highest concentration throughout this study (Table 8.1, page 156).

Comparing the amount of soluble proteins, carbohydrates and dissolved organic matter per $g.MLSS$, clearly revealed highest fluctuation for carbohydrates, especially during the first month of the growth phase of MLSS at HRT 10 hours. After two months of operation, however, the amount of carbohydrate per g.MLSS seemed to show a trend of stabilization (Figure B.1a). The organic content of the biomass presented mostly constant with a clear correlation to MLSS content (Figure B.1b). Therefore, no significant difference could be expected when normalising results to either MLSS or VSS.

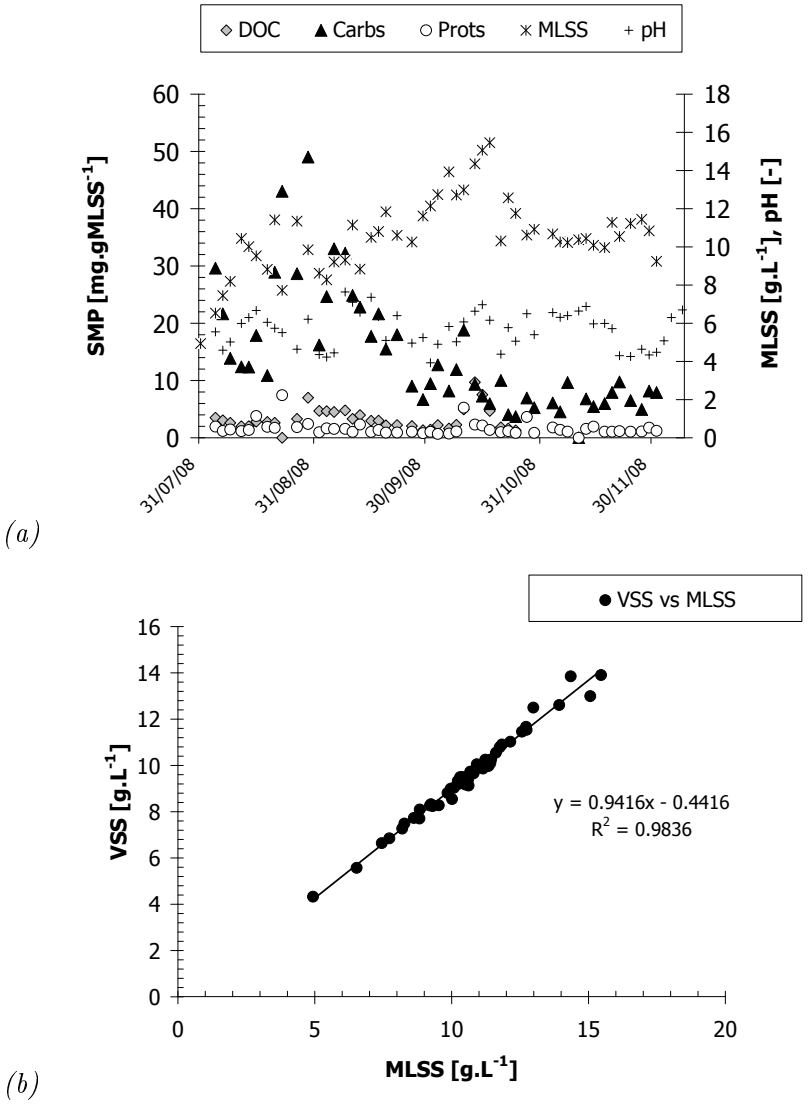

Figure B.1.: *(a)* Variation of SMP, MLSS and pH during monitoring period at HRT 10. *(b)* Correlation of MLSS vs. VSS.

B.1.1.1. Influent values

During the monitoring campaign at HRT 10 hours, supernatant of the **influent** and bulk phase of the aeration tank were compared to elucidate the origin of soluble microbial products. During this period, the determined concentrations of carbohydrates and DOC were found to be of similar range for influent and bulk phase of the aeration tank, whereas soluble proteins were consistently found to be of higher concentration for the influent samples (Figure B.2). Differences in protein concentration between the influent sample and bulk phase were on average as high as 40 to 50 mg.L^{-1}.

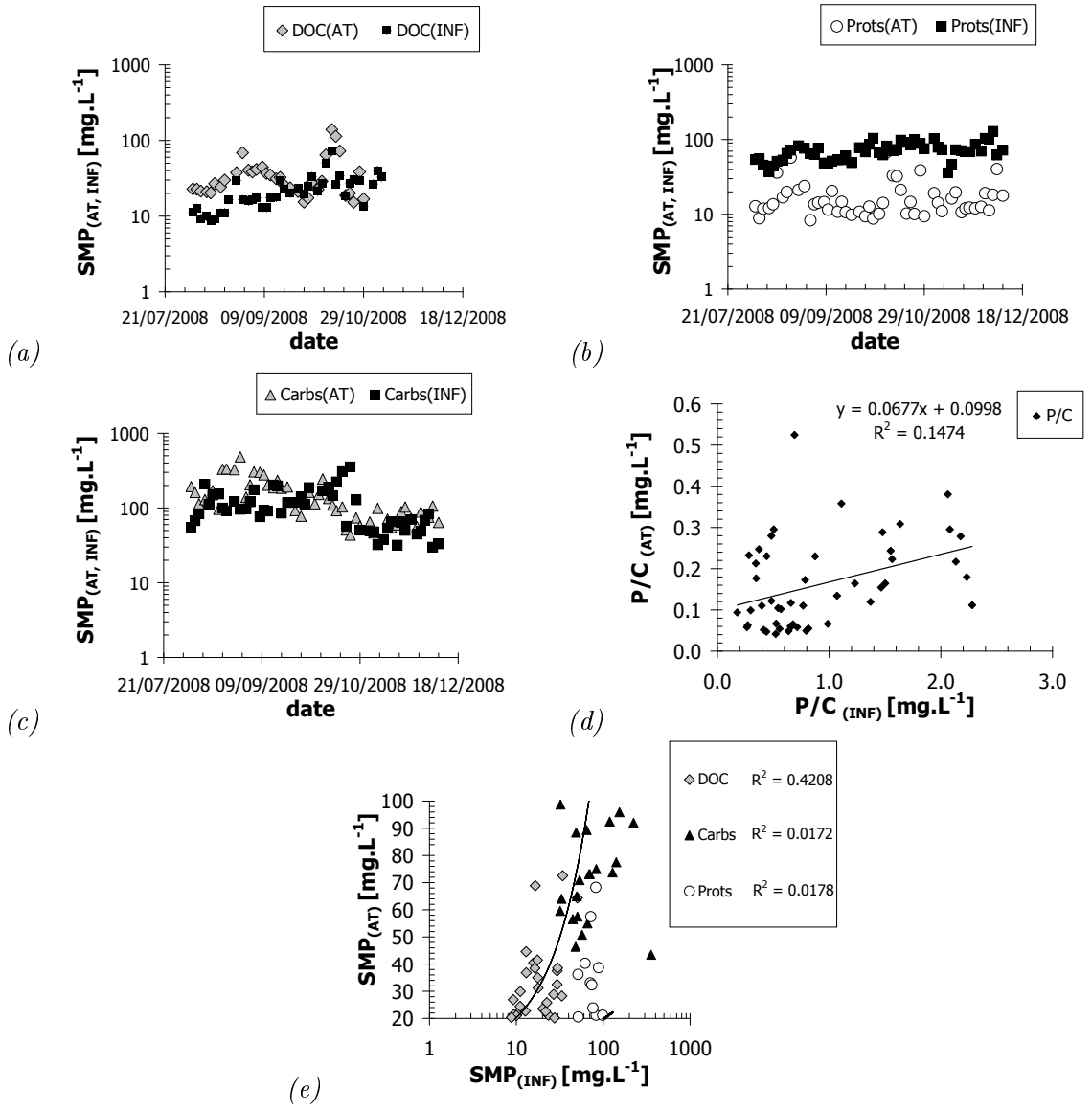

Figure B.2.: Variation of soluble microbial products measured within the influent (feed) and the supernatant of the aeration tank.

The concentrations of DOC, carbohydrates and proteins were furthermore compared for influent and supernatant of the bulk phase of the aeration tank for all trials and HRTs conducted. In general, influent values for DOC and carbohydrates were found to be higher within the supernatant of the aeration tank than within the influent samples. For instance, DOC concentration within the supernatant of the aeration tank was found for 77.6% of the determinations to be higher than within the corresponding influent sample.

Overall, the DOC concentration within the influent samples represented in average 67% of the DOC determined within the aeration tank (Table B.1). Concentrations for carbohydrates

were also found in 72.1% of the determinations to be on average 70% higher within the SMP of the aeration tank than the feed. Only ≈ 28% of the determinations showed an an average concentration 3 times higher of soluble carbohydrates for the feed than for the supernatant of the aeration tank.

This was opposed to the observation made for soluble proteins, where over 98% of the determined influent samples showed an average concentration 4.5 times higher for proteins in the feed than in the SMP of the aeration tank (Table B.1).

Table B.1.: Ratio of soluble microbial products determined in influent samples and supernatant of the aeration tank throughout the study

Ratio $\frac{c_{Inf}}{c_{AT}}$	**DOC**	**Proteins**	**Carbohydrates**
Overall results for determined ratios of $\frac{c_{Inf}}{c_{AT}} \leq 0$			
average	0.76	4.80	1.17
min	0.2	0.7	0.0
max	2.0	11.9	13.6
Determined ratios of $\frac{c_{Inf}}{c_{AT}} \leq 0$			
percentage of overall results	77.6 %	1.6 %	72.1 %
average	0.63	0.75	0.35
min	0.22	0.7	0.03
max	0.94	0.8	0.84
Determined ratios of $\frac{c_{Inf}}{c_{AT}} \geq 0$			
percentage of overall results	22.4 %	98.4 %	27.9 %
average	1.51	4.61	3.72
min	1.48	1.5	1.08
max	1.57	9.7	13.50

This consequently may have led to the assumption that even though influent values for DOC and carbohydrates were in similar range for the supernatant of the aeration tank, a certain net production or release of DOC and carbohydrates occurred by microbial activity in the aeration tank. Higher protein concentration in the feed would then suggest a net degradation of proteins inside the aeration tank and a no net production of proteins of the supernatant by microbial activity. Nevertheless, it has to be considered that the applied determination methods for SMP compounds are based on adsorption spectra measurements representing composite parameters.

Therefore, shifts of degraded proteins and produced proteins, for instance, might overall result in the same resonance of absorbance, while being different type of proteins. Furthermore, it should be mentioned that results obtained for protein concentration within this study had not been corrected for nitrogen (nitrite, nitrate, and ammonium).

In fact, comparing the HPSEC profiles between elution times for $669kDa$ to the elution time of $12kDa$ revealed a higher amount of protein like substances at higher molecular weight for the influent samples (elution time 5.8 to 7.3 minutes), while the HPSEC profile of the supernatant of the aeration tank did reveal higher quantities of compounds within the lower molecular spectra (elution time 7.3 minutes to 9.2 minutes; Figure B.3). As expected, the HPSEC curve of the permeate of the submerged HF module (HRT-control module)corresponded shape-wise to the HPSEC curve of the supernatant of the biomass, with overall lower quantities and a complete retention of substances at a higher molecular weight by the membrane module (retention of substance with higher MWCO up to elution time of 7 minutes; Figure B.3).

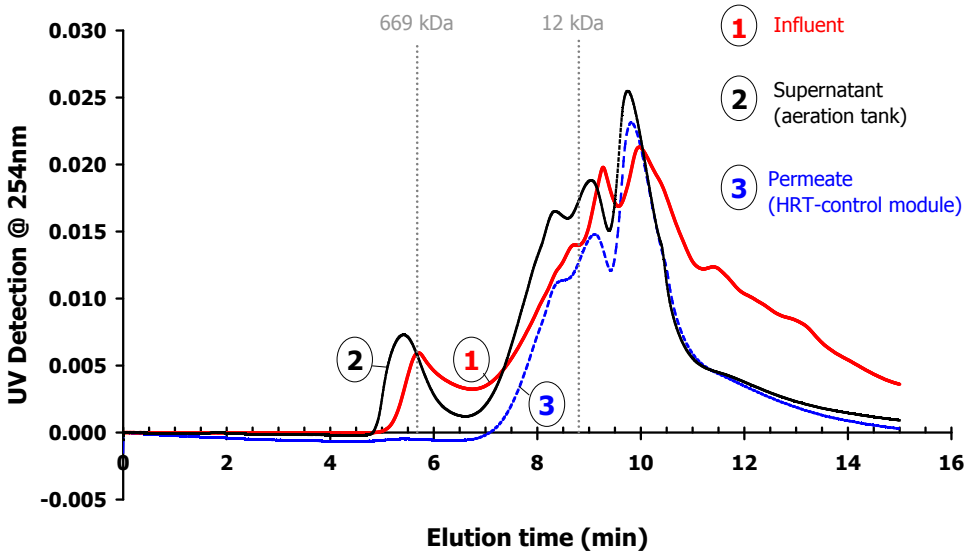

Figure B.3.: Example of HPSEC profiles of the influent, the supernatant of the aeration tank and permeate of the submerged HF module; MLSS content 12 g.L^{-1}

B.1.1.2. Elimination rates and observed retention

As the amount of SMP within the supernatant not only depends on the input from the influent and possible biomass activity, but also on the retention by the membrane module, **elimination rates** were calculated from measured SMP concentration of influent, bulk phase and permeate applying equation (B.1). Results were normalised to VSS content of the biomass to represent a specific elimination rate and specific sludge loading rate, respectively.

$$r_i = \frac{\Delta c_{i,R}}{\Delta t} + \frac{Q_{feed}}{V_R} \cdot c_{i,feed} - \frac{Q_{perm}}{V_R} \cdot c_{i,perm} - \frac{Q_{sludge}}{V_R} \cdot c_{i,R} \tag{B.1}$$

where

r_i = *determined elimination rate* $(mg.(L.h)^{-1})$

With the term for excess sludge removal ($\frac{Q_{sludge}}{V_R} \cdot c_{i,R}$) being generally zero due to no sludge wastage, specific elimination rates varied between 0.09 to 0.39 mg.(gVSS.h)$^{-1}$ for DOC and between 0.3 to 0.9 mg.(gVSS.h)$^{-1}$ and -0.4 to 2.8 mg.(gVSS.h)$^{-1}$ for proteins and carbohydrates respectively (Figure B.4**a**). Lowest variations were found for DOC, whereas highest variations were again shown for carbohydrates. Plotting the determined values for r_i against the respective values of sludge loading rates highlighted the dependency on influent loading rates (Figure B.4**b**). Specific permeate loading rates did not show any direct correlation to specific feed (sludge) loading rates (Figure B.4**c**).

Observed Retention of the HF submerged module showed to vary least for DOC with observed retention rates from 88.3% to 59.8%, whereas a higher variation was found for carbohydrates with observed retention rates varying from 92.4% to -30.9%. The observed retention for protein was determined to be on average 45.9%, with minimum of 12.% and maximum of 91.4 % (Figure B.5*a*). Interesting to note is that the observed retention for DOC, carbohydrates and proteins followed a logarithmic correlation to the amount of soluble microbial products within the bulk phase of the aeration tank, for either concentration or amount per g.VSS (Figure B.5 *b, c*). Similar results were obtained for the observed retention of turbidity (NTU) from the submerged HF module with S_{NTU} ranging from 74.2% to 98.2% providing a moderate logarithmic correlation to turbidity measured within the supernatant of the bulk phase ($R^2 = 0.6431$), and to turbidity normalised against g.VSS of the biomass ($R^2 = 0.5959$, graph not shown). However, assessing the overall obtained results throughout this study, these trends could not be verified, with the highest overall correlation for observed retention of DOC vs. DOC content or concentration being $R^2_{overall} = 0.4063$ and $R^2_{overall}$ remaining below 0.1722 for correlation of protein, carbohydrates and turbidity respectively (graph not shown).

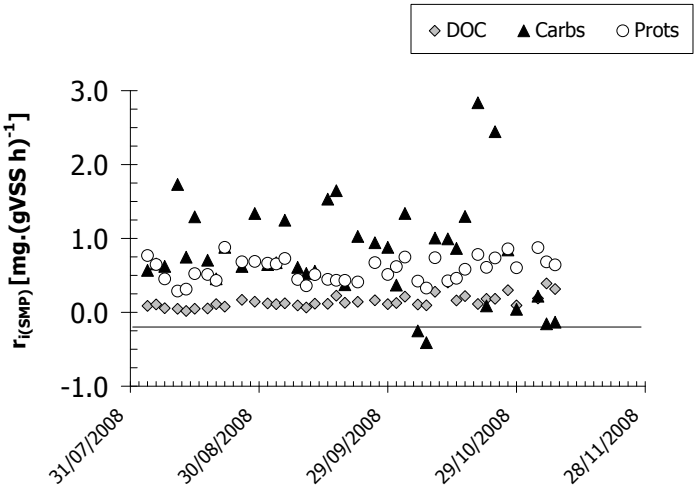

(a)

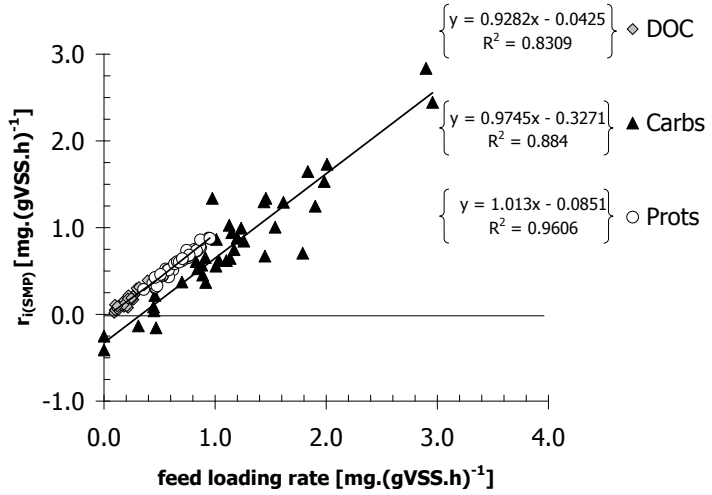

(b)

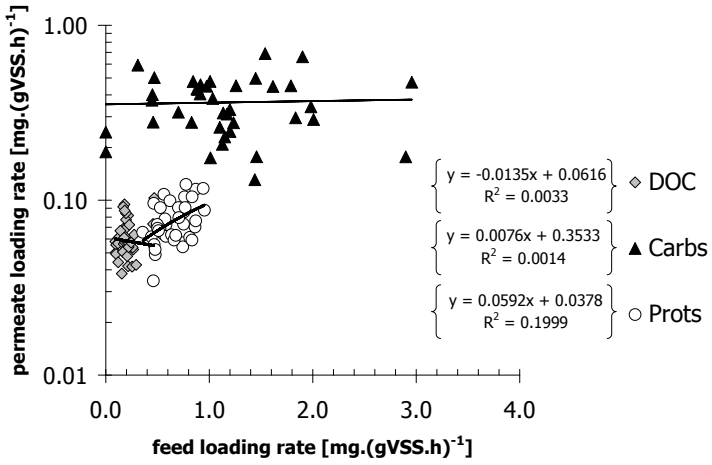

(c)

Figure B.4.: Soluble microbial products: Elimination rate vs *(a)* time and *(b)* sludge loading rate; *(b)* permeate loading rate vs sludge loading rate during monitoring period at HRT 10.

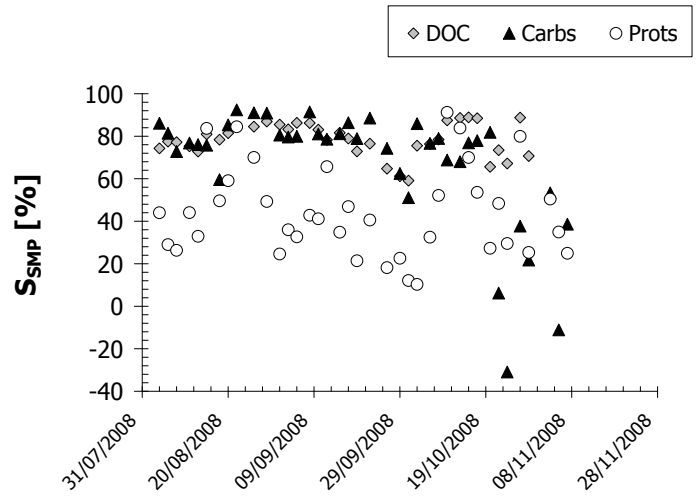

(a) *(b)*

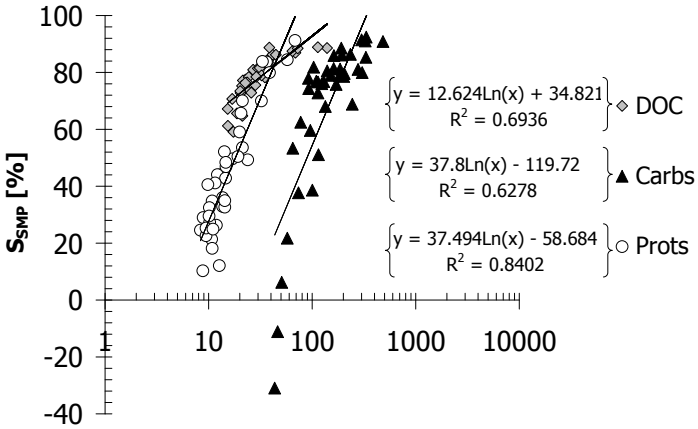

(c)

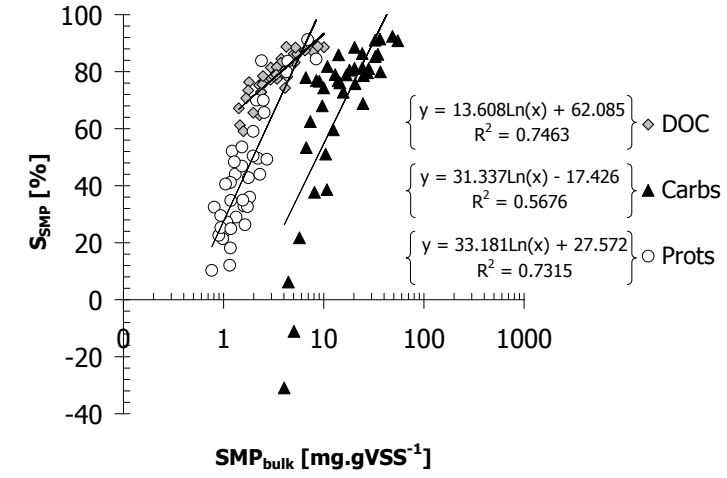

Figure B.5.: Retention of soluble microbial products during monitoring period at HRT 10.

B.1.2. Monitoring daily fluctuation of biomass properties on a 2-hourly basis

Particle size and moreover colloidal release are amongst the parameters highly discussed to cause membrane fouling. To elucidate the potential impact of shear stress due to side-stream airlift operation, the subsequent impact on floc changes and on the release of potential foulants, an overall assessment of daily variations of biomass parameters was undertaken.

Changes in flocs size distribution of the biomass of the aeration tank were monitored during constant operation mode 5 times a day on 2 consecutive days (fixed HRT, fixed aeration, no operation of side-stream modules).

Flocs size distribution monitoring was continued in the following 2 days, this time including operation of the side-stream modules where aeration was fixed and flux was set to approx. 9 LMH during the first day and 18 LMH during the following day. Particle size distributions were measured on the biomass of the aeration tank and also on the retentate lines of the side-stream modules. The tests were completed by analysing the supernatant of the aeration tank and each retentate line for SMP (DOC, proteins and carbohydrates), turbidity, pH, conductivity and dissolved oxygen.

Overall, the above described trials were repeated three times at different MLSS contents and HRTs:

- MLSS 4 $g.L^{-1}$, T = 12.5°C, HRT 24h
- MLSS 7 $g.L^{-1}$, T = 15.0°C, HRT 12h
- MLSS 4 $g.L^{-1}$, T = 20.5°C, HRT 8h

B.1.2.1. Variation of particle size distribution in the aeration tank

Surprisingly, changes in particle size within the aeration tank varied widely with the average particle size $d_{0.5}$ ranging from 39.2 μm to 80.0 μm (Figure B.6). The floc rupture, as highly discussed within literature, was shown to occur within the daily dynamic of the floc itself, even without any additional shear stress being applied.

To illustrate, the daily changes in floc size ($d_{0.5}$) were found to range between 42.2 and 80.0 μm during the monitoring at a MLSS content at of 4 $g.L^{-1}$ and low temperature (T = 12.5°C, Figure B.6*b*), which represented, at the end of the study, a coverage by 51% of the broad range of overall changes in floc size during a pilot plant operation of approximately 2 years (see Figure 8.1*b*, page 154).

The shear applied onto the biomass flocs from the operation of the side-stream membrane modules did not seem to alter the observed daily floc dynamic significantly, as the overall changes in particle size distribution within the aeration tank remained in a similar range

compared to the tests without side-stream operation (Figure B.6*b* vs. B.6*c*). Again, this could especially be observed for the test series at MLSS 4 g.L^{-1} and at temperature of 12.5°C, where floc size distribution for the low flux side-stream operation varied between 43.2 μm to 79.6 μm (Figure B.6*c*), representing 96.8% of the range in floc size change, in comparison to the respective test without side-stream operation.

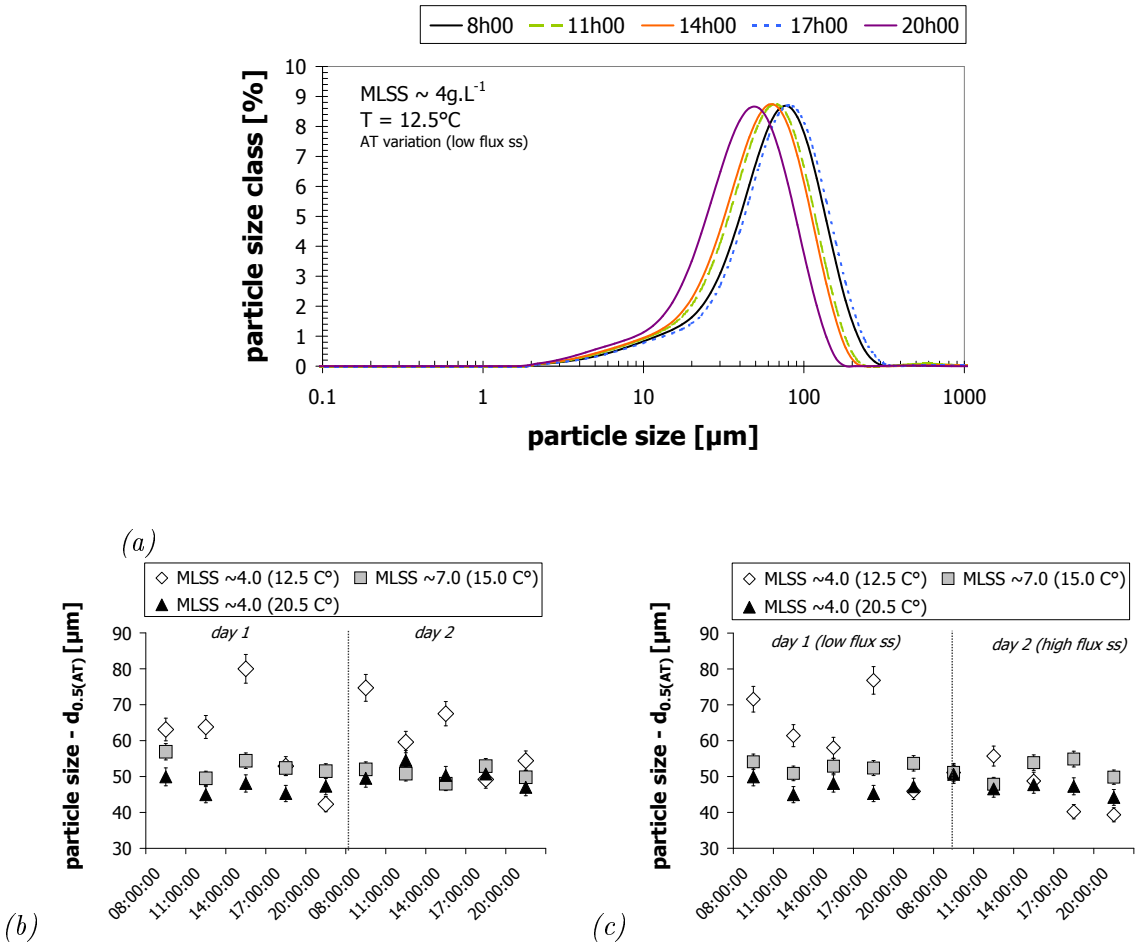

Figure B.6.: Daily variations of floc size distribution within the 2.2 m^3 membrane aeration tank. *(a)* Sample of Mastersizer profile for one monitoring day, *(b)* $d_{0.5}$ floc size development without side-stream modules operation, *(c)* $d_{0.5}$ floc size development with side-stream module operation

Nevertheless, during the operation of the side-stream modules at high fluxes in this specific test series, floc size distribution within the aeration tank was found to be an average of lower $d_{0.5}$ with less variation throughout the day. Consequently, this led to the assumption for this specific test series, that higher shear stress exhibited onto the biomass during continued

operation of the side-stream modules resulted in an overall smaller particle size distribution most likely dervived from hindered growth phases compared to lower shear stress situation. Changes in floc size distribution for the trials at lower HRT were found to be of less variation, but still within significant ranges with an average particle size $d_{0.5}$ of the biomass of the aeration tank varying from 47.9 to 51.5 μm (MLSS 7 g.L^{-1}, no sidestream operation), 48.0 to 56.9 μm (MLSS 7 g.L^{-1}, with side-stream operation), 44.3 to 50.6 μm (MLSS 4 g.L^{-1}, HRT 8 hours, no side-stream operation) and 47.0 to 54.6 μm (MLSS 4 g.L^{-1}, HRT 8 hours, with side-stream operation).

Surprisingly, the previously observed lower daily fluctuation of particle size distribution of the biomass of the aeration tank during high flux sidestream operation could not be verified during the trials at lower HRT. However, it should be mentioned that during the operation of the side-stream modules, floc sizes of all three tests run were found to be of an almost identically small size during the morning sampling of the second day (Figure B.6*c*). Considering the overall high dynamic floc changes, this might be coincidence, but it might also be assumed that during the constant shear rates which were exhibited onto the flocs during the night (also with also presumably less feed changes overall than during the day), the floc sizes approached similarity.

Finally, it should be mentioned, that the dynamic of floc size distribution found to be the highest for a highest HRT (MLSS 4 g.L^{-1}, HRT 24 hours) also coincided with the lowest sludge age and time of pilot plant operation respectively.

B.1.2.2. Variation of particle size distribution in sidestream retentate lines

Besides the daily dynamic of floc size distribution within the aeration tank, changes were monitored for biomass having passed the side-stream vessels with sidestream modules operated at constant air flow rate (35 L.min^{-1} air each module) and fluxes of 9 LMH during one day and 18 LMH the following day. Changes in floc size distribution are exemplarily represented for the trial conducted at MLSS 4 g.L^{-1}, HRT 8 hours, with low applied fluxes to the side-stream module at 8am (Figure B.7).

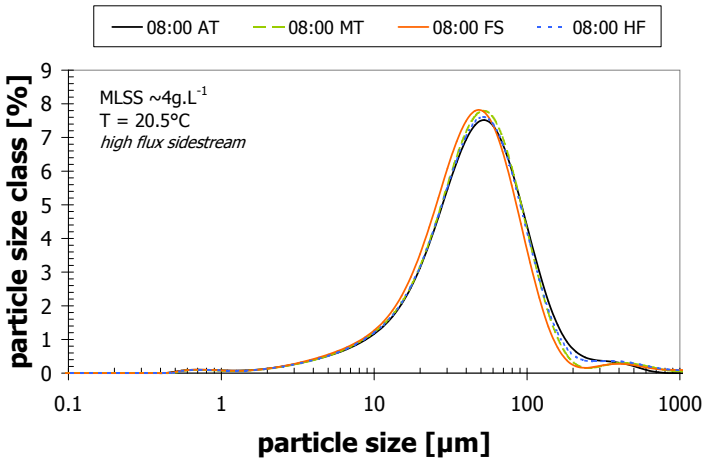

Figure B.7.: Sample of variation of floc size distribution between samples of the 2.2 m^3 membrane aeration tank and the retentate lines of the side-stream modules at 8h00 during sampling trial at MLSS 4 $g.L^{-1}$

Considering the observed high variations in particle size of the aeration tank without side-stream operation, the particle size changes monitored throughout the tests including side-stream module operation were found to be of very little significance. To illustrate, calculating the overall particle fractionation during the trial at MLSS 4 $g.L^{-1}$, 8 HRT, without side-stream operation would have resulted in 87% to 111% for particle changes within the aeration tank only (highest and lowest values on average), while particle fractionation for the retentate values of the sidestream lines during the same test trial varied from 80% to 116% for the MT module, 81% to 127% for the FS module and 91% to 105% for the HF module respectively.

Overall it could be concluded that the exhibited shear, by applying low aeration rate and moderate fluxes, did not induce significant changes in floc size distribution. In fact, during all trials, re-flocculation processes were found to have occurred during the passage of the side-stream vessel, as indicated by a particle fractionation FI $\geq$ 100 % (Figure B.8).

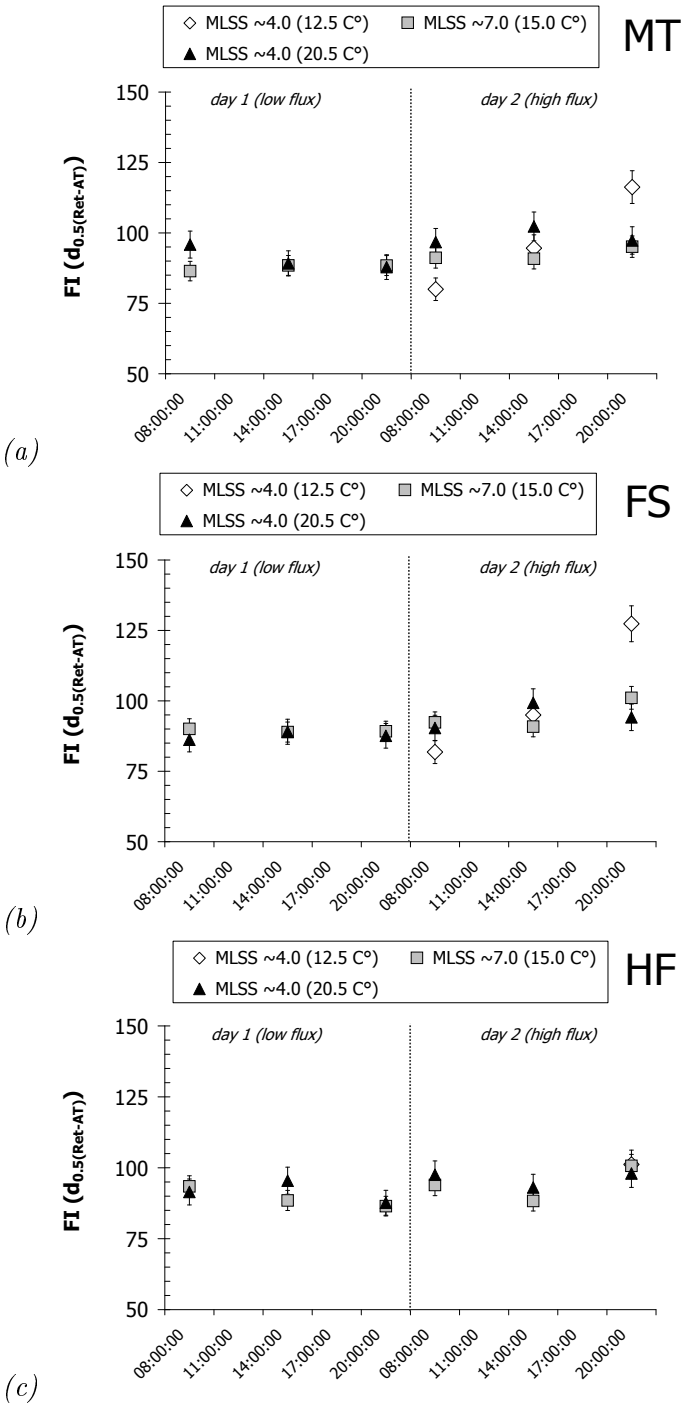

Figure B.8.: Observed particle fractionation during operation of the side-stream modules: *(a)* MT module, *(b)* FS module, *(c)* HF module

B.1.2.3. Impact of SMP variation on particle size distribution

The monitored biomass parameters, including SMP, ratio of P_{SMP}/C_{SMP}, pH and conductivity, were not found to show a statistically significant trend on the observed dynamic in the floc size distribution. Assessing, however, the impact of measured influent values on floc size changes, a slight trend became evident between the dynamic in particle changes and ratio of P/C. Plotting the hourly changes in particle size expressed as $d(d_{0.5})/dt$ against the hourly changes in ratios of P_{INF}/C_{INF} revealed a slight trend with R^2=0.756 (Figure B.9*a*). It should be noted, however, that the trend was mainly determined by one outstanding value. Nevertheless, this observation could still be validated for the 3 months monitoring period, even though significance was found to decrease (R^2=0.437; Figure B.9*b*). A generalised conclusion could, however, not be drawn for the entire study as monitoring of influent samples was not undertaken for all trials conducted.

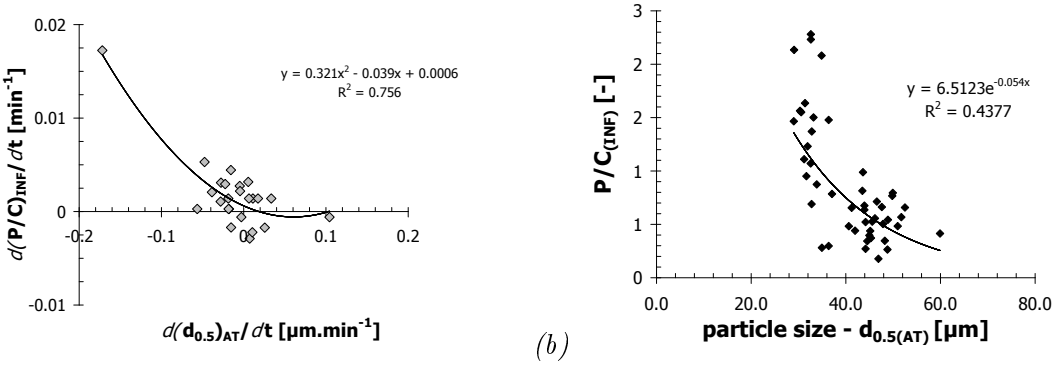

Figure B.9.: Correlation between *(a)* hourly changes of particle size $dd_{0.5}/dt$ vs. hourly changes of influent ratios P_{INF}/C_{INF} ($dP_{INF}/C_{INF}/dt$, and *(b)* correlation between P_{INF}/C_{INF} ratios and particle size of the aeration tank during the 3 months monitoring period)

B.1.2.4. Changes of SMP in supernatant due to changes in particle size distribution

A comparison of the fractionation of SMP of the supernatant and the fractionation of particle size did revealed correlations in terms of carbohydrates for all three modules. A higher fractional index for particles could be related to a higher release of carbohydrate during the sidestream passage for all membrane modules (Figure B.10).

To illustrate, with $FI_{d0.5}$ determined as 116% for both FS and MT module, the concentration of carbohydrates within the retentate line was found to represent roughly 180% of the concentration of carbohydrates determined within the supernatant of the aeration tank. Surprisingly, fractional indexes for carbohydrates of the HF module retentate were found to be above 275%,

reaching at its maximum 450% with a corresponding $FI_{d0.5}$ of only 105%. Overall, the release of SMP during the passage of the retentate line was found to be significantly higher for the HF module than for the MT module or the FS module, respectively.

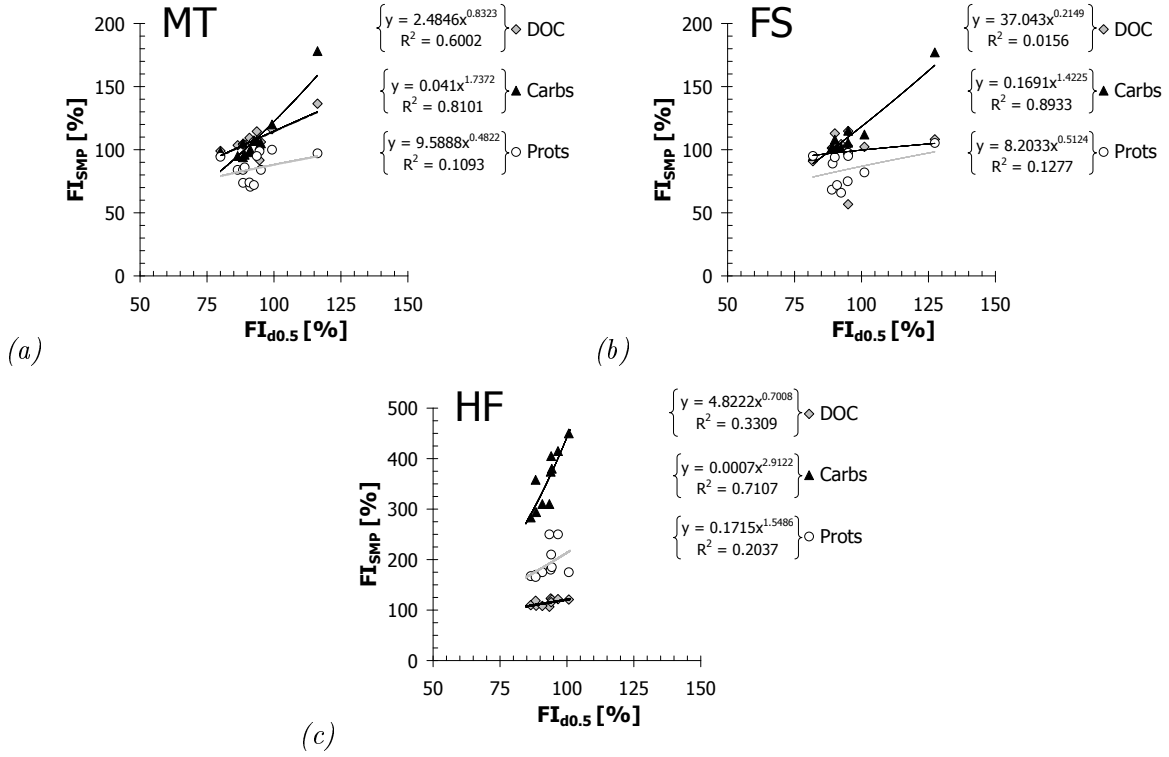

Figure B.10.: Correlation of observed particle fractionation during operation of the sidestream modules vs. fractionation of SMP during 2-hr-monitoring trial:*(a)* MT module, *(b)* FS module, *(c)* HF module

This could also be observed when comparing the HPSEC profiles for all three side-stream vessel's retentate lines, with the HF module showing highest changes of the supernatant. Overall, comparing the HPSEC profile of the HF retentate line to the biomass of the aeration tank, peaks were found to be higher for higher molecular weight ranges, but also slightly higher for lower molecular weight ranges. Changes in higher molecular weight range were also observed for the FS module retentate line, whereas the HPSEC profile of the supernatant of the MT module retentate line revealed to be almost unchanged compared to the aeration tank (Figure B.11).

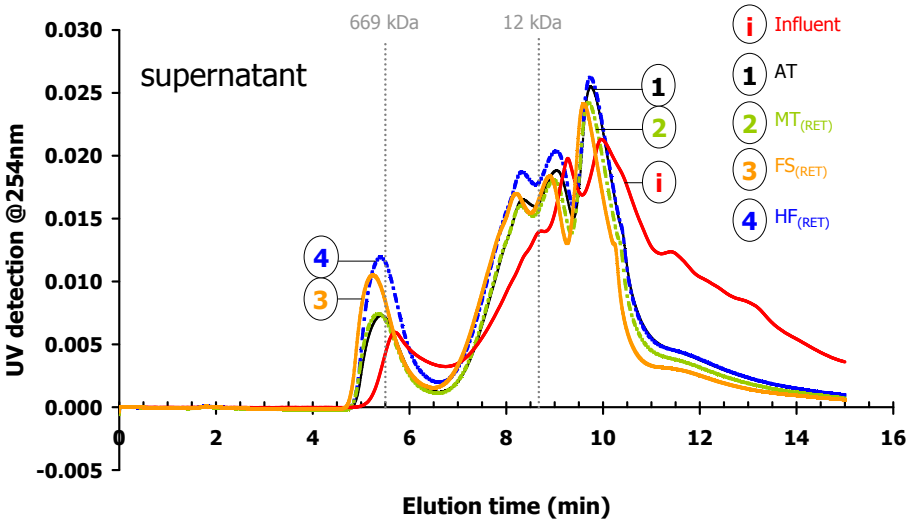

Figure B.11.: Sample of changes in supernatant molecular composition during side-stream operation - HPSEC profiles.